Biochemical and Structural Basis for the Moonlighting Function of Gephyrin

Biochemische und Strukturelle Basis für die duale Funktionalität von Gephyrin

Doctoral thesis

for a doctoral degree at the Graduate School of Life Sciences,
Julius-Maximilians-Universität Würzburg,

Section Biomedicine

Submitted by

Vikram Babu Kasaragod

from

Kasaragod, India

Würzburg 2016

Submitted on: ……..……..

Office stamp

Members of the *Promotionskomitee*:

Chairperson: Prof. Dr. Alexander Buchberger

Primary Supervisor: Prof. Dr. Hermann Schindelin

Supervisor (Second): Prof. Dr. Thomas Müller

Supervisor (Third): Prof. Dr. Carmen Villmann

Date of Public Defence: ……..……

Date of Receipt of Certificates: ……..

TABLE OF CONTENTS

Summary.....**1**

Zusammenfassung.....**3**

1. Introduction.....**10**

1.1 Synaptic transmission.....**10**

1.2 Chemical synapse.....**10**

1.2.1 Excitatory synapse.....**10**

1.2.2 Inhibitory synapse.....**11**

1.3 Gephyrin.....**13**

1.3.1 Gephyrin and its orthologs.....**16**

1.4 Molybdenum cofactor biosynthesis.....**16**

1.4.1 Terminal steps in Moco biosysnthesis.....**17**

1.5 Microtubule.....**18**

1.6 Other gephyrin interacting proteins.....**19**

1.7 Aims and objectives.....**20**

2. Modulation of gephyrin-glycine receptor affinity by multivalency.....**22**

2.1 Abstract.....**24**

2.2 Introduction.....**24**

2.3 Results and discussions.....**25**

2.3.1 A 14 residue GlyR fragment mediates almost all of the GlyR-gephyrin binding affinity.....**25**

2.3.2 A15 residue GlyR fragment is sufficient to occupy the core of gephyrin's receptor binding site.....**26**

2.3.3 Structure of apo-GephE and in complex with residues 397-410 of the GlyR β subunit.....**29**

2.3.4 Dimerization of receptor-derived peptides.....**30**

2.3.5 E domain stabilization by the bivalent peptide.....**33**

2.3.6 Thermofluor analysis suggests an increased affinity of GephE for the bivalent over the monovalent peptide.....**33**

2.3.7 Isothermal titration calorimetry (ITC) revealed the bivalent peptide to display a 25-fold enhanced affinity.....**34**

2.3.8 Similar enthalpic contributions mediate monovalent and bivalent ligand binding to gephyrin.....**36**

2.3.9 The oligomerization state of GephE modulates the receptor affinity of gephyrin.....**37**

2.4 Conclusions.....**37**

2.5 Materials and methods.....**39**

2.5.1 Protein expression and purification.....**39**

2.5.2 Peptide synthesis.....**40**

2.5.3 Peptide purification and analysis.....**40**

2.5.4 LC-MS.....**40**

2.5.5 HRMS.....**40**

2.5.6 Peptide dimerization.....**40**

2.5.7 Sample preparation for DSC, thermofluor and ITC.....**41**

2.5.8 Differential scanning calorimetry.....**41**

2.5.9 Thermofluor.....**41**

2.5.10 Isothermal titration calorimetry **41**

2.5.11 Comparative single injection total enthalpy (CSITE) analysis.....**42**

2.5.12 Crystallization and data collection.....**42**

2.5.13 Structure determination and refinement.....**42**

2.6 Accession codes.....**42**

2.7 Acknowledgement.....**43**

3. Molecular basis for alternative recruitment of $GABA_A$versus glycine receptors through gephyrin.....**44**

3.1 Abstract.....**46**

3.2 Introduction.....**46**

3.3 Results.....**48**

3.3.1 Identification of $GABA_AR\alpha3$-derived gephyrin-binding minimal peptides.....**49**

3.3.2 $GABA_AR$ α3-derived peptides are binding native full-length gephyrin.....**51**

3.3.3 Crystal structure analyses of GephE in complex with variants of $GABA_AR$ α3 fragments.....**52**

3.3.4 The $GABA_AR$ α3 and GlyR β subunits share an overlapping binding site on gephyrin.....**52**

3.3.5 Thermodynamic dissection of the receptor specificity of gephyrin.....**61**

3.4 Discussion.....**63**

3.5 Materials and methods.....**68**

3.5.1 Peptide synthesis, purification and validation.....**68**

3.5.2 Protein expression and purification.....**68**

3.5.3 Protein conjugation for chemiluminescence detection.....**68**

3.5.4 Peptide array based analysis.....**69**

3.5.5 Preparation of whole brain lysates.....**69**

3.5.6 Covalent immobilization of peptides.....**69**

3.5.7 Peptide and protein concentration determination. **70**

3.5.8 Isothermal titration calorimetry.....**70**

3.5.9 Protein complex crystallization and X-ray data collection.....**70**

3.5.10 Structure determination and refinement.....**71**

3.6 Aknowledgement **71**

3.7 Author contributions.....**71**

3.8 Additional informations.....**71**

4. Design and synthesis of high-affinity dimeric inhibitors targetting the interactions between gephyrin and inhibitory neurotransmitter receptors.....**72**

4.1 Abstract.....**74**

4.2 Introduction.....**74**

4.3 Results and discussion.....**76**

4.4 Materials and methods.....**91**

4.4.1 Peptide synthesis.....**91**

4.4.2 Synthesis of dimeric peptides.....**91**

4.4.3 HPLC purification and characterization.....**91**

4.4.4 LC-MS: Monovalent peptides.....**92**

4.4.5 Dimeric peptides.....**92**

4.4.6 MALDI-TOF-MS.....**93**

4.4.7 Protein expression and purification.....**94**

4.4.8 Preparation of whole brain lysates.....**94**

4.4.9 Covalent immobilization of peptides.....**94**

4.4.10 Pull-down and western blot detection.....**94**

4.4.11 Peptide and protein concentration determination.....**94**

4.4.12 Isothermal titration calorimetry **95**

4.4.13 Protein complex crystallization and X-ray data collection.....**95**

4.4.14 Structure determination and refinement.....**95**

4.4.15 *In vitro* serum stability assay.....**95**

4.4.16 Analytical Size Exclusion Chromatography and MALS.....**96**

5. Structural framework for metal incorporation during molybdenum cofactor biosynthesis.....**97**

5.1 Summary.....**99**

5.2 Introduction.....**99**

5.3 Results and discussions.....**101**

5.3.1 Overall Architecture of GephE-Nucleotide Complexes.....**101**

5.3.2 Structural Features of the Nucleotide-Binding Pocket **103**

5.3.3 Conformational Changes in the Nucleotide Recognition Loop.....**106**

5.3.4 Structures of Ternary GephE-ADP-Mo/W Complexes Provide Insights into Metal Ion Insertion.....**107**

5.3.5 Framework for Moco Biosynthesis is Evolutionarily Conserved.....**110**

5.3.6 Implications for Human Health.....**113**

5.3.7 Structure of a GephE-ADP-receptor derived peptide complexes provide clues towards the integration of gephyrin's dual functionality.....**114**

5.4 Conclusion.....**115**

5.5 Materials and methods.....**115**

5.5.1 Protein expression and purification.....**115**

5.5.2 Isothermal titration calorimetry.....**116**

5.5.3 Protein complex cystallization and X-ray data collection.....**116**

5.5.4 Structure determination and refinement.....**116**

5.6 Accession numbers **117**

5.7 Author contributions.....**117**

5.8 Acknowledgements.....**117**

6. Characterization of the gephyrin-microtubule interaction.....**118**

6.1 Introduction.....**118**

6.2 Aims.....**118**

6.3 Materials and methods.....**119**

6.3.1 Purification of gephyrin constructs, DARPin and RB3-SLD.....**119**

6.3.2 Microtubule purification from cow brain.....**120**

6.3.3 Microtubule co-sedimentation assay.....**121**

6.3.4 Nano-gold labelling, negative staining and electron microscopic (EM) analysis of the microtubule-gephyrin complex.....**121**

6.3.5 Analytical size exclusion chromatography coupled to MALS..... .....**121**

6.4 Results and discussions.....**122**

6.4.1 Microtubule co-sedimentation assays provide hints at multiple binding sites for tubulin on gephyrin.....**122**

6.4.2 Electron microscopy analysis of microtubules, gephyrin and the microtubule-gephyrin complex.....**124**

6.4.3 MALS provides insight into the temperature-dependent formation of the tubulin-DARPin complex.....**125**

7. Characterization of Cinnamon : gephyrin ortholog from *Drosophila*.....127

7.1 Introduction.....**127**

7.2 Aims.....**127**

7.3 Materials and methods.....**127**

7.3.1 Cloning of Cinnamon constructs.....**127**

7.3.2 Protein expression.....**129**

7.3.3 Protein purification.....**129**

7.3.4 Electron microscopy and atomic force microscopy.....**130**

7.3.5 Analytical size exclusion chromatography coupled to MALS.....**131**

7.4 Results and discussions.....**131**

7.4.1 Protein purification and separation of different Cinnamon oligomers.....**131**

7.4.2 SEC-MALS of the different Cinnamon oligomers.....**132**

7.4.3 Electron microscopy and atomic force microscopy analysis revealed a homogenous Cinnamon trimer and a heterogeneous hexamer.....**133**

8. Discussions..... .....**136**

8.1 Molecular basis of $GABA_A$ receptor clustering.....**136**

8.2 Structural basis for the terminal step of Moco biosynthesis.....**140**

8.3 Structural basis for the moonlighting function of gephyrin.....**142**

8.4 Gephyrin-microtubule interactions.....**143**

8.5 Towards structural studies of gephyrin orthologs.....**143**

8.6 Conclusion.....**144**

9. **Future perspective**.....**145**

10. **List of PDB entries**.....**147**

11. **List of publications**.....**148**

12. **Acknowledgement**.....**149**

13. **Abbreviations**.....**150**

14. **List of expression constructs**.....**154**

15. **Affidavit**.....**155**

16. **Curriculum vitae**.....**156**

17. **References**.....**158**

SUMMARY:

Neurons are specialized cells dedicated to transmit the nerve impulses throughout the human body across specialized structures called synapses. At the synaptic terminals, a crosstalk between multiple macromolecules regulates the structure and function of the presynaptic nerve endings and the postsynaptic recipient sites.

Gephyrin is the central organizer at inhibitory postsynaptic specializations and plays a crucial role in the organization of these structures by anchoring $GABA_A$ receptors ($GABA_AR$) and glycine receptors (GlyR) to the postsynaptic membrane. This 93 kDa protein features an N-terminal G domain and a C-terminal E domain and the latter interacts directly with the intracellular loop between transmembrane helices 3 and 4 of certain subunits of the GlyRs and $GABA_A$Rs. Biochemical and structural analyses have already provided valuable insights into the gephyrin-GlyR interaction. Interestingly, biochemical studies on the gephyrin-$GABA_AR$ interaction demonstrated that the $GABA_A$Rs also depend on the same binding site as the GlyRs for the interaction with the gephyrin, but the molecular basis for this receptor specific interaction of gephyrin was still unknown. Co-crystal structures of GephE-$GABA_AR$ α3- derived peptides with supporting biochemical data presented in this study deciphered the receptor-specific interactions of gephyrin in atomic detail.

In its moonlighting function, gephyrin also catalyzes the terminal step of the evolutionarily conserved molybdenum cofactor biosynthesis. Molybdenum, an essential transition element has to be complexed with a pterin-based cofactor resulting in the formation of the molybdenum cofactor (Moco). Moco is an essential component at the active site of all molybdenum-containing enzymes with the exception of nitrogenase. Mutations in enzymes involved in this pathway lead to a rare yet severe disease called Moco deficiency, which manifest itself in severe neurodevelopmental abnormalities and early childhood death. Moco biosynthesis follows a complex multistep pathway, where in the penultimate step, the N-terminal G domain of gephyrin activates the molybdopterin to form an adenylated molybdopterin intermediate. In the terminal step, this intermediate is then transferred to the C-terminal E domain of gephyrin, which catalyzes the metal insertion and deadenylation reaction to form active Moco. Previous biochemical and structural studies provided valuable insights into the penultimate step of the Moco biosynthesis but the terminal step remained elusive. Through the course of my dissertation, I crystallized the C-terminal E domain in the apo-form as well as in complex with ADP and AMP. These structures shed lightonto the deadenylation reaction and the formation of a ternary E-domain-ADP-Mo/W complex and thus provide structural insight into the metal insertion mechanism. Moreover, the structures also provided molecular insights into a mutation leading to Moco deficiency. Finally, ternary

complexes of GephE, ADP and receptor-derived peptides provided first clues regarding the integration of gephyrin's dual functionality.

In summary, during the course of the dissertation I was able to derive high resolution structural insights into the interactions between gephyrin and $GABA_A$Rs, which explain the receptor-specific interaction of gephyrin and, furthermore, these studies can be extended in the future to understand $GABA_A$R subunit-specific interactions of gephyrin. Finally, the understanding of Moco biosynthesis shed light on the molecular basis of the fatal Moco deficiency.

ZUSAMMENFASSUNG:

Neurone sind spezialisierte Zellen, die über die Synapsen Nervenimpulse im menschlichen Körper übertragen. An den synaptischen Enden reguliert ein Netzwerk aus einer Vielzahl von Makromolekülen die Struktur und die Funktion der präsynaptischen Nervenenden und der postsynaptischen Kontaktstellen.

Gephyrin ist der Hauptorganisator an inhibitorischen, postsynaptischen Spezialisierungen und spielt durch die Verankerung von $GABA_A$-Rezeptoren ($GABA_AR$) und Glycinrezeptoren (GlyR) in der postsynaptischen Membran eine zentrale Rolle für den Aufbau dieser Strukturen. Dieses 93 kDa Protein enthält eine N-terminale G-Domäne (GephG) und eine C-terminale E-Domäne (GephE), wobei letztere direkt mit der intrazellulären unstrukturierten Region zwischen Transmembranhelices 3 und 4 bestimmter Untereinheiten der GlyR und $GABA_AR$ interagiert. Biochemische und strukturelle Analysen lieferten bereits wertvolle Erkenntnisse über die Gephyrin-GlyR Interaktion. Interessanterweise zeigten Versuche zur Gephyrin-$GABA_AR$ Interaktion, dass $GABA_ARs$ die gleiche Bindungsstelle auf Gephyrin benutzen wie GlyRs, wobei die molekulare Basis für diese Interaktion nicht bekannt war. In dieser Arbeit zeige ich Co-Kristallstrukturen von GephE-$GABA_AR\alpha3$ sowie unterstützende biochemische Daten, die die atomaren Details der rezeptorspezifischen Interaktionen von Gephyrin entschlüsseln.

Als zweite Funktion katalysiert Gephyrin den terminalen Schritt der evolutionär konservierten Molybdän Cofaktor Biosynthese. Dabei muss das essentielle Übergangselement Molybdän mit einem Pterin-basierten Cofaktor komplexiert werden, um den Molybdän Cofaktor (Moco) zu bilden. Moco ist essentieller Bestandteil im aktiven Zentrum aller Molybdän-enthaltenden Enzyme mit Ausnahme der Nitrogenase. Mutationen in Enzymen, die in die Molybdän Cofaktor Biosynthese involviert sind, verursachen eine Moco Defizienz, eine seltene, jedoch schwere Erkrankung, die sich durch schwere neurologische Entwicklungsstörungen und Tod im frühen Kindesalter äußert. Die Moco Biosynthese folgt einem komplexen mehrstufigen Ablauf. Im vorletzten Schritt adenyliert GephG das Molybdopterin und ein Zwischenprodukt entsteht. Im letzten Schritt wird dieses Zwischenprodukt auf GephE übertragen, das die Insertion des Metalls und die Deadenylierungsreaktion katalysiert, wodurch der aktive Moco entsteht. Frühere biochemische und strukturelle Studien brachten wertvolle Erkenntnisse über den vorletzten Schritt der Moco Biosynthese, aber die Kenntnisse über den letzten Schritt blieben vage. Während meiner Dissertation kristallisierte ich GephE in der apo-Form sowie im Komplex mit ADP oder AMP. Diese Strukturen gaben Aufschluss über die Deadenylierungsreaktion und die Formation eines ternären GephE-ADP-Mo/W Komplexes und gewährten so einen strukturellen Einblick in den Mechanismus der Metallinsertion. Darüber hinaus ermöglichten die Strukturen eine Mutation, die zu Moco Mangel führt, auf

molekularer Ebene zu verstehen. Schließlich lieferten ternäre Komplexe aus GephE, ADP und von Rezeptoren abgeleiteten Peptiden ersten Aufschluss bezüglich der Verflechtung von Gephyrins dualer Funktion.

Zusammenfassend konnte ich während der Dissertation hochauflösende strukturelle Einblicke in den Komplex aus GephE und $GABA_AR$ α3 Untereineinheit gewinnen, die die rezeptorspezifische Interaktion von Gephyrin erklären. Weiterhin können diese Studien in der Zukunft ausgeweitet werden, um die $GABA_AR$-untereinheitenspezifische Interaktion mit Gephyrin zu verstehen. Schließlich erlauben die Studien zur Moco Biosynthese die tödliche Moco Defizienz auf molekularer Ebene zu verstehen.

This dissertation is based on the following manuscripts:

1. Maric, H.M., Kasaragod, V.B., and Schindelin, H. (2014). Modulation of gephyrin-glycine receptor affinity by multivalency. *ACS Chem. Biol*. **9**, 2554-2562.
2. Maric, H.M*., Kasaragod, V.B*., Hausrat, T.J., Kneussel, M., Tretter, V., Strømgaard, K., and Schindelin, H. (2014). Molecular basis of the alternative recruitment of $GABA_A$ versus glycine receptors through gephyrin. *Nat. Commun*. **5**, 5767.
3. Maric, H.M., Kasaragod, V.B., Kedstrom, L.H., Hausrat, T.J., Kneussel, M., Schindelin, H., Strømgaard, K. (2015) Design and synthesis of high-affinity dimeric inhibitors targeting the interaction between gephyrin and inhibitory neurotransmitter receptors. *Angew. Chem. Int. Ed.* **54**, 490-4.
4. Kasaragod, V.B. and Schindelin, H.(2016) Structural Framework for Metal Incorporation during Molybdenum Cofactor Biosynthesis.*Structure.* **24,**782-8.

*** These authors contributed equally to this work.**

"Dissertation Based on Several Published Manuscripts"

Statement of individual author contributions and of legal second publication rights

(If required please use more than one sheet)

Publication (complete reference): Maric, H.M., Kasaragod, V.B., and Schindelin, H. (2014).*ACS Chem. Biol*. **9**, 2554-2562.					
Participated in	**Author Initials,** Responsibility decreasing from left to right				
Study Design Methods Development	HMM HMM	VBK, HS VBK, HS			
Data Collection	HMM, VBK				
Data Analysis and Interpretation	HMM, VBK	HS			
Manuscript Writing Writing of Introduction Writing of Materials & Methods Writing of Discussion Writing of First Draft	 HMM, HMM, VBK HMM HMM	 VBK, HS HS VBK, HS VBK, HS			

Explanations (if applicable):

Publication (complete reference): Maric, H.M., Kasaragod, V.B., Hausrat, T.J., Kneussel, M., Tretter, V., Strømgaard, K., and Schindelin, H. (2014). Molecular basis of the alternative recruitment of $GABA_A$versus glycine receptors through gephyrin. *Nat. Commun*. **5**, 5767.					
Participated in	**Author Initials,** Responsibility decreasing from left to right				
Study Design Methods Development	HMM, VBK, HS	KS	TJH, MK	VT	
Data Collection	VBK, HMM	TJH			
Data Analysis and Interpretation	VBK, HMM	HS	KS	TJH, MK	
Manuscript Writing Writing of Introduction Writing of Materials & Methods Writing of Discussion Writing of First Draft	 HMM, VBK, VBK, HMM, HMM, VBK HMM, VBK	 HS HS HS HS	 KS KS KS KS	 TJH, MK TJH, MK TJH, MK TJH, MK	 VT VT VT VT

Explanations (if applicable):

Publication (complete reference): Maric, H.M., Kasaragod, V.B., Kedstrom, L.H., Hausrat, T.J., Kneussel, M., Schindelin, H., Strømgaard, K. (2015). Design and synthesis of high-affinity dimeric inhibitors targeting the interaction between gephyrin and inhibitory neurotransmitter receptors. *Angew. Chem. Int. Ed.***54**, 490-4.					
Participated in	**Author Initials,** Responsibility decreasing from left to right				
Study Design Methods Development	HMM, VBK HMM, VBK	KS, HS LHK, TJH	LHK, TJH KS, HS	MK MK	
Data Collection	HMM, VBK	LHK, TJH			
Data Analysis and Interpretation	HMM, VBK	KS, HS	LHK, TJH, MK		
Manuscript Writing Writing of Introduction Writing of Materials & Methods Writing of Discussion Writing of First Draft	 HMM HMM, VBK HMM HMM	 VBK, KS, HS KS, HS VBK, KS VBK, KS, HS	 LHK, TJH, MK LHK, TJH, MK LHK, TJH, MK LHK, TJH, MK		

Explanations (if applicable):

Publication (complete reference): Kasaragod, V.B., and Schindelin, H. (2016).Structural framework for metal incorporation during molybdenum cofactor biosynthesis. *Structure.***24,**782-8.					
Participated in	**Author Initials,** Responsibility decreasing from left to right				
Study Design Methods Development	VBK VBK	HS HS			
Data Collection	VBK				
Data Analysis and Interpretation	VBK	HS			
Manuscript Writing Writing of Introduction Writing of Materials & Methods Writing of Discussion Writing of First Draft	 VBK VBK VBK VBK	 HS HS			

The doctoral researcher confirms that she/he has obtained permission from both the publishers and the co-authors for legal second publication.

The doctoral researcher and the primary supervisor confirm the correctness of the above mentioned assessment.

Vikram Babu Kasaragod	2016	Würzburg	
Doctoral Researcher's Name	Date	Place	Signature

Prof. Dr. Hermann Schindelin		Würzburg	
Primary Supervisor's Name	Date	Place	Signature

"Dissertation Based on Several Published Manuscripts"

Statement of individual author contributions to figures/tables/chapters included in the manuscripts

(If required please use more than one sheet)

Publication (complete reference): Maric, H.M., Kasaragod, V.B., and Schindelin, H. (2014). Modulation of gephyrin-glycine receptor affinity by multivalency. *ACS Chem. Biol*. **9**, 2554-2562..

Figure	**Author Initials,** Responsibility decreasing from left to right				
1	VBK, HMM	HS			
2	HMM	VBK, HS			
3	VBK, HMM	HS			
4	HMM	VBK, HS			
5	HMM	VBK, HS			
6	HMM	VBK, HS			

Explanations (if applicable):

Publication (complete reference): Maric, H.M., Kasaragod, V.B., Hausrat, T.J., Kneussel, M., Tretter, V., Strømgaard, K., and Schindelin, H. (2014). Molecular basis of the alternative recruitment of $GABA_A$ versus glycine receptors through gephyrin. *Nat. Commun*. **5**, 5767.

Figure	**Author Initials,** Responsibility decreasing from left to right				
1	VBK, HMM	HS, KS	TJH, MK	VT	
2	HMM	TJH, MK	VBK, HS, KS	VT	
3	VBK	HMM, HS, KS	TJH, MK, VT		
4	VBK	HMM, HS, KS	TJH, MK, VT		
5	HMM, VBK	HS, KS	TJH, MK,VT		

Explanations (if applicable):

Publication (complete reference):Maric, H.M., Kasaragod, V.B., Kedstrom, L.H., Hausrat, T.J., Kneussel, M., Schindelin, H., Strømgaard, K. (2015). Design and synthesis of high-affinity dimeric inhibitors targeting the interaction between gephyrin and inhibitory neurotransmitter receptors. *Angew. Chem. Int. Ed.***54**, 490-4.

Figure	**Author Initials,** Responsibility decreasing from left to right				
1	HMM, VBK	LHK, TJHM MS, HS, KS			
2	HMM	TJH, VBK, LHK, MK, HS, KS			
3	HMM	VBK, LHK, TJH, MK, HS, KS			
4	VBK	HMM, HS, KS			
5					

Explanations (if applicable):

Publication (complete reference): Kasaragod, V.B., and Schindelin, H. (2016).Structural framework for metal incorporation during molybdenum cofactor biosynthesis. *Structure.***24,**782-8.					
Figure	**Author Initials,** Responsibility decreasing from left to right				
1	VBK	HS			
2	VBK	HS			
3	VBK	HS			
4	VBK	HS			
5					

I also confirm my primary supervisor's acceptance.

Vikram Babu Kasaragod		Wuerzburg	
Doctoral Researcher's Name	Date	Place	Signature

1.INTRODUCTION

1.1 Synaptic transmission:

Neurons are specialized cells which function to transmit nerve impulses throughout the human body. Each neuron consists of various dendritic terminals from which it receives the neuronal signals of adjacent neurons and transmits them through its axonic terminal. The junctions connecting two neurons are referred to as the synaptic junctions. The synapses, thus consists of two parts, the presynaptic and postsynaptic terminals, which in each case encompasses a complex array of molecules which function together in maintaining the architecture and function of the synapse. The synaptic terminals can be broadly classified into two different classes: Electrical synapses mainly consist of the gap junctions and chemical synapses containing arrays of neurotransmitter receptors (Pereda, 2014) which are regulated by small molecules, thus resulting in the transmission of either an excitatory or an inhibitory signaloriginating from a particular neuron.

1.2 Chemical synapses:

1.2.1 Excitatory synapses:

Excitatory synapses are responsible for the transmission of excitatory signals via a controlled influx of sodium/calcium ions through the presynaptic terminal into the postsynaptic neuron. Glutamate, a ubiquitous neurotransmitter, is responsible for the majority of excitatory signals through its interaction with the ionotropic glutamate receptors (iGluR) (Traynelis et al., 2010). The iGluR are cation-permeable ligand-gated ion channels, consisting of three different families, depending on their sensitivity towards different neurotransmitters. The three major classes are the α-amino-3-hydroxy-5-methyl-4-isoxazole propionic acid (AMPA)-sensitive (Keinanen et al., 1990) kainite-sensitive (Sommer et al., 1992) and *N*-methyl-D-aspartate (NMDA)-sensitive receptors (Paoletti et al., 2013). The AMPA and kainate receptors can form homomeric functional receptors whereas the NMDA receptors are obligate heteromers. Despite differences in the sensitivity towards the neurotransmitters, all receptors share structural and functional similarities (Figure 1-1, representative structure for iGluR). Structurally, the intact tetrameric receptors can be divided into three different parts; an amino terminal domain (ATD), a ligand-binding domain (LBD), which contains the agonist-binding pocket, and a transmembrane domain (TMD) consisting of four transmembrane helices. Agonist binding to the LBD results in major structural rearrangements in the LBD, in particular in the TMD, and the ATD, which, inturn, facilitate excitatory neurotransmission (Fig 1-1) (Durr et al., 2014; Sobolevsky et al., 2009).

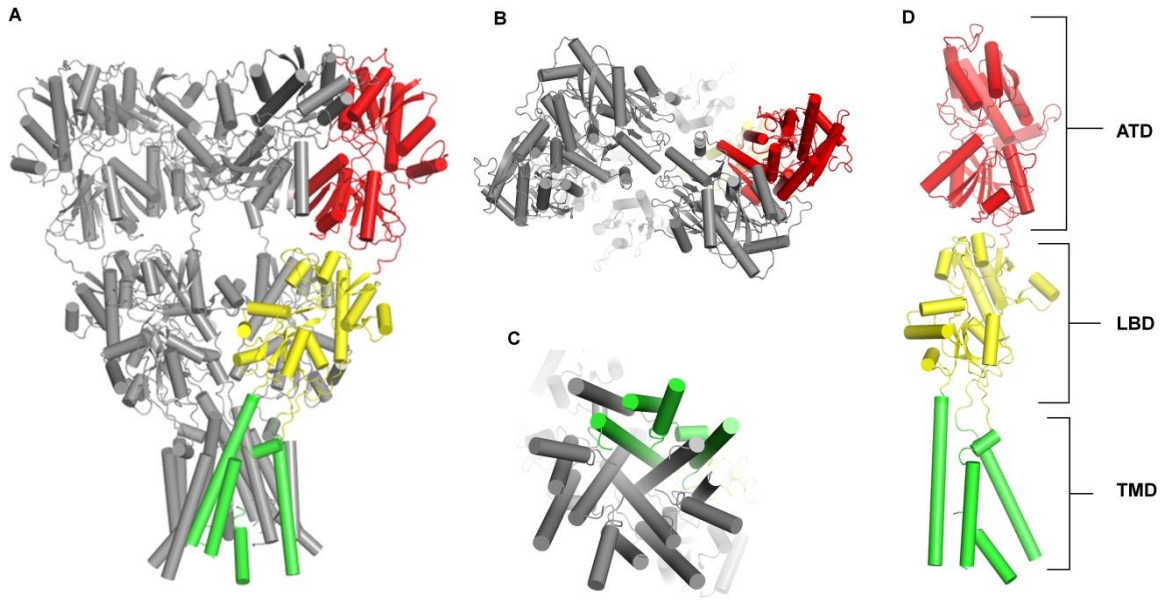

Figure 1-1: Structure of the AMPA receptor as a representative member of the iGluR family. (A) Cartoon representation of the overall architecture of the homotertrameric AMPA receptor crystal structure, where the ATD is colored in red, the LBD in yellow and transmembrane helices in green for one monomer while the other three monomers are represented in grey. **(B)** Top view of the receptor seen through the 2-fold axis of symmetry present in the ATD. **(C)** The receptor viewed along the 4-fold axis of symmetry present in the transmembrane region creating the ion channel pore. **(B)** and **(C)** clearly depict the symmetry mismatch between the individual domains, which plays crucial role in the ion channel gating mechanism. **(D)** Cartoon representation of the single subunit of the receptor. The native M3-M4 loop was replaced with a shorter sequence but even the short intracellular loop was not resolved in the crystal structure. (Sobolevsky et al., 2009)

1.2.2 Inhibitory synapses:

γ-Aminobutyric acid type A receptors ($GABA_AR$s) and glycine receptors (GlyRs) are the major classes of receptors at inhibitory postsynapses. Both $GABA_AR$ and the GlyR are pentameric ligand-gated ion channels, belonging to the Cys-loop superfamily of receptors. This class also includes the cation-selective nicotinic acetylcholine receptor (nAChR) (Albuquerque et al., 2009) and the serotonin type-3 receptor ($5\text{-}HT_3R$) (Lummis, 2012). Inhibition of neurotransmission is mediated by the permeability of these receptors to chloride (Cl^-) ions. The $GABA_AR$s are more diverse compared to the GlyRs with eight different subunit types totaling 19 different subunit classes, whereas the GlyRs only consist of two different subunit types with 5 different subunit classes (four α and one β) (Table 1-1). In the case of the $GABA_AR$, the functional receptor mainly consists of two α, two β and one γ-subunit, in contrast, GlyR can form functional homomeric receptor (Tyagarajan and Fritschy, 2014).

$GABA_AR$ subtypes, notably those containing the α1, α2 or α3 subunit along with the γ2-subunit, are localized postsynaptically with gephyrin (Tretter et al., 2012; Tyagarajan and

Fritschy, 2014). In contrast α4, α5 and δ-subunits, which mainly form extrasynaptic $GABA_AR$s, do not co-localize with gephyrin. Deficits in $GABA_AR$-mediated neurotransmission have been associated with a wide spectrum of disorders of the CNS such as epilepsy, anxiety, mood disorders, and neuro-developmental impairments including autism, fragile X syndrome, and schizophrenia (Hines et al., 2012).

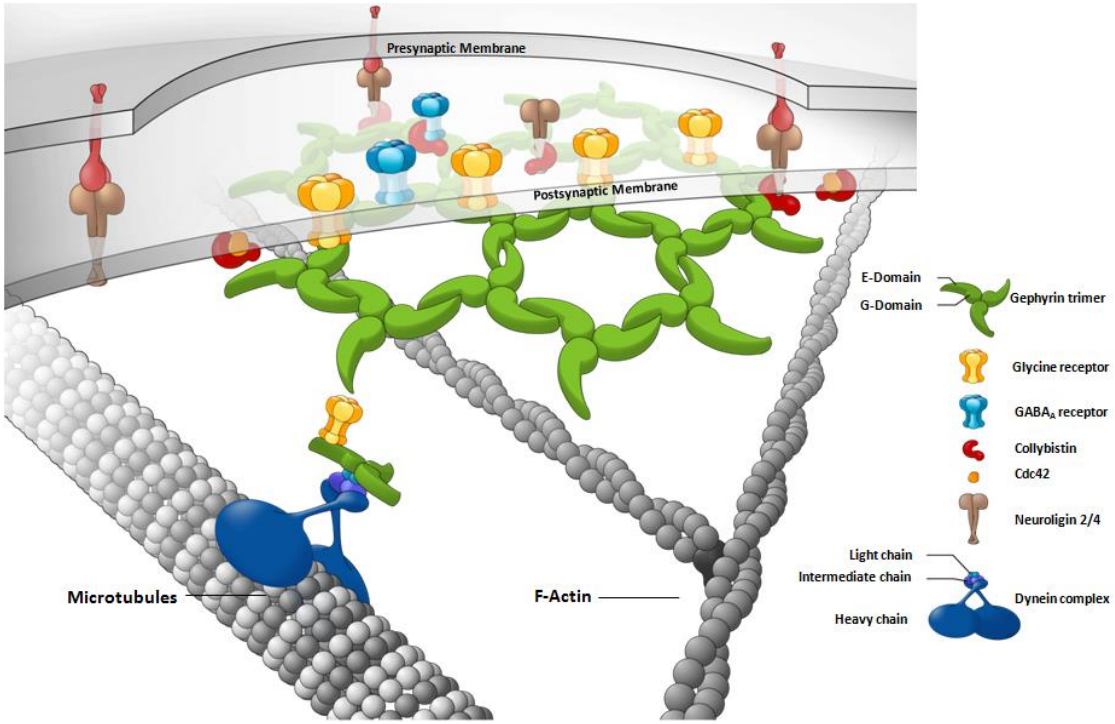

Figure 1-2: **Schematic diagram of the molecular interplay at the postsynaptic membrane.** Gephyrin (green) is proposed to form a hexagonal scaffold at inhibitory postsynapses and aids in the clustering of $GABA_AR$s (orange) and GlyRs (blue) at post-synaptic sites. Two additional interaction partners of gephyrin, Collybistin and Neuroligin-2, are represented in red and brown colours, respectively. The cytoskeletal proteins microtubule and F-actin are represented as grey filaments. (The image is used with permission from Dr. Carolyn Delto).

Crystal structures of a β3 homopentameric $GABA_AR$ (Miller and Aricescu, 2014) and an α3 homopentameric GlyR as well as a cryo-EM structure of an α1 homopentameric GlyR were recently solved (Du et al., 2015). In all cases, the structures share a similar architecture, which contains (Fig. 1-3) an extracellular domain mainly consisting of β sheets, 4 transmembrane helices and two intracellular highly unstructured loop regions, which connect the transmembrane helices (Fig. 1-3).

Subunit	Classes
α	1–6
β	1-3
γ	1-3
ε	1-3
Θ, π, δ, ρ	1

Table 1-1.Subunit class diversity of $GABA_AR$s.

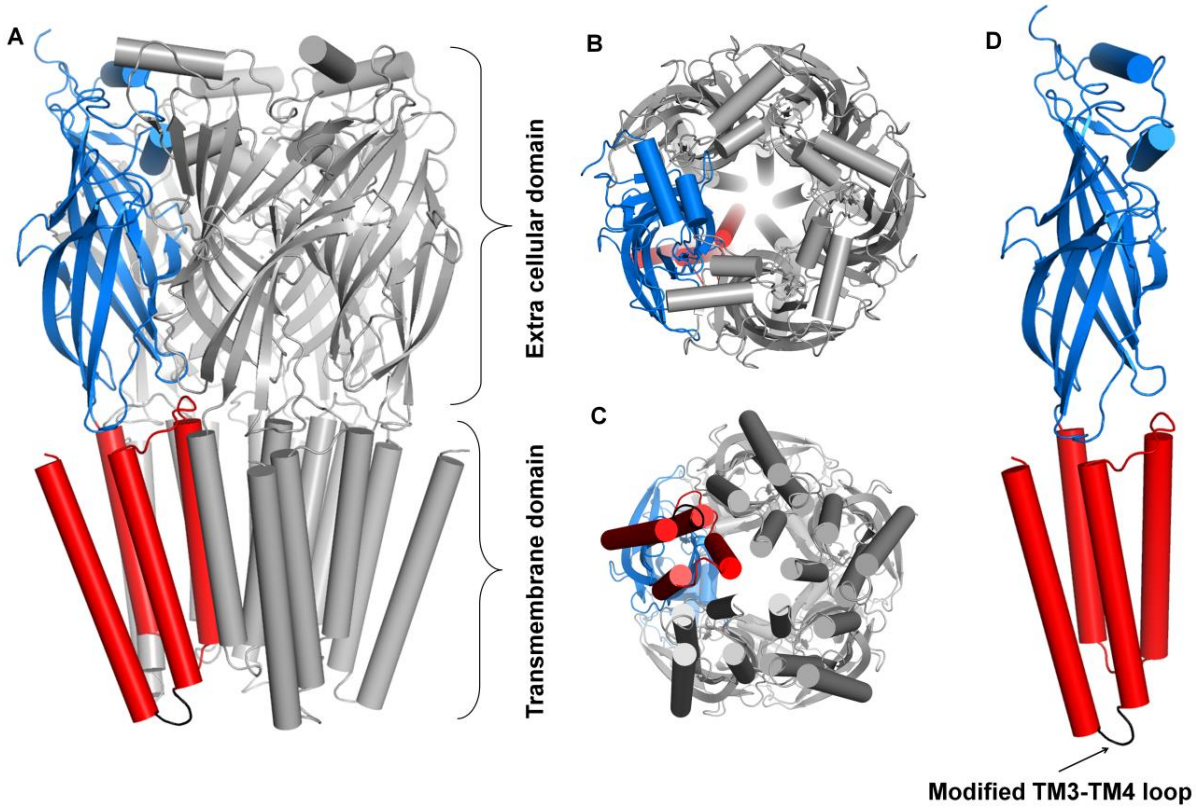

Figure 1-3: Structure of the Cys-loop $GABA_AR$. (A) Cartoon representation of the β3 homopentameric $GABA_AR$, where the extracellular domain is colored in blue, transmembrane helices in red and the intracellular loop in black. **(B)** Top view of the receptor seen along the 5-fold axis of symmetry from the extracellular side. **(C)** The receptor view from the intracellular side. **(D)** Cartoon representation of a single subunit of the receptor. Please note that the native intracellular loop between TM3 and TM4 are replaced with shortened residue stretches (colored in black) to aid in the crystallization (Miller and Aricescu, 2014).

1.3 Gephyrin:

Gephyrin, a ~93-kDa, tubulin-binding protein, is the central scaffolding protein at inhibitory postsynapses (Kirsch et al., 1991; Prior et al., 1992; Tretter et al., 2012). In its moonlighting function, gephyrin also catalyzes the terminal steps of the evolutionarily conserved Moco biosynthesis (see section 1.4 below). Gephyrin consists of an N-terminal G-domain (GephG) and a C-terminal E domain, which are connected by ~15 kDa unstructured linker region (Fig. 1-4A) (Kirsch et al., 1991; Sander et al., 2013). This linker part harbours multiple sites of post-translational modifications including phosphorylation (Herweg and Schwarz, 2012; Kuhse et al., 2012; Llamas et al., 2004) palmoytilation (Dejanovic et al., 2014) and acetylation (Tyagarajan et al., 2013) sites. Structural studies on the isolated terminal

domains showed that the G domain trimerizes (Fig. 1-4B) (Schwarz et al., 2001) while the E domain forms a dimer (Fig. 1-4C) (Kim et al., 2006) in isolation. Although the full-length protein is recalcitrant towards crystallization, studies employing small angle X ray scattering (SAXS) and atomic force microscopy (AFM) revealed that the full-length protein is predominantly trimeric, however, it is conformationally heterogeneous with a mixture of compact and extended forms (Fig. 1-4D) (Sander et al., 2013).

Knockout studies have shown that the affected mice die within a few hours after birth. Any mutation in gephyrin also results in a loss of $GABA_AR$ clusters and, inturn, causes diseases such as stiff-person syndrome (hyperekplexia) and epilepsy.

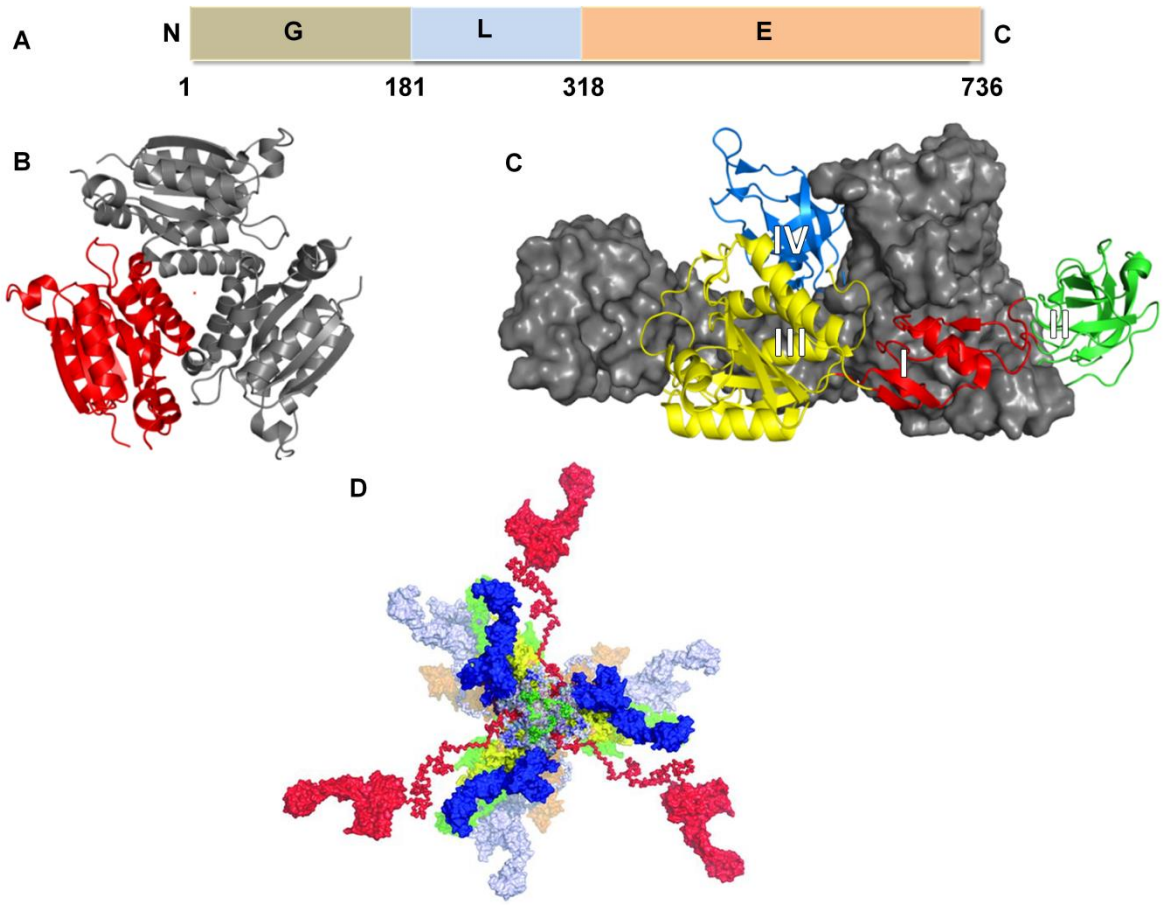

Figure 1-4: Structure of gephyrin. (A) Schematic representation of the domain architecture of gephyrin. **(B)** Cartoon representation of the N-terminal G domain where one monomer is colored in red and other two in grey. **(C)** Structure of the C-terminal E domain dimer with one monomer is represented as cartoon, colored according to the four subdomains of GephE which are numbered with roman numerals. The second monomer is shown in surface representation in dark grey. **(D)** Ensemble of models derived by SAXS for the trimeric full-length gephyrin, where different models are colored differently.

GephE is the part of gephyrin, which interacts directly with the $GABA_ARs$ and GlyRs, thereby anchoring them to the postsynaptic membrane. Biochemical and structural studies in the case of the gephyrin-GlyR complex demonstrated that the large-intracellular loop, located between transmembrane α-helices 3 and 4, interacts with gephyrin (Kim et al., 2006; Sola et al., 2004). In addition, biochemical analyses of the gephyrin-$GABA_AR$ interaction proved that both the GlyR and the $GABA_AR$, interact with gephyrin through overlapping, yet distinct receptor binding sites (Maric et al., 2011). Although the biochemical analysis shed light on the universal binding site, the molecular details of the receptor-specific interaction of gephyrin remained elusive.

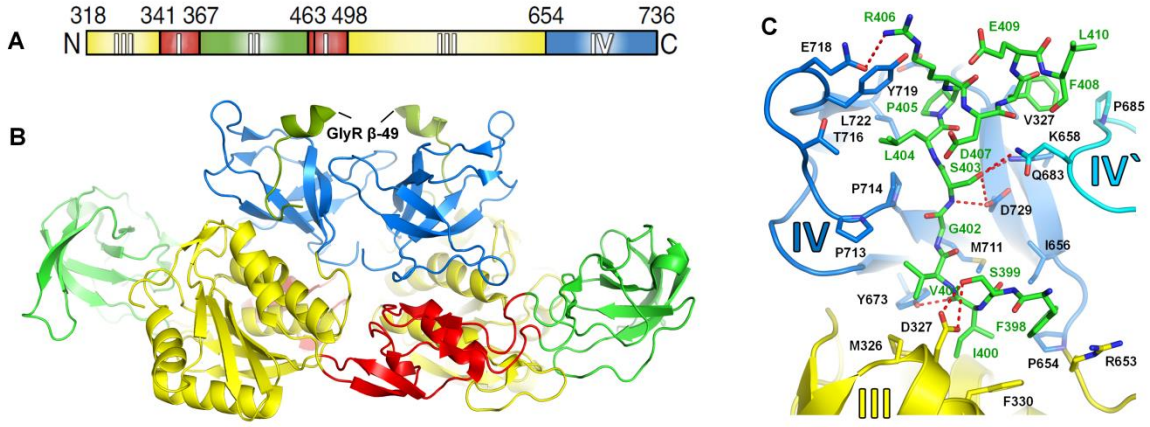

Figure 1-5: Gephyrin- GlyR interaction. (A) Schematic representation of the subdomain architecture (Roman numerals) of GephE. **(B)** Overall architecture of the GephE-GlyR β-49 complex, colored according to the scheme in **(A). (C)** Enlarged view of receptor-binding pocket with GephE represented in cartoon form and the interacting GlyR β-subunit-derived residues are represented as sticks. The red dashed lines represent hydrogen bonds.

The structure of GephE-GlyR β-49 complex revealed that the interaction is mainly mediated by hydrophobic residues, primarily residing in subdomain IV of GephE with a minor contribution from subdomain III (Fig. 1-5A). The β-49 loop adopts a "C" shape (Fig. 1-5B). Although most of the interacting residues do not fold into defined secondary structure elements, the C-terminal region of the structurally resolved part of the β-49 loop adopts an α-helical structure.

Receptor	Sequence
Gly β	^{398}FSIVGSLPRDF^{408}
$GABA_A$ α1	^{340}YAPTATSYTPN^{350}
$GABA_A$ α2	^{339}YAVAVANYAPN^{349}
$GABA_A$ α3	^{368}FNIVGTTYPIN^{378}
$GABA_A$ β2	AGLPRHSFGRNALERHVAQKKSRL
$GABA_A$ β3	QSMPKEGHGRYMGDRSIPHKKTHL

Table 1-2: Table representing the sequences of the core binding motifs in the TM3-TM4 loops from different receptor subunits that directly interact with gephyrin.

1.3.1 Gephyrin and its orthologs:

Multiple gephyrin orthologs have been identified in different organisms which always function in Moco biosynthesis but sometimes also in neurotransmitter receptor anchoring. In mammals, the homologs are involved in both of the moonlighting functions, while in other oragnisms such as prokaryotes and plants, it is solely responsible for the Moco biosynthesis. In bacteria, MogA (Liu et al., 2000) and MoeA (Xiang et al., 2001) are independent proteins which are homologous to the gephyrin G and E domains (hence the names), respectively, and also carry out the two terminal steps during Moco biosynthesis. In addition to the prokaryotes, the identified homolgs in the fungal kingdom such as *Neurospora* and *Chaetomeum*, the protein is again involved in the Moco biosynthesis. During the course of evolution, independent gene fusion events resulted in the plant protein Cnx1, containing the E and G domainsin inverted order compared to gephyrin but with a much shorter unstructured linker (Ramming et al., 2000) and, of course, gephyrin. Cnx1 is solely responsible for the catalysis of the terminal steps of Moco biosynthesis in plants. In invertebrates, such as *Drosophila,* the Cinnamon protein (Kamdar et al., 1994; Wittle et al., 1999) is not only responsible for the Moco biosynthesis but also predicted to be participating in $GABA_AR$ clustering at synaptic sites (Chapter 7). In Cinnamon the domain order is identical to that in gephyrin; however, here the domains are connected by a much shorter unstructured linker. Gephyrin homologs have also been identified in non-mammalian vertebrates such as zebra fish, where the protein inturn responsible for the Moco biosyntheis and also discovered to be involved in the glycine receptor clustering (Ogino et al., 2011). Finally the most complex form of the proteins are found in the mammalian system where the protein is involved in the clustering of both the major classes of the receptors at the inhibitory synapses and also have shown to under go multiple alternative splicing and post translational modifications, adding to the complexity of the protein.

1.4 Molybdenum cofactor biosynthesis:

Molybdenum (Mo) is an essential transition metal, which is required for the viability of all multicellular eukaryotes. To be catalytically active, Mo has to be complexed with a special tri-cyclic pterin-based cofactor called molybdopterin and the organic moiety together with the metal are referred to as molybdenum cofactor (Moco) (Fig. 1-6A) (Johnson et al., 1991; Mendel, 2013; Mendel and Leimkuhler, 2015; Schwarz et al., 2009). All Mo-containing enzymes are dependent on Moco for their catalytic activity with the exception of nitrogenase. Bacteria and archaea, which do not require Mo for their viability, inturn depend on tungsten (W) for their growth (Mendel, 2013).

Moco biosynthesis follows an evolutionarily conserved complex multistep biosynthesis pathway, which can be summarized as follows: In eukaryotes, in the first step, GTP is

rearranged by MOCS1A and MOCS1B to form a cyclic pyranopterin monophosphate, followed by the formation of the metal-ligating dithiolene moiety, which is catalyzed by MOCS2A/B and MOCS3 (Mendel and Leimkuhler, 2015).

1.4.1 Terminal steps of Moco biosynthesis:

In mammals, the terminal two steps of the biosynthesis are carried out by the moonlighting protein gephyrin (Fig. 1-6). In the penultimate step, molybdopterin (MPT) is adenylated by the N-terminal G domain (which is homologous to the plant Cnx1G and bacterial MogA proteins) in a Mg-ATP dependent manner to form an adenylated molybdopterin (MPT-AMP) intermediate (Kuper et al., 2004; Kuper et al., 2003; Llamas et al., 2004; Llamas et al., 2006). In the terminal step, MPT-AMP is transferred to the C-terminal E domain (homologous to the plant Cnx1E and bacterial MoeA proteins), which catalyzes the metal incorporation and deadenylation of MPT-AMP resulting inactive Moco (Llamas et al., 2004) (Fig. 1-6B).

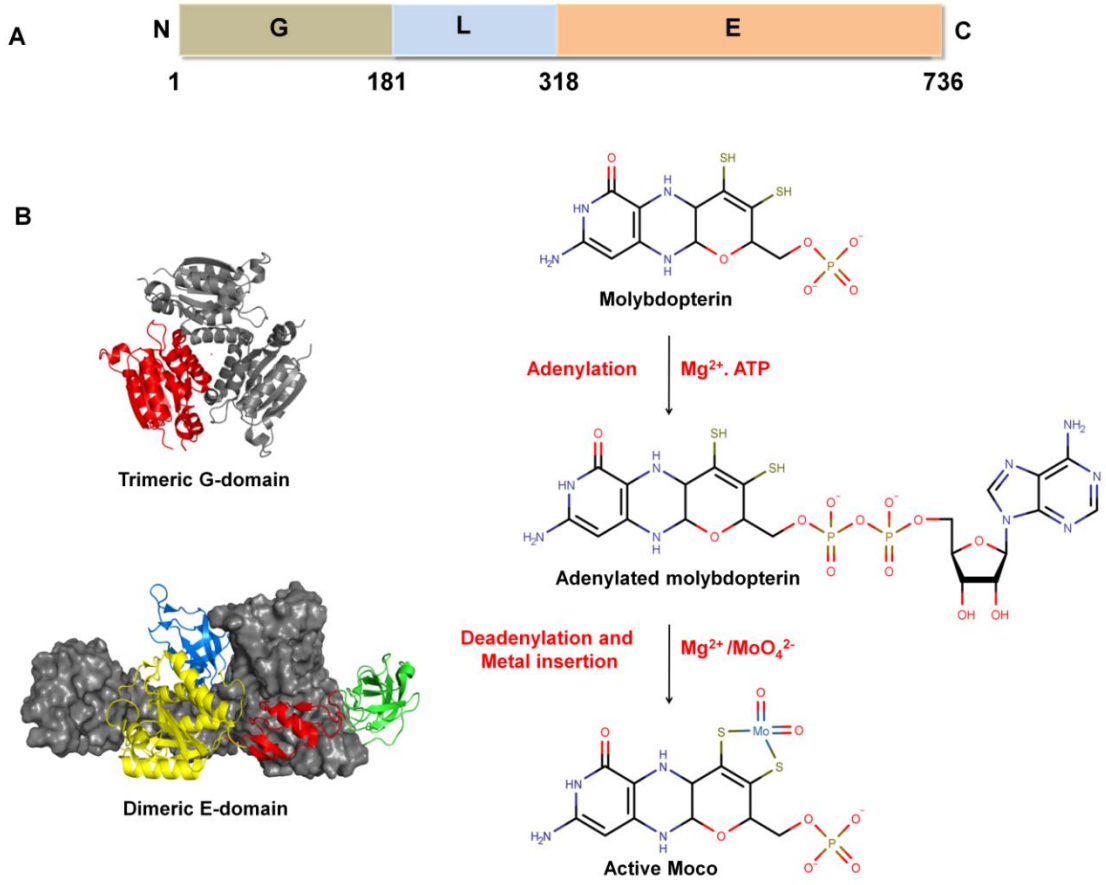

Figure 1-6: Schematic representation of the transformations during the terminal steps of Moco biosynthesis.

Prominent human enzymes, which are dependent on the Moco for their catalytic activity include sulfite oxidase, xanthine dehydrogenase and aldehyde oxidase, which carry out

critical cellular functions such as detoxification, purine catabolism and reactive oxygen species (ROS) production or, in plants, biosynthesis of the stress hormone abscisic acid. Mutations in the enzymes involved in this biosynthetic pathway result in a rare but severe autosomal recessive disease referred molybdenum cofactor deficiency (MocD) (Leimkuhler et al., 2005; Reiss and Hahnewald, 2011) which manifests itself in severe neurodevelopmental abnormalities and early childhood death. Most of the clinically reported mutations were mapped to the enzymes carrying out the initial steps of the biosynthesis. In the context of gephyrin, two mutations with clinical relevance have been reported so far which cause MocD. A frameshift mutation in the G domain, results in a stop codon already after 21 residues and results in the premature termination of the gephyrin protein (Reiss et al., 2001). The second mutation is a missense mutation in the E domain which results in the D580A substitution (Reiss et al., 2011). Both mutations completely abolish the biosynthesis, which is surprising for the D580A variant and suggests that an important residue has been eliminated, and consequently affect the functionality of the downstream proteins which are dependent on Moco, thus resulting in severe MocD.

1.5 Microtubules:

Microtubules are ubiquitously expressed cytoskeletal filaments, which play pivotal roles in crucial cellular processes such as cell division, cellular trafficking and maintenance of cell morphology. Structurally, these filaments consist of an ordered arrangement of a heterodimeric building block composed of an α and a β-tubulin subunit (Fig. 1-7A).

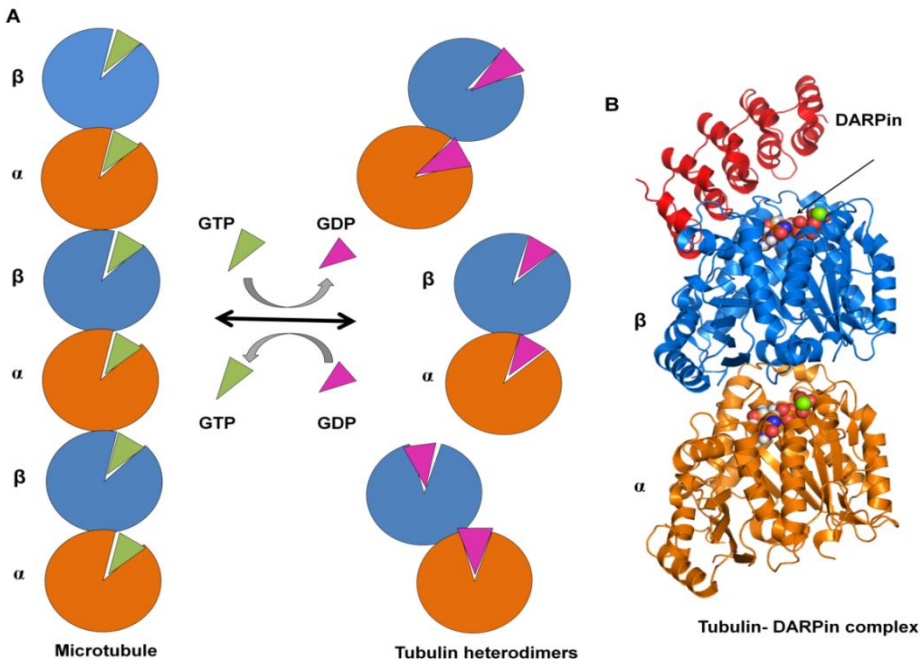

Figure 1-7. Structural dynamics of microtubules. (A) Schematic representation of the dynamic instability of microtubule depending on the presence of either GTP or GDP. GTP and GDP are shown as green

and magenta triangles. The α and β tubulins are colored in orange and blue, respectively. **(B)** Cartoon representation of the crystal structure of the tubulin α,β heterodimer in complex with DARPin. The bound GTP is shown in space filling representation and the DARPin subunit in red. The α and the β tubulin subunits are colored according to **(A).**

The dynamic instability of microtubules, i.e. the transformation of the heterodimers to the filaments and vice versa, (depending on whether GTP or GDP is bound to the tubulin) presents a major challenge to understand their structure by X-ray crystallography and most of the studies involving tubulin-filaments have been carried out by cryo-EM (Alushin et al., 2014; Zhang et al., 2015).

Recent advances in the understanding of tubulin-capping proteins such as the stathmin-like domain of RB3 (Dorleans et al., 2007; Ravelli et al., 2004) and designed ankyrin repeat protein (DARPin) (Pecqueur et al., 2012) made high resolution crystallographic studies possible (Fig. 1-7B). In the context of the inhibitory post synapses, microtubules play a crucial role as a known, high-affinity binding protein for gephyrin, which inturn anchors $GABA_A$Rs and GlyRs to the postsynaptic membrane at inhibitory postsynapses (Kirsch et al., 1991). Although gephyrin was identified initially as a tubulin-binding protein, the molecular details of the interactions remained elusive. Although the significance of the gephyrin-microtubule interaction remain unclear as the PSD has in fact a higher concentration of actin microfilaments compared to microtubules (Tyagarajan and Fritschy, 2014). The gephyrin-microtubule interaction studies were mainly carried out by the bioinformatics analysis (see chapter 6) and a detailed experimental dissection of the gephyrin-microtubule interaction was still missing.

1.6 Other gephyrin interacting proteins:

Multiple proteins regulate the functionality of gephyrin, thus contributing to the regulation of inhibitory postsynapse formation and maintenance (Fig 1-2). Gephyrin interacts for example with:Collybistin (CB), a Cdc42-specific guanine nucleotide exchange factor (GEF), Neuroligin, a cell adhesion protein (Reissner et al., 2008; Varoqueaux et al., 2006); and the cytoskeletal element F-actin. The interaction of gephyrin-actin is mainly mediated by the adaptor protein Mesa/VASP. In addition, actin binding protein Profilin also have shown to be binding to gephyrin (Giesemann et al., 2003). Gephyrin thus acts as the central organizer in maintaining the architecture of inhibitory postsynapses.

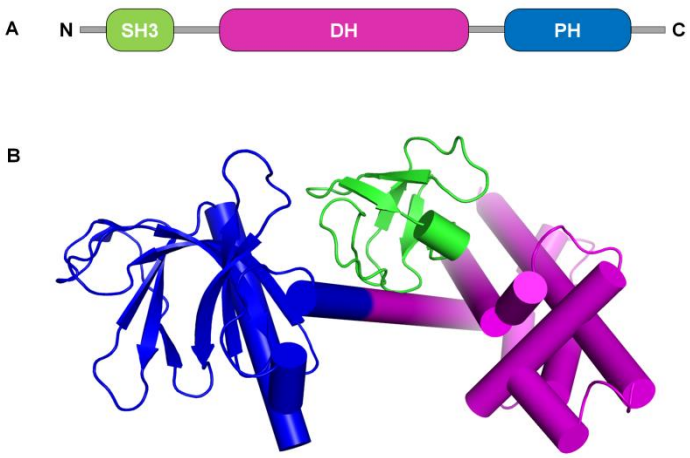

Figure 1-8.Structure of Collybistin in the closed conformation. (A) Schematic representation of the domain architecture of CB. **(B)** Cartoon representation of the crystal structure of CB in the closed conformation reveals the binding of its SH3 domain to the DH-PH domain tandem. This structure represents the auto-inhibited form of CB. Different domains are colored according to the scheme in **(A).**

Collybistin is a guanine nucleotide exchange factor (GEF) containing 3 functional domains (Fig. 1-8A). It consits of an N-terminal SH3 domain followed by a DH-PH domain tandem. Collybistin directly binds to the E domain, via abinding site which overlaps with that of the $GABA_A$Rs and GlyRs (Harvey et al., 2004; Tretter et al., 2011). Collybistin can adopt either a closed (inactive) state (Fig. 1-7B) or an open (active) conformation depending on the position of its SH3 domain. In its open conformation, it actively interacts with the cell adhesion molecule neuroligin and thus actively contributes to the formation of inhibitory postsynapses (Soykan et al., 2014).

Another protein playing a crucial role in the maintenance of synapses is the cell adhesion molecule Neuroligin, which interacts directly with Neurexin its trans-synaptic binding partner. Among four neuroligin isoforms, NL2 and NL4 are known to be selectively associated with the GABAergic and glycinergic synapses respectively. Interestingly, NL2 is the only cell adhesion molecule associated with the GABAergic synapse which is known to directly interact with gephyrin. Thus, all the described molecular interplays in and around gephyrin regulate the formation and maintenance of the inhibitory postsynaptic architecture.

1.7 AIMS AND OBJECTIVES

This dissertation work aims to biochemically and structurally characterize the two different cellular functions of moonlighting protein gephyrin. The first part of the thesis will cover the biochemical and structural characterization of the gephyrin-receptor interaction and second

part of the thesis mainly consists of the structural characterization of the terminal step during Moco biosynthesis.

The research objectives and specifically can be subdivided into the following aims, which will shed light on important questions regarding the structure and function of gephyrin:

1. **Characterization of gephyrin- $GABA_AR$ interaction.**

   What are the determinants of the gephyrin-$GABA_AR$ interaction? How does this interaction differ from the gephyrin-GlyR interaction? How is a receptor-specific interaction achieved by gephyrin, although both $GABA_AR$ and GlyR rely on a common binding site for the interaction with gephyrin? (See chapters 2, 3 and 4 for more details.)

2. **Structural studies on the terminal step of Moco biosynthesis.**

   How exactly purine bases are selected over pyrimidine bases and why is adenine preferred over guanine? Where are the binding sites for the metal and the nucleotide? What are the determining factors for the metal insertion mechanism? What determines the molecular basis for MocD? (See chapter 5 for more details.)

3. **Characterization of the gephyrin-microtubule interaction.**

   What is the molecular basis of the gephyrin-microtubule interaction? Where in gephyrin is the binding site for microtubules located? (See chapter 6 for more details.)

4. **Structural studies on gephyrin orthologs.**

   To shed light into the structure of full-length gephyrin or full-length gephyrin homologs. How exactly is the dimerization of the C-terminal E domain inhibited in the context of the full-length protein? Do interdomain interactions exist in the context of full-length gephyrin or gephyrin-like proteins and what are the participating residues? (See chapter 7 for more details.)

2. Modulation of Gephyrin-Glycine Receptor Affinity by Multivalency*

This chapter is based on the following publication:

Maric, H.M., Kasaragod, V.B., and Schindelin, H. (2014). Modulation of gephyrin-glycine receptor affinity by multivalency. *ACS Chem. Biol*. **9**, 2554-2562.

***Changes incorporated :** Supplemental information has been merged with the main text.

Statement of individual author contributions and of legal second publication rights

Participated in	**Author Initials,** Responsibility decreasing from left to right				
Study Design Methods Development	HMM HMM	VBK, HS VBK, HS			
Data Collection	HMM, VBK				
Data Analysis and Interpretation	HMM, VBK	HS			
Manuscript Writing Writing of Introduction Writing of Materials & Methods Writing of Discussion Writing of First Draft	 HMM, HMM, VBK HMM HMM	 VBK, HS HS VBK, HS VBK, HS			

Statement of individual author contributions to figures/tables/chapters included in the manuscripts

Figure	**Author Initials,** Responsibility decreasing from left to right				
1	VBK, HMM	HS			
2	HMM	VBK, HS			
3	VBK, HMM	HS			
4	HMM	VBK, HS			
5	HMM	VBK, HS			
6	HMM	VBK, HS			

2.Modulation of Gephyrin-Glycine Receptor Affinity by Multivalency

Hans Michael Maric, Vikram Babu Kasaragod, and Hermann Schindelin*

Department Institute of Structural Biology, Rudolf Virchow Center for Experimental Biomedicine, University of Würzburg, Josef-Schneider-Str. 2, 97080 Würzburg, Germany.

*Corresponding author: Hermann Schindelin (e-mail: hermann.schindelin@virchow.uni-wuerzburg.de)

TITLE RUNNING HEAD: Multivalency of the Gephyrin-Receptor Interaction

Current address of Maric, H.M.: Department of Drug Design and Pharmacology, University of Copenhagen, Universitetsparken 2, DK-2100 Copenhagen, Denmark

2.1ABSTRACT

Gephyrin is a major determinant for the accumulation and anchoring of glycine receptors (GlyRs) and the majority of γ-aminobutyric acid type A receptors ($GABA_ARs$) at postsynaptic sites. Here we explored the interaction of gephyrin with a dimeric form of a GlyR β-subunit receptor-derived peptide. A 2 Å crystal structure of the C-terminal domain of gephyrin (GephE) in complex with a 15-residue peptide derived from the GlyR β-subunit defined the core binding site which we targeted with the dimeric peptide. Biophysical analyses via differential scanning calorimetry (DSC), thermofluor and isothermal titration calorimetry (ITC) demonstrated that this dimeric ligandis capable of binding simultaneously to two receptor binding sites and that this multivalency results in a 25-fold enhanced affinity. Our study therefore suggests that the oligomeric state of gephyrin and the number of gephyrin-binding subunits in the pentameric $GABA_ARs$ and GlyRs together control postsynaptic receptor clustering.

2.2 INTRODUCTION

The scaffold protein gephyrin is a central player at inhibitory synapses (Fritschy and Panzanelli, 2014; Tyagarajan and Fritschy, 2014), mediating postsynaptic receptor localization and accumulation via direct interactions with γ-aminobutyric acid type A and glycine receptors ($GABA_AR$ and GlyR, respectively), a process that is crucial for synapse function and plasticity. Gephyrin is composed of an N-terminal domain (GephG) and a C-terminal domain (GephE) connected by an unstructured linker. Our crystal structure of GephE in complex with a 49 residue peptide derived from the large cytoplasmic loop of the GlyR β subunit defined this interaction in atomic detail (Kim et al., 2006), while our recent studies (Maric et al., 2011) demonstrated that this binding site universally mediates the interactions with the $GABA_AR$ α1-3 (Maric et al., 2011; Mukherjee et al., 2011b; Tretter et al., 2008) and possibly also the $GABA_AR$ β2-3 (Kowalczyk et al., 2013) subunits. Interestingly, the large majority of synaptic $GABA_ARs$ and GlyRs do contain more than a single gephyrin-binding subunit. At the same time, structural studies revealed GephG to trimerize and GephE to dimerized (Schwarz et al., 2001; Sola et al., 2004; Sola et al., 2001), while the full-length protein predominantly forms trimers in solution (Herweg and Schwarz, 2012; Sander et al., 2013; Schrader et al., 2004). The trimerization of full-length gephyrin is thought to come at the expense of the GephE dimer interface (Herweg and Schwarz, 2012; Sander et al., 2013; Schrader et al., 2004).

Initially, gephyrin was proposed to form a hexagonal lattice beneath the postsynaptic membrane (Kneussel and Betz, 2000), however,a recent electron tomographic analysis of GABAergic synapses (Linsalata et al., 2014) instead revealed a rather loose assembly of

gephyrin oligomers ranging from dimers to dodecamers that contribute to the inhibitory postsynaptic density. Furthermore, high-resolution microscopy (Specht et al., 2013) revealed different states of $GABA_AR$ and GlyR saturation of the gephyrin scaffold and thereby established gephyrin as a dynamic platform for competing receptors. While initially a 1:1 stoichiometry between pentameric receptor complexes and gephyrin (Kirsch et al., 1991) was proposed, the presence of two gephyrin-binding subunits within the $GABA_AR$ (Kowalczyk et al., 2013; Maric et al., 2011; Mukherjee et al., 2011b; Olsen and Sieghart, 2008; Tretter et al., 2008) and three (Yang et al., 2012) gephyrin binding β-subunits within the GlyR (Meyer et al., 1995) suggested that the receptors sites simultaneously interact with the gephyrin scaffold at more than one binding site, either within the same gephyrin trimer (Fritschy et al., 2008) or by crosslinking adjacent trimers (Herweg and Schwarz, 2012; Sola et al., 2004). Such a process would be driven by an enhanced affinity, which should be directly measureable.

Until now biophysical and biochemical studies of the gephyrin receptor subtype interactions (Herweg and Schwarz, 2012; Kim et al., 2006; Kowalczyk et al., 2013; Maric et al., 2011; Meyer et al., 1995; Mukherjee et al., 2011b; Schrader et al., 2004; Sola et al., 2004; Specht et al., 2011) involved monovalent receptor subunit fragments and recombinant forms of gephyrin. These binary systems disregard the possibility of enhanced affinity due to plurivalent interactions mediated by the complex assembly of the receptor subunits and the multimeric nature of gephyrin. To address this limitation we generated a dimeric gephyrin-binding GlyR fragment and explored its interaction with either dimeric GephE or trimeric full-length gephyrin (FL-Geph).

2.3 RESULTS AND DISCUSSION

2.3.1 A 14 residue GlyR fragment mediates almost all of the GlyR-gephyrin binding affinity. Using a 49-residue receptor fragment (GlyR β 378-425, here referred to as β49), the GlyR-gephyrin interaction was extensively analyzed with different biophysical methods. Based on a biphasic binding behavior in isothermal titration calorimetry (ITC) experiments, two binding sites were proposed with K_d values in the nanomolar and low micromolar range (Herweg and Schwarz, 2012; Kim et al., 2006; Meyer et al., 1995; Schrader et al., 2004; Sola et al., 2004; Specht et al., 2011). To resolve the apparent discrepancy of the single binding site observed in the crystal structure and the repeatedly suggested two binding site, we studied in detail two truncated GlyR fragments:i) β14 (GlyR residues Phe398-Ser411) which encompasses the 13 GlyR residues (GlyR residues Phe398-Leu410) visible in the electron density maps of the GephE-β49 crystal structure (Kim et al., 2006; PDB: 2FTS), plus an additional serine as well as an intermediate-length fragment (β19) that contains

additional C-terminal residues (GlyR residues Phe398-Tyr416). ITC experiments revealed that all three peptides (β14, β19 and β49) can be fitted with a model assuming a single binding site, and that peptide truncation, especially when β49 and β19 are compared, is accompanied by a significant loss in the enthalpic contribution to the free energy, which is offset by a more favorable entropic contribution (Figure 2-1a). However, fitting of the isotherms revealed comparably low micromolar affinities for all three GlyR fragments (Figure 2-1a).

2.3.2 A 15 residue GlyR fragment is sufficient to occupy the core of gephyrin's receptor binding site. Based on the thermodynamic analysis we concluded that gephyrin binding is mediated by a single site within the β14 peptide. To verify this and to understand the differences in the enthalpic contributions on the molecular level we determined the crystal structure of GephE in complex with β15 (GlyR residues Asp397-Ser411) (PDB: 4PD1), which encompasses β14 from the ITC studies together with an additional Asp at the N-terminus.

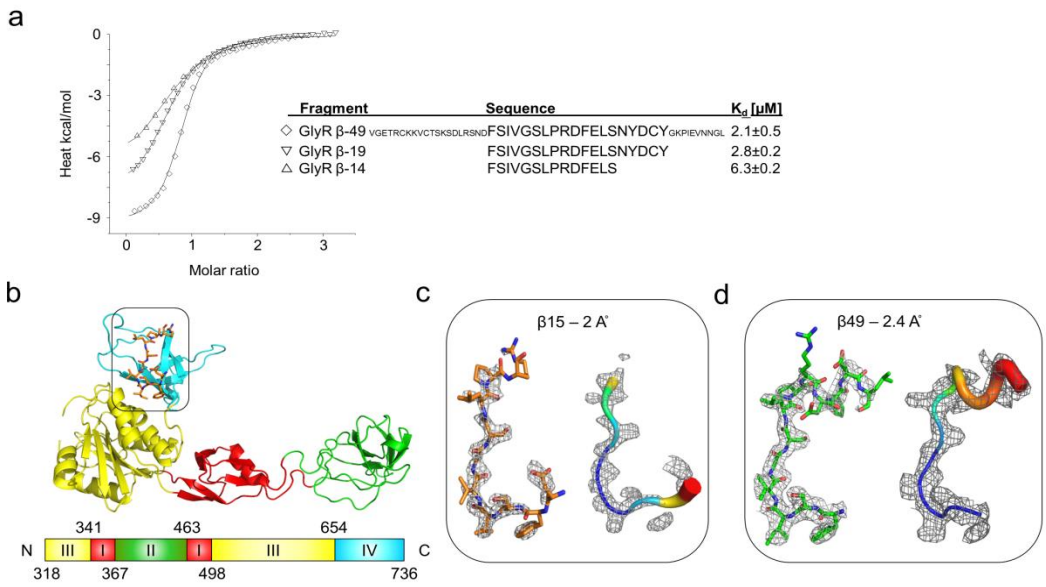

Figure 2-1. GlyRs mediate gephyrin binding via a single core region. (Fig.1 in the published manuscript). (a) ITC reveals very similar GephE affinities for GlyR β-derived peptides of different lengths. Measured binding enthalpies are plotted as a function of the molar ratio of ligand to gephyrin and reveal a loss of binding enthalpy upon peptide truncation. Sequence alignment of the β49, β19 and β14 peptides together with their dissociation constants calculated with a one-site binding model. **(b)** Ribbon diagram of GephE shown in the same color code as the GephE subdomain architecture (below). The bound β15-fragment is displayed as a stick model. **(c)** Electron density (F_o-F_c omit map contoured at a root mean square deviation (rmsd) of 3 and the assigned stick model (left) as well as the B-factor representation (right) of the GephE-β15 complex (PDB: 4PD1). **(d)** Electron density ($2F_o$-F_c map contoured at 1σ (PDB: 2FTS)) and the assigned stick model (left) and the corresponding B-factor representation (right) of the GephE-β49 complex. Note that the GephE-β15 complex lacks several C-terminal residues, while the GephE-β49 complex lacks one N-terminal

residue (Asp397). Arg406 adopts different conformations, while the core sequence (Phe398-Pro405) displays a highly similar and tight binding.

In this process we also improved theoriginal GephE apo-structure from 2.7 to 1.7 Å resolution (PDB: 4PD0). The 2 Å GephE-β15 crystal structure confirmed that β15 occupies the same binding site as β49 (Figure2-1b), which has also been implicated in $GABA_AR$ binding (Maric et al., 2011). However, there are also important differences: Asp397, the N-terminal residue of β15, could be assigned, albeit weakly, in the electron density of the GephE-β15 complex (Figure 2-1c), while there was no density for this residue in the GephE-β49 structure (Figure 2-1d, Kim et al., 2006; PDB: 2FTS). Furthermore, Arg406 adopts different conformations in both crystal structures, although the side chain remains poorly resolved in both structures (Figure 2-1c,d). Finally, GlyR β residues Asp407-Ser411, which form a flexible α-helix in the GephE-β49 complex, are disordered in the GephE-β15 complex (Figure 2-1c,d). Notably, the stretch of residues encompassing Phe398 to Pro405 are highly similar in both structures and can be superimposed with an rmsd of 0.29 Å for Cα atoms (1.0 Å for all atoms).

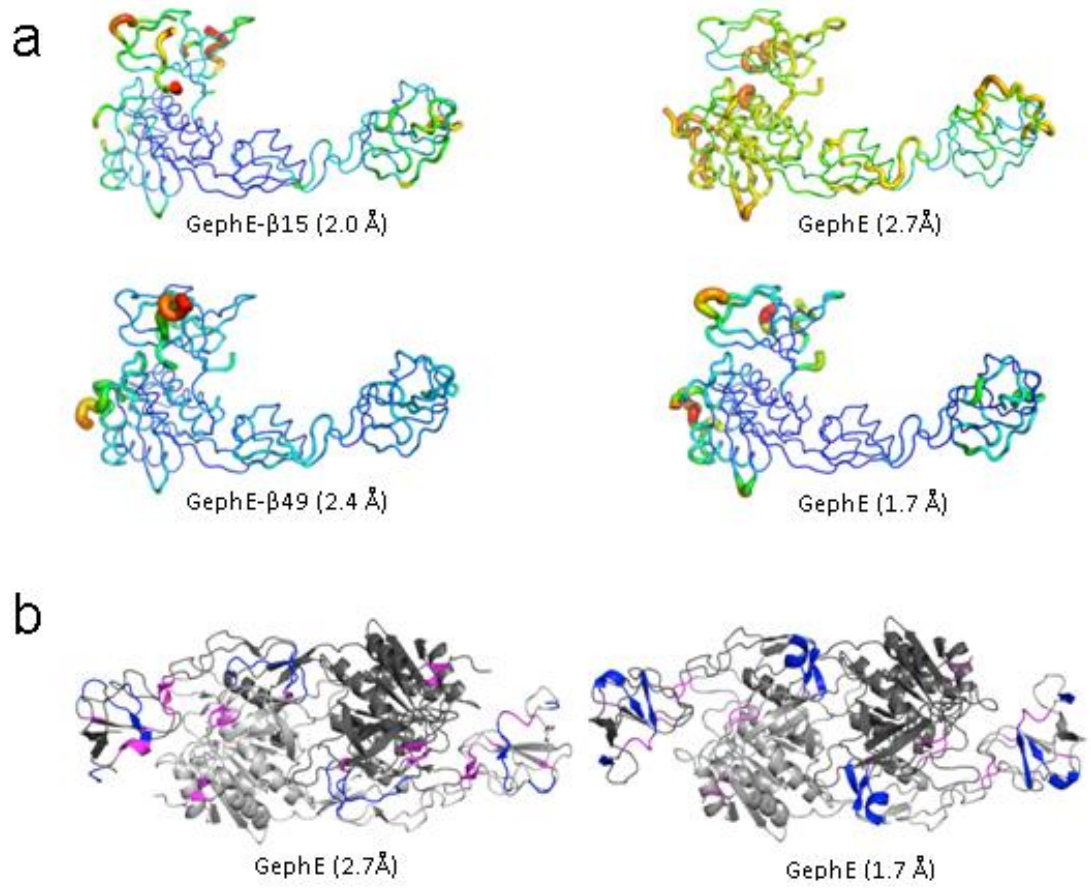

Figure 2-2 . Overview of crystal structures of GephE alone or in complex with GlyR-derived peptides. (Supplemental Fig.1 in the published manuscript). (a) B-factor

representation (red and blue colors represent high and low B-factors, respectively) of the earlier published (Kim et al., 2006) GephE structure refined at 2.7Å (PDB: 2FU3), the apo-GephE structure refined at 1.7Å and presented in this work (PDB: 4PD0) together with the earlier published GephE-β49 complex (Kim et al., 2006) (PDB: 2FTS) and the GephE-β15 complex(PDB: 4PD1) presented here. **(b)** Cartoon model of the old 2.7 Å (Kim et al., 2006) (PDB: 2FU3) and new 1.7 Å GephE structures (PDB: 4PD0). The improved data quality allowed for the reassignment of secondary structure elements. New features are marked in blue, while secondary structure elements, which are no longer present, have been marked in magenta.

Table 2-1. Data collection and refinement statistics

	Apo GephE	**GephE-β15**
Wavelength (Å)	0.9198	0.9184
Space group	I222	I222
Unit cell Parameters		
a, b, c (Å)	87.65, 100.00, 113.7	85.66, 100.10, 117.50
Resolution limit (Å)	43.83-1.7	36.47- 2.0
R_{sym}[a]	0.105 (1.717)	0.111 (1.134)
R_{pim}[b]	0.044 (0.698)	0.043 (0.462)
$CC_{1/2}$	0.999 (0.678)	0.999 (0.729)
Redundancy	13.0 (13.6)	14.7(13.5)
Unique reflections	55179	35783
Completeness	1.0 (1.0)	1.0 (1.0)
$\langle I/\sigma I \rangle$[c]	15.0 (1.9)	17.7(2.4)
R[d] /R_{free}[e]	0.160 /0.184	0.158 /0.196
Deviations from ideal values in		
Bond distances (Å)	0.011	0.011
Bond angles (°)	1.322	1.300
Torsion angles (°)	12.626	13.708
Planar groups (Å)	0.007	0.007
Chirality centers (Å^3)	0.080	0.080
Ramachandran statistics (Preferred/Allowed/Outliers)	97.54/1.48/0.98	97.99/1.76/1.25
Overall average B factor (Å^2)	37.6	45.6
Coordinate error (Å)	0.16	0.17

[a]$R_{sym} = \Sigma_{hkl}\Sigma_i | I_i - \langle I \rangle | / \Sigma_{hkl}\Sigma_i I_i$ where I_i is the i^{th} measurement and $\langle I \rangle$ is the weighted mean of all measurements of I.

[b]$R_{pim} = \Sigma_{hkl} 1/(N-1)^{1/2} \Sigma_i | I_i(hkl) - \overline{I(hkl)} | / \Sigma_{hkl}\Sigma_i I(hkl)$, where N is the redundancy of the data and $\overline{I(hkl)}$ the average intensity.

[c]$\langle I/\sigma I \rangle$ indicates the average of the intensity divided by its standard deviation.

[d]$R = \Sigma_{hkl} ||F_o| - |F_c|| / \Sigma_{hkl}|F_o|$ where F_o and F_c are the observed and calculated structure factor amplitudes.

[e]R_{free}same as R for 5% of the data randomly omitted from the refinement. The number of reflections includes the R_{free} subset.

[f]Ramachandran statistics were calculated with MolProbity in PHENIX.

[g]The coordinate errors were calculated based on maximum likelihood.

Moreover, their B-factors indicate that they are highly ordered (Figure 2-1c,d) and, together with earlier mutational studies (Kim et al., 2006; Maric et al., 2011; Specht et al., 2011), this suggests a major contribution of these residues to the overall binding affinity in both structures. Taken together our combined structural and thermodynamic studies demonstrate that the elongated β49 and truncated β15 peptides both target only a single binding site within gephyrin. Truncation to 15 residues results in the loss of interaction surface between gephyrin and residues Asp407-Ser411 as reflected in a less favorable binding enthalpy, but this does not interfere with the tight binding of the core binding site (Phe398 to Pro405) due to a corresponding decrease in the entropic penalty.

2.3.3 Structure of apo-GephE and in complex with residues 397-410 of the GlyR β-subunit. The E domain of rat gephyrin (residues 318-736) in the absence of a receptor-derived peptide was crystallized in the orthorhombic space group I222. In contrast to the published E domain structure (PDB: 2FU3), which crystallized in space group $P2_12_12$ with one E domain dimer per asymmetric unit, the new apo-structure contains one monomer per asymmetric unit. It was refined at a resolution of 1.7 Å, thus significantly enhancing model quality compared to the earlier apo-structure at 2.7 Å (Fig 2-2a-b). As described earlier, the E domain can be divided into four subdomains (I-IV), and the new structure shows a close similarity with the structure previously published (Kim et al.,PDB: 2FU3) as reflected by an rmsd of 1.87 Å for the Cα atoms of all residues. Omitting subdomain II, which can adopt various positions relative to the remainder of the structure, reduces the rmsd to 0.82 Å. Because of the improved resolution, additional secondary structure elements could be defined (Fig 2-2b). Notably, residues 352-355 and 474-477 were found to form two β strands, although the rmsd between subdomains I where these elements are located is only 0.31 Å (Fig 2-2b, marked in blue). In addition, a short α-helix is formed by amino acids 699-704 (Fig 2-2b, marked in blue), which belongs to subdomain IV. This domain displays the highest rmsd of 2.89 Å compared to the 2.7 Å structure, however, the rmsd for subdomain IV reduces to 0.58 Å after omitting residues 693-703, which form a flexible loop in the 2.7 Å structure in contrast to a short α-helix and a few disordered residues in the new apo-structure (Fig 2-2a,b).

The structure of the GephE-β15 complex (residues 397-410 of the GlyR β-subunit) crystallized in the same I-centered orthorhombic space group (I222) as the apo-structure with closely related unit cell dimensions. In contrast, the previously published structure of GephE in complex with a GlyR-derived peptide crystallized in space group $C222_1$. The individual subdomains differ to some degree between the β-short complex and the new apo-structure as reflected by rmsd values of 0.15 Å, 0.21 Å, 0.34 Å and 0.57 Å for subdomains I, II, III and IV, respectively. Taking into account coordinate errors of 0.16 Å and 0.17 Å for the apo-structure and the β short complex the structural differences in subdomains III and, in particular, subdomain IV where the binding site is primarily located seem significant and most likely are a consequence of peptide binding.

2.3.4 Dimerization of receptor-derived peptides.The C-terminal ends of the receptor fragments within the GephE homodimer are roughly 16 Å apart from each other (Figure 2-3a). Using sulfhydryl-specific PEG crosslinkers we dimerized the 19-residue peptide in solution via a naturally occurring cysteine residue (Figure 2-3 a,b), the penultimate C-terminal residue. The quantitative dimerization was monitored in a calorimeter to allow for real-time control of the temperature, stirring speed, incubation time and stoichiometry of the reaction (Figure 2-3c). Upon titration of the sulfhydryl-reactive crosslinker into the cysteine-containing peptide, a stoichiometric conversion to the bivalent peptide was indicated by an abolishment of the heat signature (Figure 2-3c).

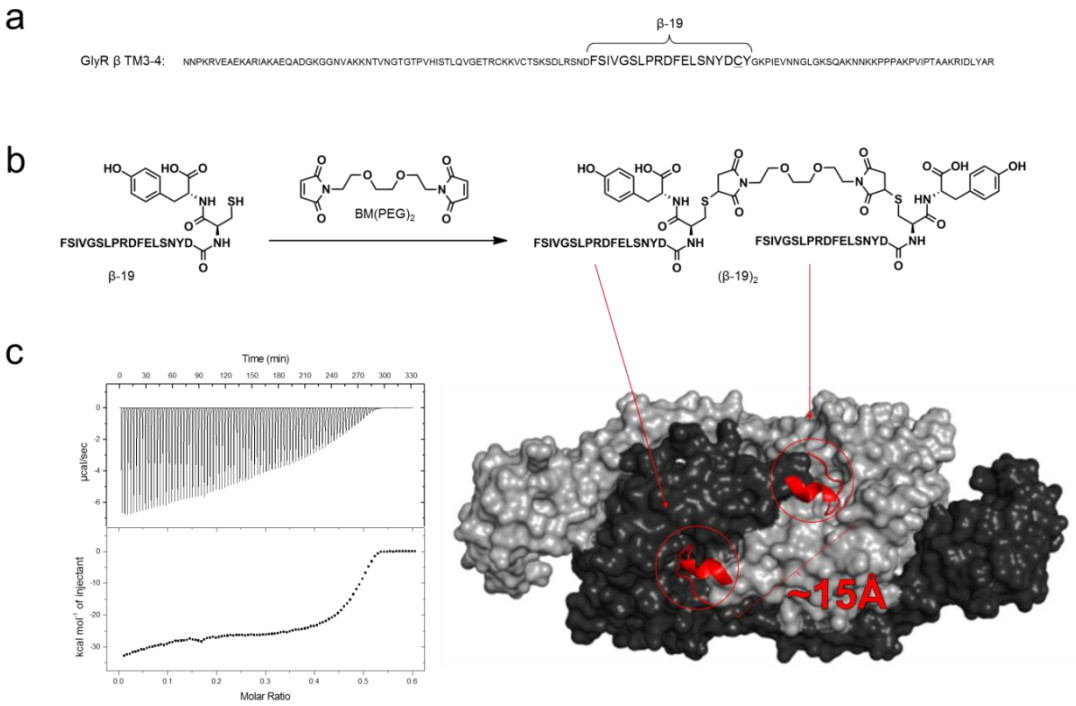

Figure 2-3. (Fig.2 in the published manuscript). Design and synthesis of a receptor-derived, gephyrin-targeting bivalent peptide.(a) Sequence of the intracellular loop of the GlyR β

subunit. Residues used for subsequent bivalent peptides (larger letters) and the naturally occurring cysteine (underlined) used for dimerization are indicated. **(b)** Maleimide-based dimerization of peptides. The maleimide groups within the crosslinkers react in a thiol-specific Michael addition to form succinimide-linked dimers. Schematic representation of the GephE-GlyR β-loop complex crystal structure viewed along the twofold axis of symmetry. The GephE dimer is shown in surface representation with the monomers either in light or dark gray, respectively. The β-loops are shown in cartoon representation in red. **(c)** Heat signature of the stoichiometric one-step peptide dimerization. Note that the endpoint of the conversion is at a 0.5 molar excess of the bivalent crosslinker over the peptide.

Table 2-2. Crystallization conditions for apo-GephE and the GephE-β15 complex.

Location	Salt [M]	Salt	[Buffer] [M]	Buffer	Precipitant [%]	Precipitant
A1	-	-	0.1	Citric acid pH 3.5	24	2-Methyl-2,4-pentanediol
A2	0.3	Sodium chloride	0.1	Citric acid pH 3.5	26	2-Methyl-2,4-pentanediol
A3	-	-	0.1	Citric acid pH 3.5	28	2-Methyl-2,4-pentanediol
A4	0.3	Sodium chloride	0.1	Citric acid pH 3.5	30	2-Methyl-2,4-pentanediol
A5	-	-	0.1	Citric acid pH 3.5	32	2-Methyl-2,4-pentanediol
A6	0.3	Sodium chloride	0.1	Citric acid pH 3.5	34	2-Methyl-2,4-pentanediol
A7	-	-	0.1	Sodium citrate pH 4.5	24	2-Methyl-2,4-pentanediol
A8	0.3	Sodium chloride	0.1	Sodium citrate pH 4.5	26	2-Methyl-2,4-pentanediol
A9	-	-	0.1	Sodium citrate pH 4.5	28	2-Methyl-2,4-pentanediol
A10	0.3	Sodium chloride	0.1	Sodium citrate pH 4.5	30	2-Methyl-2,4-pentanediol
A11	-	-	0.1	Sodium citrate pH 4.5	32	2-Methyl-2,4-pentanediol
A12	0.3	Sodium chloride	0.1	Sodium citrate pH 4.5	34	2-Methyl-2,4-pentanediol
B1	-	-	0.1	Sodium citrate pH 5	24	2-Methyl-2,4-pentanediol
B2	0.3	Sodium chloride	0.1	Sodium citrate pH 5	26	2-Methyl-2,4-pentanediol
B3	-	-	0.1	Sodium citrate pH 5	28	2-Methyl-2,4-pentanediol
B4	0.3	Sodium chloride	0.1	Sodium citrate pH 5	30	2-Methyl-2,4-pentanediol
B5	-	-	0.1	Sodium citrate pH 5	32	2-Methyl-2,4-pentanediol
B6	0.3	Sodium chloride	0.1	Sodium citrate pH 5	34	2-Methyl-2,4-pentanediol
B7	-	-	0.1	Sodium citrate pH 5.5	24	2-Methyl-2,4-pentanediol
B8	0.3	Sodium chloride	0.1	Sodium citrate pH 5.5	26	2-Methyl-2,4-pentanediol
B9	-	-	0.1	Sodium citrate pH 5.5	28	2-Methyl-2,4-pentanediol
B10	0.3	Sodium chloride	0.1	Sodium citrate pH 5.5	30	2-Methyl-2,4-pentanediol
B11	-	-	0.1	Sodium citrate pH 5.5	32	2-Methyl-2,4-pentanediol
B12	0.3	Sodium chloride	0.1	Sodium citrate pH 5.5	34	2-Methyl-2,4-pentanediol
C1	-	-	0.1	Sodium citrate pH 6	24	2-Methyl-2,4-pentanediol
C2	0.3	Sodium chloride	0.1	Sodium citrate pH 6	26	2-Methyl-2,4-pentanediol
C3	-	-	0.1	Sodium citrate pH 6	28	2-Methyl-2,4-pentanediol
C4	0.3	Sodium chloride	0.1	Sodium citrate pH 6	30	2-Methyl-2,4-pentanediol
C5	-	-	0.1	Sodium citrate pH 6	32	2-Methyl-2,4-pentanediol
C6	0.3	Sodium chloride	0.1	Sodium citrate pH 6	34	2-Methyl-2,4-pentanediol
C7	-	-	0.1	Sodium acetate pH 4	24	2-Methyl-2,4-pentanediol
C8	0.3	Sodium chloride	0.1	Sodium acetate pH 4	26	2-Methyl-2,4-pentanediol
C9	-	-	0.1	Sodium acetate pH 4	28	2-Methyl-2,4-pentanediol
C10	0.3	Sodium chloride	0.1	Sodium acetate pH 4	30	2-Methyl-2,4-pentanediol
C11	-	-	0.1	Sodium acetate pH 4	32	2-Methyl-2,4-pentanediol
C12	0.3	Sodium chloride	0.1	Sodium acetate pH 4	34	2-Methyl-2,4-pentanediol
D1	-	-	0.1	Sodium acetate pH 4.5	24	2-Methyl-2,4-pentanediol
D2	0.3	Sodium chloride	0.1	Sodium acetate pH 4.5	26	2-Methyl-2,4-pentanediol
D3	-	-	0.1	Sodium acetate pH 4.5	28	2-Methyl-2,4-pentanediol
D4	0.3	Sodium chloride	0.1	Sodium acetate pH 4.5	30	2-Methyl-2,4-pentanediol
D5	-	-	0.1	Sodium acetate pH 4.5	32	2-Methyl-2,4-pentanediol

D6	0.3	Sodium chloride	0.1	Sodium acetate pH 4.5	34	2-Methyl-2,4-pentanediol
D7	-	-	0.1	Sodium acetate pH 5	24	2-Methyl-2,4-pentanediol
D8	0.3	Sodium chloride	0.1	Sodium acetate pH 5	26	2-Methyl-2,4-pentanediol
D9	-	-	0.1	Sodium acetate pH 5	28	2-Methyl-2,4-pentanediol
D10	0.3	Sodium chloride	0.1	Sodium acetate pH 5	30	2-Methyl-2,4-pentanediol
D11	-	-	0.1	Sodium acetate pH 5	32	2-Methyl-2,4-pentanediol
D12	0.3	Sodium chloride	0.1	Sodium acetate pH 5	34	2-Methyl-2,4-pentanediol
E1	-	-	0.1	Sodium acetate pH 5.5	24	2-Methyl-2,4-pentanediol
E2	0.3	Sodium chloride	0.1	Sodium acetate pH 5.5	26	2-Methyl-2,4-pentanediol
E3	-	-	0.1	Sodium acetate pH 5.5	28	2-Methyl-2,4-pentanediol
E4	0.3	Sodium chloride	0.1	Sodium acetate pH 5.5	30	2-Methyl-2,4-pentanediol
E5	-	-	0.1	Sodium acetate pH 5.5	32	2-Methyl-2,4-pentanediol
E6	0.3	Sodium chloride	0.1	Sodium acetate pH 5.5	34	2-Methyl-2,4-pentanediol
E7	-	-	0.1	Sodium succinate pH 5.5	24	2-Methyl-2,4-pentanediol
E8	0.3	Sodium chloride	0.1	Sodium succinate pH 5.5	26	2-Methyl-2,4-pentanediol
E9	-	-	0.1	Sodium succinate pH 5.5	28	2-Methyl-2,4-pentanediol
E10	0.3	Sodium chloride	0.1	Sodium succinate pH 5.5	30	2-Methyl-2,4-pentanediol
E11	-	-	0.1	Sodium succinate pH 5.5	32	2-Methyl-2,4-pentanediol
E12	0.3	Sodium chloride	0.1	Sodium succinate pH 5.5	34	2-Methyl-2,4-pentanediol
F1	0.3	Calcium chloride	0.1	Sodium citrate pH 4.5	24	2-Methyl-2,4-pentanediol
F2	-	-	0.1	Sodium citrate pH 4.5	26	2-Methyl-2,4-pentanediol
F3	0.3	Calcium chloride	0.1	Sodium citrate pH 4.5	28	2-Methyl-2,4-pentanediol
F4	-	-	0.1	Sodium citrate pH 4.5	30	2-Methyl-2,4-pentanediol
F5	0.3	Calcium chloride	0.1	Sodium citrate pH 4.5	32	2-Methyl-2,4-pentanediol
F6	-	-	0.1	Sodium citrate pH 4.5	34	2-Methyl-2,4-pentanediol
F7	0.3	Calcium chloride	0.1	Sodium acetate pH 4.5	24	2-Methyl-2,4-pentanediol
F8	-	-	0.1	Sodium acetate pH 4.5	26	2-Methyl-2,4-pentanediol
F9	0.3	Calcium chloride	0.1	Sodium acetate pH 4.5	28	2-Methyl-2,4-pentanediol
F10	-	-	0.1	Sodium acetate pH 4.5	30	2-Methyl-2,4-pentanediol
F11	0.3	Calcium chloride	0.1	Sodium acetate pH 4.5	32	2-Methyl-2,4-pentanediol
F12	-	-	0.1	Sodium acetate pH 4.5	34	2-Methyl-2,4-pentanediol
G1	0.3	Sodium chloride	0.1	Sodium acetate pH 4.5	24	PEG 400
G2	-	-	0.1	Sodium acetate pH 4.5	26	PEG 400
G3	0.3	Sodium chloride	0.1	Sodium acetate pH 4.5	28	PEG 400
G4	-	-	0.1	Sodium acetate pH 4.5	30	PEG 400
G5	0.3	Sodium chloride	0.1	Sodium acetate pH 4.5	32	PEG 400
G6	-	-	0.1	Sodium acetate pH 4.5	34	PEG 400
G7	0.3	Magnesium chloride	0.1	Sodium acetate pH 4.5	24	PEG 400
G8	-	-	0.1	Sodium acetate pH 4.5	26	PEG 400
G9	0.3	Magnesium chloride	0.1	Sodium acetate pH 4.5	28	PEG 400
G10	-	-	0.1	Sodium acetate pH 4.5	30	PEG 400
G11	0.3	Magnesium chloride	0.1	Sodium acetate pH 4.5	32	PEG 400
G12	-	-	0.1	Sodium acetate pH 4.5	34	PEG 400
H1	0.02	cobalt (II) chloride hexahydrate	0.1	Sodium acetate pH 4.5	0.7	1,6-Hexanediol
H2	-	-	0.1	Sodium acetate pH 4.5	0.75	1,6-Hexanediol
H3	0.02	cobalt (II) chloride hexahydrate	0.1	Sodium acetate pH 4.5	0.8	1,6-Hexanediol
H4	-	-	0.1	Sodium acetate pH 4.5	0.85	1,6-Hexanediol
H5	0.02	cobalt (II) chloride hexahydrate	0.1	Sodium acetate pH 4.5	0.9	1,6-Hexanediol
H6	-	-	0.1	Sodium acetate pH 4.5	0.95	1,6-Hexanediol
H7	0.02	cobalt (II) chloride hexahydrate	0.1	Sodium acetate pH 4.5	1	1,6-Hexanediol
H8	-	-	0.1	Sodium acetate pH 4.5	1.05	1,6-Hexanediol
H9	0.02	cobalt (II) chloride hexahydrate	0.1	Sodium acetate pH 4.5	1.1	1,6-Hexanediol
H10	-	-	0.1	Sodium acetate pH 4.5	1.15	1,6-Hexanediol
H11	0.02	cobalt (II) chloride hexahydrate	0.1	Sodium acetate pH 4.5	1.2	1,6-Hexanediol
H12	-	-	0.1	Sodium acetate pH 4.5	1.25	1,6-Hexanediol

2.3.5 E domain stabilization by the bivalent peptide. To test whether binding of the bivalent ligand by trimeric full-length gephyrin (FL-Geph) results in larger structural rearrangements and to control for GephE specificity, we analyzed its thermal denaturation in the presence and absence of a 1:1 molar ratio of monovalent and bivalent ligands using differential scanning calorimetry (DSC). DSC determined the melting temperature of GephE as 62.5 °C and GephG as 78.9 °C. In line with a GephE-specific binding, ligand-binding stabilized the E domain by 0.6 °C (β14), 1.1 °C (β19) and 2.0 °C $(β19)_2$ (Figure 2-4a-d). The increased stabilizing effect of the bivalent peptide compared to the monovalent peptides indicated a stronger affinity of GephE for the bivalent peptide. In contrast, GephG showed a destabilization (by 0.9 °C (β14), 0.8 °C (β19) and 1.0 °C $(β19)_2$ (Figure 2-4a-d) upon ligand binding which was nearly identical for all ligands.

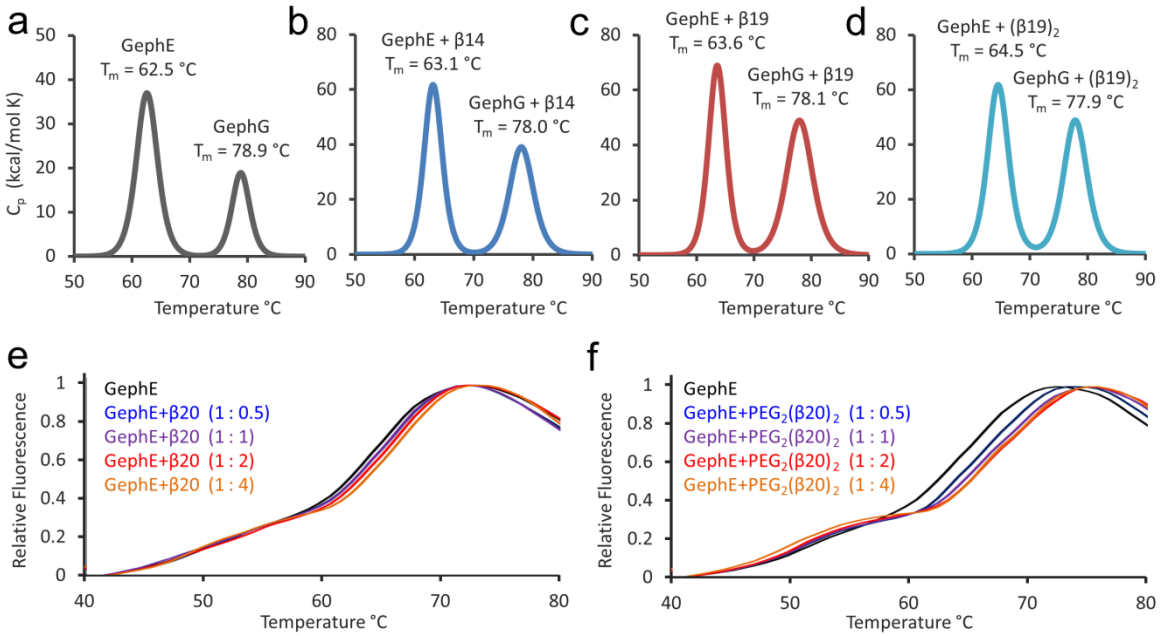

Figure 2-4.(Fig.3 in the published manuscript). Bivalent peptides specifically target GephE. (a-d) Differential scanning calorimetry (DSC) demonstrates that the dimeric peptides specifically target GephE. Shown are the thermograms of full-length gephyrin in the apo-form **(a)** and in the presence of different peptides: β14 **(b),** β19 **(c)** and $(β19)_2$ **(d)** at a molar ratio of 1:1. The graphs show the fits according to a two-state scaled model. **(e-f)** Thermofluor analysis suggests an increased affinity of GephE for the bivalent over the monovalent peptide.

2.3.6 Thermofluor analysis suggests an increased affinity of GephE for the bivalent over the monovalent peptide. To further explore the stabilizing effect of mono- and bivalent receptor fragments on GephE we used thermofluor, which, similar to DSC, monitors thermal protein unfolding, however, several different conditions can be tested in parallel. To verify an

increased stabilizing effect of GephE for the bivalent over the monovalent peptide we compared GephE melting at different molar ratios of both ligands. In particular, we used a 0.5, 1, 2 and 4-fold excess of the respective ligand (Figure 2-4 e,f). As expected, increasing ligand concentrations raised the melting temperature of GephE. Notably, the bivalent peptide displayed a more pronounced shift of the melting temperature and the shift reached its maximum at a lower stoichiometric excess. Specifically, we found a 5 °C shift for the bivalent peptide which was already reached at a 2-fold excess, while the monovalent peptide exhibited only a moderate 2.5 °C shift even at a 4-fold molar excess. Taken together the thermofluor data confirmed the DSC measurements but additionally indicated a stronger affinity for the bivalent over the monovalent peptide to GephE.

2.3.7 Isothermal titration calorimetry (ITC) revealed the bivalent peptide to display a 25-fold enhanced affinity. Next we used isothermal titration calorimetry (ITC) to define dissociation constants (K_D) and the underlying thermodynamic parameters ΔH and ΔS as well as the binding stoichiometry. As expected, the titration of GephE with the monovalent (Figure 2-5a) and bivalent (Figure 2-5b) β19 fragments resulted in fundamentally different binding data. The dimerization resulted in a ~25-fold enhanced affinity to GephE, decreasing the K_D from 2.8 µM to 0.11 µM, and, in line with the idea that both binding sites can be occupied simultaneously, the increase in binding strength was accompanied by a doubled enthalpic contribution and a stoichiometry of 0.5 (Figure 2-5a,b and Table 2-3).

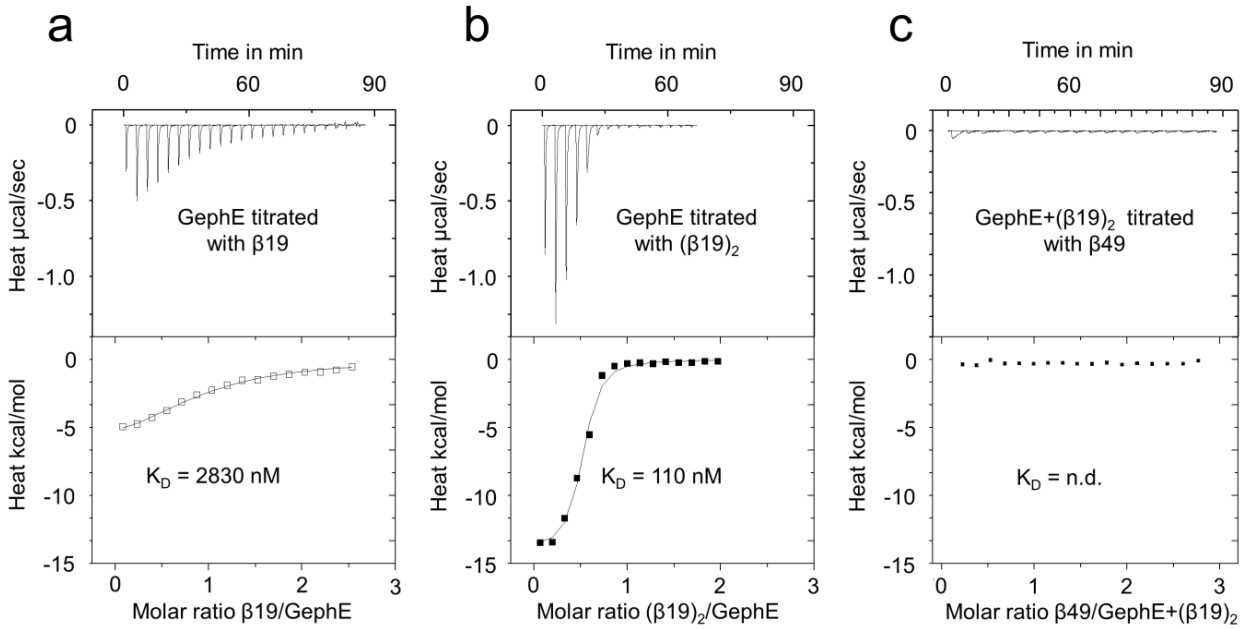

Figure 2-5.(Fig.4 in the published manuscript). Calorimetric analysis of GephE interacting with monovalent and bivalent ligands. Titration of GephE with **(a)** monovalent β19 and **(b)** bivalent $(β19)_2$ peptides. In line with a multivalent binding, the isothermal binding curves display an

enhancedaffinity, accompanied by a doubling of the molar enthalpy and a stoichiometry of roughly 0.5. **(c)** ITC competition assay between mono- and bivalent gephyrin ligands. Titration of the preformed GephE-β-19)$_2$ complex with β-49. The lack of any thermal signature in this competition experiment indicates that there are no additional binding contributions mediated by the elongated peptide sequence.

Next, to test whether the bivalent peptide described here is sufficient to act as a specific inhibitor of gephyrin's receptor binding activity and to rule out secondary binding effects, we performed ITC competition assays. First, we pre-equilibrated GephE with the bivalent peptide (β19)$_2$ at a molar ratio of 1:1. The resulting complex was titrated with the strongest conventional monovalent peptide, namely β49. Strikingly, the bidentate peptide indeed completely abolished any trace of GephE interaction with the elongated monovalent fragment (Figure 2-5c). We conclude that, due to simultaneous binding to two binding sites, the bivalent peptide displays a significantly higher affinity compared to the receptor fragments that have so far been used to target gephyrin and that β49 does not contain an additional secondary binding site compared to β19.

Table 2-3. Dissociation constants, enthalpy, entropy and stoichiometry values from ITC experiments.

Ligand	Protein[e]	K_D[μM][f]	ΔH [kcal mol^{-1}][f]	-TΔS[kcalmol^{-1}][f]	N[f]
β14[a]	GephE (D)	6.3±0.2	-5.5±0.07	2.5	0.98±0.04
β19[b]	GephE (D)	2.8±0.15	-6.2±0.4	2.7	0.96±0.06
β49 [d]	GephE (D)	2.1±0.5	-9.4±0.5	5.8	0.91±0.04
β19[b]	Gephyrin (M)	2.5±0.2	-6.8±0.6	3.3	0.88±0.04
β49 [d]	Gephyrin (M)	2.4±0.6	-10.4±0.8	6.8	0.83±0.03
(β19)$_2$[c]	GephE (D)	0.11±0.03	-13.4±0.2	8.0	0.46±0.04
(β19)$_2$[c]	Gephyrin (M)	0.59±0.08	-13.9±0.3	9.5	0.59±0.06
β49[d]	GephE (D) in complex with BM(PEG)$_2$(β19)$_2$	n.d.[g]	n.d.	n.d.	n.d.

[a] FSIVGSLPRDFELS.[b] FSIVGSLPRDFELSNYDCY.

[c] BM(PEG)2(FSIVGSLPRDFELSNYDCY)$_2$.

[d] VGETRCKKVCTSKSDLRSNDFSIVGSLPRDFELSNYDCYGKPIEVNNGL.

[e] Putative oligomeric state of the E domain: M = monomer (when present in trimeric full-length gephyrin) D = dimer (when GephE was analyzed)

[f] Titrations were fitted using a single binding site model. Represented as the mean±standard deviation from at least three measurements.

[g] n.d., no binding could be detected.

2.3.8 Similar enthalpic contributions mediate monovalent and bivalent ligand binding to gephyrin. To further rule out secondary effects we also monitored the maximal possible heat release upon simultaneous saturation of all gephyrin-binding sites using either the monovalent or bivalent ligands. In such an experiment the heat release solely depends on the number of gephyrin molecules and should be independent of ligand concentration, activity, purity and number of binding sites (Figure 2-6a). In line with earlier studies, which attributed the effect of simultaneous binding to two binding sites on binding strength to kinetic contributions (Jencks, 1981; Zhou, 2001, 2003), the single injection of an eight-fold ligand excess over GephE displayed similar enthalpic contributions for the monomeric and dimeric fragments despite the 25-fold difference in affinity (Figure 2-6a). It should be pointed out that the binding enthalpies of the titrations with β19 and $(β19)_2$ presented in Table 2-3 cannot be directly compared, instead the values for the dimeric peptide have to be divided by two to account for the fact that there are twice as many peptides on a molar basis in the dimerized peptide. The nearly identical enthalpies derived by single injection calorimetry suggest that both fragments occupy an identical binding site on GephE resulting in comparable van der Waals and hydrogen bonding interactions, which give rise to the total heat signature.

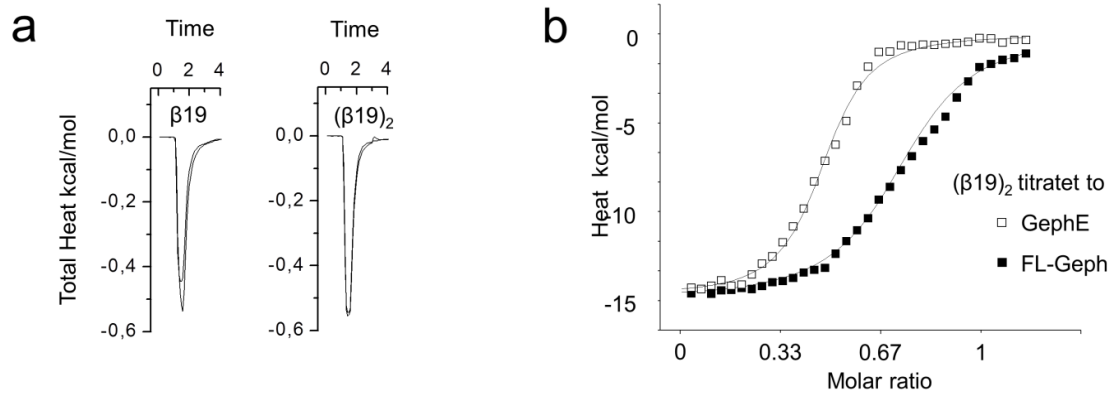

Figure 2-6. **(Fig.5 in the published manuscript). Calorimetric analysis of monovalent and bivalent ligands interacting with GephE and FL-Geph and determination of the total binding enthalpy. (a)**Single injection calorimetry (overlay of two independent experiments) reveals similar enthalpic contributions of different GephE ligands. Single injection of an 8-fold molar excess of either the

monovalent GlyR β derived minimum peptide β19 (left) or its bivalent counterpart $(β19)_2$ (right). Note that the heat release measured in µcal/sec is nearly identical despite the 25-fold difference in affinity. **(b)** Binding isotherms of GephE and FL-Geph titrated with $(β19)_2$.

2.3.9 The oligomerization state of GephE modulates the receptor affinity of gephyrin.

Prompted by the enhanced affinity of the GephE dimer for the dimeric peptides we asked whether trimericFL-Geph (Herweg and Schwarz, 2012; Sander et al., 2013; Schrader et al., 2004) would show a similar effect. Trimerization of FL-Geph occurs via the G domain at the expense of the E domain dimer interface (Bedet et al., 2006; Sander et al., 2013) and, following this idea, titration with a dimerized peptide should not yield an increased affinity, unless there is a large flexibility in the trimeric arrangement (Sander et al., 2013). As expected from earlier studies (Schrader et al., 2004) FL-Geph and GephE showed largely identical binding parameters for the monomeric β19 peptides (Table 2-3). Titration of FL-Geph with the dimeric fragment displayed, similar to GephE, a sharp increase in the enthalpic contribution and affinity (Figure 2-6b). Nonetheless, the 4-fold affinity potentiation for FL-Geph is rather limited which is due to the less favorable entropicterm of 9.5 kcal mol^{-1} for FL-Geph compared to 8.0 kcal mol^{-1} for GephE, and the resulting stoichiometry is slightly larger than expected (Figure 2-6b and Table 2-3). One possible scenario would be that trimeric FL-Geph allows two of its E domains to approach each other closely enough to offer a dimeric receptor binding interface, similar to the arrangement present in the GephE crystal structures; however, this is coupled to a decrease in entropy. Following this idea, one third of the offered receptor binding sites would be monovalent, while two thirds would be bivalent. This hypothesis would offer a possible explanation for the reduced stoichiometry and moderately enhanced affinity of FL-Geph for bivalent peptides, which is mediated by the fraction of bivalent receptor binding sites.

2.4 CONCLUSIONS

So far gephyrin-receptor interactions were analyzed with monovalent receptor-derived fragments (Herweg and Schwarz, 2012; Kim et al., 2006; Kowalczyk et al., 2013; Maric et al., 2011; Meyer et al., 1995; Mukherjee et al., 2011b; Schrader et al., 2004; Sola et al., 2004; Specht et al., 2011), which do not fully reflect the situation *in vivo*. Using a two site binding model the high affinity binding site of the elongated GlyR β was described to be in the nanomolar range with values varying between 22 nM (Specht et al., 2011), 30 nM (Herweg and Schwarz, 2012), 90-120 nM (Kim et al., 2006) and 200-400 nM (Schrader et al., 2004). Based on similar affinities of truncated peptides (β15 and β19) and the single binding site observed in the structures with (β15 and β49) we instead suggest the presence of a single binding site. In line with this idea the elongated 49-mer peptide does not show

additional binding contributions when GephE was pre-incubated with the $(\beta19)_2$ peptide (Figure 2-6b). Our results also suggest that the low K_D values obtained for the high affinity interaction, when the binding data were analyzed with a two-site binding model, possibly representing an artifact of the fitting procedure.

Our bivalent peptides presented here might mimic the simultaneous binding of pentameric GlyRs and $GABA_ARs$ approaching the gephyrin scaffold at postsynaptic sites *in vivo* (Scheme 2-1). Indeed, it was proposed earlier that simultaneous binding of more than one subunit could explain the outstandingly slow exchange rates (Specht et al., 2013) of GlyRs at postsynaptic sites, and the only moderate binding affinities of single $GABA_AR$ subunits to gephyrin (Tretter et al., 2012). In line with this idea, synaptic $GABA_ARs$ are thought to most commonly contain two gephyrin binding α1-3 and/or two β2/3 subunits (Kowalczyk et al., 2013; Maric et al., 2011; Mukherjee et al., 2011b; Olsen and Sieghart, 2008; Tretter et al., 2008), while GlyRs were shown to contain three gephyrin-interacting β subunits (Yang et al., 2012). However, trimeric peptidic ligands that are able to cover long distances between intra- and intermolecular GephE binding sites within the FL-Geph protein have not been included in our study.

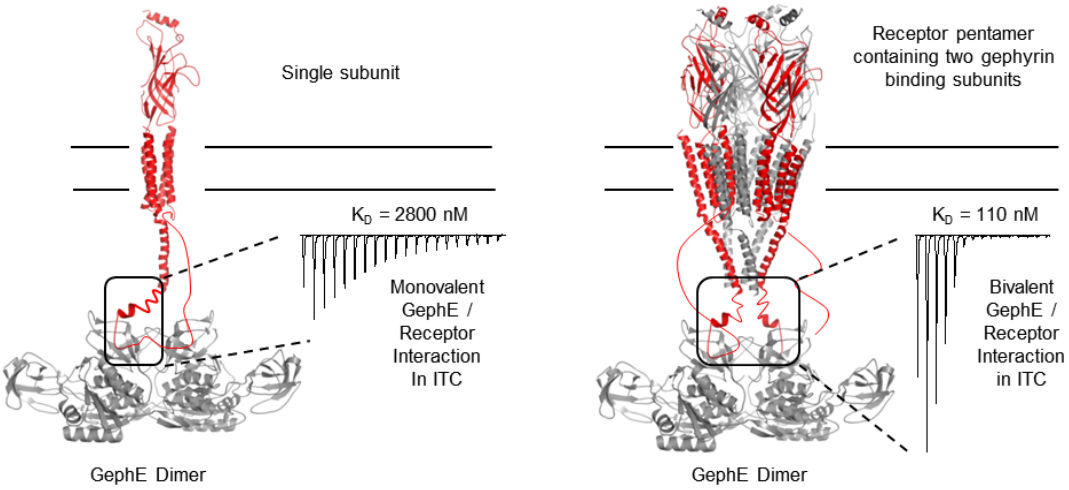

Scheme 2-1. Receptor clustering at inhibitory postsynaptic sites is a multivalent process. Our biophysical studies revealed that dimeric receptor fragments (right) bind dimeric E domains with a ~25-fold enhanced affinity compared to their monovalent counterparts (left). Accordingly our studies identified that the number of gephyrin-binding subunits in each inhibitory receptor pentamer together with gephyrin's oligomeric state are major determinants of receptor accumulation at inhibitory postsynaptic sites.

The concept of enhancing the gephyrin-binding affinity of its cognate receptors by dimerization presented in this study opens new avenues of research: 1. Variants of the dimeric peptide may be used for future crystallographic studies of low affinity $GABA_AR$

subunits (Kowalczyk et al., 2013; Maric et al., 2011; Mukherjee et al., 2011b; Tretter et al., 2008), which, so far, have not been amenable to crystallization in our hands. 2. By competing with naturally occurring receptor-gephyrin interactions, the dimerized β19 fragment and related compounds might be used as tools to specifically target gephyrin's receptor binding activity in a fashion analogous to compounds targeting interactions between PDZ domains and excitatory neurotransmitter receptors or other disease-relevant ligands (Bach et al., 2008; Bach et al., 2009; Bach et al., 2012; Bach et al., 2011; Bard et al., 2010; Chi et al., 2010; Iskenderian-Epps and Imperiali, 2010; Klosi et al., 2007; Sainlos et al., 2013; Sainlos et al., 2011).

Indeed, the results described here resemble the situation at excitatory synapses, which rely on the multivalent interaction of receptors containing more than one PDZ-binding subunit and PDZ-containing proteins. Not surprisingly, the 25-fold affinity potentiation described here is comparable to what has been described earlier for the scaffold-receptor interactions at excitatory synapses. Namely, a 8-30 fold affinity potentiation for Shank3-PDZ (Iskenderian-Epps and Imperiali, 2010; Sainlos et al., 2011) and a 1-145 fold increase of PDZ1-2 for PSD95 (Bach et al., 2009). On the other hand, there are also important differences between the multivalent receptor/scaffold interactions. ManyPDZ-containing scaffold proteins contain more than a single PDZ domain and therefore the multivalency of their ligand binding sites is an intrinsic feature of their primary structure. Shank and gephyrin, however, contain only a single receptor-binding site and the multimeric receptor-binding interface is instead formed upon homomerization of the full-length protein. We propose that the interdependence of gephyrin's oligomeric state and its receptor affinity described here provides a possible explanation for the prominent link between gephyrin clustering and receptor clustering *in vivo* (Essrich et al., 1998; Vlachos et al., 2013). Taken together, our results suggest that the number of gephyrin-binding subunits in each inhibitory receptor pentamer together with gephyrin's oligomeric state determine receptor accumulation at the postsynaptic membrane. *Vice versa*, receptor interactions might induce and/or stabilize gephyrin aggregation.

2.5 MATERIALS AND METHODS

2.5.1 Protein expression and purification. FL-Geph (Gephyrin P2 splice variant, residues 1-736), GephE (residues 318-736) and β49 (GlyR residues 378-425, VGETRCKKVCTSKSDLRSNDFSIVGSLPRDFELSNYDCYGKPIEVNNGL) were expressed and purified as described (Kim et al., 2006; Maric et al., 2011; Schrader et al., 2004). Pure fractions were pooled and concentrated to 1-20 mg/ml using Vivaspin 3 kDa molecular weight cutoff (MWCO) centrifugal filter devices (Sartorius Stedim Biotech), flash-frozen in 0.5 ml aliquots, and stored at -80 °C.

2.5.2 Peptide synthesis. Peptides were initially purchased as lyophilized powder (Genscript) at a minimal purity of 90% and later synthesized using Fmoc solid phase peptide synthesis. All peptides, GlyR β 398-411 (β14, FSIVGSLPRDFELS), GlyR β 397-411 (β15, DFSIVGSLPRDFELS), GlyR β 398-416 (β19, FSIVGSLPRDFELSNYDCY), were water soluble at neutral pH.

2.5.3 Peptide purification and analysis. Preparative HPLC was performed on an Agilent 1100 system using a C18 reversed phase column (Zorbax 300 SB-C18, 21.2×250 mm) with a linear gradient of 0.1 % trifluoroacetic acid (TFA) in water/acetonitrile (ACN) (A: 95/5 and B: 5/95 (v/v)) with a flow rate of 20 mL/min. Mass spectra were obtained with an Agilent 6410 triple quadrupole mass spectrometer instrument using electron spray ionization coupled to an Agilent 1200 HPLC system (ESI-LC/MS) with a C18 reversed phase column (Zorbax Eclipse XBD-C18, 4.6×50 mm), autosampler and diode-array detector using a linear gradient of 0.1% formic acidin water/ACN (A: 95/5 and B: 5/95 (v/v)) with a flow rate of 1 mL/min. During ESI-LC/MS analysis evaporative light scattering (ELS) traces were obtained with a SedereSedex 85 light scattering detector. The identity of all tested compounds was confirmed by ESI-LC/MS, which also provided purity data (all >90%; ELS-detector). High resolution mass spectrometry (HRMS) spectra were acquired in positive-ion mode, using a drying temperature of 200 °C, a capillary voltage of 4100 V, a nebulizer pressure of 2.0 bar, and a drying gas flow of 7 L/min on amicrOTOF-Q II mass spectrometer (BrukerDaltonik) equipped with an electrospray ionization interface.

2.5.4 LC-MS: Calculated for β19: $[M + 2H]^{3+}$: 1113,72, found: *m/z* 1113.20; $[M + 3H]^{2+}$: 742.81, found: *m/z* 742.70. Calculated for $(β19)_2$: $[M + 3H]^{3+}$, 1587.38, found: m/z 1587.00, $[M + 4H]^{4+}$: 1190.79, found *m/z* 1190.70; $[M + 5H]^{5+}$: 952.83, found: *m/z* 952.60; $[M + 6H]^{6+}$: 794.20, found *m/z*: 794.20.

2.5.5 HRMS: Calculated for β19: $[M + 3H]^{3+}$, 742.81; found: *m/z* 742.583. Calculated for $(β19)_2$: $[M + 5H]^{5+}$,952.83, found: 952.8368; $[M + 6H]^{6+}$: 794.20; found: 794.0314; $[M + 7H]^{7+}$:680,88, found: 680.7425.

2.5.6 Peptide dimerization. The GlyR β peptide β19 was dissolved in buffer (100 mM Hepes pH 7.3) to a final concentration of 0.4 mM as determined by absorption at 280 nm due to two tyrosine residues ($ε_{280}$ (Tyrosine) = 1480 $M^{-1}cm^{-1}$). 1,8-Bismaleido-diethylenglycol ($BM(PEG)_2$) (ThermoFischer Scientific) was dissolved at 2 mM in the same buffer. The $BM(PEG)_2$ concentration was determined by absorption measurement at 302 nm ($ε_{302}$ (Maleimide) = 620 $M^{-1}cm^{-1}$(Singh, 1994)). Using a VP-ITC (MicroCal) as reaction vessel, 1 µl portions of crosslinker (300 µl total) were added to 1.5 ml solution of the cysteine-containing peptide at 30°C while stirring at 400 rpm, resulting in a final stoichiometry of nearly 1:1. Each 1 µl injection was elongated to last 10 seconds to prevent heat release to

surpass the maximal limit of 34 µcal/sec. Additionally the incubation time after each injection was adjusted to last at least 7 minutes to ensure complete conversion of each portion of crosslinker and hence to minimize excess of crosslinker resulting in irreversible mono-substituted peptides. After addition of 500 mM BME to quench residual reactive maleimides, the bivalent peptide was dialyzed twice overnight against 10 mM Tris/HCl pH 8.0, 250 mM NaCl, 1 mM β-ME using a Slide-A-Lyzer Dialysis Cassette, 3.5 kDa MWCO, 3 ml (ThermoFischer Scientific).

2.5.7 Sample preparation for DSC, thermofluor and ITC. Protein and peptide samples were prepared by extensive dialysis against 10 mM Tris-HCl pH 8.0, 250 mM NaCl, 1 mM β-ME at 4°C overnight. Directly prior to the respective experiment, samples were filtrated and degassed.

2.5.8 Differential scanning calorimetry (DSC). DSC experiments were performed with a NanoDSC (TA instruments) with FL-Geph at a concentration of 20 µM in the apo-form and the different peptides at a molar ratio of 1:1. The calorimetric data of the protein samples were obtained between 20 and 90°C at a scan rate of 1 min/°C, corrected for the buffer scan and analyzed with a two-state scaled model and the NanoAnalyze Software (TA instruments).

2.5.9 Thermofluor. Prior to thermal unfolding 9 µl of GephE (30 µM) were mixed with 1µl of a 1:100 dilution of Sypro Orange (Sigma-Aldrich) dissolved in 100% DMSO. In a 96 PP-PCR-plate (Greiner Bio-One) the prepared GephE-Sypro solution was mixed with monovalent or bivalent 19 residue peptides at final molar ratios of 0.5, 1, 2 and 4 and a final volume of 15 µl. The experiment was performed on a real-time Mx3005PTM PCR system (Stratagene), which performed 70 steps starting at 25°C. With each step, the temperature was increased by 1°C and fluorescence was measured. The analysis was carried out with an excel sheet (Structural Genomics Consortium).

2.5.10 Isothermal titration calorimetry (ITC). The experiments were performed using an ITC_{200} (MicroCal) at 25°C and 1000 rpm stirring and designed so that c-values were generally within 1–1000 (c-value = K_A x [protein] x N with K_A, equilibrium association constant; [protein], protein concentration; N, stoichiometry). Specifically, 40 µl of a solution containing 150-300 µM of β49, β19, β14, $PEG_2(β19)_2$ were titrated into the 200 µl sample cell containing 25-50 µM GephE. A volume of 1-2 µl of ligand was added at a time resulting in 20-40 injections and a final molar ratio between 1:1 and 1:3. Ligand-to-buffer titrations were carried out analogously, so that the heat produced by injection, mixing and dilution could be subtracted. The binding enthalpy was directly measured, while the dissociation constant (K_D), entropy and stoichiometry (N) were obtained by data analysis using the Origin

software (OriginLab). Measurements were conducted several times as indicated and are given as mean values with the resulting standard derivation.

2.5.11 Comparative single injection total enthalpy (CSITE) analysis. These experiments were performed using an ITC_{200} (MicroCal) at 25°C and 1000 rpm stirring. 40 µl of a solution containing 160 µM of β19 or $PEG_2(β19)_2$ were added with a single injection (30 sec) into the 200 µl sample cell containing 4 µM GephE resulting in a final molar ratio of 1:8. Corresponding buffer-to-buffer titrations were carried out in an analogous fashion. Measurements were conducted at least twice.

2.5.12 Crystallization and data collection. For the complex crystal structure GephE (c=200 µM in 5 mM Tris pH 8 and 50 mM NaCl) was mixed with β15 (1:2) and adjusted to a final complex concentration of 350 µM in the same buffer. Using a Lissy liquid handling robot (Zinsser Analytik) a customized GephE fine screen was generated Table 2-2). A HoneyBee 963 crystallization robot (Genomic Solutions) dispensed 0.3 µl protein solution and 0.3 µl crystallization solution which were equilibrated against 40 µl reservoir solution in a 96-well crystallization plate (Greiner Bio-One). Prism-shaped GephE and GephE-β15 crystals were obtained after two days at 25 °C against a reservoir solution containing 0.1 M sodium citrate pH 4.5 and 28-34% (v/v) 2-methyl-2,4-pentanediol. Crystals were directly flash cooled in liquid nitrogen. Diffraction data were collected at wavelengths of 0.9198 Å and 0.9184 Å for apo-GephE and GephE-β15 crystals, respectively. Data collection statistics are summarized in Table 2-1.

2.5.13 Structure determination and refinement. Data were indexed and integrated with iMosflm for the GephE-β15 complex(Battye et al., 2011) and with XDS for apo-GephE. For scaling and all other subsequent steps the CCP4 software package was used (1994). Molecular replacement was carried with PDB entry 2FU3 (Kim et al., 2006) as initial model with PhaserMR, followed by refinement with Phenix including TLS refinement in which each GephE monomer was divided into four TLS bodies according to its subdomain architecture. Clear density corresponding to at least 10 residues of the GlyR β-loop was already visible in the first electron density maps and assignment of the sequence was straightforward. The structures were refined to 1.7 and 2.0 Å resolution for apo and GephE-β15, respectively.

2.6 ACCESSION CODES

The structures have been deposited in the protein data bank with accession numbers (4PD0, apo-GephE) and (4PD1, GephE-β15).

2.7 ACKNOWLEDGMENTS

This work was supported by the Deutsche Forschungsgemeinschaft (FZ 82, SFB487 C7 and Schi 425/8-1), HM was supported by a grant of the German Excellence Initiative to the Graduate School of Life Sciences, University of Würzburg. We thank B. Sander and M. Amato for their contributions, U.Dietzel for his help with structure solution and refinement, P.Gimeson for help with initial DSC measurements, S.G.Wubshet for the high resolution mass spectrometry analysis and K. Strømgaard for the use of his facilities.

3. Molecular basis of the alternative recruitment of $GABA_A$ versus glycine receptors through gephyrin*

This chapter is based on the following publication:

Maric, H.M., Kasaragod, V.B., Hausrat, T.J., Kneussel, M., Tretter, V., Strømgaard, K., and Schindelin, H. (2014). Molecular basis of the alternative recruitment of $GABA_A$ versus glycine receptors through gephyrin. *Nat. Commun*. ***5***, 5767.

*Changes incorporated: Supplemental informations have been merged with main text.

Statement of individual author contributions and of legal second publication rights

Participated in	**Author Initials,** Responsibility decreasing from left to right				
Study Design Methods Development	HMM, VBK, HS.	KS	TJH, MK	VT	
Data Collection	VBK, HMM	TJH			
Data Analysis and Interpretation	VBK, HMM	HS	KS	TJH, MK	
Manuscript Writing					
Writing of Introduction	HMM, VBK,	HS	KS	TJH, MK	VT
Writing of Materials & Methods	VBK, HMM,	HS	KS	TJH, MK	VT
Writing of Discussion	HMM, VBK	HS	KS	TJH, MK	VT
Writing of First Draft	HMM, VBK	HS	KS	TJH, MK	VT

Statement of individual author contributions to figures/tables/chapters included in the manuscripts

Figure	**Author Initials,** Responsibility decreasing from left to right				
1	VBK, HMM	HS, KS	TJH, MK	VT	
2	HMM	TJH, MK	VBK, HS, KS	VT	
3	VBK	HMM, HS, KS	TJH, MK, VT		
4	VBK	HMM, HS, KS	TJH, MK, VT		
5	HMM, VBK	HS, KS	TJH, MK,VT		

3. Molecular basis of the alternative recruitment of $GABA_A$ versus glycine receptors through gephyrin

Hans Michael Maric[1,2,*], Vikram Babu Kasaragod[1,*], Torben Johann Hausrat[3], Matthias Kneussel[3], Verena Tretter[4], Kristian Strømgaard[2]& Hermann Schindelin[1]

[1]Rudolf Virchow Center for Experimental Biomedicine, University of Würzburg, Josef-Schneider-Straβe 2, Building D15, D-97080 Würzburg, Germany.

[2]Department of Drug Design and Pharmacology, University of Copenhagen, Universitetsparken 2, DK-2100 Copenhagen, Denmark.

[3]Center for MolecularNeurobiology, ZMNH, University Medical Center Hamburg-Eppendorf, D-20251 Hamburg, Germany.

[4]Department of General Anesthesia and Intensive Care, Medical University Vienna, Währinger Gürtel 18-20, 1090 Vienna, Austria.

*These authors contributed equally to this work.

Correspondence and requests for materials should be addressed to H.S. (e-mail: hermann.schindelin@virchow.uni-wuerzburg.de).

3.1 ABSTRACT

γ-Aminobutyric acid type A and glycine receptors ($GABA_A$Rs, GlyRs) are the major inhibitory neurotransmitter receptors and contribute to many synaptic functions, dysfunctions and human diseases. $GABA_A$Rs are important drug targets regulated by direct interactions with the scaffolding protein gephyrin. Here, we deduce the molecular basis of this interaction by biochemical, biophysical and structural studies of the gephyrin-$GABA_A$R α3 complex, revealing that the N-terminal region of the α3 peptide occupies the same binding site as the GlyR βsubunit, whereas the C-terminal moiety, which is conserved among all synaptic $GABA_A$R α-subunits, engages in unique interactions. Thermodynamic dissections of the gephyrin-receptor interactions identify two residues as primary determinants for gephyrin's subuni tpreference. This first structural evidence for the gephyrin-mediated synaptic accumulation of $GABA_A$Rs offers a framework for future investigations into the regulation of inhibitorysynaptic strength and for the development of mechanistically and therapeutically relevant compounds targeting the gephyrin-$GABA_A$R interaction.

3.2 INTRODUCTION

γ-Aminobutyric acid type A receptors ($GABA_A$Rs) are ligand-gated ion channels, which mediate the majority of fast inhibitory synaptic transmission in the mammalian central nervous system (CNS). Deficits in $GABA_A$R-mediated neurotransmission have been implicated in a wide spectrum of disorders of the CNS such as epilepsy, anxiety, mood disorders, and neuro-developmental impairments including autism, fragile X syndrome, and schizophrenia (Hines et al., 2012b). Accordingly, $GABA_A$Rs are important, validated drug targets and compounds targeting $GABA_A$Rs have been extensively explored and successfully used clinically as sedatives, anxiolytics and anticonvulsive drugs, narcotics and anesthetics, anti-spasmodics, anti-epileptics, hypnotic and analgesic drugs.

$GABA_A$Rs are pentameric hetero-oligomers assembled from seven different subunit classes with the most common receptor combination being two α, two β and a single γ subunit (Kittler et al., 2002). The majority of synaptic $GABA_A$R subtypes are localized and accumulated by the scaffolding protein gephyrin. Gephyrin is a central player at inhibitory synapses and, besides its structural role as a receptor scaffold, it also acts as a platform for additional protein-protein interactions, bringing receptors, cytoskeletal elements and signaling proteins into close spatial proximity (Fritschy and Panzanelli, 2014; Tretter et al., 2012; Tyagarajan and Fritschy, 2014). Therefore, insights into the molecular basis of $GABA_A$R clustering at synaptic sites might allow the advance of new therapeutic principles in the treatment of $GABA_A$R-related disorders. Gephyrin iscomposed of an N-terminal domain (GephG, residues 1-181) and a C-terminal domain (GephE, residues 318-736), which are

connected by an unstructured linker (residues 182-317). Gephyrin was discovered (Pfeiffer et al., 1982) by co-purification with glycine receptors (GlyRs) and found to be responsible for anchoring and accumulating GlyRs at postsynaptic sites, which is accomplished by the simultaneous binding of gephyrin to the GlyR β subunit (Kim et al., 2006; Kneussel et al., 1999b; Meyer et al., 1995; Schrader et al., 2004) and elements of the cytoskeleton (Giesemann et al., 2003; Kirsch et al., 1991). A number of gene knock-out studies have addressed the role of the gephyrin-$GABA_AR$ interaction *in vivo*. Gephyrin knock-out mice die within hours after birth (Feng et al., 1998) and analysis of these mice revealed a loss of GlyR clusters (Feng et al., 1998) and a subset of $GABA_AR$ clusters (Kneussel et al., 1999a). Similarly, gene knock-outs of single $GABA_AR$ subunits, such as the γ2 and α3 subunit, not only interfere with $GABA_AR$ but also with gephyrin clustering (Essrich et al., 1998; Studer et al., 2006; Winsky-Sommerer et al., 2008). An X-ray crystal structure of GephE in complex with a 49-residue peptide derived from the large cytoplasmic loop of the GlyR β subunit defined the gephyrin-GlyR interaction in atomic detail (Kim et al., 2006). Recently, we demonstrated that the same region of gephyrin can act as a universal receptor binding site (Maric et al., 2011), which also mediates the interactions with the $GABA_AR$ α1, α2 and α3 subunits (Maric et al., 2011; Mukherjee et al., 2011b; Tretter et al., 2008), and that this interaction is modulated by the oligomeric state of gephyrin together with the number of receptor-binding subunits (Maric et al., 2014c), possibly explaining the extremely slow exchange rates of GlyRs at synaptic sites (Specht et al., 2013). Recent studies have highlighted the critical role of the $GABA_AR$ α subunits in gephyrin-mediated synaptic versus extrasynaptic targeting of $GABA_ARs$, which has been verified in cell-based, electrophysiological (Wu et al., 2012) and immunohistochemical experiments (Kneussel et al., 1999a; Maric et al., 2011; Mukherjee et al., 2011b; Tretter et al., 2008).

Despite its fundamental function in synaptic receptor localization (Fig. 3-1), receptor diffusion dynamics (Mukherjee et al., 2011b) and synaptic plasticity (Vlachos et al., 2013), the gephyrin-$GABA_AR$ interaction has not yet been elucidated on the molecular level. The aim of this study was therefore to determine the crystal structure of a gephyrin-$GABA_AR$ complex and to identify key residues in gephyrin and the $GABA_AR$ that drive the gephyrin-mediated recruitment of $GABA_ARs$ to postsynaptic sites. This will allow for a rational approach to develop compounds that could perturb the gephyrin-$GABA_AR$ interaction, which would be of great mechanistic and pharmacological interest and could pave the way for new approaches in targeting $GABA_ARs$ in drug development.

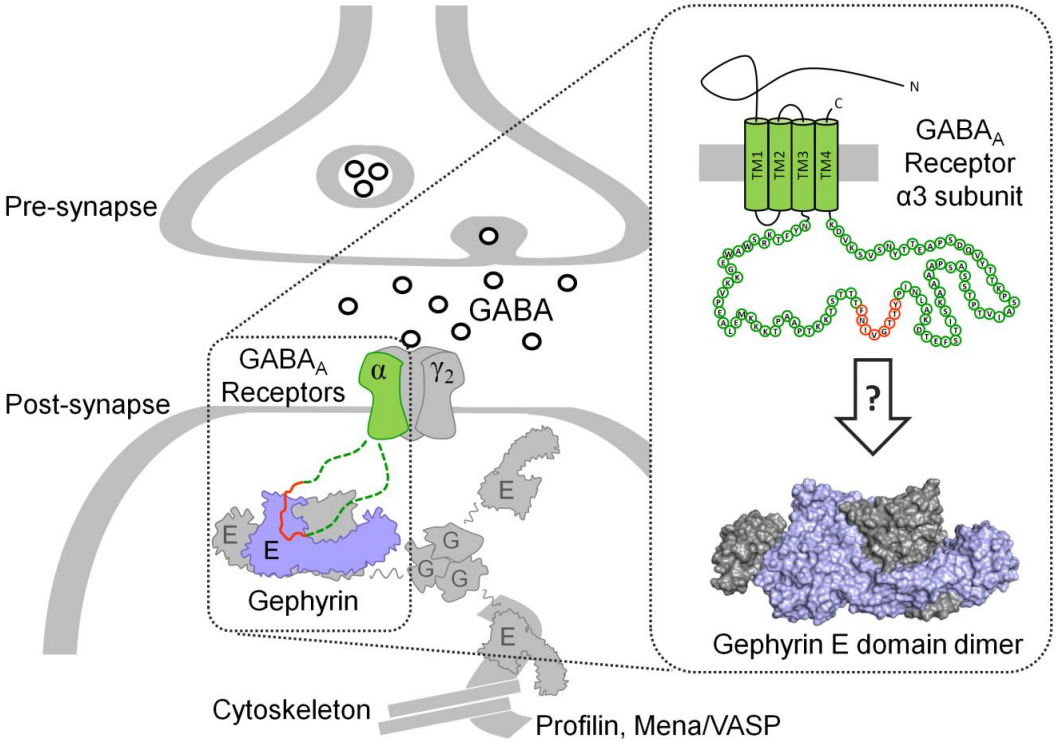

Figure 3-1 (Fig.1 in the published manuscript) . Schematic view of a GABAergic synapse. Ionotropic γ-aminobutyric acid type A receptors ($GABA_AR$s) are pentameric membrane receptors that are clustered at synaptic sites by direct interactions with the anchoring protein gephyrin. Gephyrin is believed to form higher oligomers at synaptic sites by homotrimerization of its G domain and homodimerization of its E domain. Eleven residues, which are conserved among the synaptic $GABA_AR$ α-subunits, directly engage with the E domain (PDB entry 4PD0) near the dimer interface (boxes). Gephyrin-binding tethers the receptors to the cytoskeleton by direct interaction with profilin and Mena/VASP.

3.3 RESULTS

Previous attempts to structurally characterize the interactions between GephE and the full-length intracellular loops of the $GABA_AR$ α1, α2 and α3 subunit were hampered by the low affinities and low solubility of the loops. Accordingly, a primary challenge was to identify $GABA_AR$-derived peptides appropriate for crystallization. The α3 subunit was selected as a template since it displays the highest *in vitro* gephyrin affinity of all $GABA_AR$ subunits with a K_D of 5.3 µM for the full-length intracellular loop (Kowalczyk et al., 2013; Maric et al., 2011; Mukherjee et al., 2011b). $GABA_AR$s containing α3 subunits co-localize with gephyrin in the cerebellar cortex (Sassoe-Pognetto et al., 2000), thalamic reticular nucleus (Winsky-Sommerer et al., 2008) and at perisomatic synapses in the globus pallidus (Gross et al., 2011), and a knock-out of the α3 subunit results in disruption of postsynaptic gephyrin clusters (Studer et al., 2006; Winsky-Sommerer et al., 2008). Additionally, structural insights into the gephyrin-α3 interaction would allow one to predict the interactions with the α1 and

α2 subunits to gephyrin, since the binding motifs of these α subunits are conserved (Maric et al., 2011).

3.3.1 Identification of GABA$_A$Rα3-derived gephyrin-binding minimal peptides

Based on the conserved N-terminal gephyrin-binding motif (FXIVG) in the GlyR β and GABA$_A$R α3 subunits (Maric et al., 2011) we synthesized a 20-residue GABA$_A$R α3 fragment (α20) (^{367}TFNIVGTTYPINLAKDTEFS^{386}). However, the affinity of this 20-mer peptide was too low to be assessed by isothermal titration calorimetry (ITC)(Maric et al., 2011). Hence, we first used peptide SPOT synthesis to perform a complete Ala-scan of the α20 peptide to characterize the molecular details of the GephE-GABA$_A$R α3 interaction. For this assay GephE was recombinantly expressed, purified and conjugated to horseradish peroxidase (HRP) to allow tracking of its peptide binding by chemiluminescence with high sensitivity.

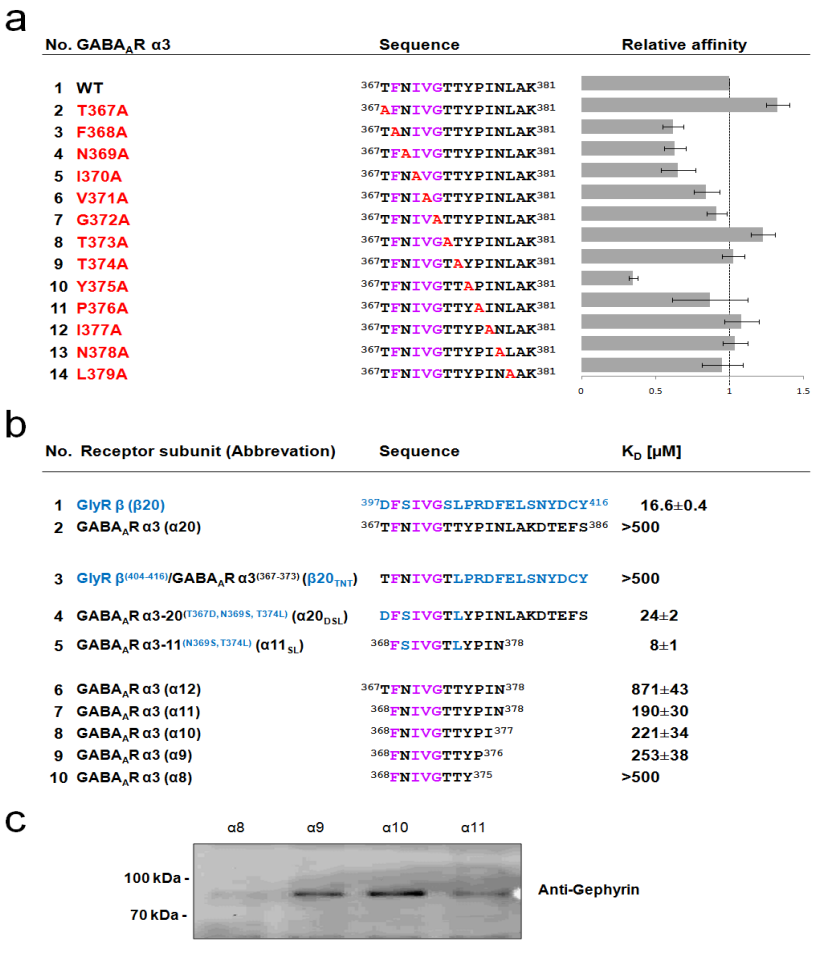

Figure 3-2. Identification of short GABA$_A$R-derived peptides as gephyrin-binding probes. (Fig.2 in the published manuscript). (a) Peptide-array-based alanine-scan of the gephyrin corebinding site within the GABA$_A$R α3 subunit. Residues shown in pink are conserved in the GABA$_A$R α3 and GlyR β subunits. Gephyrin binding to peptides was detected by chemiluminescence of conjugated horse-radish peroxidase. Shown are the relative averaged intensities of six peptide sets together with their standard deviations (error bars). Notably, T367A and T374A increase the gephyrin affinity, whereas an alanine exchange of residues 368–373 as well as residue 376 reduces gephyrin binding. **(b)** ITC analysis of gephyrin binding to GABA$_A$R α3 and GlyR β/GABA$_A$R α3 chimeric peptides. Peptide sequences and respective GephE affinities are shown. Peptides containing the seven N-terminal residues of the GlyR β peptide display a potentiated gephyrin affinity. N-terminal elongation reduces the affinity, whereas C-terminal elongation has an affinity-enhancing effect. **(c)** Short GABA$_A$R-derived peptides were sufficient to retain native gephyrin. Pull-down of native gephyrin from whole mouse brain lysate using

immobilized short $GABA_AR$-derived peptides. Immunedetection of gephyrin reveals that peptides with a length of 9–11 residues (α9-α11) were sufficient for gephyrin binding, whereas an octamer (α8) did not display binding.

Table 3-1. LC-MS analysis of synthesized peptides.

Receptor subunit variant	Sequence	$[M+H]^{1+}$,$[M+H]^{2+}$ (Calculated)	$[M+H]^{1+}$,$[M+H]^{2+}$ (LC-MS)
$GABA_AR$ α3	^{367}TFNIVGTTYPIN^{378}	670.26, 1339.51	670.50, 1339.70
$GABA_AR$α3	^{368}FNIVGTTYPIN^{378}	619.7, 1238.40	620.00, 1238.60
$GABA_AR$ α3	^{368}FNIVGTTYPI^{377}	562.65, 1124.30	562.70, 1124.70
$GABA_AR$ α3	^{368}FNIVGTTYP^{376}	506.07, 1011.14	506.00, 1010.80
$GABA_AR$ α3	^{368}FNIVGTTY^{375}	457.52, 914.03	457.30, 913.50
$GABA_AR$ α3	^{368}FNIVGTTYPIN^{378}C	671.28, 1341.55	671.50, 1341.60
$GABA_AR$ α3	^{368}FNIVGTTYPI^{377}C	614.22, 1227.44	614.60, 1227.60
$GABA_AR$α3	^{368}FNIVGTTYP^{376}C	557.64, 1114.28	557.90, 1114.60
$GABA_AR$ α3	^{368}FNIVGTTY^{375}C	509.09, 1017.17	-, 1017.50
GlyR β WT	^{398}FSIVGSLPRDF^{408}	619.21, 1237.42	619.50, 1237.70
GlyR β S399N, L404T	^{398}FNIVGSTPRDF^{408}	626.70, 1252.40	626.96, 1252.60
GlyR β S403T, P405Y	^{398}FSIVGTLYRDF^{408}	659.26, 1317.51	659.50, 1317.70
GlyR β S399N	^{398}FNIVGSLPRDF^{408}	632.73, 1264.45	633.00, 1264.69
GlyR β S403T	^{398}FSIVGTLPRDF^{408}	626.23, 1251.45	626.50, 1251.69
GlyR β L404T	^{398}FSIVGSTPRDF^{408}	613.19, 1225.37	613.50, 1225.69
GlyR β P405Y	^{398}FSIVGSLYRDF^{408}	652.24, 1303.48	652.50, 1303.69
GlyR β P405A	^{398}FSIVGSLARDF^{408}	606.20, 1211.39	606.50, 1211.69
$GABA_AR$ α3 WT	^{368}FNIVGTTYPIN^{378}	619.71, 1238.41	620.00, 1238.70
$GABA_AR$ α3 P376R, I377D, N378F	^{368}FNIVGTTYRDF^{378}	666.74, 1332.48	667.00, 1332.70
$GABA_AR$ α3 N369S, T374L	^{368}FSIVGTLYPIN^{378}	612.22, 1223.44	612.50, 1223.70
$GABA_AR$ α3 T374L	^{368}FNIVGTLYPIN^{378}	625.73, 1250.46	626.00, 1250.70
$GABA_AR$ α3 N369S	^{368}FSIVGTTYPIN^{378}	606.19, 1211.38	606.50, 1211.70

14 different alanine mutants of the α20 peptide were immobilized in high density on a cellulose-based microarray (Celluspot^{TM}, Intavis, Germany). After incubation with GephE-HRP the chemiluminescence was quantified for each alanine mutant. We observed that Ala substitutions of residues 368 to 372 as well as 375 significantly impaired binding to GephE, whereas Ala substitutions of Thr373 and, in particular, Thr367 resulted in an increased binding affinity (Fig. 3-2a).

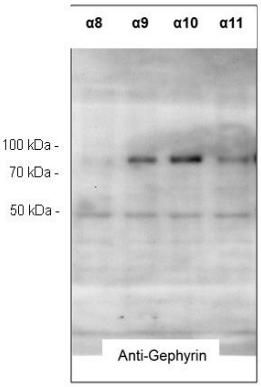

Figure 3-3. (Supplemental Fig.1 in the published manuscript). Immunodetection of gephyrin from whole mouse brain lysate (complete plot). Short $GABA_AR$-derived peptides were sufficient to retain native gephyrin. Pull-down of native gephyrin from whole mouse brain lysate using immobilized short $GABA_AR$-derived peptides. Immunodetection of gephyrin reveals that peptides with a length of 9-11 residues (α9- α11) were sufficient for gephyrin binding, while an octamer (α8) did not display binding of the 93 kDa protein gephyrin.

In an attempt to increase the affinity of the $GABA_AR$-derived binding peptide and to map differences in the way $GABA_AR$ and GlyR interact with gephyrin, we designed and prepared $GABA_AR$ α3/GlyR β chimeric peptides and quantified their binding affinity by ITC (Fig. 3-2b). We found that the affinity of the α20 peptide could be increased by substituting seven N-terminal residues with those derived from the GlyR β subunit (Fig. 3-2b, sequences No. 4 and 5), whereas substitution with 13 C-terminal residues from GlyR βdid not lead to detectable changes in affinity (Fig. 3-2b, sequence no. 3). Based on the Ala-scan and chimeric peptides, we then synthesized optimized variants of $GABA_AR$ α3-derived peptides corresponding to the N-terminal region of the GlyR β gephyrin-binding site lacking the N-terminal Thr367 (Fig. 3-2b, sequences no. 5 to 10). Strikingly, three $GABA_AR$ α3 subunit peptide fragments varying in length from 9 to 11 residues displayed a micromolar affinity to GephE in ITC experiments (Fig. 3-2b, sequences no. 6-9). This correlates with the Ala-scan showing that the Thr367Ala mutation increased affinity to GephE (Fig. 3-2b), and this possibly explains why binding of gephyrin to longer $GABA_AR$-derived synthetic peptides could not be quantified by ITC earlier (Maric et al., 2011). Thus, we identified short and soluble $GABA_AR$ α3-derived peptides, α9-11, exhibiting micromolar affinity to GephE, which was essential for our overall aim of delineating the gephyrin-$GABA_AR$ interaction.

3.3.2 Short $GABA_AR$ α3-derived peptides are binding native full-length gephyrin

Phosphorylation (Demirkan et al., 2011; Herweg and Schwarz, 2012; Tyagarajan et al., 2013; Zita et al., 2007), palmitoylation (Dejanovic et al., 2014; Kang et al., 2008) and acetylation (Choudhary et al., 2009; Schwer et al., 2009) of gephyrin have been reported and these post-translational modifications have been shown to affect the structure, trafficking, half-life, and importantly the ability of gephyrin to interact with partner proteins. To test whether the identified short $GABA_AR$ derived peptide fragments α9-11 also mediate binding to native full-length gephyrin comprising post-translational modifications, the peptides were covalently immobilized on iodoacetyl-activated beads and subsequently incubated with mouse brain lysates. In accordance with the recombinant GephE-based ITC

results, α9-11 but not α8, could retain wild-type gephyrin on the beads (Fig. 3-2c). Thus, our peptides not only bind to GephE *in vitro*, but also to full-length wild-type gephyrin from adult mouse brain. The presence of phosphorylations in native gephyrin was verified using phosphospecific (Kuhse et al., 2012) antibodies (data not shown).

3.3.3 Crystal structure analyses of GephE in complex with variants of $GABA_AR$ α3 fragments

Co-crystallization trials with GephE in combination with either the medium-affinity $α11_{WT}$ peptide (FNIVGTTYPIN) or the high-affinity $α11_{SL}$peptide (FNIVGSLYPIN) yielded four co-crystal-structures belonging to two crystal forms (Table 3-4): (1) Hexagonal crystals (space group $P6_1$), which were previously described for the GephE-GlyR complex (Sola et al., 2004), diffracting to resolutions of 3.6 and 4.1 Å (Table 3-4). (2) Orthorhombic crystals (space group $P2_12_12$) diffracting to 2.7 Å resolution (Fig.3-4,5 and Table 3-4) which were related to GephE-GlyR complexes and GephE apo-structures (Kim et al., 2006; Maric et al., 2014c).The $α11_{WT}$ and $α11_{SL}$ peptides were clearly defined in the electron density maps (Fig. 3-6 and 3-9) in both crystal forms, allowing us to model either all or the first 9 residues of the 11-mer $GABA_AR$ peptide fragment (Fig. 3-4,5 and 3-6 and 3-9).

3.3.4 The $GABA_AR$ α3 and GlyR β subunits share an overlapping binding site on gephyrin

The crystal structures of GephE in complex with the $GABA_AR$ α3 derived peptide fragments revealed (Fig. 3-4a) that GephE is present as a homodimer with each subunit consisting of foursubdomains (Kim et al., 2006; Maric et al., 2014c; Sola et al., 2004). The GephE dimer is in complex with two symmetrically arranged receptor fragments (Fig. 3-4a) where subdomains III and IV of one GephE monomer as well as subdomain IV of a second monomer (IV') together from a common receptor binding site (Fig. 3-4b,c) for peptides derived from either the $GABA_AR$ α3 or the GlyR β subunit (Kim et al., 2006; Maric et al., 2014c; Sola et al., 2004). The interactions of the peptides derived from either receptor with subdomain III are nearly identical, while the interactions with subdomain IV and IV` are receptor-specific (Fig.3-5, 3-7 and 3-8).

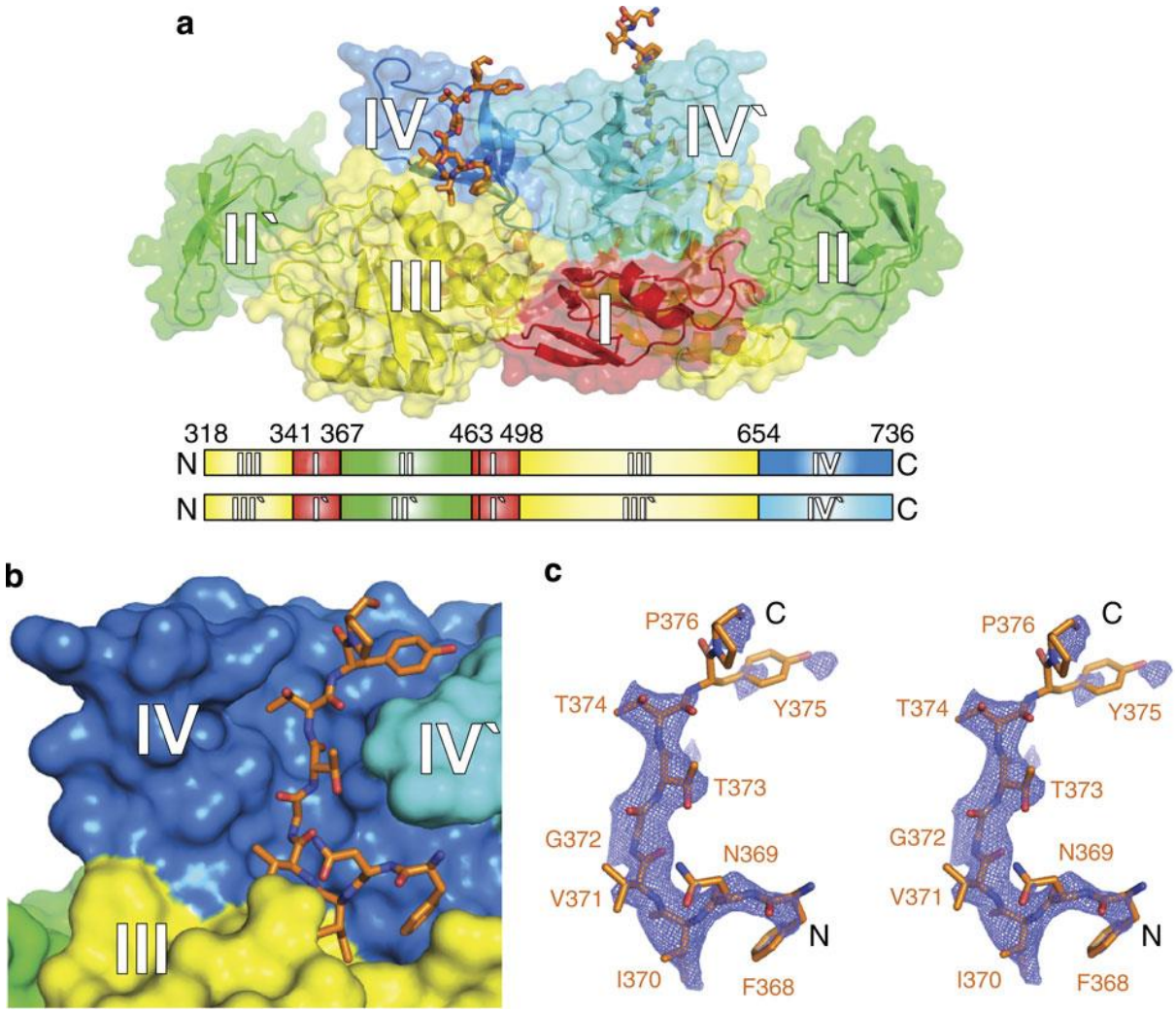

Figure 3-4. (Fig.3 in the published manuscript). X-ray crystal structure of GephE in complex with the GABA$_A$R α3 peptide fragment. (a) Cartoon representation of GephE in complex with the GABA$_A$R α3-derived peptide α11$_{WT}$ (PDB-ID: 4TK1) colour-coded according to its subdomain architecture as indicated (scheme at the bottom). The residues of α11$_{WT}$ resolved in the structure (^{368}FNIVGTTYP^{376}) are shown as a stick model in orange. **(b)** Close-up view into the binding pocket. Surface representation of the GephE-binding pocket coloured according to **a**. The GABA$_A$R peptide is tightly packed into the cleft formed by subdomains III and IV from one monomer, as well as subdomain IV' from the other monomer. **(c)** F_o-F_c omit electron density map of the GABA$_A$R α3 peptide (stereo representation) contoured at an rmsd of 2.5 in blue with the modeled peptide in stick representation.

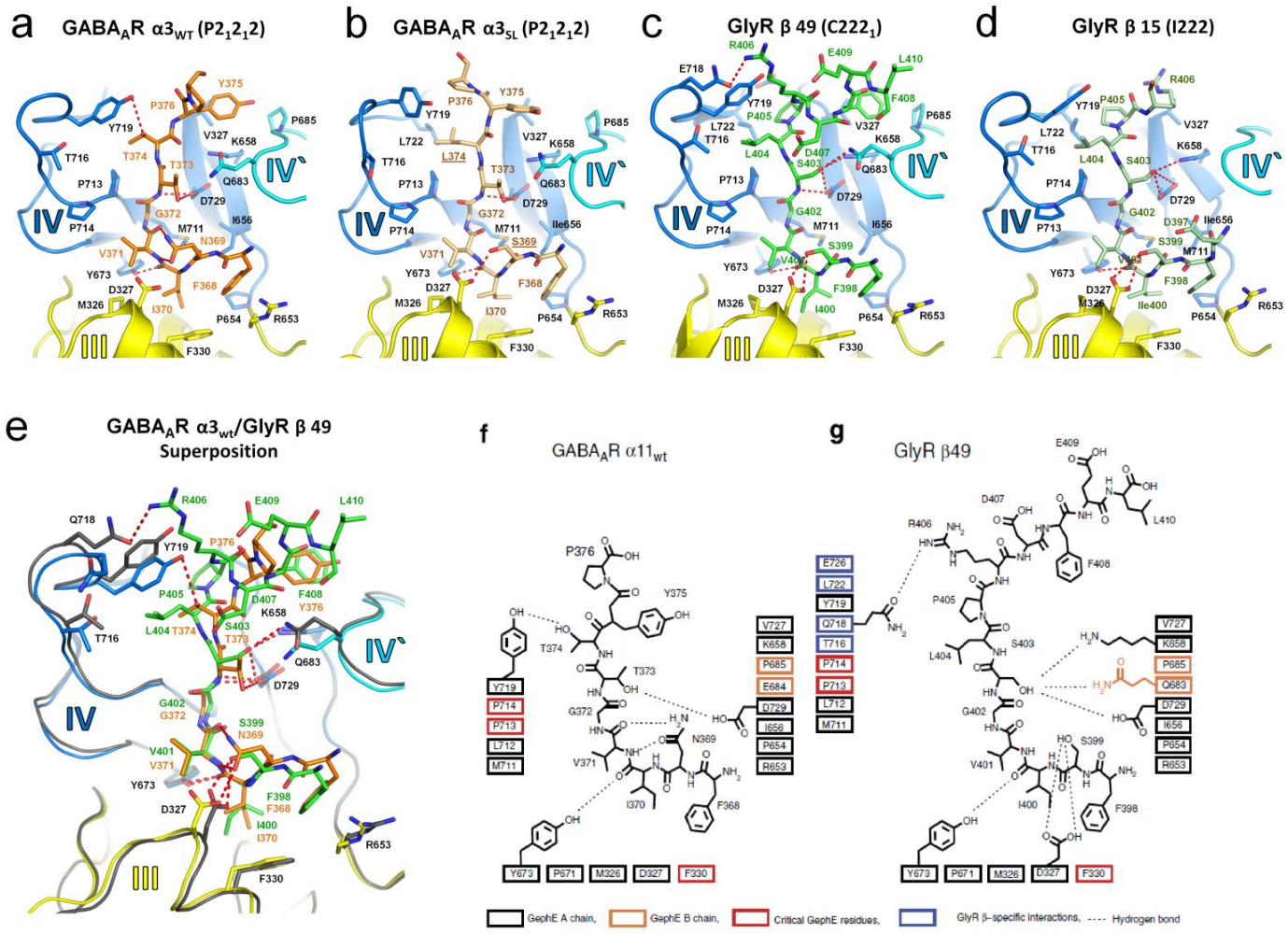

Figure 3-5. Molecular details of subunit-specific gephyrin interactions. (Fig.4 in the published manuscript) Close up view of the interactions between GephE with **(a)** GABA$_A$R α3 wild-type-derived peptide (PDB-ID 4TK1), **(b)** α11$_{SL}$ peptide (PDB-ID 4TK3) and **(c,d)** GlyR β-derived peptides (PDB-ID 2FTS and 4PD1) as well as **(e)** a superposition and **(f,g)** schematic 2D representations of the GlyR β wild-type and GABA$_A$R α3 wild-type interactions. In **a–d**, residues mediating the interactions are highlighted in stick representation and are numbered (coloured for the peptides, black for GephE). GephE residues located in subdomain III are coloured in yellow, residues from subdomain IV in marine blue and GephE residues derived from the other subdomain IV' in cyan. Hydrogen bonds are shown as dotted red lines. Note that the N-terminal-binding motifs engage in conserved interactions, whereas the C-terminal halves interact differentially with GephE.

GABA$_A$R α3 and GlyR β-derived peptides also engagein receptor-specific interactions. A direct comparison of the two GephE- α11$_{WT}$ structures with the two GephE- α11$_{SL}$ structures (Fig. 3-5a,b and 3-7) as well as the corresponding GlyR β structures (Fig. 3-5 c,d) (Kim et al., 2006; Maric et al., 2014c) revealed distinct interactions with either receptor (Fig. 3-5 e-g).

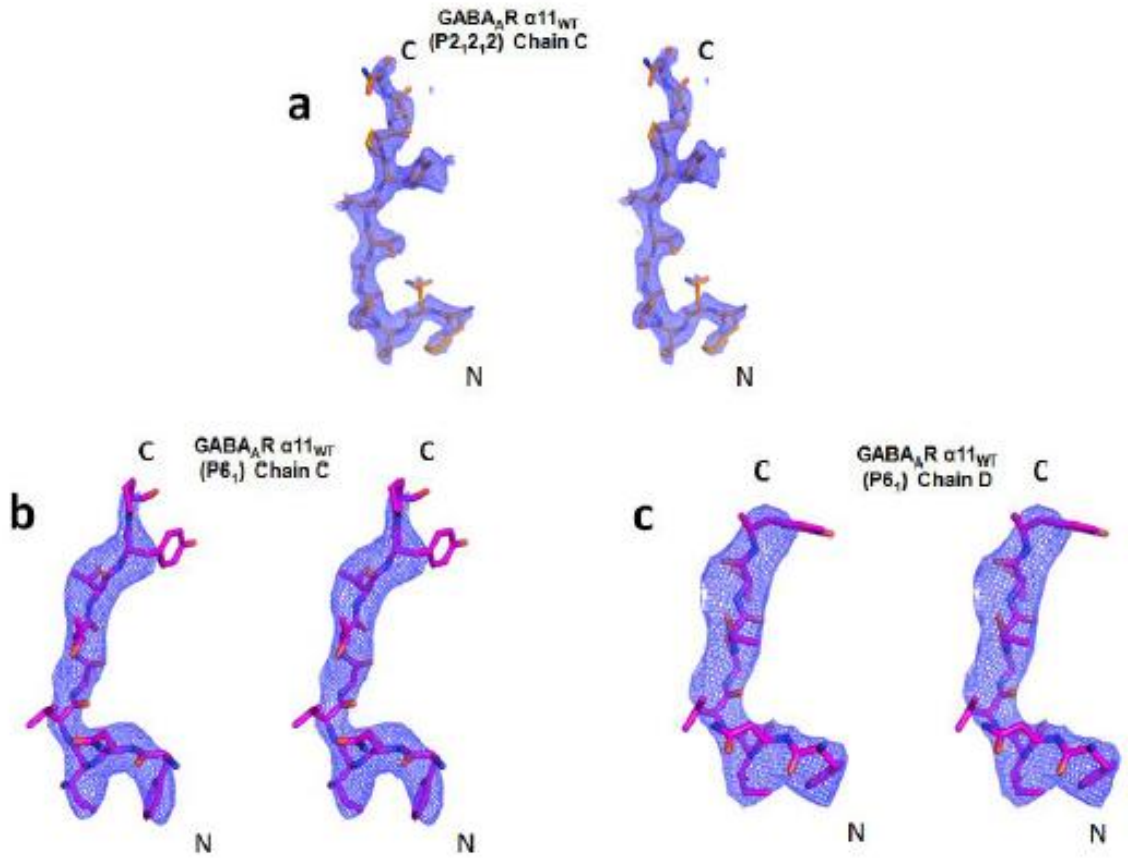

Figure 3-6. Omit electron density of the GABA$_A$R α3 peptides. (Supplemental Fig.4 in the published manuscript). Stereo images of F_o-F_c omit electron density maps for the GABA$_A$R α11$_{WT}$ peptides contoured at an rms deviation of 2.5.

Based on the largely identical N-terminal interactions for $\alpha 11_{WT}$ and GlyR β derived peptides, we defined the critical N-terminal aromatic residue, which is conserved in all gephyrin-binding receptor derived peptides as position 1 (Phe368 in GABA$_A$R α3, Phe398 in GlyR β) and, based on previous mutational studies (Maric et al., 2011), this residue corresponds to Tyr340 in GABA$_A$R α1 and Tyr339 in GABA$_A$R α2.The main chains of the conserved N-terminal residues (positions 1-7: GABA$_A$R α3^{368}FNIVGTT^{374}, GlyRβ ^{398}FSIVGSL^{404} (Kim et al., 2006; Maric et al., 2014c) adopted highly similar conformations (Fig. 3-5e), while their side chains formed subunit-specific interactions with gephyrin (Fig. 3-5e).

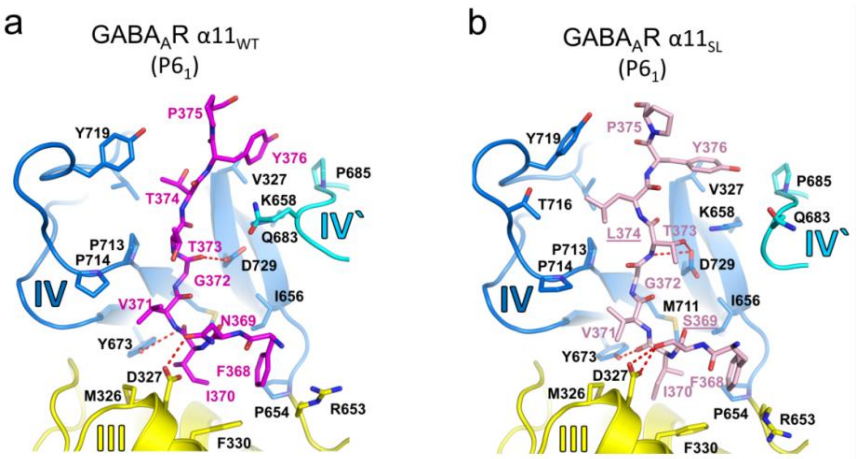

Figure 3-7. Molecular details of subunit-specific gephyrin interactions.(Supplemental Fig.2 in the published manuscript). Close up view of the interactions between GephE with **(a)** the α11$_{WT}$ peptide (PDB-IDs: 4TK2) and **(b)** the α11$_{SL}$ peptide (PDB-IDs: 4TK4) based on the hexagonal crystals (space group P6$_1$) diffracting to resolutions of 4.1 and 3.6 Å, respectively. Residues mediating the gephyrin-receptor interaction are shown in stick representation superimposed on ribbon diagrams of gephyrin. GephE residues located in subdomain II are colored in yellow, residues from subdomain IV in marine blue and GephE residues derived from the other subdomain IV' in cyan as indicated. Critical residues of GephE are numbered in black and all residues of the peptides are numbered in color. Hydrogen bonds are shown as dotted red lines.

The central four-stranded β-sheet of GephE subdomain IV and the first α-helix and several neighboring residues of subdomain III engaged inidentical interactions with the peptides from either the GABA$_A$R α3 or GlyR β subunits (positions 1-5 corresponding to GABA$_A$R ^{368}FNIVG^{372} and GlyR ^{398}FSIVG^{402}),with the exception of position 2 (Asn369 in GABA$_A$R, Ser399 in GlyR). Notably, the hydrogen-bonded interactions of GABA$_A$R Asn369 with GephE Asp327 appeared to be less optimal when compared to the corresponding hydrogen bonds of Ser399 in GlyR β, thereby contributing to the lower affinity of the GABA$_A$R. The subsequent residues of the GABA$_A$R and GlyR loops (positions 6-7, GABA$_A$R ^{373}TT^{374}, GlyR ^{403}SL^{404}) interacted with gephyrin differently: GlyR β Ser403 allows the formation of additional hydrogen bonds compared to GABA$_A$R Thr373 and, in addition, GABA$_A$R Thr374 could not engage as efficiently with the large hydrophobic pocket formed by Thr716, Tyr719 and Leu722 of gephyrin compared to the corresponding Leu404 in the GlyR β subunit. The C-terminal residues (positions 8-11:GABA$_A$R^{375}YPIN^{378}, GlyR ^{405}PRDFEL^{410}) differed substantially in both their side chain interactions and main chain conformations. Nonetheless, GABA$_A$R α3 Tyr375 at position 8 contacted roughly the same hydrophobic interface on the second GephE monomer as GlyR β Phe408 at position 11. Remarkably, the elongated 49 residue GlyR βloop (β49) forms a short α-helical element, while the GABA$_A$R-derived peptides displayed no secondary structure, and, as a result, the overall GephE-GlyR β-binding interface is significant larger (991 Å^2 buried surface area upon complex formation) than the corresponding GephE-GABA$_A$R α3-binding interface (835 Å^2 buried surface area)

(Tables 3-2 and 3-3). This may additionally contribute to the reduced affinity of $GABA_AR$ α3 to gephyrin compared to GlyR β.

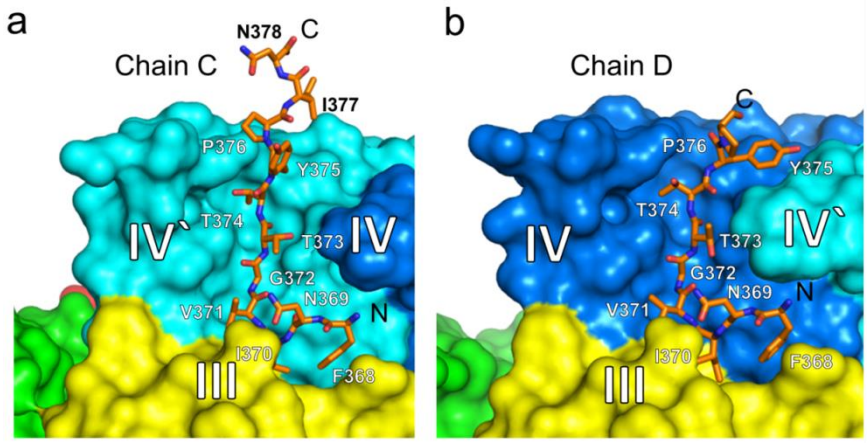

Figure 3-8. Comparison of the $GABA_AR$ $α11_{WT}$ peptide fragments bound to a single GephE dimer. (Supplemental Fig.3 in the published manuscript). Surface representation of the GephE binding pocket colored according to the subdomain architecture of GephE. The $GABA_AR$ $α11_{WT}$ peptides are bound in the cleft formed by subdomains III and IV from one monomer, as well as subdomain IV from the other monomer. Note that Tyr375 adopts a different orientation in chain C due to a crystal contact as shown in (**a**). Additionally, two more $GABA_AR$ residues are resolved in chain C (**a**) compared to chain B (**b**), which are stabilized by contacts with a symmetry related GephE molecule.

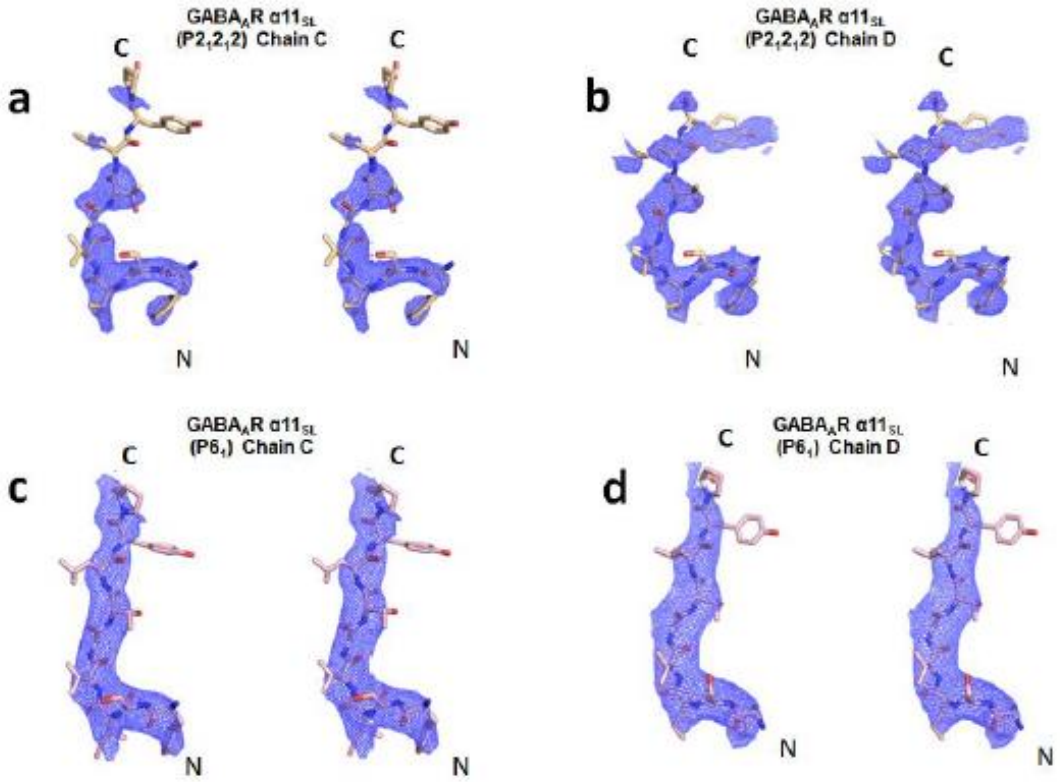

Figure 3-9. Omit electron density of the $GABA_AR$ α3 peptides. (Supplemental Fig.3 in the published manuscript). Stereo images of F_o-F_c omit electron density maps for the $GABA_AR$ $α11_{SL}$ peptides contoured at an rms deviation of 2.5.

Comparisons of the GephE- α_{11}WT (PDB: 4TK1, 4TK2), GephE- $\alpha11_{SL}$ (PDB: 4TK3, 4TK4), GephE-apo (PDB: 4PDO, 2FU3) and GephE-GlyR β (PDB: 4PD1 and 2FTS) complex structures derived from four different crystal forms revealed that the structure of the gephyrin E-domain remains largely unchanged upon ligand binding. The observed structural differences are primarily due to crystal packing and the differences in the sequences of the bound ligands.

.Table 3-2. Comparison of the gephyrin interfaces of $GABA_AR$ α3 and GlyR β.

##	$GABA_AR$ α3	H-bond	ASA	BSA	Δ^iG	##	GlyR	H-bond	ASA	BSA	Δ^iG
1	PHE 368		236.37	119.22 |||||	1.88	1	PHE 398		235.84	105.31 |||||	1.63
2	ASN 369		98.89	34.69 ||||	-0.48	2	SER 399	H	77.06	29.34 ||||	-0.14
3	ILE 370	H	152.90	148.98 |||||||||	1.80	3	ILE 400	H	159.40	159.24 |||||||||	1.77
4	VAL 371		102.83	84.29 ||||||||	1.31	4	VAL 401		117.16	87.25 |||||||	1.33
5	GLY 372		77.21	73.10 |||||||||	0.40	5	GLY 402		73.13	66.47 |||||||||	0.40
6	THR 373	H	114.47	53.04 |||||	-0.20	6	SER 403	H	90.86	59.57 ||||||	-0.55
7	THR 374		122.81	89.53 |||||||	1.01	7	LEU 404		122.39	95.53 |||||||	1.50
8	TYR 375		209.27	79.09 ||||	1.06	8	PRO 405		121.15	100.25 ||||||||	1.59
9	PRO 376		166.51	1.84 |	0.03	9	ARG 406	H	185.70	60.46 ||||	0.16
						10	ASP 407		80.45	0.00	0.00
						11	PHE 408		180.34	81.92 |||||	1.30
						12	GLU 409		124.14	0.00	0.00
						13	LEU 410		208.27	0.00	0.00

##	$GABA_AR$ α3	H-bond	ASA	BSA	Δ^iG	#	GlyR	H-bond	ASA	BSA	Δ^iG
1	PHE 368		236.37	37.89 ||	-0.16	1	PHE 398		235.84	15.30 |	0.07
2	ASN 369		98.89	12.57 ||	0.08	2	SER 399		77.06	2.59 |	-0.01
3	ILE 370		152.90	0.00	0.00	3	ILE 400		159.40	0.00	0.00
4	VAL 371		102.83	0.00	0.00	4	VAL 401		117.16	0.00	0.00
5	GLY 372		77.21	0.00	0.00	5	GLY 402		73.13	0.00	0.00
6	THR 373		114.47	27.09 |||	0.33	6	SER 403	H	90.86	20.93 |||	-0.06
7	THR 374		122.81	4.54 |	-0.05	7	LEU 404		122.39	0.13 |	-0.00
8	TYR 375		209.27	64.13 ||||	0.25	8	PRO 405		121.15	0.00	0.00
9	PRO 376		166.51	5.03 |	0.08	9	ARG 406		185.70	0.00	0.00
						10	ASP 407		80.45	12.44 ||	0.03
						11	PHE 408		180.34	74.27 |||||	1.17
						12	GLU 409		124.14	0.00	0.00
						13	LEU 410		208.27	19.64 |	-0.01

ASA = Accessible Surface Area in Å², BSA = Buried Surface Area in Å², ^iG = Solvation energy effect in kcal/mol, |||| = Buried area percentage, one bar per 10% , Conserved residues are colored.

PDBePISA (http://www.ebi.ac.uk/pdbe/pisa/) calculation of accessible surface area (ASA), buried surface area (BSA) and free energy contribution on a per residue basis (PDB entries 4TK1 and 2FTS). Strictly conserved positions are highlighted in red. The top tables describe the primary interface of one receptor peptide with one monomer of the GephE-dimer and the bottom tables the secondary interface formed by the same peptide with the other GephE monomer.

Table 3-3. Overall comparison of the gephyrin interfaces of $GABA_AR$ α3 and GlyR β.

Interaction	$GABA_AR$ α3		GephE (Chain A)		GlyR		GephE (Chain A)	
Solvent-accessible area, $Å^2$								
Interface	683.8	53.4%	519.2	2.5%	845.3	47.6%	664.8	3.1%
Total	1281.3	100.0%	20596.8	100.0%	1775.9	100.0%	21148.1	100.0%
Solvation energy, kcal/mol								
Isolated structure	-2.4	100.0%	-390.5	100.0%	-4.0	100.0%	-404.6	100.0%
Gain on complex formation	-6.8	285.1%	-1.8	0.5%	-9.0	227.3%	-2.6	0.6%
Interaction	$GABA_AR$ α3		GephE (Chain B)		GlyR		GephE (Chain B)	
Solvent-accessible area, $Å^2$								
Interface	151.2	11.8%	155.1	0.7%	145.3	8.2%	157.7	0.7%
Total	1281.3	100.0%	21206.4	100.0%	1775.9	100.0%	21131.3	100.0%
Solvation energy, kcal/mol								
Isolated structure	-2.4	100.0%	-397.1	100.0%	-4.0	100.0%	-404.8	100.0%
Gain on complex formation	-0.5	22.4%	0.5	-0.1%	-1.2	30.4%	-0.8	0.2%
Interaction	$GABA_AR$ α3		GephE (Chain A and B)		GlyR		GephE (Chain A and B)	
Solvent-accessible area, $Å^2$								
Interface	835.0	67.2%	674.3	3.2%	990.6	55.8%	822.5	3.8%
Total	1281.3	100.0%	20901.6	100.0%	1775.9	100.0%	21139.7	100.0%
Solvation energy, kcal/mol								
Isolated structure	-2.4	100.0%	-393.8	100.0%	-4.0	100.0%	-404.7	100.0%
Gain on complex formation	-7.3	307.5%	-1.3	0.4%	-10.2	257.7%	-3.4	0.8%

Calculations of the solvent-accessible surface and the resulting solvation energy (PDB entries 4TK1 and 2FTS) with PDBePISA (http://www.ebi.ac.uk/pdbe/pisa/). Shown are the interfaces of the $GABA_AR$ α3(left) and the GlyR β(right) peptide engaging with GephE chain A (top), chain B (middle) and both simultaneously (bottom). The total GlyR peptide surface (1776 $Å^2$) is larger than the total $GABA_AR$ surface (1281$Å^2$). 67% of the $GABA_AR$ peptide and 56% of the GlyR peptide surface directly contact gephyrin. Together this results in large gephyrin interaction surfaces for the GlyR (991 $Å^2$) and the $GABA_AR$ (835$Å^2$) peptides. Note that both peptides primarily interact with one monomer of the GephE dimer, which contributes 79.5% in case of the $GABA_AR$ peptide and 85.3% in case of the GlyR peptide to the total interaction surface.

Table3-4. Data collection and structure refinement

		GephE+ $\alpha11_{WT}$		GephE+ $\alpha11_{SL}$	
Beamline		ID 23-2	ID 14-4	ID 23-2	ID 14-4
Wavelength (Å)		0.8726	0.9393	0.8726	0.9393
Space group		P 2_1 2_1 2	P 6_1	P 2_1 2_1 2	P 6_1
Unit cell Parameters a, b, c (Å)		110.44, 157.69, 51.01	164.5, 164.5, 129.4	110.00, 157.20, 51.03	160.2, 160.2, 127.9
Resolution limits (Å)		48.6- 2.7	49.72- 4.1	48.53-2.7	67.88- 3.6
R_{sym}[a]		0.212 (1.150)	0.202 (1.030)	0.164 (1.283)	0.158 (0.956)
R_{pim}[b]		0.144 (0.793)	0.115 (0.586)	0.107 (0.848)	0.071 (0.433)
$CC_{1/2}$		0.980 (0.583)	0.984 (0.456)	0.993 (0.444)	0.993 (0.427)
Redundancy		5.7 (5.7)	4.1 (4.1)	6.1 (6.2)	5.6 (5.7)
Unique reflections		25198	15728	25090	21728
Completeness		0.99 (0.99)	0.99 (1.0)	1.0 (1.0)	1.0 (1.0)
<I/ σI>[c]		7.8 (1.6)	6.0 (1.6)	9.1 (1.3)	7.6 (1.7)
R [d] /R_{free}[e]		0.215/ 0.262	0.183/ 0.236	0.229/ 0.267	0.176/ 0.216
Deviation from ideal values					
Bond distances (Å)		0.007	0.002	0.002	0.003
Bond angles (°)		1.295	0.584	0.656	0.707
Torsion angles (°)		15.947	11.441	12.150	11.574
Planar groups (Å)		0.005	0.003	0.003	0.003
Chiral centers (Å^3)		0.074	0.022	0.023	0.026
Ramachandran statistics (%) (Preferred/Allowed/Outliers)[f]		96.4/ 3.4/ 0.2	98.2/ 1.7/ 0.1	98.1/ 1.9/ 0.0	97.4/ 2.6/ 0.0
Overall average B factor(Å^2)		50.5	160.4	72.1	128.5
No of atoms	Protein	6209	6277	6296	6259
	Peptide	159	136	133	141
	Monomer A	50.0	151.4	73.0	121.4
	Monomer B	52.3	166.8	74.6	133.9
	Peptide A	48.4	225.8	97.4	165.8
	Peptide B	72.6	213.9	87.0	165.6
Coordinate error (Å)[g]		0.30	0.53	0.39	0.51

All the terms in the table are defined as according to the table 2-1.

3.3.5 Thermodynamic dissection of the receptor specificity of gephyrin

Based on the gephyrin-GABA$_A$R α3 X-ray crystal structures, we designed and synthesized a range of point mutated GABA$_A$R α3 peptide fragments and determined the thermodynamic basis of their gephyrin binding by ITC (Fig.3-10). Between the structurally resolved GABA$_A$R (^{368}FNIVGTTYPIN^{378}) and GlyR (^{398}FSIVGSLPRDFEL^{410}) fragments, only the four underlined residues are conserved (Fig.3-10a). Three of seven non-conserved residues are located at the C-terminal end (GABA$_A$R ^{376}PIN^{378}, GlyR ^{406}RDF^{408}), which is the region where the primary structural differences are found. Nonetheless, exchange of these residues between peptides derived from either GABA$_A$R or GlyR did not alter the overall binding affinity significantly (Fig. 3-10 a), thus indicating comparable binding contributions. Among the four remaining receptor subunit-specific residues, position 2 (GABA$_A$R α3 Asn369, GlyR β Ser399) is located within the conserved N-terminal motif, which mediates the mutually exclusive receptor-binding to gephyrin. ITC measurements verified the structural evidence (Fig.3-10 a-d); Ser399 could engage in more optimal hydrogen bonding interactionswith GephE compared to Asn369. The exchange of Ser399 with an Asn369 in GlyR resulted in an at least 4-fold reduced affinity (8.3±0.1 to 25.5 µM), *vice versa*, introduction of Ser for Asn369 in GABA$_A$R increased the affinity at least 6-fold (190±30 to 33±6 µM) (Fig.3-10a).

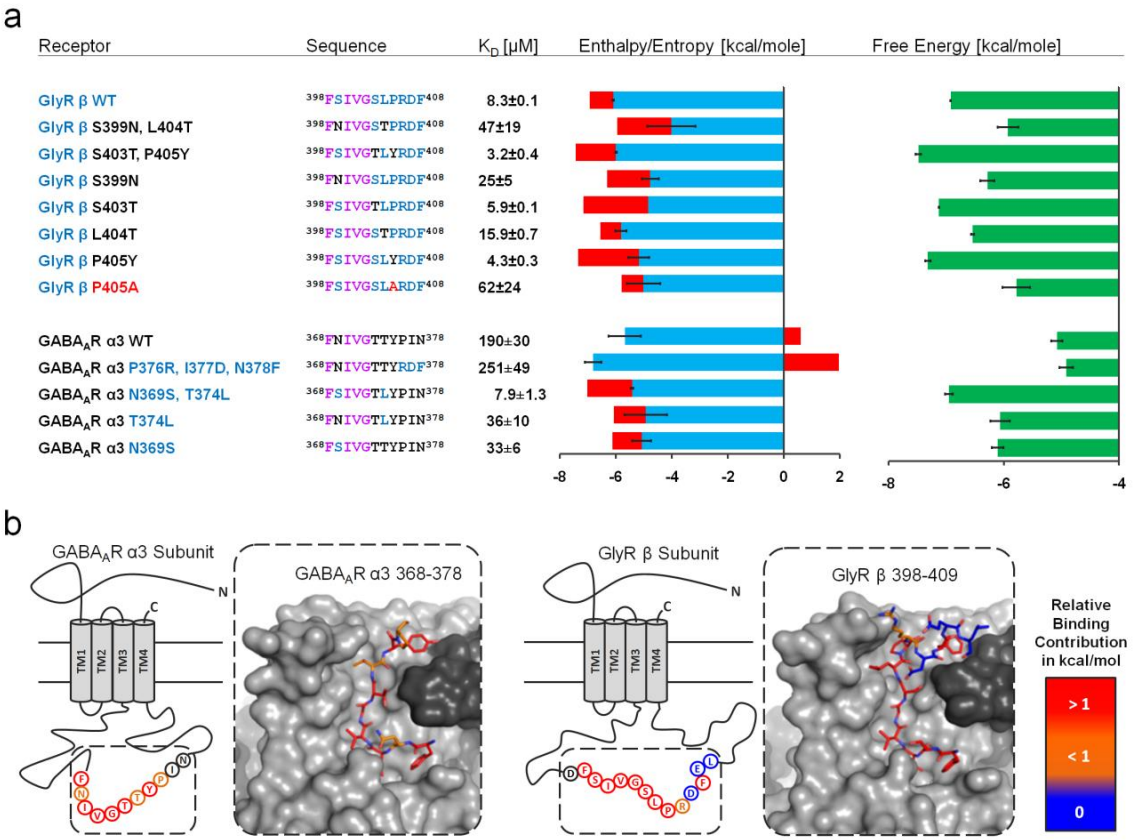

Figure 3-10. Thermodynamic dissection of the subunit specificity of gephyrin. (Fig.5 in the published manuscript) (a) Different contributions of the binding enthalpy and entropy to the overall

free energy. Residues conserved among the GlyR β and $GABA_AR$ α3 subunits are shown in magenta, GlyR β residues in blue and $GABA_AR$ α3 residues in black. The GlyR β peptide displayed a 23-fold higher affinity than the corresponding $GABA_AR$ peptide. Subunit-specific residues were exchanged between both receptor subunits. Note that the gephyrin affinity can be maximized by combining hydrophobic residues of GlyRs and $GABA_ARs$ (GlyR S403Tand $GABA_AR$ P405Y). Remarkably, full GlyR-like binding affinity can be reconstituted for the $GABA_AR$ fragment by only two mutations, N369S and T374L. Enthalpy, entropy and free energy bar graphs are averages (with their standard deviations indicated by the error bars) of at least three ITC measurements. **(b)** Differential binding of $GABA_ARs$ and GlyRs to an overlapping gephyrin-binding site. Structures of the GlyR and $GABA_AR$ peptides in stick representation colour-coded according to the relative binding contribution (high (>1 kcal mol^{-1}) in red, low (0-1 kcal mol^{-1}) in orange and none (0 kcal mol^{-1}) in blue) with the gephyrin surface shown in grey. The corresponding sequences of the full-length intracellular loops of $GABA_AR$ α3 and GlyR β are shown below using the same colour code. Note that different ligand residue positions mediate the critical gephyrin interactions.

The three remaining subunit-specific residues were located near the center of the receptor peptide fragments (positions 6-8, $GABA_AR$ ^{373}TTY^{375}, GlyR ^{403}SLP^{405}). The ITC analysis revealed that both, the Ser403Thr as well as the Pro405Tyr exchange, enhanced the peptide fragment affinity (8.3±0.1 to 5.9±0.1 and 8.3±0.1 to 4.3±0.3 µM, respectively), and that this effect was based on additional hydrophobic interactions as reflected by the larger contribution of the entropy term to the overall affinity (Fig.3-10a). Exchange of GlyR Leu404 with the corresponding $GABA_AR$ Thr reduced the GlyR affinity 2-fold (8.3±0.1 to 15.9±0.7 µM). In contrast, the corresponding exchange yielded a 5-fold higher affinity (190±30 to 36±10 µM) for the $GABA_AR$ accompanied by a gain in entropy. This finding was in line with the additional hydrophobic interactions as indicated by the structural analysis (Fig.3-4a-d). Remarkably, at position 8, the GlyR and the $GABA_AR$ subunit engaged in critical, yet different hydrophobic interactions, with either a Pro in case of the GlyR β subunit or a Tyr in the $GABA_AR$ α3 subunit. The critical nature of this ligand position was demonstrated by the corresponding Pro-to-Ala variant which showed an at least 7-fold reduced affinity (8.3±0.1 to 62±24 µM) (Fig.3-10a) and was in line with a loss of a large hydrophobic contact area as indicated by the crystal structure.

Finally, a double mutation at positions 2 and 7 within both receptor peptide fragments reduced the GlyR fragment affinity 6-fold (8.3±0.1 to 47±19) and improved the $GABA_AR$ fragment affinity 25-fold (190±30 to 7.9±1.3 µM), yielding in the latter case an affinity identical to the GlyR fragment (8.3± 0.1 µM) (Fig. 3-11). Thus, the ITC experiments provide a detailed picture of the thermodynamic basis of the subunit-specific gephyrin interactions. Together with the crystal structures the thermodynamic data complete the picture of how $GABA_ARs$ and GlyRs are recruited alternatively to postsynaptic sites by engaging with gephyrin as summarized in Fig. 3-10b.

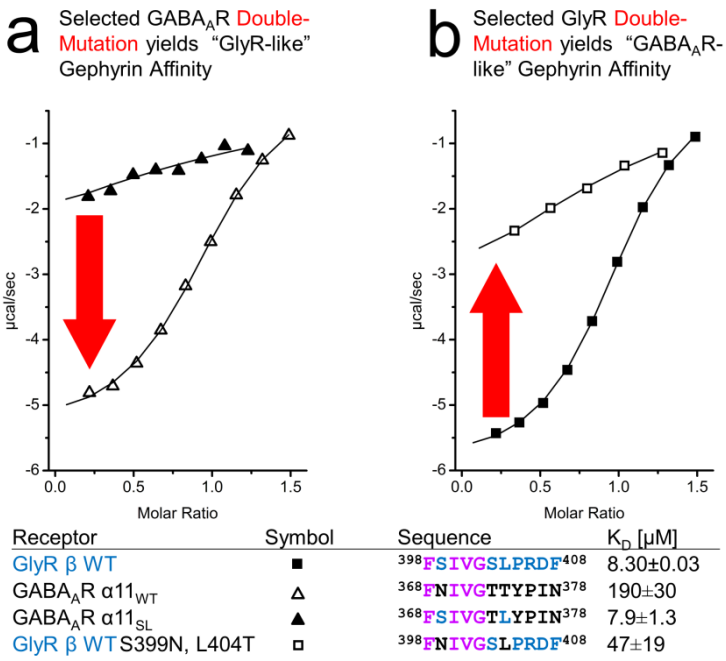

Figure 3-11. Two residues primarily contribute to the difference in affinity between GABA$_A$R α3 and GlyR β. (Supplemental Fig.6 in the published manuscript).

Binding isotherms of GephE titrated with **(a)** the GABA$_A$R α11$_{WT}$ or the GABA$_A$R α11$_{SL}$double mutant and **(b)** with the GlyR βwild type or the GlyR β S399N/L404T double mutant. The corresponding sequences and calculated K_D values are shown below. Note that positions 2 and 7 within the receptor ligands largely determine the receptor subunit affinity to gephyrin and hence gephyrin's distinct subunit preference for GlyR β over GABA$_A$R α3.

3.4 DISCUSSION

Despite its fundamental importance for the function of the inhibitory synapse, the interactions with gephyrin that mediate the anchoring and accumulation of synaptic GABA$_A$Rs are poorly understood. To address this we designed GABA$_A$R α3-derived gephyrin-binding peptides, which enabled the structural analysis of the gephyrin-GABA$_A$R complex and revealed how GABA$_A$Rs containing the α3 subunit are clustered at synaptic sites. Despite their binding to an overlapping site in the gephyrin protein compared to GlyRs, GABA$_A$Rs engage in subunit-specific interactions allowing for an alternative recruitment of inhibitory receptors by gephyrin. Specifically, our study identifies two residues as major determinants for gephyrin´s distinct preference for the GlyR β subunit over the GABA$_A$R α3 subunit. Thus, we have provided the structural basis for the mutually exclusive binding of GABA$_A$R and GlyR to the scaffold protein gephyrin (Maric et al., 2011).

Here, we present the structural and thermodynamic analysis of gephyrin binding to short peptides, either native to the GABA$_A$R α3 subunit or rationally designed. Notably, the full-length intracellular loop of GABA$_A$R α3 displays an enhanced affinity (K_D = 5.3 µM)(Maric et al., 2011) compared to the truncated α11$_{WT}$ variant analyzed here. The 11-mer mediates ~70% of the free energy and ~86% of the enthalpy compared to the GABA$_A$R α3 full-length intracellular loop (Tretter et al., 2011) when interacting with gephyrin. While the molecular basis of the enhanced binding cannot be fully explained, the beneficial entropic contribution

of the full-length fragment suggests that secondary/tertiary structure effects in the full-length intracellular loop present the core binding site in a more favorable orientation and are thus responsible for its stronger binding. Furthermore, the $\alpha11_{WT}$ peptide (^{368}FNIVGTTYPIN^{378}) occupies an overlapping binding site (Fig. 3-4e) compared to the GlyR fragment resolved earlier (^{398}FSIVGSLPRDFELS^{411}), which, in turn, could be used to completely block gephyrin-binding of $GABA_AR$-derived full-length intracellular loops (Maric et al., 2011). Additionally, single point-mutations within the core region of the peptides (^{368}FNIVGTTY^{375}) that could be resolved in the structural analysis presented here were shown (Maric et al., 2011) to completely abolish gephyrin-binding of the full-length loop and, *vice versa*, loops missing the core motif were demonstrated to completely lose their ability to mediate receptor clustering in neurons or to mediate binding in yeast-two hybrid experiments (Maric et al., 2011). Taken together, it can be concluded that the remainder of the intracellular loop exerts a critical enhancing effect but does not provide a second independent binding site that would be sufficient for binding in primary hippocampal neurons, yeast-two hybrid, ITC or pull-down assays.

A direct comparison of the gephyrin affinity to the core binding sites of GlyR and $GABA_AR$ confirmed an approximately 25-fold preference of gephyrin for GlyRs containing the β subunit over $GABA_ARs$ containing the α3 subunit. The structural and thermodynamic mutational analysis revealed that Ser399 of the GlyR binds more effectively than the corresponding Asn369 in the $GABA_AR$ α3 subunit, while Leu404 of the GlyR creates a larger hydrophobic binding interface than the corresponding $GABA_AR$ α3 residue Thr374 (Fig. 3-5 and Fig. 3-8). Together the slight differences in the side chain interactions synergistically result in the distinct subunit preference of gephyrin for GlyRs over α3-containing $GABA_ARs$.

Gephyrin mediates $GABA_AR$ α3 and GlyR β binding via a large groove formed by subdomainsIII and IV (Fig. 3-4b) within GephE. The N-terminal part of the receptor core binding sites relies on highly conserved receptor interactions and involves hydrophobic contacts between Phe330 of gephyrin and the respective aromatic residues in the receptors, but also critical hydrogen bonds mediated by Tyr673 and Asp327 of gephyrin. We observed that the seven N-terminal residues contribute the majority of the overall receptor-binding strength, and that the peptide-binding motif derived from the GlyR β subunit displays the highest gephyrin-binding potency. GlyR and $GABA_AR$ colocalization and agonist co-transmission were reported earlier (Muller et al., 2006; Rahman et al., 2013). It was shown that up to 35% of all GlyRs colocalize with $GABA_ARs$ in the hypoglossal nucleus (Muller et al., 2006) and that 20-40% of all miniature postsynaptic currents (mIPSCs) recorded from respiratory glycinergic neurons are mixed mIPSCs (Rahman et al., 2013) that result from the co-release of GABA and glycine. The competition between $GABA_ARs$ and GlyRs for an overlapping gephyrin binding site, as shown here, suggests an interdependence of their

clustering as well as their transport to the synapse. Major determinants of the competition would be the ratio of free receptor binding sites in gephyrin and among the gephyrin-binding receptor subunits, the gephyrin-binding subunit number within a pentameric receptor and the posttranslational modifications of the respective motifs within these subunits (Mukherjee et al., 2011b; Specht et al., 2011). While $GABA_AR$ transport remains poorly characterized, GlyRs were shown to be retrogradely co-transported with gephyrin by the dynein motor complex via an interaction of the dynein light chain with the central linker of gephyrin (Maas et al., 2006). If $GABA_ARs$ would rely on the same pathway for their retrograde transport, both inhibitory receptor families would also compete for a common transport pathway, thus further intertwining their presence at inhibitory synapses. Finally, a recent study of the ultrastructure of spinal cord inhibitory synapses suggested that the $GABA_AR$/GlyR competition for gephyrin binding sites is regulated in an activity-dependent manner (Specht et al., 2013).

Overall the GephE-peptide structures (Table 3-3) display a high similarity,however, two out of eight peptide chains in the GephE-peptide complexes derived from the orthorhombic and hexagonal space groups exhibit obvious differences in the orientation of $GABA_AR$ Tyr375 (Fig. 3-7). We find that these changes are due to crystal contacts with a neighboring symmetry related molecule and therefore do not indicate a difference between the two receptor binding sites within a GephE dimer as suggested earlier (Sola et al., 2004). Accordingly, our structures clearly support the view that both receptor-binding sites within a single GephE dimer are identical and hence are occupied in a non-cooperative manner.

Our structural analysis demonstrates that the C-terminal halves of the GlyR and $GABA_AR$ gephyrin-binding core regions interact differently with gephyrin and occupy partially non-identical binding surfaces. The analysis of the chimeric peptide variants demonstrated that the C-terminal regions are crucial for the binding event by exhibiting an important enhancing effect. Furthermore, the structural and thermodynamic dissections revealed that the side chain interactions of $GABA_AR$ α3 residues Thr373, Thr374 and Tyr375 within this C-terminal receptor region are of major importance. Particularly, Tyr375, which is conserved among the α1, α2 and α3 $GABA_AR$ subunits, engages in critical hydrophobic interactions. Based on the sequence similarity of the gephyrin-binding region of the $GABA_AR$ α3 and α1 subunits and a previous mutagenesis study (Maric et al., 2011), the gephyrin-binding interface of the $GABA_AR$ α1 subunit can be predicted (Fig. 3-12).

The fact that different receptor subunits target gephyrin with unique binding motifs, which nonetheless engage in tight and specific interactions, allows for a subunit-specific posttranslational regulation of this interaction. To this end, our study provides a possible structural explanation for the previously described regulation of GABAergic transmission by the extracellular signal-regulated kinases/mitogen-activated protein kinases (ERK/MAPK) pathway mediated by phosphorylation of $GABA_AR$ α1 Thr345, which is conserved within the

gephyrin binding site of $GABA_AR$ α1-3 and corresponds to $GABA_AR$ α3 Thr373 (Fig. 3-12) (Bell-Horner et al., 2006). Furthermore, we provide a structural framework for future functional studies of phosphorylations at $GABA_AR$ α3Thr374 and Tyr375 and their corresponding $GABA_AR$ α1 and α2 residues, which are phosphorylated *in vivo* (Ballif et al., 2008; Munton et al., 2007). It can be assumed that post-translational modifications of these residues modulate the gephyrin-$GABA_AR$ affinity, and hence the residence time at the synapse in a similar fashion as reported for the protein kinase C (PKC) mediated phosphorylation of GlyR β Ser399 (Specht et al., 2011).

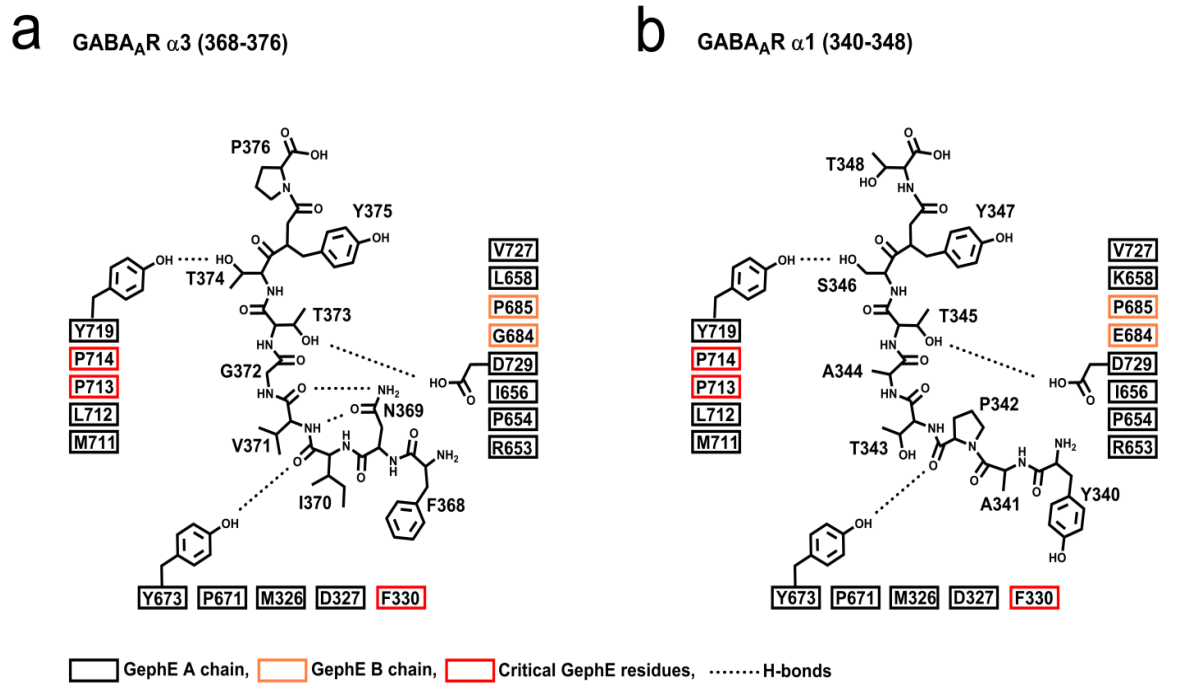

Figure 3-12. Schematic 2D representations of $GABA_AR$ α1 and α3 peptides binding to gephyrin. (Supplemental Fig.7 in the published manuscript). (a) Schematic representation of the GephE-$GABA_AR$ α3 interactions as derived from our crystal structures. **(b)** Based on the GephE-$GABA_AR$ α3 interactions, the sequence conservation between the corresponding residues in the α1 and α3 subunits and an earlier mutagenesis study (Maric et al., 2011) the interactions between gephyrin and the $GABA_AR$ α1 subunit were predicted.

In contrast to glutamate receptors for which bacterial homologs have been identified, no GlyR-related receptors have been identified in bacteria. Furthermore, GlyRs are also absent from invertebrates (Xue, 1998) and, in agreement with this observation, only those residues that are required for the receptor interaction are conserved among gephyrin proteins from vertebrates (Kim et al., 2006). In contrast, $GABA_AR$ α subunit related proteins have been identified in invertebrates (Xue, 1998) and, in order to decipher how the gephyrin-binding

motif evolved within the $GABA_AR$ family, we compared the corresponding sequences (Fig. 3-13). Similar to the gephyrin-binding motif of GlyRs, only vertebrate $GABA_ARs$, but not invertebrate $GABA_ARs$, contain a largely conserved gephyrin-binding sequence. This suggests that gephyrin-mediated $GABA_AR$ clustering evolved later than gephyrin-mediated GlyR clustering and that both motifs evolved independently.

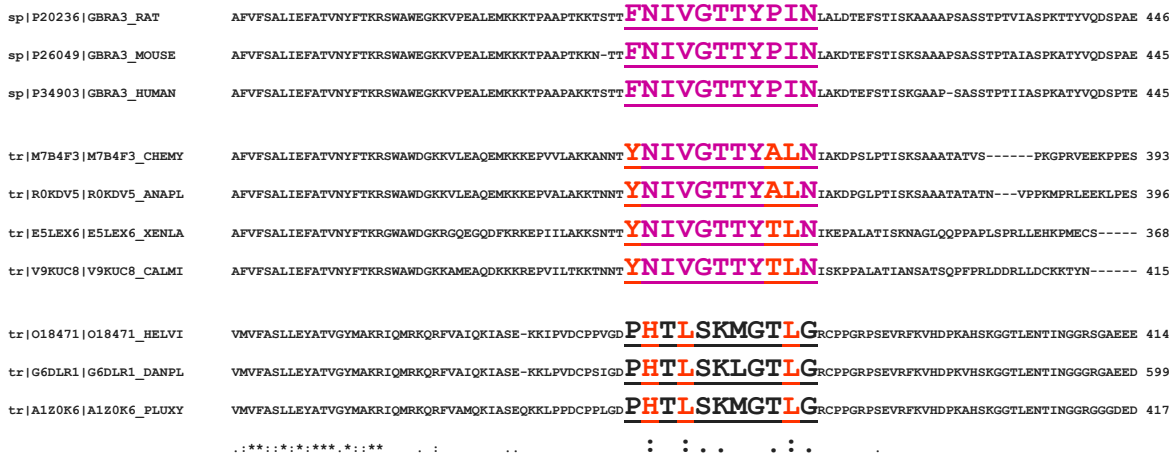

Figure 3-13. Multiple sequence alignment of $GABA_AR$ α3 homologs. (Supplemental Fig.8 in the published manuscript). Alignment of $GABA_AR$ α3 sequences from rat (*Rattus norvegicus)*, mouse (*Mus musculus*), human (*Homo sapiens*), green sea-turtle (*Chelonia agassizi*, CHEMY), domestic duck (*Anas boschas*, ANAPL), African clawed frog (*Xenopus laevis,* XENLA), Australian ghost shark (*Callorhynchus milii*, CALMI), tobacco budworm moth (*Heliothis virescens,* HELVI), monarch butterfly *(Danaus plexippus*, DANPL) anddiamondback moth(*Plutella xylostella*, PLUXY). Conserved residues interacting with gephyrin are highlighted in magenta, type-conserved residues in orange. Note that the gephyrin-binding motif is conserved among mammals (top), type-conserved among vertebrates (middle) and not conserved in invertebrates (bottom). Alignments were performed using ClustalW(http://www.ebi.ac.uk/clustalw).

As major mediators of fast synaptic inhibition $GABA_ARs$ are clinically relevant drug targets, and molecules that uncouple the central receptor-scaffold interaction at post-synaptic sites would therefore provide a powerful pharmacological tool with a possible therapeutic relevance. This principle has been demonstrated for the interaction between the *N*-methyl-d-aspartate (NMDA) type glutamate receptors and the scaffolding postsynaptic density protein 95 (PSD-95), which has been targeted by peptide-based inhibitors (Bach et al., 2008; Bach et al., 2009; Bach et al., 2012; Bach et al., 2011; Iskenderian-Epps and Imperiali, 2010; Sainlos et al., 2011). This approach has shown great promise both as a pharmacological tool (Chi et al., 2012; Sainlos et al., 2011) and, in particular, in the development of therapeutically relevant compounds (Dolgin, 2012; Flemming, 2012). We therefore propose that conceptually similar molecules could be used to interfere with the receptor-scaffold

interactions *in vivo* to modulate GABAergic and/or glycinergic transmission. Molecules that bind the universal N-terminal receptor-binding site with high affinity could be used as competitive inhibitors of gephyrin-mediated synaptic GlyR and $GABA_AR$ clustering. Additionally, the described alternative receptor recruitment of $GABA_ARs$ *versus* GlyRs by gephyrin, could form the basis for the development of subunit-specific modulators of either GABAergic or glycinergic transmission.

3.5 MATERIALS AND METHODS

3.5.1 Peptide synthesis, purification and validation.

Apart from four chimeric peptides, which were purchased as lyophilized powder from Genscript (USA), peptides were synthesized using Fmoc solid phase peptide synthesis. Preparative HPLC was performed on an Agilent 1100 system using a C18 reverse phase column (Zorbax 300 SB-C18, 21.2×250 mm) with a linear gradient of the binary solvent system of 0.1% trifluoroacetic acid (TFA) in H_2O/acetonitrile (ACN) (A: 95/5 and B: 5/95) with a flow rate of 20 ml/min. Analytical HPLC was performed on an Agilent 1100 system with a C18 reverse phase column (Zorbax 300 SB-C18 column, 4.6×150 mm), a flow rate of 1 ml/min, and a linear gradient of the binary solvent system of 0.1% TFA in H_2O/ACN (A: 95/5 and B: 5/95). Mass spectra were obtained with an Agilent 6410 Triple Quadrupole Mass Spectrometer instrument using electron spray ionization coupled to an Agilent 1200 HPLC system (ESI-LC/MS) with a C18 reverse phase column (Zorbax Eclipse XBD-C18, 4.6×50 mm), autosampler and diode-array detector using a linear gradient of the binary solvent system of 0.1% formic acid in H_2O/ACN (A: 95/5 and B: 5/95) with a flow rate of 1 ml/min. During ESI-LC/MS analysis evaporative light scattering (ELS) traces were obtained with a SedereSedex 85 Light Scattering Detector. The identity of all tested compounds was confirmed by ESI-LC/MS (Table 4-1), which also provided purity data (all >90%; UV and ELSD). All used peptides were water soluble at neutral pH in the millimolar range.

3.5.2 Protein expression and purification.

GephE (gephyrin P1 splice variant residues 318-736) as well as residues 378-425 of the large cytoplasmic loop of the GlyR β subunit (β-49) were expressed and purified as described earlier (Kim et al., 2006; Maric et al., 2011; Schrader et al., 2004). Pure fractions were pooled and concentrated using Vivaspin 3 kDa molecular weight cut-off (MWCO) centrifugal filter devices (Sartorius Stedim Biotech) to 1-20 mg/ml, aliquoted, flash-frozen and stored at -80 °C.

3.5.3 Protein conjugation for chemiluminescence detection. Purified GephE was conjugated with horse radish peroxidase (HRP) (Sigma Aldrich) as described earlier (Nakane and Kawaoi, 1974) to enable its detection by chemiluminescence. 5 mg lyophilized

HRP were dissolved in 1 ml conjugation buffer (50 mM Na_2CO_3, pH 8.0). After incubation with 1 ml of 50 mM $NaIO_4$ for 30 minutes and 1 ml 160 mM ethylene glycol for 1h the reaction mixture was dialyzed against 10 mM Na_2CO_3, pH 9.5 at 4°C overnight. 5 mg GephE were added to the dialyzed activated HRP containing solution and after incubation for 3 h 5 mg of $NaBH_4$ were added and the reaction was stirred for another 3 h at 4°C. After dialysis against SEC-buffer (10 mM Tris/HCl pH 8.0, 250 mM NaCl, 1 mM β-mercaptoethanol (BME)) the solution was centrifuged for 5 min at 10000 x *g* and the supernatant was applied to a 26/60 Superdex 200 size exclusion column (Amersham Biosciences) equilibrated with SEC-buffer. Pure fractions of the GephE-HRP-conjugate were identified via SDS-PAGE and pooled according to chemiluminescence and concentrated using Vivaspin 3 kDa molecular weight cut-off (MWCO) centrifugal filter devices (Sartorius Stedim Biotech) to 1 mg/ml, flash-frozen in 0.1 ml aliquots, and stored at -80 °C.

3.5.4 Peptide array based analysis.

The wild-type $GABA_AR$ α3 peptide (^{369}TFNIVGTTYPINLAK^{384}) and its respective Ala-variants were purchased from Intavis AG in a CelluSpot™ format. After rinsing of the peptide array slides with TBS (50mM Tris, 150 mM NaCl, pH 7.6) and 0.05% Tween-20 (TBST) for 5 min the peptide array was incubated with HRP-conjugated GephE (1 µM) in blocking buffer (TBST+5% nonfat dry milk) for 5 h at RT. After extensive washing bound GephE-HRP-conjugate was detected by chemiluminescence using the Amersham ECL Prime Western Blotting Detection Reagent (GE Healthcare) using the chemiluminescent bio-imaging system MicroChemi (DNR Bio-imaging Systems). The resulting dot-blots were analyzed using the array analyze software (Active Motif). Three peptide array duplicates were used to calculate the average spot densities and the rmsd values.

3.5.5 Preparation of whole brain lysates.

After cervical dislocation, whole brains from 54 week old C57Bl/6J male mice were removed from the scull and rapidly homogenized in 1 ml lysate buffer (20 mM Hepes, 100 mM CH_3COOK, 40 mM KCl, 5 mM EGTA, 5 mM $MgCl_2$, 5 mM DTT, 1 mM PMSF, 1% Triton X, protease inhibitor Roche complete, pH 7.2) per 200 mg using a pistol homogenizer (8 strokes at 900 rpm). The homogenate was centrifuged at 10,000 x *g* for 15 min. Subsequently, the supernatant was removed and aliquots were flash-frozen in liquid nitrogen and stored at -80 °C.

3.5.6 Covalent immobilization of peptides.

$GABA_AR$ α3 peptide fragments with an additional C-terminal Cys (^{368}FNIVGTTY^{375}C, ^{368}FNIVGTTYP^{376}C, ^{368}FNIVGTTYPI^{377}C, ^{368}FNIVGTTYPIN^{378}C) were coupled to UltraLink Iodoacetyl Gel (Thermo Scientific) according to the protocol of the manufacturer: The peptides were dissolved in coupling buffer (50 mM Tris, 5mM EDTA, pH 8.5) at a concentration of 1 mM and incubated for 2 h at RT with UltraLink beads, which had been

washed and equilibrated with coupling buffer before. After removing excess peptides, the UltraLink beads were subjected to 1 mM cysteine for 2 h to quench possible unreacted iodoacetyl groups. The resin was washed three times and equilibrated with 1 M NaCl and stored at 4 °C.

Pull-down and western blot detection. The resin with the immobilized peptides was incubated with brain lysate for 1 h at 4 °C. After three washing steps with lysate buffer, the beads were boiled with Laemmli buffer containing 10% SDS. Subsequently, the supernatant was applied to an SDS-PAGE followed by western blotting against gephyrin using the mAb7a antibody (Kuhse et al., 2012) (Synaptic Systems) at a dilution of 1:500.

3.5.7 Peptide and protein concentration determination.

The concentration of the GephE stock-solution was determined by amino acid analysis and aliquots of an identical stock were used for all experiments to ensure comparability of all experiments and rule out effects of protein activity, degradation, concentration determination and aggregation. Peptide stocks were prepared by weighing the lyophilized powders. All ITC titrations displayed stoichiometries between 0.96 and 1.04, thus, demonstrating a high accuracy of the measured concentrations and comparability of the results.

3.5.8 Isothermal titration calorimetry (ITC).

The experiments were performed using an ITC200 (MicroCal, Northampton, MA, USA) at 25 °C and 1000 rpm stirring and designed so that c-values were generally within 0.5–100 (c-value = K_A x [protein] x N with K_A, equilibrium association constant; [protein], protein concentration; N, stoichiometry). Specifically, 40 µl of a solution containing 1-3 mM of the peptide were titrated into the 200 µl sample cell containing 25-100 µM GephE. In each experiment, a volume of 1-2 µl of ligand was added at a time resulting in 20-40 injections and a final molar ratio between 1:3 and 1:6. Ligand-to-buffer titrations were carried out in an analogous fashion, so that the heat produced by injection, mixing and dilution could be subtracted. The binding enthalpy was directly measured, while the dissociation constant (K_D) and stoichiometry (N) were obtained by data analysis using the Origin software (OriginLab). Measurements were conducted at least three times and are given as mean values with the resulting standard deviations.

3.5.9 Protein complex crystallization and X-ray data collection.

Complexes of GephE and peptides $\alpha11_{WT}$ and $\alpha11_{SL}$ were prepared by mixing both in a 1:5 (protein:peptide) molar ratio followed by incubation at 4 °C for 15min. The complexes were crystallized by the hanging drop vapor diffusion method at 20 °C at a concentration of 10 mg/ml in the presence of 0.2 M calcium acetate, 0.1 M MES pH 6 and 6-10% isopropanol as precipitant. Both complexes were also crystallized at 4 °C at a concentration of 2.5 mg/ml with 0.1 M Tris pH 7.5 and 21-27% PEG 4000 as precipitant. The crystals were transferred to the respective mother liquor solution containing 25% glycerol as cryo protectant and flash

frozen in liquid nitrogen. The datasets were collected at beamlines ID14-4 and ID 23-2 at the ESRF, Grenoble (Table 3-1).

3.5.10 Structure determination and refinement.

The datasets were indexed and integrated with iMosflm or XDS, further scaling and merging were done by using the CCP4 suite. The structures were solved by molecular replacement with PhaserMR using 2FU3 as initial model. Refinements were carried out with PHENIX and Refmac5. The crystals grown at 4°C belonged to space group $P2_12_12$ and diffracted to a resolution of 2.7 Å, the crystals grown at 20 °C to space group $P6_1$ and diffracted only to low resolutionsof 3.6-4.1 Å. For low resolution refinement the 1.7 Å resolution apo-E domain structure (PDB: 4PDO) was used as reference model. Figures involving molecular representations were prepared using PyMol (http://www.pymol.org). The coordinates have been deposited in the Protein Data Bank with the following PDB codes: 4TK1 and 4TK2 for GephE-α11$_{WT}$, 4TK3 and 4TK4 for GephE-α11$_{SL}$structures.

3.6 ACKNOWLEDGEMENTS

This work was supported by the Deutsche Forschungsgemeinschaft (H.S.: FZ 82, SFB 487 C7, SCHI 425/8-1 and M.K.: GRK1459 and KN 556/6-1), H.M.M. was supported by Lundbeckfonden (R118-A11469) and a grant of the German Excellence Initiative to the Graduate School of Life Sciences, University of Würzburg.

3.7 AUTHOR CONTRIBUTIONS

H.M.M. carried out all experiments except the crystallization and structure determination, which was carried out by V.B.K., and the preparation of brain lysates, pull-down and WB experiments, which were carried out by T.J.H. Research was designed by H.M.M., T.J.H., H.S., K.S., M.K. and V.T. The manuscript was written by H.M.M., V.B.K. and H.S.

3.8 ADDITIONAL INFORMATION

Accession codes: The coordinates have been deposited in the Protein Data Bank with the following codes: 4TK1 (orthorhombic) and 4TK2 (hexagonal) for GephE-α11$_{WT}$, 4TK3 (orthorhombic) and 4TK4 (hexagonal) for GephE-α11$_{SL}$ structures.

4. Design and Synthesis of High-Affinity Dimeric Inhibitors of the Interactions between Gephyrin and Inhibitory Neurotransmitter Receptors*

This chapter is based on the following publication:

Maric, H.M., Kasaragod, V.B., Kedstrom, L.H., Hausrat, T.J., Kneussel, M., Schindelin, H., Strømgaard, K. (2015) Design and synthesis of high-affinity dimeric inhibitors targeting the interaction between gephyrin and inhibitory neurotransmitter receptors. *Angew. Chem. Int. Ed.***54**, 490-4.

***Changes incorporated :**1. Supplemental information has been merged with the main text.

2. Supplemental figures 3, 4 and 5 have been merged to Fig 4-6.

Statement of individual author contributions and of legal second publication rights

Participated in	**Author Initials,** Responsibility decreasing from left to right				
Study Design Methods Development	HMM, VBK HMM, VBK	KS, HS LHK, TJH	LHK, TJH KS, HS	MK MK	
Data Collection	HMM, VBK	LHK, TJH			
Data Analysis and Interpretation	HMM, VBK	KS, HS	LHK, TJH, MK		
Manuscript Writing Writing of Introduction Writing of Materials & Methods Writing of Discussion Writing of First Draft	 HMM HMM, VBK HMM HMM	 VBK, KS, HS KS, HS VBK, KS VBK, KS, HS	 LHK, TJH, MK LHK, TJH, MK LHK, TJH, MK LHK, TJH, MK		

Statement of individual author contributions to figures/tables/chapters included in the manuscripts

Figure	**Author Initials,** Responsibility decreasing from left to right				
1	HMM, VBK	LHK, TJHM MS, HS, KS			
2	HMM	TJH, VBK, LHK, MK, HS, KS			
3	HMM	VBK, LHK, TJH, MK, HS, KS			
4	VBK	HMM, HS, KS			

4. Design and Synthesis of High-Affinity Dimeric Inhibitors of the Interactions between Gephyrin and Inhibitory Neurotransmitter Receptors[$]

Hans Michael Maric[1], Vikram Babu Kasaragod[2], Linda Haugaard-Kedström[1],Torben Johann Hausrat[3], Matthias Kneussel[3], Hermann Schindelin[2] and Kristian Strømgaard[1]*

[1]Department of Drug Design and Pharmacology, University of Copenhagen, Universitetsparken 2, DK-2100 Copenhagen, Denmark.

[2]Rudolf Virchow Center for Experimental Biomedicine, University of Würzburg, Josef-Schneider-Straβe 2, Building D15, D-97080 Würzburg, Germany.

[3]Center for Molecular Neurobiology, ZMNH, University Medical Center Hamburg-Eppendorf, D-20251 Hamburg, Germany.

*Corresponding author : Kristian Strømgaard (e-mail: kristian.stromgaard@sund.ku.dk)

4.1 ABSTRACT

Gephyrin is the central scaffolding protein for inhibitory neurotransmitter receptors in the brain. Here, we describe the development of dimeric peptides that modulate the interaction between gephyrin and these receptors, a process which is fundamental to numerous synaptic functions and diseases of the brain. First receptor-derived minimal gephyrin-binding peptides were identified, that displayed exclusive binding towards native gephyrin from brain lysate. We then designed and synthesized series of dimeric ligands, which led to a remarkable 1220-fold enhancement of the gephyrin affinity (K_D = 6.8 nM). Two X-ray crystal structures visualize the simultaneous dimer-to-dimer binding in atomic detail revealing compound-specific binding modes.Thus, we reveal the molecular basis of the affinity enhancing effect of multivalent inhibitors of gephyrin and provide conceptually novel compounds allowing the elucidation of the gephyrin-receptor interplay, and its therapeutic potential**.**

4.2 INTRODUCTION

Regulation of the number of the primary inhibitory neurotransmitter receptors in the brain, namely glycine receptors (GlyRs)(Kneussel et al., 1999b; Maas et al., 2006; Meyer et al., 1995) and γ-aminobutyric acid type A receptors ($GABA_A$Rs) (Kneussel et al., 1999a; Maric et al., 2011; Mukherjee et al., 2011b; Tretter et al., 2008), is regulated by the scaffolding protein gephyrin through direct interactions (Wu et al., 2012). Accordingly, a gephyrin knockout in mice is lethal and accompanied by loss of receptor clusters (Essrich et al., 1998; Feng et al., 1998; Kneussel et al., 1999a). It is known that gephyrin interacts with GlyRs and $GABA_A$Rs via auniversal binding site (Maric et al., 2011) located within the gephyrin E domain (GephE)(Kim et al., 2006), although distinct GlyR and $GABA_A$R interactions have very recently been described (Maric et al., 2014a). The affinity of the gephyrin-receptor interaction is dependent on factors such as the oligomeric state of gephyrin and the number of gephyrin-binding receptor subunits in the functional receptor (Maric et al., 2014c).Consequently, oligomerization of gephyrin, GlyRs and $GABA_A$Rs were found to be interdependent (Essrich et al., 1998; Vlachos et al., 2013).

Dysregulation of particularly $GABA_A$R-mediated neurotransmission has been implicated in a wide range of disorders in the brain (Hines et al., 2012b). Accordingly, compounds targeting $GABA_A$Rs have been extensively explored and are widely used as clinically relevant drugs (Johnston, 1996). In the search for improved drugs and potentially novel indications, there has been a large effort directed towards the development of compounds with improved receptor subtype-selectivity (Rudolph and Knoflach, 2011), with limited success so far. As a conceptually different approach, one could imagine targeting the interaction between $GABA_A$R and its intracellular scaffolding protein gephyrin. This is substantiated by the fact

that GlyR and $GABA_AR$ functions are markedly affected by gephyrin-binding-deficient mutations (Maric et al., 2011; Mukherjee et al., 2011b; Tretter et al., 2008). Additionally, in a principally similar approach, compounds with great therapeutic promise have been developed for other receptor/scaffolding protein interactions(Bach et al., 2009; Bach et al., 2012; Chi et al., 2012; Sainlos et al., 2013; Sainlos et al., 2011). We envisioned that receptor-derived peptides could be used as templates to generate high-affinity ligands that could modulate the gephyrin-receptor interaction *in vivo* and potentially have therapeutic relevance (Dolgin, 2012; Flemming, 2012). Importantly, such molecules could help decipher the details of $GABA_AR$ and GlyR population dynamics (Specht et al., 2013), which so far have remained poorly defined due to the lack of tools for acutely and specifically controlling the underlying gephyrin binding interactions (Tretter et al., 2012; Tyagarajan and Fritschy, 2014).

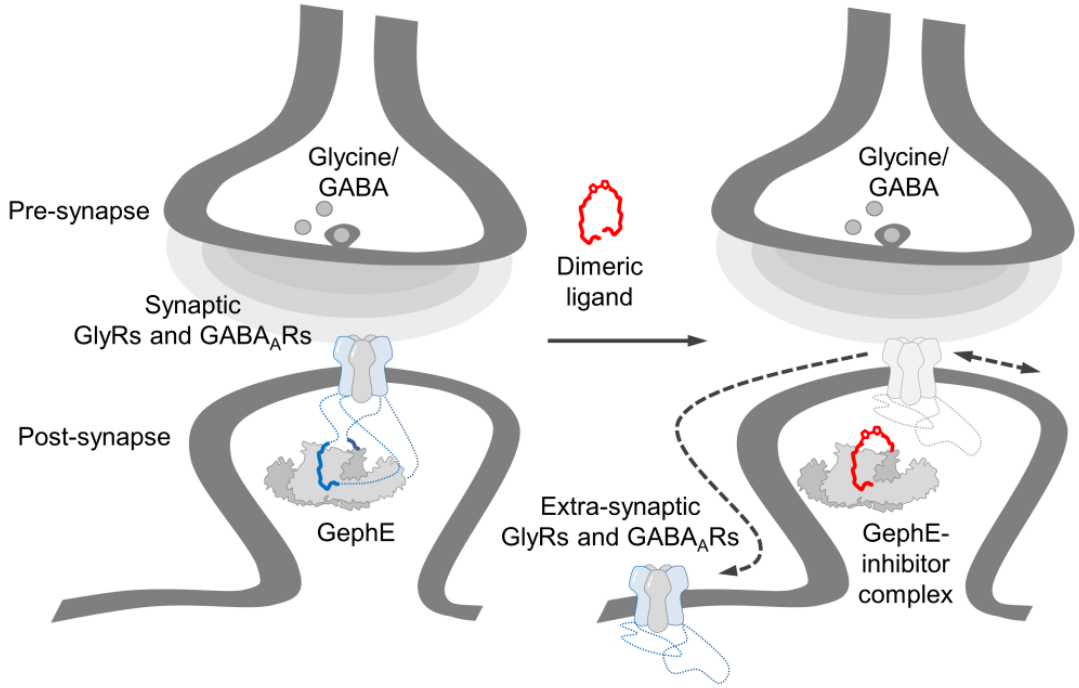

Figure 4-1. (Fig.1 in the published manuscript). Principle action of dimeric gephyrin inhibitors on the synaptic localization of GlyRs and $GABA_AR$s. $GABA_AR$s and GlyRs are concentrated at synaptic sites via direct interaction of their large intracellular loops with an overlapping gephyrin binding site. The receptor-binding C-terminal gephyrin E domain (GephE) dimerizes and offers two receptor-binding sites in close proximity. Dimeric ligands could simultaneously target two receptor-binding sites and thereby interfere with the accumulation of a specific subset of the receptors at post-synaptic sites by completion, thus acting as modulators of GABAergic and glycinergic transmission.

Here we present the design and synthesis of dimeric peptide ligands that target gephyrin with a remarkable specificity and display unprecedented high affinity to gephyrin and hence could open a new pathway to modulate inhibitory synaptic transmission (Figure 4-1).

4.3 RESULTS AND DISCUSSION

The 50 residue GlyR fragment **1a** that displays wild-type gephyrin-affinity (Meyer et al., 1995) with a K_D of 2.1±0.5 µM was used as a starting point and reference. Shorter peptide sequences were chosen on the basis of earlier mutagenesis and structural studies (Kim et al., 2006; Kneussel et al., 1999b; Maric et al., 2014a; Maric et al., 2014c; Maric et al., 2011; Meyer et al., 1995; Schrader et al., 2004). Truncation of **1a** to a 14 residue core binding peptide (**1b**), that could be resolved in a X-ray crystal structure (Kim et al., 2006), results in a roughly three-fold weaker affinity (K_D = 6±2 µM). From peptide **1b** a range of modifications was made in order to characterize a truncated peptide with good affinity to GephE; the modification included C-terminal truncations **1c**–**k**, point mutations **1l**–**o**, truncated amide-variants **1p**–**r** and N-terminally elongated amide-variants **1s**–**v**. This SAR study additionally provided a number of key features for gephyrin-binding, which are described in the subsequent sections, and additionally identified an octapeptide ligand **1r** which still exhibits ~90% of the free energy upon binding GephE when compared to the 50-mer peptide **1a**.

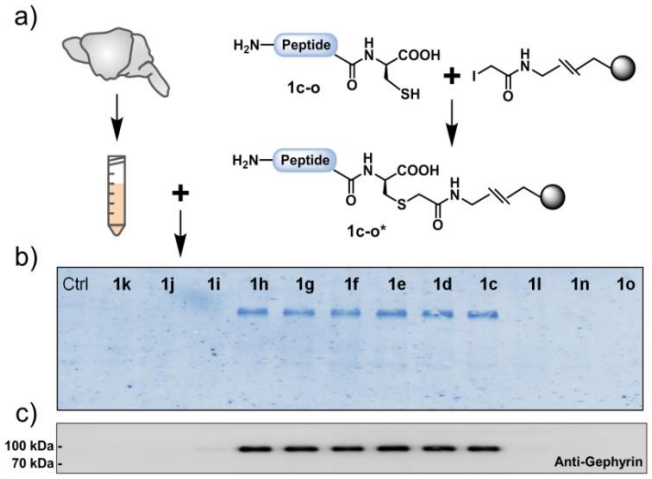

Figure 4-2.(Fig.2 in the published manuscript). Short GlyR-derived peptides bind native gephyrin. a) Scheme of the pull-down of native gephyrin. Whole mouse brain lysate was freshly prepared and GlyR-derived peptides **1c-k** as well as mutated variants **1l-o** were immobilized (*****) using iodoacetyl reactive resin. **b)** The Coomassie stained gel reveals that the peptides **1c-h*** exclusively bind gephyrin, while the Ala-mutants **1l-o*** and 5-6 residues wild-type variants **1k*** and **1j*** do not. **c)** Immune detection verifies the identity of gephyrin.

Having identified truncated peptides displaying a high affinity for recombinant GephE, we were interested in assessing the affinity and specificity for wild-type gephyrin. We employed an affinity-based approach, where the identified peptides were challenged with a murine whole-brain homogenate, as a highly complex gephyrin-containing matrix. Peptides **1c**-**k** with a systematic variation in length and affinity to GephE were covalently immobilized on iodoacetyl-activated beads and subsequently incubated with mouse whole-brain lysate

(Figure 4-2). Satisfyingly, there was an excellent correlation between the *in vitro* ITC data, and the ability to recover wild-type gephyrin from mouse brain: The six peptides **1c**-**h**, but not peptides **1i**-**k**, bound gephyrin as visualized by Western blot (Figure 4-2c). Importantly, a Coomassie-stained gel of the same resin-bound peptides (Figure 4-2b) demonstrates a remarkably high specificity of the peptides, as they exclusively bind native gephyrin. Thus, we demonstrate that the peptides bind native gephyrin from mouse brain with high efficiency.

Table 4-1.Identification of minimal gephyrin-specific peptides. Shown are the peptides **1a-z**, their residue numbers, sequences as well as their dissociation constants (K_D in µM) obtained from ITC by titration against GephE. ‡ **1w-z** were measured and analysed before.(Maric et al., 2014a)

No.	AA	Sequence	K_D [µM]
1a	50	$^{377}H_2N$-…SND F S I V G S L P R D F E L S…-COOH^{426}	2.1±0.5
1b	14	$^{398}H_2N$-F S I V G S L P R D F E L S-COOH^{411}	6±2
1c	13	$^{398}H_2N$-F S I V G S L P R D F E L-COOH^{410}	4.5±0.2
1d	12	$^{398}H_2N$-F S I V G S L P R D F E-COOH^{409}	13±7
1e	11	$^{398}H_2N$-F S I V G S L P R D F-COOH^{408}	8.3±0.1
1f	10	$^{398}H_2N$-F S I V G S L P R D-COOH^{407}	15±4
1g	09	$^{398}H_2N$-F S I V G S L P R-COOH^{406}	19±18
1h	08	$^{398}H_2N$-F S I V G S L P-COOH^{405}	20±4
1i	07	$^{398}H_2N$-F S I V G S L-COOH^{404}	>500
1j	06	$^{398}H_2N$-F S I V G S-COOH^{403}	>500
1k	05	$^{398}H_2N$-F S I V G-COOH^{402}	>500
1l	11	$^{398}H_2N$-A S I V G S L P R D F-COOH^{408}	>500
1m	11	$^{398}H_2N$-F S I V G S L A R D F-COOH^{408}	42±22
1n	11	$^{398}H_2N$-A S I V G S L A R D F-COOH^{408}	>500
1o	11	$^{398}H_2N$-A S A V G S L A R D F-COOH^{408}	>500
1p	06	$^{398}H_2N$-F S I V G S-CONH$_2$^{403}	>500
1q	07	$^{398}H_2N$-F S I V G S L-CONH$_2$^{403}	>500
1r	08	$^{398}H_2N$-F S I V G S L P-CONH$_2$^{405}	8.9±0.3
1s	07	$^{399}H_2N$-S I V G S L P-CONH$_2$^{405}	>500
1t	09	$^{397}H_2N$-D F S I V G S L P-CONH$_2$^{405}	71±20
1u	10	$^{396}H_2N$-N D F S I V G S L P-CONH$_2$^{405}	69±18
1v	11	$^{395}H_2N$-S N D F S I V G S L P-CONH$_2$^{405}	79±7
1w	11	$^{370}H_2N$-F N I V G T T Y P I N-CONH$_2$^{380}	190±30‡
1x	10	$^{370}H_2N$-F N I V G T T Y P I-CONH$_2$^{379}	221±34‡
1y	9	$^{370}H_2N$-F N I V G T T Y P-CONH$_2$^{378}	253±38‡
1z	8	$^{370}H_2N$-F N I V G T T Y-CONH$_2$^{377}	>500‡

Next, we employed the identified monomeric peptides in the design and synthesis of dimeric ligands, which we envisionto bind the dimeric GephE domain simultaneously, thereby enhancing affinity to act as potent inhibitors of this interaction. Specifically, GlyR-derived peptides **1c**-**h** and $GABA_AR$-derived peptides **1w**-**y**, peptides were dimerized using a variety of different linkers.

The SAR study of the monovalent peptides (Figure 4-2, Table 4-2 and Figures 4-3 and 4-5) provided a number of key features for gephyrin binding. First, removal of Phe398 at the N-terminus impairs binding of **1s**, while elongation at the N-terminal does not improve the affinity for **1t–v**. At the C-terminal end, removal of Pro405 results in a complete loss of gephyrin binding for **1h–l**, while removal of Phe408 in **1e–f** and Leu410 in **1c–d** reduces the affinity slightly. The shortest peptide capable of binding gephyrin is the octapeptide **1h** with a K_D of 20±4 µM, however, the corresponding C-terminal amide peptide (**1r**) displayed improved binding affinity with a K_D of 8.9±0.3 µM. The critical impact of point mutations in gephyrin and the receptors was demonstrated earlier in ITC and cell-based assays (Kim et al., 2006; Maric et al., 2011). In this study we included seven point mutated variants of the monovalent (1l-o) and dimeric (3w-y) receptor-derived peptides (Fig 4-2) and studied them via ITC. In excellent agreement with earlier findings the selected mutations strongly interfere with gephyrin-binding.

Since, the N-terminal region of these peptides are presumed to display important interaction points with gephyrin, the dimeric peptide ligands were synthesized by dimerization at the C terminus. Linker moieties with variations in hydrophobicity, length and flexibility were employed, and systematically combined with the different peptide ligands. Specifically, rigid phenyl-based linkers **2a**–**c**, short alkyl-linkers **2d** and longer flexible PEG-based **2e** linkers were used to dimerizes peptides**1e**–**y**, which varied in length between 8 to 13 residues, yielding 25 different dimeric peptide compounds **3a**–**y** (Figure 4-4a and 4-6c). The dimeric peptides were evaluated for their affinity to recombinant GephE using ITC (Figure 4-4b-d and 4-5, 4-6a, 4-6b and Table 4-2).

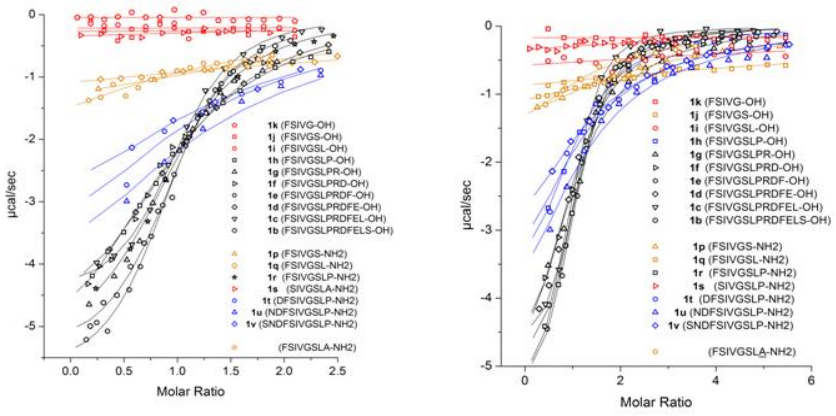

Figure 4-3. Isothermal titration calorimetry raw heat diagrams upon titration of 1b-v to GephE. (Supplemental Fig.1 in the published manuscript). Raw heat diagrams (symbols as defined on the right) obtained from

ITC and the resulting fits (lines) upon titration of **1b-v** to GephE at a maximal ligand excess of 2.5 (left) or 6 (right). No binding was detected for **1i-k** (red). Binding was detected for **1p-q** (orange) but binding parameters could not be obtained under these conditions. **1t-v** (blue) display weak binding whereas **1b-h** (black) exhibit strong binding.

Gratifyingly, all dimeric ligands displayed a significant increase in affinity compared to the equivalent monomeric peptide. The potentiation of affinity upon dimerization followed two basic principles: 1)The nature of the linker determines the overall affinity of dimeric peptides with PEG being the most optimal linker and *m*-phenyl the least optimal. 2) The length and not the affinity of the peptide ligands determine the gephyrin-binding potency over a range of more than one magnitude with 11 residues being optimal. The synergistic effect of linker and peptide optimization together led to a 1220-fold improved binding affinity of dimeric ligand **3m** with a K_D of 6.8±0.6 nM, compared to the corresponding monovalent peptide **1e** (K_D = 8.3±0.1 µM).

We also extended the concept to the $GABA_AR$ α3 subunit-derived peptides, which displayed the highest gephyrin-affinity among all so far analyzed $GABA_AR$ subunit peptides. Here, dimerization yielded a K_D of 288±86 nM, corresponding to an 880-fold increase in affinity, which is hence in the same range as found for the best GlyR-derived dimeric fragment. Evaluation of the dimeric ligands **3x–z** exclude contributions to the affinity by the linker region and therefore the described affinity potentiation is solely based on the simultaneous binding of the two peptide arms.

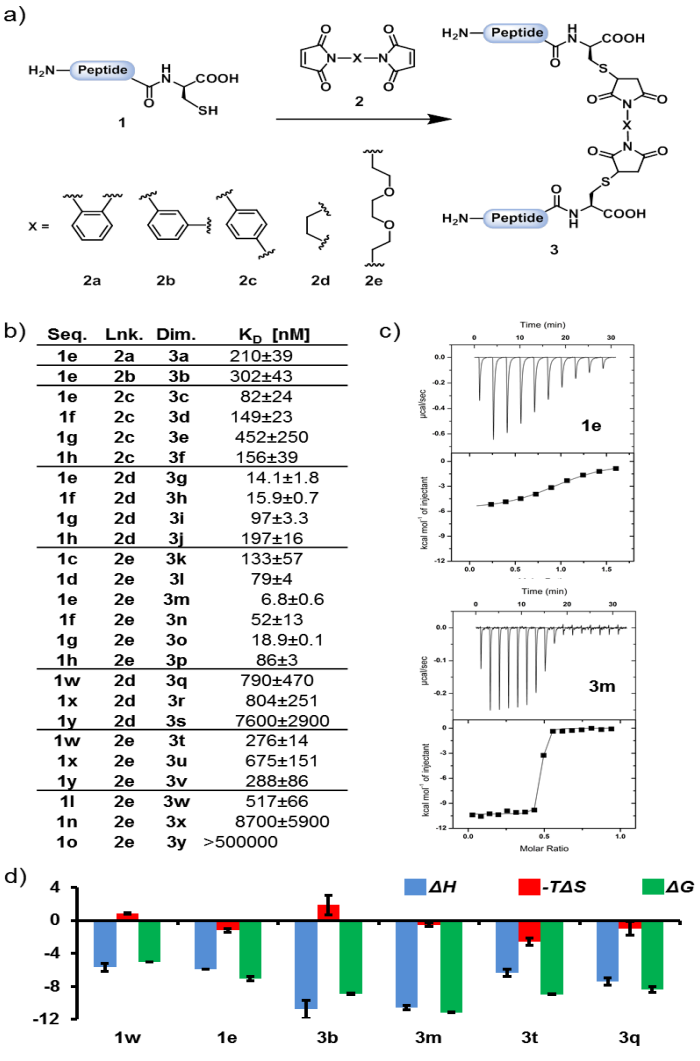

Seq.	Lnk.	Dim.	K_D [nM]
1e	2a	3a	210±39
1e	2b	3b	302±43
1e	2c	3c	82±24
1f	2c	3d	149±23
1g	2c	3e	452±250
1h	2c	3f	156±39
1e	2d	3g	14.1±1.8
1f	2d	3h	15.9±0.7
1g	2d	3i	97±3.3
1h	2d	3j	197±16
1c	2e	3k	133±57
1d	2e	3l	79±4
1e	2e	3m	6.8±0.6
1f	2e	3n	52±13
1g	2e	3o	18.9±0.1
1h	2e	3p	86±3
1w	2d	3q	790±470
1x	2d	3r	804±251
1y	2d	3s	7600±2900
1w	2e	3t	276±14
1x	2e	3u	675±151
1y	2e	3v	288±86
1l	2e	3w	517±66
1n	2e	3x	8700±5900
1o	2e	3y	>500000

Figure 4-4. (Fig.3 in the published manuscript). Design and synthesis of dimeric peptides and their *in vitro* binding evaluation by ITC. a) Monomeric GlyR β-derived **1c-o** or $GABA_AR$ α3-derived **1w-y** peptides were dimerized in solution via a C-terminally added Cys, which reacted with different

bismaleamide containing linkers **2a-e** to yield their dimerized variants **3a-y**. **b)** Dissociation constants of dimeric compounds **3a-y** determined by ITC together with their linker type **2a-e** and their peptide sequence **1e-y**. **c)** Representative ITC-diagrams of the monovalent peptide **1e** and its dimeric variant **3m**. **d)** Thermodynamic bar graphs for selected compounds (ΔH, ΔG and $-T\Delta S$ in kcal mol^{-1}).

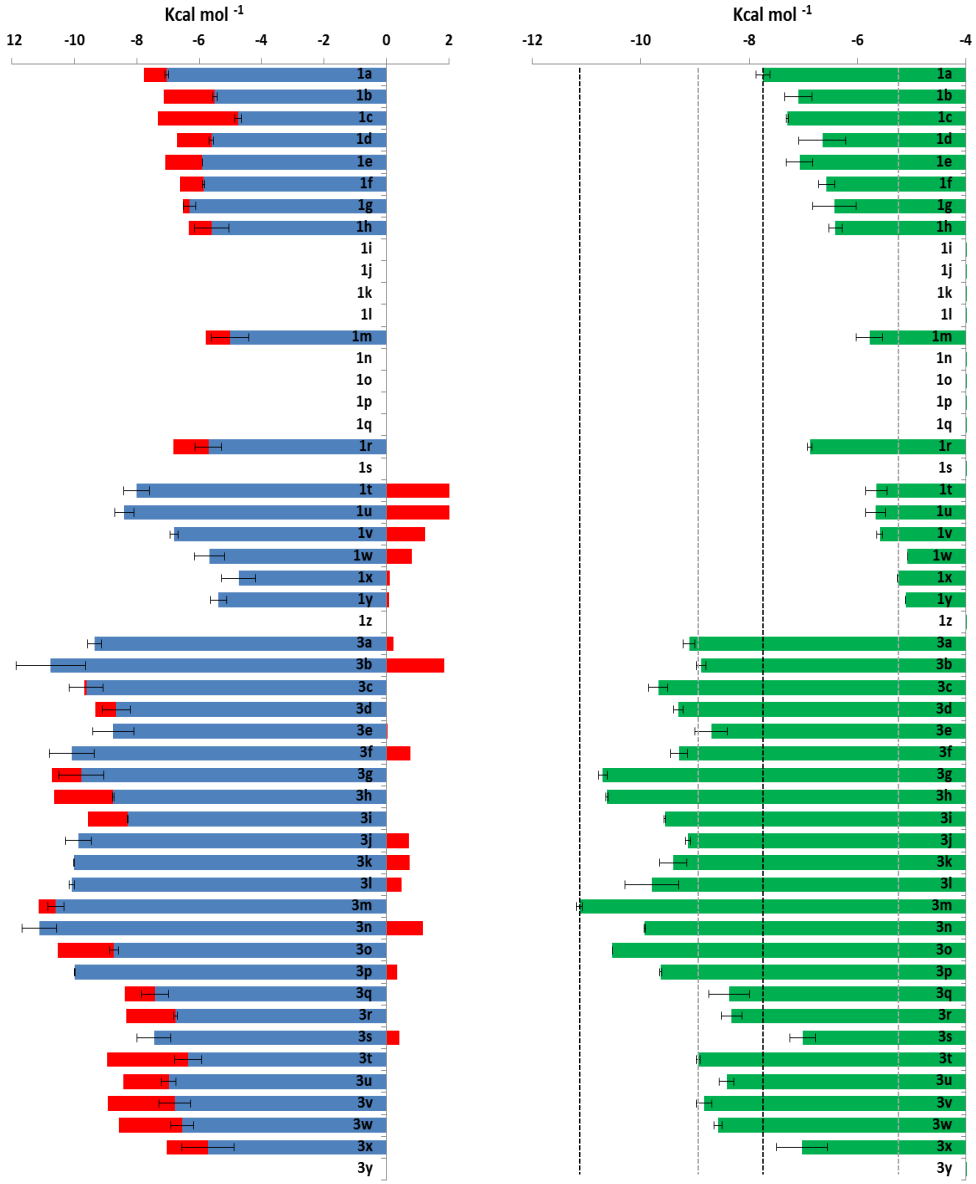

Figure 4-5. Thermodynamic parameters of GephE-peptide binding deduced by ITC.(Supplemental Fig.2 in the published manuscript). Bar graphs of the enthalpy (blue), entropy (red) and free energy (green) of GephE-peptide binding determined by ITC. Bold dashed lines indicate the free energy for the tightest binding dimeric and monomeric GlyR (black) and $GABA_AR$ (grey) peptides. Error bars show the standard deviation derived from at least three different measurements.

From the ITC experiments, we found that the dimeric peptide ligands bound with a 1:2 stoichiometry to GephE, in line with a simultaneous binding of both peptide moieties to dimeric GephE. This was confirmed by analytical size exclusion chromatography (SEC) and

multi angle light scattering (MALS) which both clearly demonstrated the dimeric oligomerization state of GephE in the presence and absence of the dimeric peptide ligands (Figure 4-7).

To elucidate the binding mode of the peptide dimeric ligands to GephE, we examined the corresponding structures by X-ray crystallography. Two dimeric ligands were selected for co-crystallization with GephE: The dimeric ligand **3v** containing a flexible PEG linker and a $GABA_AR$-derived peptide and the dimeric ligand **3d** with shorter GlyR-derived peptides and a rigid phenyl-based linker. The X-ray crystal structures of GephE in complex with **3v** (PDB ID: 4U90) (Figure 4-9 a-c) and **3d** (PDB ID: 4U91) (Figure 4-9d-f) illustrate how both peptide ligands engage simultaneously with two GephE proteins and how the supra-molecular GephE-dimeric peptide complex is spatially arranged (Figure 4-8).

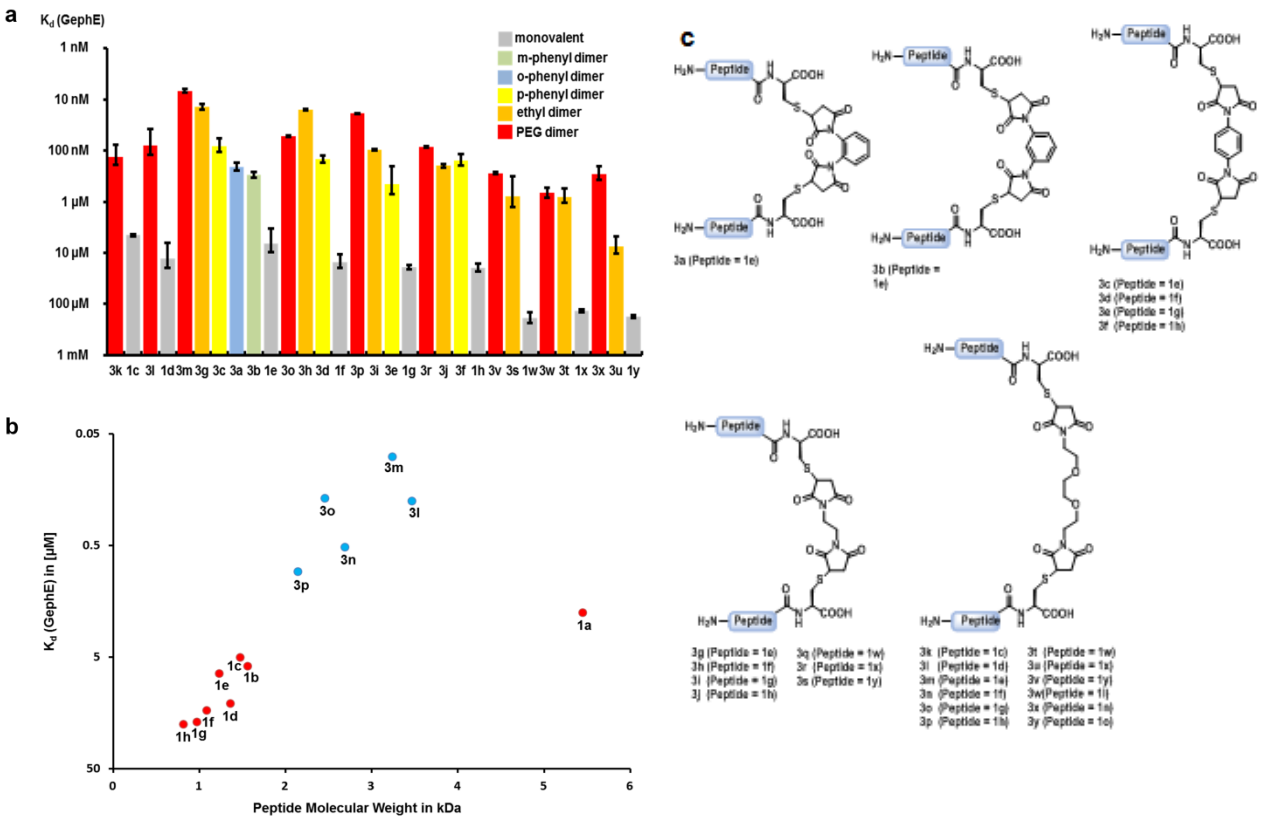

Figure 4-6. Structures of dimeric peptides 3a-y. (Supplemental Fig.3, 4 and 5 in the published manuscript). Overview of the structures of the dimeric peptides **3a-y**. Monomeric Cys-containing receptor-derived peptides **1c-y** were dimerized with either phenyl-based linkers **2a-c** to yield rigid dimers **3a-f** or with ethyl-based **2d** and PEG-based **2e** linkers to yield more flexible dimeric peptides **3g-y.**

Since our MALS data (Figure 4-7) demonstrated that each dimeric ligand binds to just one GephE dimer, the binding modes observed in the two structures (Figure 4-8 and Figure 4-9) represent interesting examples of domain swapping (Gronenborn, 2009). Despite the different domain swapped arrangements, in both GephE-dimeric peptide structures all GephE binding sites are occupied.

Table 4-2. Thermodynamic parameters of **1a-z** and **3a-y** binding to GephE as determined by ITC.

Compound	**Δ*H*** [kcal mol^{-1}]	**-*T*Δ*S***[kcal mol^{-1}]	**Δ*G***[kcal mol^{-1}]	K_D **[nM]**
1a	-7.04±0.05	-0.73±0.01	-7.75±0.13	2090±460
1b	-5.50±0.07	-1.63±0.02	-7.09±0.25	6300±2200
1c	-4.75±0.11	-2.57±0.21	-7.29±0.02	4500±200
1d	-5.60±0.07	-1.12±0.40	-6.65±0.43	13100±6700
1e	-5.90±0.01	-1.20±0.21	-7.07±0.24	8300±30
1f	-5.85±0.04	-0.76±0.20	-6.57±0.15	15100±4400
1g	-6.31±0.21	-0.21±0.09	-6.43±0.40	19100±18300
1h	-5.60±0.57	-0.74±0.11	-6.41±0.12	19800±3600
1i	n.d.	n.d.	n.d.	n.d.
1j	n.d.	n.d.	n.d.	n.d.
1k	n.d.	n.d.	n.d.	n.d.
1l	n.d.	n.d.	n.d.	n.d.
1m	-5.01±0.60	-0.79±0.84	-5.78±0.24	618000±23600
1n	n.d.	n.d.	n.d.	n.d.
1o	n.d.	n.d.	n.d.	n.d.
1p	n.d.	n.d.	n.d.	n.d.
1q	n.d.	n.d.	n.d.	n.d.
1r	-5.70±0.42	-1.13±0.20	-6.88±0.04	8900±300
1s	n.d.	n.d.	n.d.	n.d.
1t	-8.00±0.41	2.48±0.11	-5.65±0.20	71000±20000
1u	-8.40±0.31	2.75±0.10	-5.67±0.18	69000±18000
1v	-6.80±0.13	1.25±0.04	-5.59±0.05	79000±7000
1w	-5.68±0.48	0.82±0.03	-5.08±0.01	190000±30000
1x	-4.73±0.54	0.10±0.13	-5.26±0.01	221000±34000

1y	-5.38±0.26	0.09±0.12	-5.11±0.01	253000±38000
1z	n.d.	n.d.	n.d.	n.d.
3a	-9.35±0.22	0.23±0.23	-9.11±0.11	210±39
3b	-10.76±1.11	1.86±1.17	-8.89±0.09	302±43
3c	-9.62±0.54	-0.07±0.66	-9.68±0.18	82±24
3d	-8.66±0.45	-0.66±0.42	-9.31±0.09	149±23
3e	-8.76±0.66	0.04±0.73	-8.70±0.30	452±250
3f	-10.08±0.73	0.77±0.73	-9.29±0.15	159±39
3g	-9.78±0.71	-0.94±0.64	-10.70±0.08	14.1±1.8
3h	-8.75±0.03	-1.89±0.01	-10.63±0.03	15.9±0.7
3i	-8.30±0.01	-1.28±0.03	-9.56±0.02	97±3.3
3j	-9.87±0.41	0.72±0.37	-9.14±0.05	197±16
3k	-10.02±0.01	0.74±0.36	-9.40±0.25	133±57
3l	-10.08±0.08	0.48±0.65	-9.80±0.50	79±4
3m	-10.59±0.27	-0.55±0.22	-11.13±0.05	6.8±0.6
3n	-11.12±0.56	1.17±0.54	-9.92±0.02	52±13
3o	-8.73±0.14	-1.81±0.13	-10.52±0.00	18.9±0.1
3p	-9.99±0.01	0.35±0.03	-9.63±0.02	86±3
3q	-7.42±0.44	-0.97±0.82	-8.37±0.37	790±470
3r	-6.76±0.05	-1.58±0.15	-8.32±0.19	804±251
3s	-7.44±0.54	0.43±0.67	-7.01±0.24	7570±2860
3t	-6.36±0.44	-2.59±0.42	-8.94±0.03	276±14
3u	-6.98±0.23	-1.45±0.36	-8.42±0.13	675±151
3v	-6.78±0.51	-2.14±0.51	-8.83±0.14	288±86
3w	-6.55±0.37	-2.03±0.34	-8.57±0.07	517±66
3x	-5.72±0.83	-1.32±0.12	-7.02±0.47	8670±5930
3y	n.d.	n.d.	n.d.	n.d.

n.d., no binding could be detected

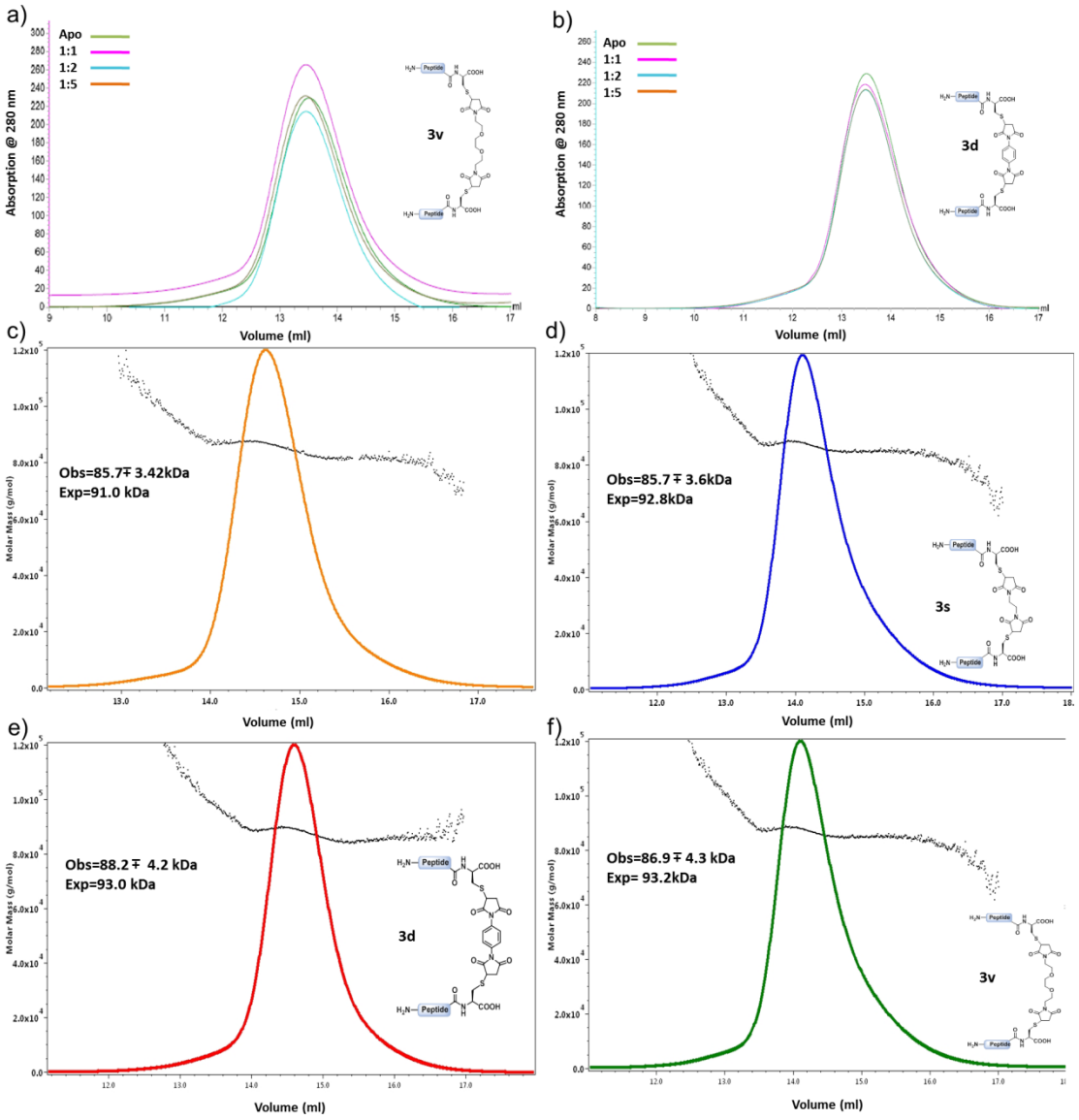

Figure 4-7. Analysis of the oligomeric state of selected GephE-dimeric peptide complexes and apo-GephE. (Supplemental Fig.6 in the published manuscript). Analytical SEC and MALS of selected GephE-dimeric peptide complexes as well as of apo-GephE. Analytical size exclusion chromatography (SEC) of GephE in the presence or absence of a 1-fold to 5-fold molar excess of either **3v (a)** or **3d (b)**verifies that the oligomeric state of GephE is not altered upon binding of the dimeric ligands. Multi angle light scattering (MALS) confirms GephE dimerization of apo-GephE **(c)** and demonstrates the binding of one GephE dimer to **3s (d)**, **3d (e)**, and **3v (f)**. The differential refractive index (dRI) has been represented as curves of different colours and the respective molecular mass measured is represented by the black scatter.

Table 4-3. Data collection and refinement statistics

Parameters	**Structure**	
Protein Complex	**GephE- $GABA_AR$ α3 dimer**	**GephE-GlyR β dimer**
Beamline	ESRF, ID 23-1	BESSY, ID 14-1
Wavelength (Å)	0.9100	0.9184
Space group	I222	I222
Unit cell Parameters		
a, b, c (Å)	88.54, 99.24, 114.40	87.44, 99.21, 112.50
Resolution limit (Å)	44.2 – 2.0	56.2- 2.0
R_{sym}[a]	0.065 (0.623)	0.091 (0.576)
R_{pim}[b]	0.045 (0.432)	0.061 (0.412)
$CC_{1/2}$	0.999 (0.852)	0.992 (0.627)
Redundancy	5.5 (5.7)	5.9 (5.3)
Unique reflections	34354	33407
Completeness	0.99 (1.0)	1.0 (1.0)
$\langle I/\sigma I \rangle$[c]	14.1 (2.2)	10.0 (2.5)
R [d] /R_{free}[e]	0.166/ 0.211	0.168/ 0.225
Deviations from ideal values in		
Bond distances (Å)	0.018	0.015
Bond angles (°)	1.906	1.705
Torsion angles (°)	21.521	19.899
Planar groups (Å)	0.009	0.009
Chirality centers ($Å^3$)	0.111	0.097
Ramachandran statistics (Preferred/Allowed/Outliers)	98.3/ 1.7/ 0.0	97.4/ 2.6/ 0.0
Overall average B factor ($Å^2$)	53.2	48.4
Coordinate error (Å)	0.11	0.12

All the terms in the table are defined as according to the table 2-1.

In both structures the peptide binding pocket is mainly created by GephE subdomain IV and partially by subdomain III (Figures, 4-8 and 4-9a,d), which acts as a universal binding site for the GlyR β and $GABA_AR$ α subunit derived peptides (Maric et al., 2011). Nonetheless, both

compounds also engage in unique GephE interactions (Figure 4-9 c,f). Remarkably, the linkers of the PEG-based **3v** and the phenyl-based **3d** dimeric ligands are fully resolved in the electron density (Figure 4-9b,e), indicating a tight and rigid arrangement of both linkers. Due to the high resolution (2Å), the co-crystal structure of the $GABA_AR$ α3 derived peptide **3v** also reveals new features, which are described in the supporting information.

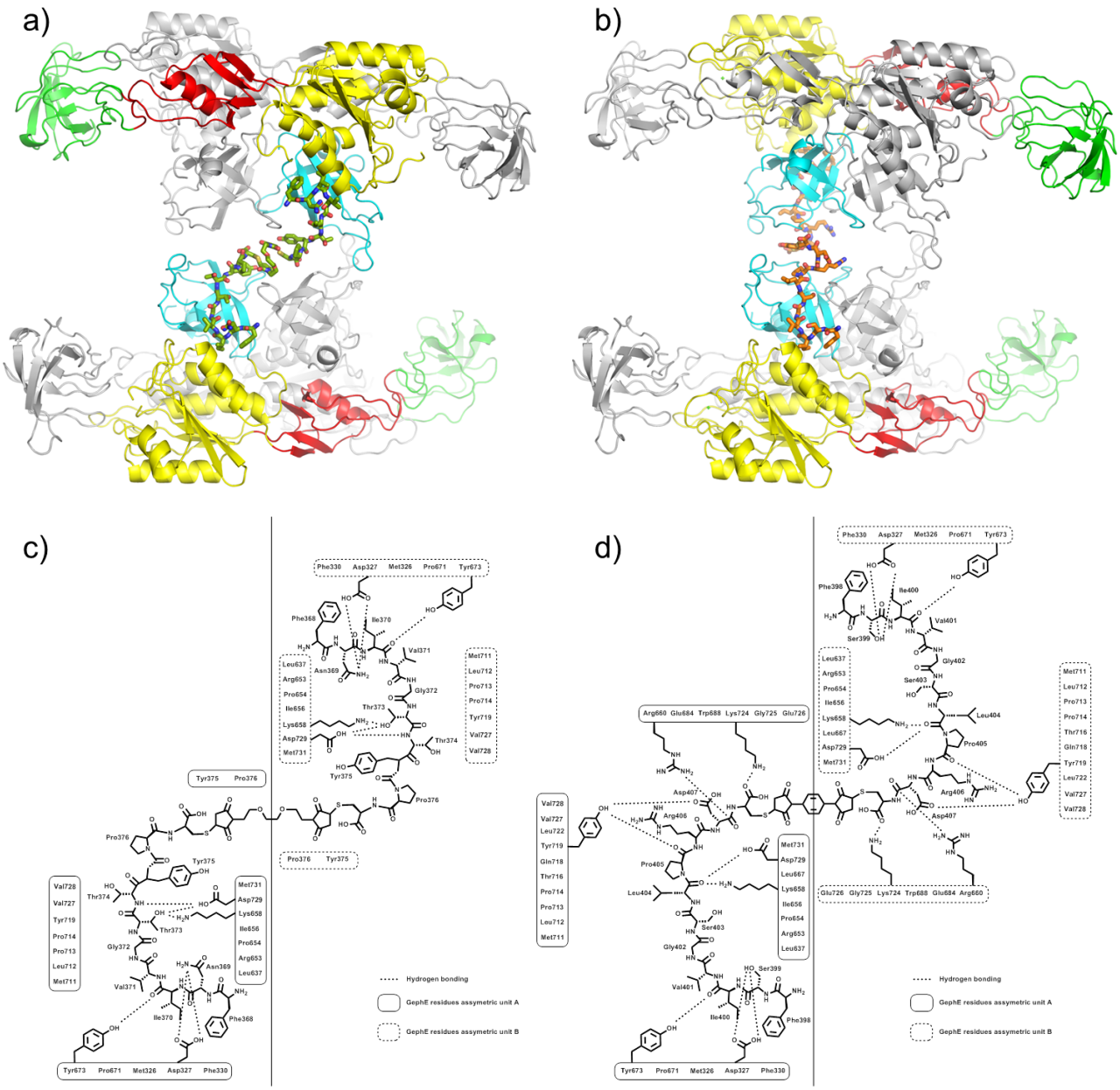

Figure 4-8. Overall and schematic views of the GephE-dimeric peptide complexes. (Supplemental Fig.7 in the published manuscript). Overall structures and schematic views of the GephE-dimeric peptide complexes. **(a)** Binding of the $GABA_AR$ α3-derived PEG-linked dimeric peptide **3v** in stick representation (PDB-ID: 4U90) to GephE in the context of the two adjacent GephE dimers. Subdomains 1-4 are colour coded in one subunit of each dimer as in Figure 5, while the other monomer is shown in grey. **(b)**

Binding of **3d** in the context of the two adjacent GephE dimers, **(c)** Detailed 2D representation of the interactions between the $GABA_AR$ α3-derived PEG-linked dimeric peptide **3v** (PDB-ID: 4U90) and both GephE monomers**. (d)** Detailed 2D representation of the interactions between the GlyR β-derived p-phenyl-linked dimeric peptide and both GephE monomers (PDB:4U91).

GephE (318-736) was crystallized with **3v**, a $GABA_A$ α3-derivedand PEG-linkeddimeric peptide (PDB ID: 4U90) and **3d**, a GlyR β-derived *p*-phenyl linked dimeric peptide (PDB ID: 4U91). Crystallisation of both GephE-peptide complexes occurred in the orthorhombic space group I222 with closely related unit cell dimensions as also found in the GephE apo-structure (PDB ID: 4PD0) (Maric et al., 2014c).

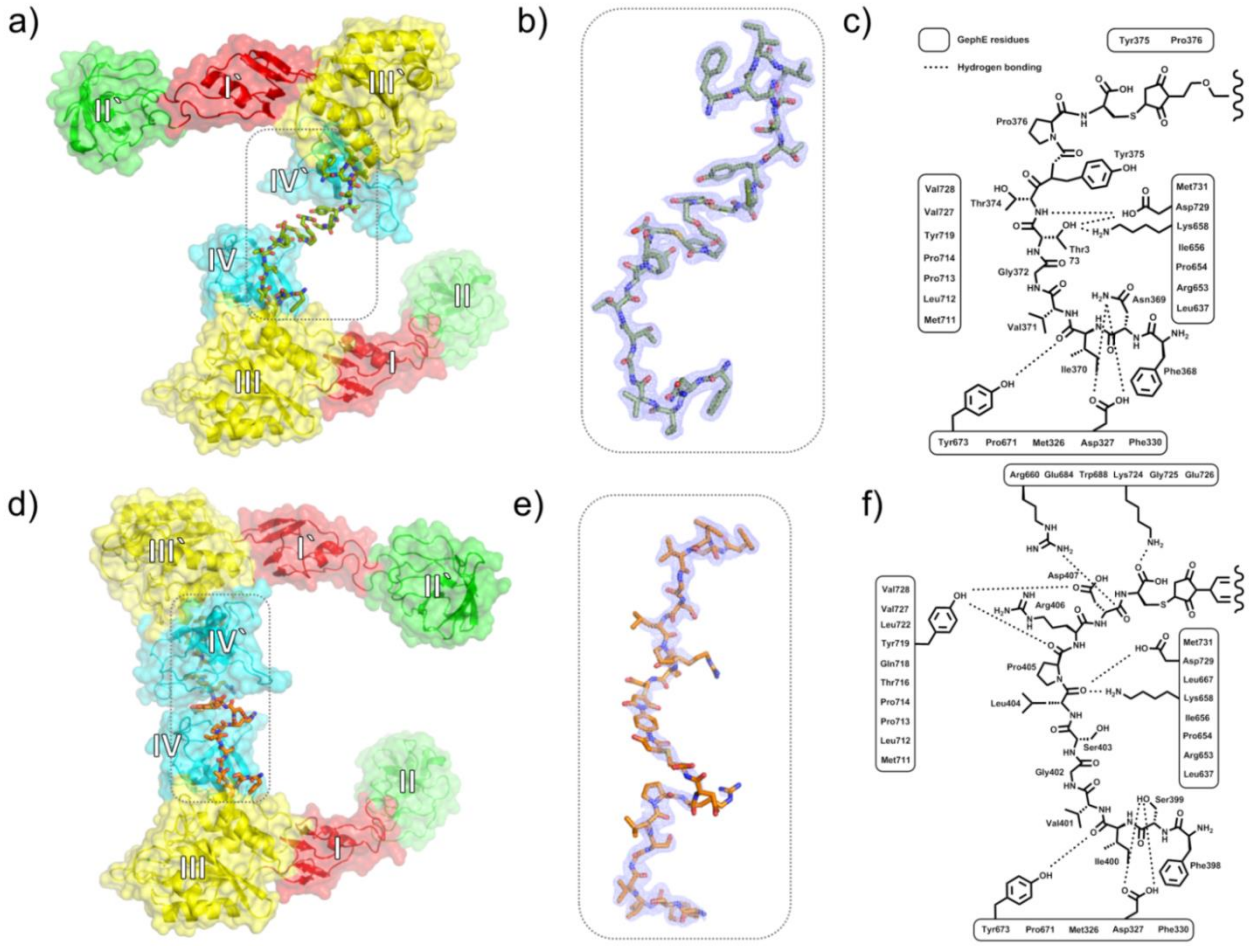

Figure 4-9. (Fig.4 in the published manuscript). X-ray crystallographic analyses of two GephE-dimeric peptide complexes. (a) Binding of the $GABA_AR$ α3-derived PEG-linked dimeric peptide **3v** in stick representation (PDB-ID: 4U90) to GephE. Subdomains 1-4 are indicated in roman numbers and are coloured differently. **(b)** Stick model and feature enhanced electron density map (FEM) at one times the rmsd for the bound dimeric peptide **3v**. **(c)** Detailed 2D representation of the GephE interactions of one half of the dimeric peptide **3v**. **(d)** Structure of **3d**, a GlyR β-derived p-phenyl-linked dimeric peptide, engaging with two GephE proteins molecules simultaneously (PDB: 4U91). **(e)** Stick model and FEM at one times the rmsd of **3d** bound to GephE. **(f)** 2D representation of one half of the GephE-**3d** complex.

Both complexes contain one GephE monomer and half of the dimeric peptide per asymmetric unit, however, the crystal structures differ significantly from each other and also from the expected interaction of one GephE dimer with one dimeric peptide (Figures4-5a-b and 4-7 a-b). While the standard GephE dimer (dimer A) is formed via a crystallographic twofold axis of symmetry, a second GephE dimer (dimer B) is in close spatial proximity (Figure 4-8 a-b). The dimeric peptides bind in such a way that they occupy one monomer of dimer A and one monomer in dimer B, however, it is a different monomer in each case (Figure 4-8 c-d). Despite the fact that the dimeric peptides have undergone domain swapping (Gronenborn, 2009), the structures still unambiguously resolve the GephE-peptide interactions, which are defined by the content of the asymmetric unit which contains one GephE monomer and half of the dimeric peptide. Differences between the crystal structures and the situation in solution could only be observed for the respective linkers, only with respect to the path of the one half of the peptide in the domain swapped arrangement, which do not contribute to the binding affinity by direct interactions to GephE. One possible explanation for the widely different arrangement of the GephE-peptide complexes might be based on differential C-terminal GephE-peptide interactions of both dimeric peptides.

Due to the higher resolution and tighter peptide-binding, the **3v** co-crystal structure reveals additional details of the GephE-$GABA_AR$ α3 interaction that could not be resolved using the corresponding monovalent fragment, (Maric et al., 2014a) which displays only a low affinity. Notably, $GABA_AR$ α3 Tyr375 is now clearly resolved in the electron density. This residue was identified to be critical for the binding interaction of the synaptic $GABA_AR$ α1-3 subunits (Maric et al., 2011), and more importantly, to engage $GABA_AR$ distinct gephyrin interactions. It displays an inward facing conformation which engages in hydrophobic interactions with GephE Lys658, Val727, Pro685 and Leu686. Additionally, $GABA_AR$ α3 Asn369, a major determinant of the preference of gephyrin for the GlyR β subunit over the $GABA_AR$ α3 (Maric et al., 2014a) could now be assigned precisely. This side chain replaces a Ser in the GlyR β subunit and, in contrast to the Ser, which can engage in productive hydrogen-bonded interactions with the main chain nitrogen of Val371 in the peptide and the side chain of Asp327 in gephyrin, the Asn cannot simultaneously satisfy both interactions, hence explaining its negative impact on the binding affinity. The $GABA_AR$ α3 Asn369 was modelled with two different side chain confirmations, one where its side chain oxygen points towards the main chain of the peptide and a second conformation in which it points towards GephE Asp327. The approach to use dimerized receptor fragments could also be used to analyse binding of yet uncharacterized GephE-binding receptor subunits such as $GABA_AR$ α1, α2, β2 and β3 which display affinities in the micromolar range that so far prevented their co-crystallization with GephE.

As mentioned before, the $GABA_AR$ α3 and GlyR β peptides occupy an overlapping binding site, and compared to apo-GephE (PDB : 4PD0)(Maric et al., 2014e), the overall architecture of the complex is conserved with rmsd values of 0.34 and 0.53 Å for the Cα atoms of the GephE-$GABA_AR$ α3 and GephE-GlyR β dimer complexes, respectively. Surprisingly, subdomain IV also shows minor structural changes where the peptide is bound (rmsd values of 0.41 Å for GephE-$GABA_AR$ α3 PEG and 0.47 Å for GephE-GlyR β *p*-phenyl). In comparison to the monomeric counterparts of the complexes (GephE-$GABA_AR$ α3, PDB ID: 4TK1 and GephE-GlyR β, PDB ID: 4PD1), the GephE-$GABA_AR$α3 PEG complex shows rmsd values of 1.40 Å for all Cα atoms of and 2.41 Å for those in subdomain IV where the ligand binding pocket is located. GephE-GlyR β *p*-phenyl shows rmsd values of 0.69 Å and 0.40 Å for the overall architecture and subdomain IV, respectively. The GlyR β *p*-phenyl peptide interaction is conserved with the monomeric variant (rmsd values of 0.18 Å for the Cα atoms and 1.54 Å for all atoms in the peptide) with notable differences inthe conformations of Arg406 and Asp407 at the C terminal part of the peptide. The visible part of the peptide in GephE-$GABA_AR$ α3 PEG shows significant structural changes with rmsd values of 1.52 Å for the Cα and 2.84 Å for all atoms in the peptide.

Peptide-based ligands are generally subject to enzymatic cleavage by proteases *in vivo*, which often is the major limiting factor for advanced biological studies. We therefore evaluated the stability on a subset of both monomeric and dimeric peptide ligands in an *in vitro* serum stability assay (Figure 4-10). In contrast to the monomeric peptides **1x–w,** which were degraded relatively fast with half-lives ($t_{1/2}$) of 4-6 minutes, the dimeric ligands **3q–r** and **3t–u** comprising different linkers displayed a 24- to 41-fold increase in stability, with a maximal $t_{1/2}$ of over 4 hours (Figure S4-8). Thus, dimerization of peptide ligands leads to a superior stability compared to standard, monomeric peptides (Dolgin, 2012; Flemming, 2012).

In conclusion, we first identified short gephyrin binding peptides with moderate affinity, which, however, showed exclusive and efficient binding to wild-type gephyrin. Dimerization of these peptide ligands with a subset of different linkers, led to dimeric ligands that target gephyrin with unprecedented high affinity, with the most potent ligand displaying an affinity in the low nanomolar range.Additionally, dimerization also substantially improved the serum stability, thus providing compounds with great promise for further studies of gephyrin-receptor interactions. Finally, the atomic details of the interaction between the dimeric ligands and gephyrin was revealed by X-ray crystallography, showing several interesting features including that both peptide ligands engage with two GephE proteins simultaneously and in specific binding modes.

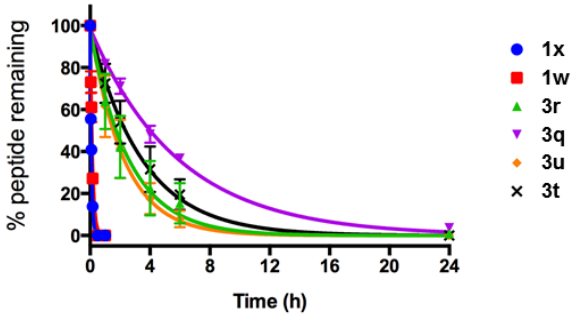

Peptide	$t_{1/2}$
1x	4 min
1w	6 min
3r	1.8 h
3q	4.1 h
3u	1.6 h
3t	2.4 h

Figure 4-10.*In vitro* serum stability assay of selected compounds. (Supplemental Fig.8 in the published manuscript). The monomeric peptides **1x-w**show half-lives ($t_{1/2}$) of only 4 to 6 minutes.The ethyl-based bis-maleamide linked dimers **3r** and **3q** display a 27 and 41-fold increase in $t_{1/2}$ in serum, while the PEG-linked peptides **3u** and **3t** show a 24 and 27-fold increase in $t_{1/2}$.

It is known that GABAergic transmission can be modulated by changing the lateral diffusion of $GABA_A$Rs (Triller and Choquet, 2005) and that small peptide fragments can effectively compete with binding of full-length intracellular receptor loops (Maric et al., 2014c; Maric et al., 2011). Accordingly, we propose that the compounds presented here act on the anchoring of a defined subset of $GABA_A$R and GlyR receptors, namely receptors that rely on gephyrin-mediated anchoring such as $GABA_A$Rs containing the α1 (Mukherjee et al., 2011b) or α3 (Tretter et al., 2011) subunits and GlyRs featuring the β subunit (Meyer et al., 1995) (Figure4-1). We speculate that the presented molecules could exert their effects in different ways: (1) Act as a highly receptor subtype-specific functional antagonist by uncoupling receptors from synaptic sites and hence tune down fast-synaptic inhibition. (2) Function as a subtype-specific functional agonist, by accelerating the exchange rate of desensitized receptors at post-synaptic sites (Heine et al., 2008; Petrini et al., 2009). Such subtype specific $GABA_A$R agonists hold promise to overcome the limitations of classical benzodiazepines(Rudolph and Knoflach, 2011). (3) Shift the balance of phasic inhibition, mediated by post-synaptic receptors, to tonic inhibition, mediated by extra-synaptic receptors. Extra-synaptic $GABA_A$Rs hold great potential as therapeutic targets.

4.4 MATERIALS AND METHODS

4.4.1 Peptide synthesis.

Peptides **1b-y** were manually synthesized by Fmoc-based solid-phase peptide synthesis (SPPS) at a 0.25 mmol scale on aMiniBlock (Mettler-Toledo, OH, USA) using a 2-chlorotrityl chloride resin (200-400 mesh, 1% DVB). After swelling the resin in dry DCM for 15-30 min,the first amino acid was loaded by dissolving (4 equiv) in dry DCM (1ml/g resin) and adding the solution to the resin with DIPEA (8 equiv), followed by agitation for 1 h and washing of the resin with DCM. Capping of the resin was performed with DCM/MeOH/DIPEA (17:2:1, 3 ml) for 3 × 1 min followed by washing with DCM and DMF. Fmoc deprotection was carried out with 20% piperidine in DMF (2 × 2 min) washing with DMF in-between and after. Coupling steps were carried out using N-[1H-benzotriazol-1-yl)(dimethylamino)methylene]-N-methyl-methanaminium hexafluorophosphate N-oxide(HBTU) and diisopropylethylamine (DIPEA) (resin/amino acid/HBTU/DIPEA, 1:4:4:8) or N-[(dimethylamino)-1H-1,2,3-triazolo-[4,5-b]pyridin-1-ylmethylene]-N-methylmethanaminium hexafluorophosphate N-oxide (HATU) and 2,4,6-trimethylpyridine with a resin/linker/HATU/2,4,6-trimethylpyridine ratio of 1:2:2:3, in dry DMF (3 mL) for 30 min. Finally, the Fmoc group was removed from the terminal residue. Cleavage from thesolid support was conducted by treatment of the resin for 2 h with a cleavage mixture containing TFA/triisopropylsilane(TIPS)/H2O/Ethanedithiol/ Thioanisol (90:2.5:2.5:2.5:2.5, 3 mL). After evaporation *in vacuo*, cold ether precipitation and reverse phase HPLC purification, the peptides were lyophilised and characterized by LC-MS.

4.4.2 Synthesis of dimeric peptides.

General procedure for dimerization of **1c-y** to yield dimeric peptides **3a-y**: 5-10 µmol **1c-y** were dissolved in 5 mlH2O/ACN (2:1) adjusted with 50 mM bicarbonate buffer to pH 8.0. 2.5-5 µmol bismaleamide building blocks **2a-e** (Sigma-Aldrich, Pierce, ThermoScientific) were dissolved in 200 µl ACN and added dropwise over 1h to a final molar ratio of peptide/bismaleamide of 2:1.05 or until LC-MS verifiedfull conversion of the monovalent peptide. Reaction mixtures were directly subjected to reverse phase HPLC purification, followed by lyophilization,which yielded the dimeric peptide ligands as white solids. All final compounds were characterized by LC-MS.

4.4.3 HPLC purification and characterization.

Preparative HPLC was performed on an Agilent 1100 system using a C18 reverse phase column (Zorbax 300 SB-C18, 21.2×250 mm) with a linear gradient of the binary solvent system of H_2O/acetonitrile (ACN)/trifluoroacetic acid (TFA) (A: 95/5/0.1 and B:5/95/0.1) with a flow rate of 20 ml/min. Analytical HPLC was performed on an Agilent 1100 system with a C18 reverse phase column (Zorbax 300 SBC18column, 4.6×150 mm), at a flow rate of 1 ml/min, and a linear gradient of the binary solvent system of H2O/ACN/TFA (A: 95/5/0.1 and

B: 5/95/0.1). Mass spectra were obtained with an Agilent 6410 Triple Quadrupole Mass Spectrometer instrument using electron spray ionization coupled to an Agilent 1200 HPLC system (ESI-LC/MS) with a C18 reverse phase column (Zorbax Eclipse XBD-C18, 4.6×50 mm), autosampler and diode-array detector using a linear gradient of the binary solvent system of H_2O/ACN/formic acid (A: 95/5/0.1 and B: 5/95/0.086) with a flow rate of 1 ml/min.During ESI-LC/MS analysis evaporative light scattering (ELS) traces were obtained with a SedereSedex 85 Light Scattering Detector. The identity of all tested compounds was confirmed by ESI-LC/MS, which also provided purity data (all >90%; ELSD). Peptides were water soluble at neutral pH in the millimolar range.

4.4.4 LC-MS: Monovalent peptides:

Calculated for **1b**: $[M + 1H]^{1+}$: 1567, found 1566.80; [*M* + 2H]2+: 784, found 784.10. Calculated for **1c**: $[M + 1H]^{1+}$: 1479,found 1478.80; $[M + 2H]^{2+}$: 740.6, found 740.59. Calculated for **1c**+Cys: $[M +1H]^{1+}$, 1583, found 1582.8. Calculated for **1d**: $[M + 1H]^{1+}$: 1367, found1366.70; $[M + 2H]^{2+}$: 684, found 684.00. **1d**+Cys: $[M +1H]^{1+}$, 1470, found 1469.7. Calculated for **1e**: $[M + 1H]^{1+}$: 1238, found 1237.7; $[M + 2H]^{2+}$: 620,found 619.5. Calculated for **1f**: $[M + 1H]^{1+}$: 1091, found 1090.70; $[M + 2H]^{2+}$: 545.9, found 545.90. Calculated for **1g**: $[M + 1H]^{1+}$: 976, found 975.60; $[M+ 2H]^{2+}$: 488, found 488.40. Calculated for **1h** $[M + 1H]^{1+}$: 820, found 819.60; $[M + 2H]^{2+}$: 410, found 410.30. Calculated for **1i**: $[M + 1H]^{1+}$: 722, found722.40; $[M + 2H]^{2+}$: 362, found 361.70. Calculated for **1j**: $[M + 1H]^{1+}$: 609, found 609.3; $[M + 2H]^{2+}$: 296, found 296.20. **1j**+Cys: $[M + 1H]^{1+}$: 711, found:711.4. Calculated for **1k**: $[M + 1H]^{1+}$: 522, found 522.30. Calculated for **1k**+Cys: $[M + 1H]^{1+}$, 624, found: 624.3. Calculated for **1l**+Cys: $[M + 1H]^{1+}$: 1265,found 1264.60, $[M + 2H]^{2+}$: 633, found 633.0. Calculated for **1n**+Cys: $[M + 1H]^{1+}$: 1239, found 1238.60; $[M + 2H]^{2+}$: 620, found 620.0. Calculated for**1o**+Cys: $[M + 1H]^{1+}$: 1197, found 1196.60; $[M + 2H]^{2+}$: 599, found 598.90. Calculated for **1p**: $[M + 1H]^{1+}$: 608, found 608.30. Calculated for **1q**: $[M +1H]^{1+}$: 721, found 721.40; $[M + 2H]^{2+}$: 353, found 352.80. Calculated for **1r**: $[M + 1H]^{1+}$: 819, found 818.50; $[M + 2H]^{2+}$: 410, found 409.80. Calculated for**1s**: $[M + 1H]^{1+}$: 671, found 671.3. Calculated for **1t**: $[M + 1H]^{1+}$: 933, found 933.40. Calculated for **1u**: $[M + 1H]^{1+}$: 1048, found 1047.50. Calculated for**1v**: $[M + 1H]^{1+}$: 1135, found 1134.60; $[M + 2H]^{2+}$: 568, found 567.90.Calculated for **1w**: $[M + 1H]^{1+}$: 1239, found 1238.70; $[M + 2H]^{2+}$: 620, found 620.0.Calculated for **1w**+Cys: $[M + 1H]^{1+}$: 1342, found 1341.60; $[M + 2H]^{2+}$: 672, found 671.50. Calculated for **1x**+Cys: $[M + 1H]^{1+}$: 1228, found 1227.60; $[M +2H]^{2+}$: 615, found 614.50. Calculated for **1y**+Cys: $[M + 1H]^{1+}$: 1115, found 1114.6; $[M + 2H]^{2+}$: 558, found 557.90. Calculated for **1z**: $[M + 1H]^{1+}$: 914,found 913.50; $[M + 2H]^{2+}$: 457, found 457.30. Calculated for **1z**+Cys: $[M + 1H]^{1+}$: 1018, found 1017.50.

4.4.5 Dimeric peptides: Calculated for **3a** $[M +2H]^{2+}$: 1475, found 1475.20; $[M +3H]^{3+}$: 984, found 984.00; $[M +3H]^{3+}$: $[M +4H]^{4+}$: 738, found 738.10.Calculated for **3b**: $[M +2H]^{2+}$: 1475,

found 1475.30; [*M* +3H]$^{3+}$: 984, found 983.90, [*M* +4H]$^{4+}$: 738, found 738.20. Calculated for **3c**: [*M* +2H]$^{2+}$: 1475,found 1475.30; [*M* +3H]$^{3+}$: 984, found 983.80; [*M* +4H]$^{4+}$: 738, found 738.30. Calculated for **3d**: [*M* +2H]$^{2+}$: 1328, found 1328.20; [*M* +3H]$^{3+}$: 886, found885.80; [*M* +4H]$^{4+}$: 665, found 664.70. Calculated for **3e**: [*M* +2H]$^{2+}$: 1213, found 1213.20; [*M* +3H]$^{3+}$: 809, found 809.10; [*M* +4H]$^{4+}$: 607, found 607.10.Calculated for **3f**: [*M* +2H]$^{2+}$: 1057, found 1056.70; [*M* +3H]$^{3+}$: 705, found 704.90. Calculated for **3g**: [*M* +2H]$^{2+}$: 1451, found 1451.20; [*M* +3H]$^{3+}$: 968,found 967.90; [*M* +4H]$^{4+}$: 726, found 726.20. Calculated for **3h**: [*M* +2H]$^{2+}$: 1304, found 1304.20; [*M* +3H]$^{3+}$: 870, found 869.80; [*M* +4H]$^{4+}$: 653, found652.6. Calculated for **3i**: [*M* +2H]$^{2+}$: 1189, found 1188.80; [*M* +3H]$^{3+}$: 793, found 793.10; [*M* +4H]$^{4+}$: 595, found 595.10. Calculated for **3j**: [*M* +2H]$^{2+}$:1033, found 1032.70; [*M* +3H]$^{3+}$: 689, found 689.00. Calculated for **3k**: [*M* +2H]$^{2+}$, 1734, found 1734; [*M* +3H]$^{3+}$, 1156, found 1156, [*M* +4H]$^{4+}$, 867,found 867. Calculated for **3l**: [*M* +2H]$^{2+}$: 1624, found 1624.30; [*M* +3H]$^{3+}$: 1083, found 1083.30; [*M* +4H]$^{4+}$: 813, found 812.80; [*M* +5H]$^{5+}$: 650, found650.40. Calculated for **3m**: [*M* +2H]$^{2+}$: 1495, found 1495.30; [*M* +3H]$^{3+}$: 997, found 997.30, [*M* +4H]$^{4+}$: 748, found 748.20. Calculated for **3n**: [*M* +2H]$^{2+}$:1348, found 1348.30; [*M* +3H]$^{3+}$: 899, found 899.10; [*M* +4H]$^{4+}$: 675, 674.70. Calculated for **3o**: [*M* +2H]$^{2+}$: 1233, found 1232.80; [*M* +3H]$^{3+}$: 822, found822.40; [*M* +4H]$^{4+}$: 617, found 617.10. Calculated for **3p**: [*M* +2H]$^{2+}$: 1077, found 1076.70; [*M* +3H]$^{3+}$: 718, found 718.30. Calculated for **3q**: [*M* +2H]$^{2+}$:1452, found 1452.30; [*M*+3H]$^{3+}$: 969, found 968.60. Calculated for **3r**: [*M* +2H]$^{2+}$: 1338, found 1338.10; [*M* +3H]$^{3+}$: 892, found 892.40. Calculated for**3s**: [*M* +2H]^{2}+: 1225, found 1225.20; [*M* +3H]$^{3+}$: 817, found 817.10. Calculated for **3t**: [*M* +2H]^{2}+: 1496, found 1496.30; [*M* +3H]$^{3+}$: 998, found 998.00;[*M* +4H]$^{4+}$: 749, found 748.80. Calculated for **3u**: [*M* +2H]$^{2+}$: 1382, found 1382.30; [*M* +3H]$^{3+}$: 922, found 921.90; [*M* + 4H]$^{4+}$: 692, found 691.60.Calculated for **3v**: [*M* +2H]$^{2+}$: 1269, found 1268.8; [*M* +3H]$^{3+}$: 846, found 846.30. Calculated for **3w**: [*M* +2H]$^{2+}$: 1419, found 1419.30; [*M* +3H]$^{3+}$: 947,found 946.6; [*M* +4H]$^{4+}$: 710, found 710.20. Calculated for **3x**: [*M* +2H]$^{2+}$: 1393, found 1393.30; [*M* +3H]$^{3+}$: 929, found 929.10; [*M* +4H]$^{4+}$: 697, found697.20. Calculated for **3y**: [*M* +2H]$^{2+}$: 1351, found 1351.20; [*M* +3H]$^{3+}$: 901, found 901.10; [*M* + 4H]$^{4+}$: 676, found 676.20.

4.4.6 MALDI-TOF-MS:

Calculated for **3e**: [*M* +H]$^{1+}$: 2425.82, found 2425.782. Calculated for **3r**: [*M* +H]$^{1+}$: 2676.07, found 2675.981. Calculated for **3c**: [*M*+H]$^{1+}$: 2950.35, found 2950.493. Calculated for **3g**: [*M* +H]$^{1+}$: 2902.31, found 2902.899. Calculated for **3d**: [*M* +H]$^{1+}$: 2656.00, found 2656.105.Calculated for **3n**: [*M* +H]$^{1+}$: 2696.06, found 2696.497. Calculated for **3h**: [*M* +H]$^{1+}$: 2608.40, found 2608.482. Calculated for **3s**: [*M* +Na]$^{1+}$: 2471.40,found 2471.417. Calculated for **3t**: [*M* +Na]$^{1+}$: 3014.60, found 3014.937. Calculated for **3v**: [*M* +Na]$^{1+}$: 2559.60, found 2559.680. Calculated for **3q**: [*M*+Na]$^{1+}$: 2926.60, found 2926.212. Calculated for **3u**: [*M* +Na]$^{1+}$: 2786.6, found 2786.281.

4.4.7 Protein expression and purification.

GephE (gephyrin P1 splice variant residues 318-736) as well as residues 378-425 of the large cytoplasmic loop of the GlyR β subunit were expressed and purified as described earlier. In the final purification step protein-containing fractions were collected,concentrated and applied to a 26/60 Superdex 200 size exclusion column (Amersham Biosciences) equilibrated with buffer (10 mM Tris/HCl pH 8.0, 250 mM NaCl, 1 mM β-mercaptoethanol (BME)). Pure fractions were pooled and concentrated using Vivaspin 3 kDa molecular weight cut-off (MWCO) centrifugal filter devices (Sartorius Stedim Biotech) to 20 mg/ml, aliquoted, flash-frozen and stored at -80 °C.

4.4.8 Preparation of whole brain lysates.

Mouse brains from adult C57BL/6J animals were removed and homogenized with a pistol homogenizer in 1ml/200 mg lysate buffer (20 mM Hepes, 100 mM K-acetate 40 mM KCl, 5 mM EGTA, 5 mM $MgCl_2$, 5 mM DTT, 1 mM PMSF, 1% Triton X, protease inhibitor Roche complete, pH 7.2). After centrifugation at 10.000 x *g* for 15 min the full brain lysate was removed as supernatant and flash-frozen asaliquots and stored at -80 °C.

4.4.9 Covalent immobilization of peptides.

GlyR β peptide fragments **1c-k** and **1l-o** with an additional C-terminal Cys were coupled to UltraLink IodoacetylGel (Thermo Scientific) according to the protocol of the manufacturer: The peptides were dissolved in coupling buffer (50 mM Tris, 5 mM EDTA, pH8.5) at a concentration of 1 mM and incubated on buffer-washed and equilibrated UltraLink beads for 2 h at RT. After removing excess peptides the UltraLink beads were subjected to 1 mM cysteine for 2 h to quench possible unreacted iodoacetyl groups. The resin was washed three times and equilibrated with 1M NaCl and stored at 4°C.

4.4.10 Pull-down and western blot detection.

The resin with the immobilized peptides was incubated with brain lysate for 1 h at 4 °C. After three washing steps with the lysate buffer the beads were boiled with Laemmeli buffer containing 10% SDS and the supernatant was applied to a SDS-PAGE followed by western blotting against gephyrin using the mAb7a antibody (Synaptic Systems) at a dilution of 1:500, a phospho-specific antibody directed against the central unstructured linker domain of gephyrin.

4.4.11 Peptide and protein concentration determination.

The concentration of the GephE stock-solution was determined by amino acid analysis and aliquots of an identical stock were used for all experiments to ensure comparability of all experiments and rule out effects of protein activity, degradation, concentration determination and aggregation. Peptide stocks were prepared by weighing the lyophilized powders. All ITC titrations displayed stoichiometries between 0.95 and 1.05 for monomeric peptides and

between 0.45 and 0.55 for the dimeric peptides, thus, demonstrating ahigh accuracy of the measured concentrations and comparability of the results.

4.4.12 Isothermal titration calorimetry (ITC).

The experiments were performed using an ITC200 (MicroCal, Northampton, MA, USA) at 25 °C and 1000 rpm stirring and designed so that c-values were generally within 0.5–100 (c-value = KA x [protein] x N with KA, equilibrium association constant; [protein], protein concentration; N, stoichiometry). Specifically, 40 µl of a solution containing 1-3 mM of the peptide were titrated into the 200 µl sample cell containing 25-100 µM GephE. In each experiment, a volume of 1-2 µl of ligand was added at a time resulting in 20-40 injections and a final molar ratio between 1:3 and 1:6. Ligand-to-buffer titrations were carried out in an analogous fashion, so that the heat produced by injection, mixing and dilution could be subtracted. The binding enthalpy was directly measured, while the dissociation constant (K_D) and stoichiometry (N) were obtained by data analysis using the Origin software (OriginLab). Measurements were conducted at least three times and are given as mean values with the resulting standard deviations.

4.4.13 Protein complex crystallization and X-ray data collection.

Complexes of GephE and dimeric peptides ($GABA_AR$ α3- PEG and GlyR β- *p*-phenyl) were prepared by mixing both in a 1:2 (protein:peptide) molar ratio followed by incubation at 4 °C for 15 min. The complexes were crystallized by the sittingdrop vapour diffusion method at 4 ° C at a concentration of 2.5 mg/ml. GephE-GlyR β-*p*-phenyl was crystallized in the presence of 0.2 M calcium acetate, 0.1 M sodium acetate pH 4.5 and 20-30 % PEG 400 as precipitant. GephE-$GABA_A$ α3-PEG was crystallized in the presence of 0.1 M sodium acetate pH 4.5 and 20-30 % 2-methyl-2, 4-pentanediol (MPD) as precipitant. Crystals were directly flash frozen in the liquid nitrogen. Data werecollected at beam lines ID14-1, BESSY, Berlin and ID 23-1, ESRF, Grenoble.

4.4.14 Structure determination and refinement.

The datasets were indexed and integrated with XDS, further scaling and merging were done by using the CCP4 suite. The structures were solved by molecular replacement with PhaserMR using 2FU3 as initial model. Refinements were carried out with Refmac5. The restraints for the crosslinker were generated by using the PRODRG server (http://davapc1.bioch.dundee.ac.uk/cgi-bin/prodrg). Figures involving molecular representations were prepared using PyMol (http://www.pymol.org). The coordinates have been deposited in the Protein Data Bank with the following PDB codes: 49U0 for GephE-$GABA_AR$ α3-PEG and 49U1 for GephE-GlyR β- *p*-phenyl dimeric peptide complex.

4.4.15 *In vitro* serum stability assay.

Human male serum (Sigma-Aldrich) was pre-incubated at 37 °C for 15 min, before being spiked with selected peptides. All peptides were tested at a final concentration between 50-

100 µM, depending on solubility. Samples were taken out at different time points (0, 3, 5,10, 30 and 60 min for monovalent peptides and at 0, 1, 2, 4, 6, 24 h for bivalent peptides) and quenched by adding 50 µl of 6 M urea followed by 10 min incubation on ice and an addition of 50 µl of 20% trichloroacetic acid followed by 10 min incubation on ice. The samples were centrifuged at 14,000 x *g* for 10 min. The supernatant was analysed by analytical RP-HPLC (1% buffer B/min gradient and a C18 column) at 214 nm. Each experiment wasrepeated three times and normalized against time point 0 min.

4.4.16 Analytical Size Exclusion Chromatography (SEC) and Multi Angle Light Scattering (MALS).

Analytical SEC and MALS were carried out by using a Superdex 200 10/300 GL analytical SEC column (GE healthcare). Analytical SEC experiments were carried at 4°C in buffer composition, 20mM Hepes pH 8, 150 mM sodium chloride and 5 mM β-mercaptoethanol and the MALS experiments were carried out at room temperature (Wyatt technologies).

5.Structural Framework for Metal Incorporation during Molybdenum Cofactor Biosynthesis*

This chapter is based on the following publication:

Kasaragod, V.B., and Schindelin, H. (2016). Structural framework for metal incorporation during molybdenum cofactor biosynthesis. *Structure.***24,**782-8.

***Changes incorporated :**

1. Supplemental information has been merged with the main text.

2.Parts of this chapter which concern the moonlighting function of gephyrin are unpublished.

Statement of individual author contributions and of legal second publication rights

Participated in	**Author Initials,** Responsibility decreasing from left to right				
Study Design Methods Development	VBK VBK	HS HS			
Data Collection	VBK				
Data Analysis and Interpretation	VBK	HS			
Manuscript Writing Writing of Introduction Writing of Materials & Methods Writing of Discussion Writing of First Draft	 VBK VBK VBK VBK	 HS HS			

Statement of individual author contributions to figures/tables/chapters included in the manuscripts

Figure	**Author Initials,** Responsibility decreasing from left to right				
1	VBK	HS			
2	VBK	HS			
3	VBK	HS			
4	VBK	HS			

5. Structural Framework for Metal Incorporation during Molybdenum Cofactor Biosynthesis

Vikram Babu Kasaragod[1] and Hermann Schindelin[1]*

[1]Institute of Structural Biology, Rudolf Virchow Center for Experimental Biomedicine, University of Würzburg, Josef-Schneider-Str. 2, 97080 Würzburg, Germany.

*Correspondence: hermann.schindelin@virchow.uni-wuerzburg.de

5.1 SUMMARY

With the exception of nitrogenase, the molybdenum cofactor (Moco) is essential for the catalytic activity of all molybdenum-containing enzymes, which in humans include sulfite oxidase and xanthine dehydrogenase. Moco biosynthesis follows an evolutionarily highly conserved pathway and genetic deficiencies in the corresponding human enzymes result in Moco deficiency, which manifests itself in severe neurological symptoms and death in childhood. In humans the final steps of Moco biosynthesis are catalyzed by gephyrin, specifically the penultimate adenylation of molybdopterin (MPT) by its N-terminal G-domain (GephG) and the final metal incorporation by its C-terminal E-domain (GephE). To better understand the poorly defined molecular framework of this final step we determined high-resolution crystal structures of GephEin its apo-state and incomplex with ADP,AMP and molybdate. Our data provide novel insights into the catalytic steps leading to final Moco maturation, namely deadenylation as well as molybdate binding and insertion.

5.2 INTRODUCTION

All eukaryotes with the exception of *Saccharomyces cerevisiae* as well as most prokaryotes require the transition element molybdenum (Mo) for viability. To be catalytically active, Mo has to be complexed with the so-called molybdenum cofactor (Moco) (Johnson et al., 1991). Some bacteria and anaerobic archaea, which are independent of Mo for viability, inturn depend on tungsten (W) for their growth (Mendel, 2013). The tungsten and molybdenum cofactors are synthesized through overlapping biosynthetic pathways, with the only difference being that W is inserted into the cofactor instead of Mo to form the tungsten cofactor (Leimkuhler and Iobbi-Nivol, 2015).

Moco biosynthesis is carried out through a conserved multistep pathway (Rizzi and Schindelin, 2002; Schwarz et al., 2009). In humans, GTP is rearranged by MOCS1A and MOCS1B in the first step to form a cyclic pyranopterin monophosphate and in the ensuing step MOCS2A/B and MOCS3 mediate the formation of the metal-ligating dithiolene moiety in the pyran ring (Mendel and Leimkuhler, 2015). The two terminal steps are carried out by gephyrin, a 93 kDa moonlighting protein, which has an N-terminal G (GephG) and a C-terminal E (GephE) domain connected by a ~15 kDa unstructured linker (Prior et al., 1992; Sander et al., 2013). GephG carries out the penultimate step during Moco biosynthesis in which the apo-pyranopterin gets adenylated (Llamas et al., 2004) in an ATP-dependent manner and is then transferred to GephE, where the metal ion (Mo/W) is inserted into the dithiolene group of the pterin coupled to the deadenylation of the AMP-MPT dinucleotide, resulting in active Moco(Belaidi and Schwarz, 2013; Llamas et al., 2006) (Figure 1A). GephG and GephE are homologous to the bacterial MogA (Liu et al., 2000) and MoeA

(Xiang et al., 2001) proteins as well as to the plant Cnx1 G and E (Schwarz et al., 2001) which carry out the respective biosynthetic steps in these organisms.

Mutations in the enzymes responsible for Moco biosynthesis in humans result in an autosomal recessive disorder, referred to as Moco deficiency, which is accompanied by severe neurological symptoms and usually leads to early childhood death (Reiss and Hahnewald, 2011). The majority of mutations affect the upstream proteins MOCS1 and MOCS2, however, two mutations have been reported for gephyrin, which both result in a severe form of Moco deficiency (Bayram et al., 2013).

Gephyrin is a moonlighting protein (Copley, 2003), which also anchors glycine receptors (GlyRs) and a subset of γ-aminobutyric acid type A receptors ($GABA_ARs$) at inhibitory postsynaptic membranes. These receptors mediate inhibitory neurotransmission in the central nervous system (Feng et al., 1998; Tyagarajan and Fritschy, 2014). Biochemical and structural analyses revealed that the receptors interact with GephE through a universal binding site, located within the intracellular loop between transmembrane α-helices 3 and 4 of the GlyR β-subunit and the $GABA_AR$ α1-3 subunits (Kim et al., 2006; Maric et al., 2011; Mukherjee et al., 2011a; Tretter et al., 2008). Via this binding site the receptors are recruited to inhibitory synapses where they are anchored through simultaneous interactions with cytoskeletal componentsand thus critically regulate GABAergic and glycinergic signal transmission (Kirsch et al., 1991). Mutations affecting the anchoring process have been implicated in disease states such as epilepsy and mental retardation (Dejanovic et al., 2014a; Hines et al., 2012a).

Although previous biochemical and structural studies of Cnx1G have provided valuable insights into the understanding of the penultimate step during Moco biosynthesis (Kuper et al., 2004; Kuper et al., 2003), the molecular details of the terminal step are only poorly defined. The GephE-nucleotide and GephE-nucleotide-Mo/W structures presented in this study provide critical insights into Moco maturation. In addition, GephE-ADP-receptor derived peptide ternary complexes provide first structural insights into the integration of two functions of gephyrin.

5.3 RESULTS AND DISCUSSION

5.3.1 Overall Architecture of GephE-Nucleotide Complexes

To understand the mechanism of the deadenylation reaction on a molecular level, structures of GephE in complex with ADP (in the presence of Mg^{2+} or Ca^{2+} or Mn^{2+}) and AMP (with Mg^{2+})were solved. I will focus on the nucleotide complexes in the presence of Mg^{2+} as this is the physiologically relevant metal ion (Llamas et al., 2004). ADP constitutes one half of the adenylated pyranopterin substrate of GephE (Figure 5-1A) while AMP is the second product besides the mature cofactor. All structures were derived from the orthorhombic spacegroup I222 with similar unit cell dimensions (Tables 5-1 and 5-2) and thus any structural changes I report for the complex structures can be attributed to interactions with the ligands rather than differences in crystal packing environments (Figure 5-2).

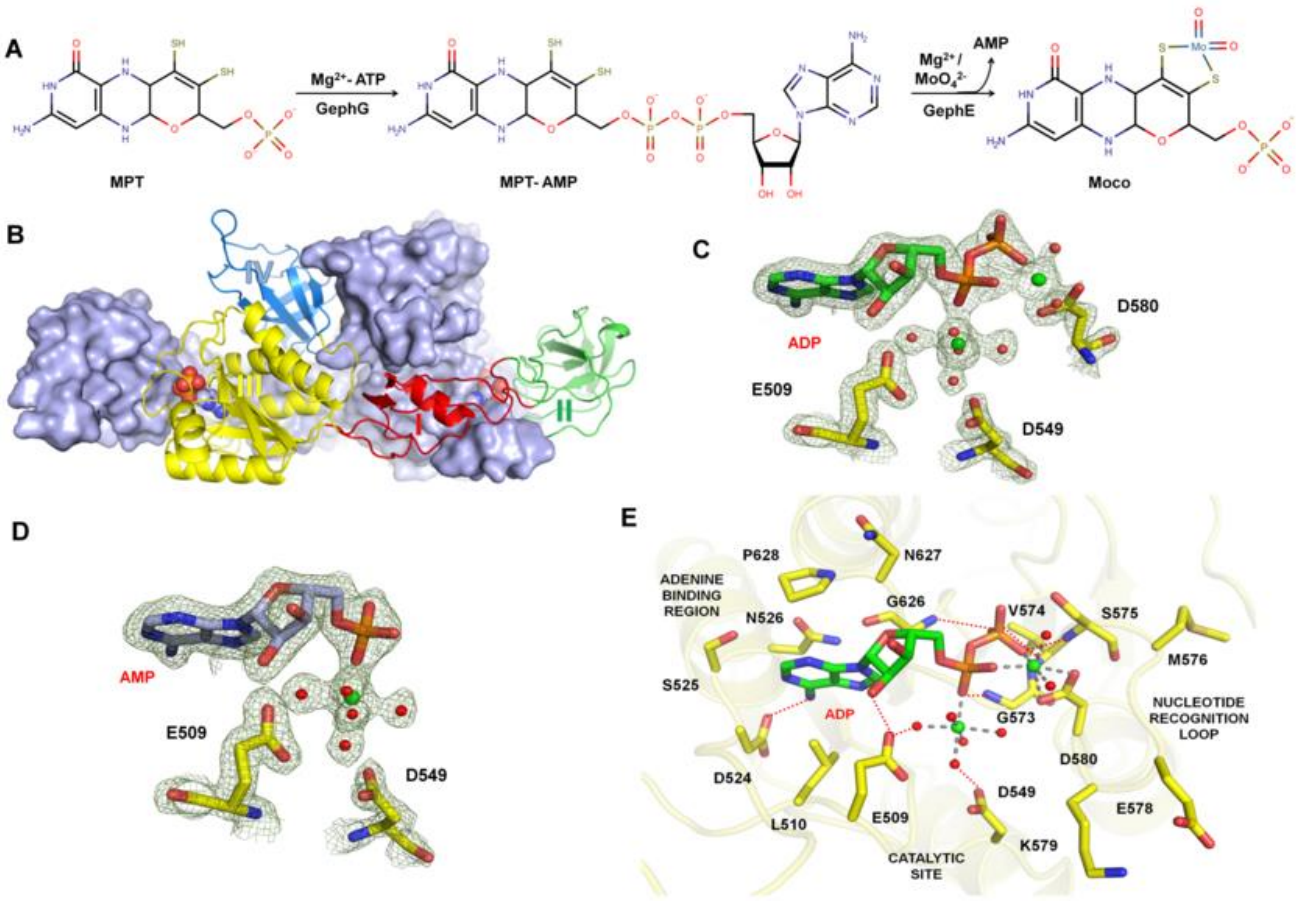

Figure 5-1. (Fig.1 in the published manuscript). Ligand Binding to the E Domain. (A) Reaction scheme of the last two steps during Moco biosynthesis. **(B)** Overall architecture of the GephE-ADP complex. One monomer is shown in ribbon representation with subdomain I in red, subdomain II in green, subdomain III in yellow and subdomain IV in blue, the other in surface representation in grey-blue. The bound ADP molecules are shown in space filling representation. **(C)** $2F_o$-F_c omit maps for ADP contoured at an rmsd level of 1.0 with Mg^{2+} ions in green and water molecules in red. **(D)** $2F_o$-F_c omit maps for AMP at an rmsd level of

1.0. **(E)** Close-up view of the nucleotide binding pocket with hydrogen bonds as red dotted lines and Mg^{2+}-coordinating interactions as dashed gray lines.

Table 5-1. Summary of Crystallization Conditions.

Protein	Crystallization condition
GephE-apo	0.1 M sodium acetate pH 4.5, 25% 2-Methyl-2,4-pentanediol
GephE-ADP-$MgCl_2$	0.1 M sodium acetate pH 4.5, 20% 2-Methyl-2,4-pentanediol
GephE-AMP-$MgCl_2$	0.1 M sodium acetate pH 4.5, 34% 2-Methyl-2,4-pentanediol
GephE-ADP-Na_2WO_4	0.1 M sodium acetate pH 4.5, 0.02 M calcium chloride, 30% 2-Methyl-2,4-pentanediol
GephE-ADP-Na_2MoO_4	0.1 M sodium acetate pH 4.5, 0.02 M calcium chloride, 24% 2-Methyl-2,4-pentanediol
GephE-ADP-$MnCl_2$	0.1 M sodium acetate pH 4.5, 26% 2-Methyl-2,4-pentanediol
GephE-ADP- $GABA_AR$	0.2 M sodium acetate pH 4.5,0.02 M calcium chloride, 26% 2-Methyl-2,4-pentanediol
GephE-ADP- Glyβ R	0.3 M sodium acetate pH 4.5,0.02 M calcium chloride, 34% 2-Methyl-2,4-pentanediol

Structurally, GephE can be divided into four subdomains (I-IV) with the nucleotide-binding pocket residing in subdomain III, which is composed of residues 318-341 and 498-654 (Figure 5-1B), however, in the context of dimeric GephE, the nucleotide is also close to subdomain II of the other monomer. Subdomain III features a Rossmann fold with seven central β-strands surrounded by five α-helices. Interestingly, it is structurally similar to GephG and the apo-structures can be superimposed resulting in an rmsd of 2.06 Å as stated earlier (Schwarz et al., 2001). ADP/AMP are well defined (Figure 5-1C and 5-1D) and both are bound in the vicinity of the C-terminal ends of three β-strands, in agreement with the general location of the ligand-binding site in the Rossmann fold.

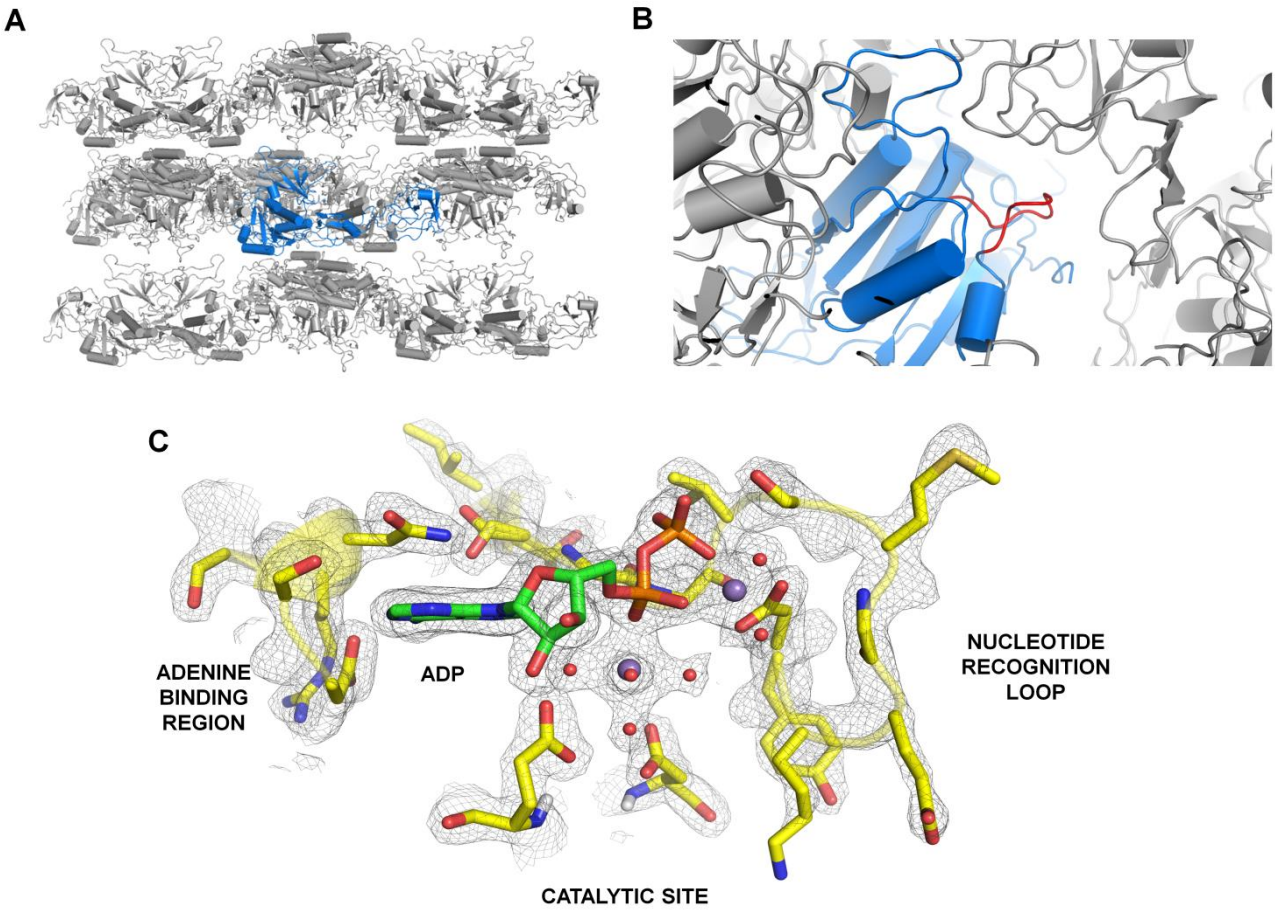

Figure 5-2. Structural Features of GephE Complexes: (Supplemental Fig.1 in the published manuscript). (A) Crystal packing of GephE and its various complexes in spacegroup I222. The single molecule present in the asymmetric unit is colored in blue and its symmetry related molecules in gray. **(B)** Enlarged view of the nucleotide recognition loop (red) clearly shows that its conformation is not influenced by crystal contacts. **(C)** $2F_o$-F_c map contoured at an rmsd of 1.5 of the nucleotide-binding pocket for the GephE-Mn^{2+}-ADP bound structure.

5.3.2 Structural Features of the Nucleotide-Binding Pocket

The nucleotide-binding pocket can be subdivided intoan adenine-binding region, a nucleotide recognition loop and a catalytic site for AMP-MPT hydrolysis. The adenine-binding region is mainly comprised of residues 524-526, which interact with the adenine ring of ADP/AMP (Figure 5-1E) and preclude the binding of guanine due to a non-compatible hydrogen bond donor/acceptor profile. The nucleotide recognition loop is composed of residues 573-582, which recognize the phosphate(s) of ADP/AMP and, by analogy, the pyrophosphate moiety of AMP-MPT and harbor the most significant conformational changes upon nucleotide binding (see below). The catalytic region features the acidic side chains of Glu509, Asp549 and Asp580. In both the ADP and AMP bound structures, Glu509 interacts

directly with the 2'-OH group of the ribose and also coordinates the α-phosphate through one of the Mg^{2+}-ion coordinating water molecules. In a similar way, Asp549 coordinates the same Mg^{2+}-ion via a metal-coordinating water molecule. This Mg^{2+}-ion is octahedrally coordinated by five water molecules and one oxygen from the α-phosphate. Possibly even more critical is Asp580,which, in a bidentate fashion, directly coordinates the second Mg^{2+}-ion, present only in the ADP-bound structure. The coordination sphere of this Mg^{2+}-ion is completed by one oxygen each from α-and β-phosphate and two water molecules resulting again in an octahedral arrangement (Figure 5-1E).

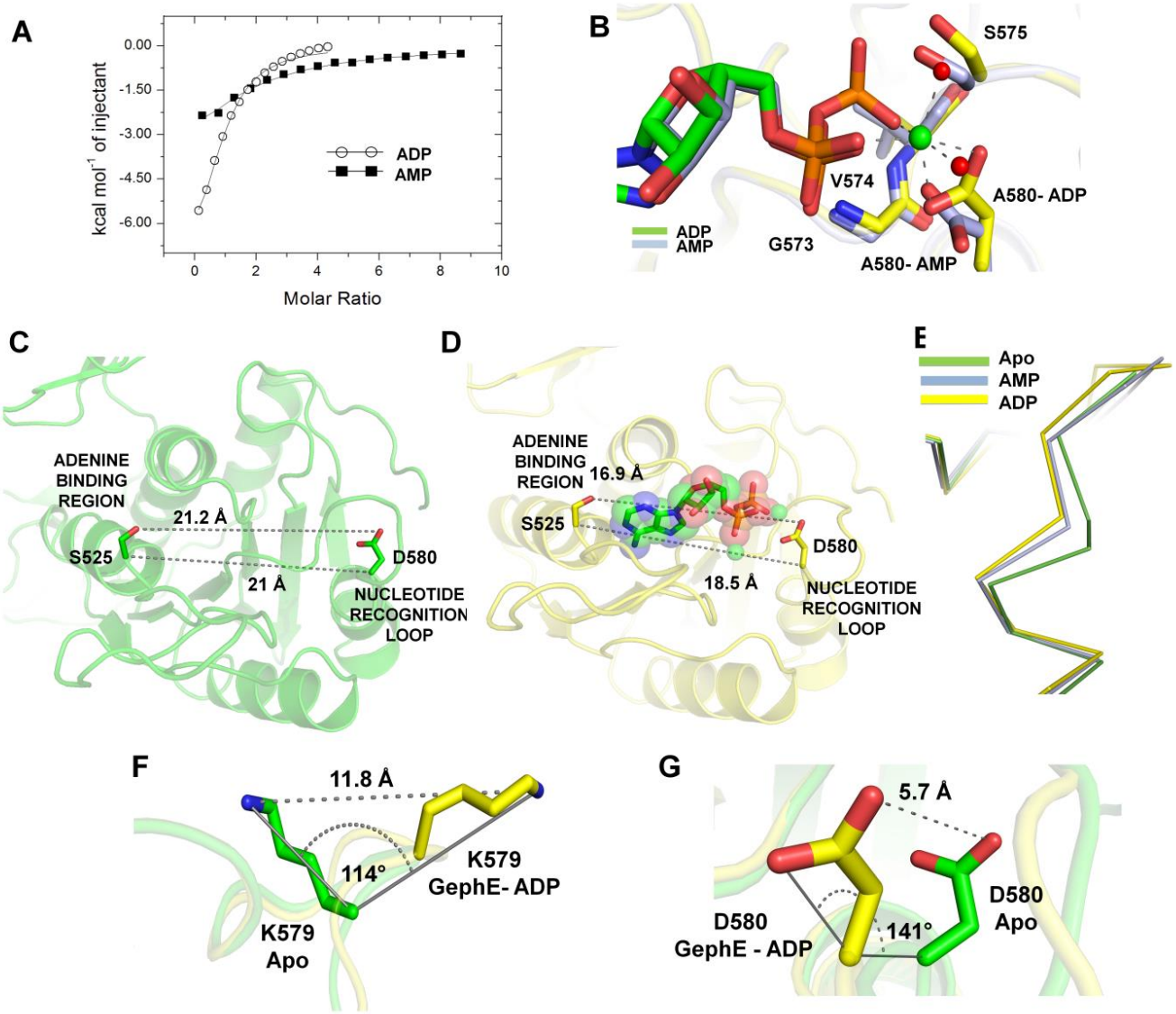

Figure 5-3. (Fig.2 in the published manuscript). Nucleotide Binding and Conformational Changes: (A) ITC curves for the titrations of ADP and AMP to GephE. **(B)** Superposition of the ADP and AMP bound structures of GephE. **(C)** Distances between the Cα and Oγ-Oδ2 atoms of Ser525 in the adenine binding region and Asp580 in the nucleotide recognition loop in the apo-structure. **(D)** Distances between the Cα and Oγ-Oδ2 atoms of Ser525 in the adenine binding region and

Asp580 in the nucleotide recognition loop in GephE -Mg^{2+}-ADP. **(E)** Superposition of the nucleotide recognition loops in the apo-state (green) as well as the ADP (yellow) and AMP bound (blue) states. **(F)** Structural rearrangements of Lys579 between the apo and ADP bound states. **(G)** Structural rearrangements of Asp580 between the apo and ADP bound states.

Table 5-2. Data Collection and Refinement Statistics.

	GephE-Apo	GephE-ADP	GephE-AMP	GephE-ADP-W	GephE-ADP-Mo
Beamline	ESRF-ID 29	ESRF-ID 30A-3	ESRF-ID 30A-3	PETRA IIIP13	PETRA IIIP14
Wavelength (Å)	0.9762	0.9640	0.9640	1.2148	0.6187
Space group	I222	I222	I222	I222	I222
Unit cell Parameters a, b, c (Å)	87.67, 99.29, 113.72	87.68, 99.53, 113.03	87.00, 99.28, 112.79	87.66, 99.68, 113.24	87.68, 99.10, 113.06
Resolution limits (Å)	43.0 - 1.55	43.84- 1.65	49.64- 1.70	74.82-1.80	74.52- 1.60
R_{sym}	0.055 (0.808)	0.091 (0.998)	0.145 (1.081)	0.180 (2.134)	0.093 (1.724)
R_{pim}	0.049 (0.710)	0.056 (0.615)	0.093 (0.729)	0.074 (0.875)	0.030 (0.553)
$CC_{1/2}$	0.998 (0.502)	0.998 (0.564)	0.992 (0.562)	0.996 (0.577)	1.0 (0.700)
Redundancy	3.7 (3.8)	6.8 (6.9)	6.5 (6.1)	13.2 (13.5)	20.5 (20.8)
Unique reflections	71,703	59,012	53,903	46,251	65,106
Completeness	0.988 (0.982)	0.99(0.98)	1.0 (1.0)	1.0 (1.0)	1.0 (1.0)
$\langle I/\sigma I \rangle$	11.1 (1.5)	12.3 (1.7)	8.0 (1.5)	12.3 (1.8)	19.2 (2.0)
R / R_{free}	0.154/ 0.186	0.153/ 0.182	0.153/ 0.180	0.157/ 0.200	0.144/ 0.174
Deviations from ideal values in					
Bond distances (Å)	0.007	0.004	0.008	0.008	0.007
Bond angles (°)	0.952	0.825	0.981	0.990	0.971
Ramachandran statistics (%)	97.9/ 1.9/ 0.2	98.8/ 1.2/ 0.0	98.6/ 1.4/ 0.0	99.1/ 0.9/ 0.0	99.1/ 0.5/ 0.4
Overall average B factor ($Å^2$)	32.11	28.53	24.55	30.45	30.51
Coordinate error (Å)	0.17	0.18	0.16	0.22	0.15

All quantitities in this table are defined according to Table 2-1.

A biochemical characterization of the interaction of GephE and the nucleotides AMP and ADP by isothermal titration calorimetry (ITC) revealed that ADP binds to the E domain with a dissociation constant (K_D) of ~260 µM, in contrast to AMP, which bound with a ~7-fold lower

affinity (K_D ~2 mM). In both cases, the interactions displayed a stoichiometry of 1:1(Figure 5-3A), in accordance with our structures (Figure 5-3B).

5.3.3 Conformational Changes in the Nucleotide Recognition Loop

Although the overall architecture of the GephE-nucleotide structures were similar to the apo-structure with rmsd values of 0.81 Å and 0.78 Å for the ADP and AMP complexes, respectively, nucleotide-binding triggered localized conformational changes in subdomain III, specifically in the nucleotide recognition loop. To quantify the movement of the loop regions I relied on two marker residues, Ser525 and Asp580 (Figure 5-3C), and measured the distances between their Cα atoms and selected atoms in their side chains. Ser525 interacts with the adenine in all of our structures and, quite importantly, does not display differences in any of our structures. On the other hand Asp580, located in the nucleotide recognition loop, underwent conformational changes and the distance pairs thus yielded an indication of the relative movement of the nucleotide recognition loop in the different structures. In the apo-structure, the nucleotide recognition loop adoptedan open conformation, where Ser525 and Asp580 were at distances of 21.0 Å (Cα-Cα) and 21.2Å (Oγ-Oδ2) (Figure 5-3C), however, in the ADP-bound structure, the nucleotide recognition loop was present in a closed conformation, where the marker residues were at distances of 18.5 Å (Cα-Cα) and 16.9 Å (Oγ-Oδ2) (Figure 5-3D). Thus, binding of ADP triggered an inward movement of the nucleotide recognition loop with a maximal displacement of 2.5 Å for the Cα (4.3 Å for the Oδ2) of Asp580 (Figure 5-3D).

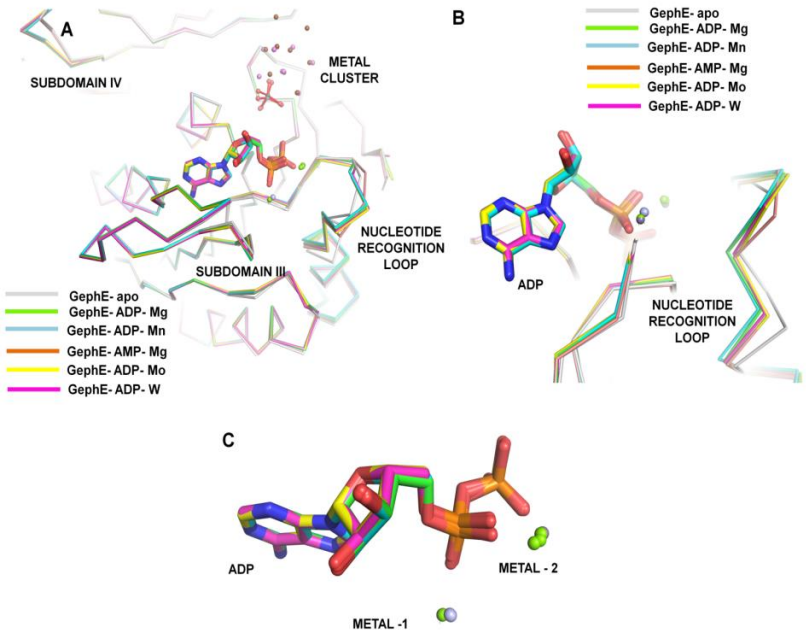

Figure 5-4. Comparison of Structures: (Supplemental Fig.2 in the published manuscript). (A) Superposition of GephE-apo, and its binary and ternary complexes. **(B)** Enlarged view of the nucleotide recognition loop illustrating its conformational heterogeneity and flexibility. **(C)** Superposition of ADP moieties in the binary and ternary complexes indicating the limited flexibility in the phosphates and associated metal ions.

In addition to these overall structural rearrangements of the nucleotide recognition loop (Figure 5-3E and Figure 5-4), striking changes were observed for Lys579 and Asp580. In the apo-structure, Lys579 pointed towards the ADP binding site while Asp580 was oriented roughly in the opposite direction. Nucleotide binding triggered an outward movement of Lys579 characterized by a rotation of 114° coupled to a maximal displacement of 11.8 Å for the Nε atom (Figure 5-3G). In contrast, Asp580 flipped into the nucleotide binding siteby undergoing a 141° rotation which was coupled to an inward movement by 5.7 Å (Figure 5-3F).The conformational change of Asp580 appears to becritical for the binding of the nucleotides as it allows this residue to coordinate the second metal ion.

5.3.4 Structures of Ternary GephE-ADP-Mo/W Complexes Provide Insights into Metal Ion Insertion

Mo is taken up by all organisms which rely on this trace metal in the form of the highly water soluble molybdate anion and Mo is also incorporated into the metal-free form of the Moco in the form of this anion (Bittner, 2014; Tejada-Jimenez et al., 2007). To identify and characterize the molybdate-binding region of GephE, GephE-ADP co-crystals were soaked in either sodium molybdate or sodium tungstate solutions (15 mM) and diffraction data were collected at the absorption edge of the respective metal (Figure 5-6).

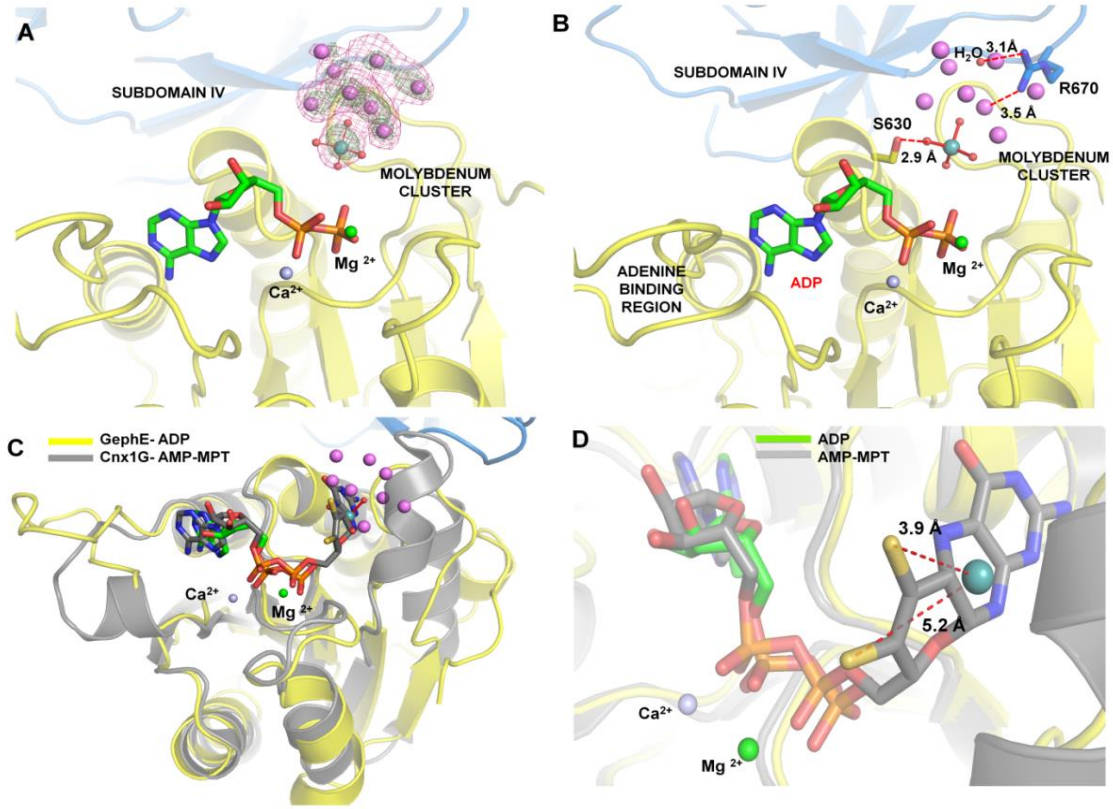

Figure 5-5. Metal Binding and Incorporation: (Fig.3 in the published manuscript). (A) Structure of the GephE-ADP-Mo complex with the anomalous density (green) contoured at an rmsd of 6.0 and the corresponding $2F_o$-F_c density (purple) at an rmsd of 1.5. The apical Mo is colored in cyan, all other Mo in

purple and Ca^{2+} in gray. **(B)** Architecture of the GephE-ADP-Mo ternary complex where the apical Mo (blue) is represented with its bound oxygen atoms (red) and the other molybdenum atoms as purple spheres. **(C)** Superposition of the Cnx1G domain in complex with the AMP-MPT dinucleotide (gray, PDB: 1UUY) and the GephE-ADP-Mo complex (yellow). **(D)** Close-up view of the superposition with only the apical Mo atom shown. Distances between this atom and the dithiolene S-atoms of the pterin are depicted as red dashed lines.

In both cases a strong anomalous signal could be detected which in case of the tungstate-soaked crystal allowed straightforward structure solution by single wavelength anomalous diffraction with data collected at the W-L_{III}edge (1.2148 Å). The data collected with the molybdate-soaked crystals provide, to the best of my knowledge, the first example of data collected at the Mo-K edge (0.6187 Å).

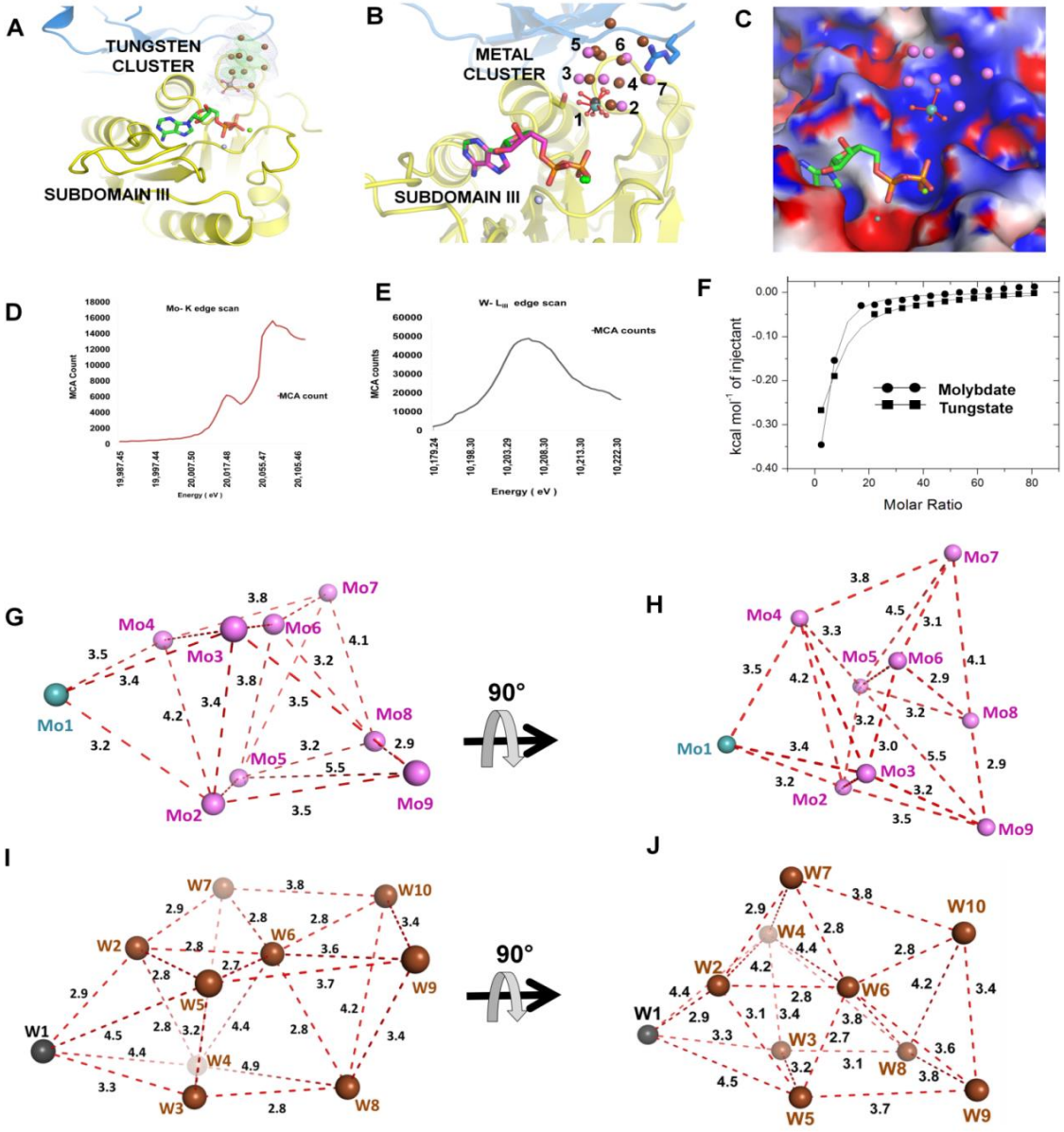

Figure 5-6. Mo and W Cluster:(Supplemental Fig.3 in the published manuscript). (A) Anomalous density (green, rmsd of 6) and $2F_o$-F_c (blue, rmsd of 1.5) for the tungsten cluster in the GephE-ADP-

tungsten ternary complex. **(B)** Superposition of the GephE-ADP-Mo complex (yellow) with the W-cluster in the GephE-ADP-W structure. The apical molybdenum (blue) and tungsten (black) atoms are shown with their bound oxygen atoms (red). The Arabic numbers 1-7 indicate the conserved positions in the metal clusters. **(C)** Electrostatic surface potential of the nucleotide and metal-binding pocket in the GephE-ADP-Mo complex (electropositive in blue and electronegative in red, contoured at ±5kT). ADP is represented with sticks and metals as spheres, with the apical Mo in blue and all other Mo atoms in purple.Energy scans at the Mo-K **(D)**and W-L_{III} **(E)** edge. **(F)** ITC titration curves of the molybdate and tungstate titrations to the GephE-ADP complex. **(G)-(J)** Two different views of the molybdenum and the tungsten clusters with inter-metallic distances given in Å. All sites in the molybdenum cluster **(G and H)** are colored in purple except for one (blue), which is in close proximity of Ser630. Mo3, Mo4, Mo6 and Mo7 constitute the first plane and the second plane of metals is constituted by Mo2, Mo5, Mo8 and Mo9.All sites in the tungsten cluster **(I and J)**are colored in brown except for one (black), which is in close proximity of Ser630.The first plane of metals is constituted by W2, W5, W6, W7, W9 and W10, while W3, W4 and W8 constitute the second plane in the metal cluster.

Surprisingly, multiple anomalous scatterers located in close spatial proximity were detected in both datasets at the same electrostatically positive location (Figure 5-6C), which is in close proximity of the nucleotide-binding pocket (Figures 5-5A and 5-5B). For the molybdate soaked crystals nine sites (Figure 5-6) were detected with peak heights varying between 18 and 7 rmsd, while ten sites (Figure 5-6) were observed for the tungstate treated crystals ranging in peak height between 39 and 4 rmsd. In addition to the slight difference in the total number of metal sites the order of peaks was also different between the two structures; nevertheless there are sevenpositions, which were conserved (defined as being at distances of less than 1.5 Å) between the two clusters (Figure 5-6). In the W-containing structure nine of the ten W atoms are arranged in two parallel layers (Figure 5-6) with one plane containing six sites in a pentagonal arrangement surrounding a central Wand the other three sites adopting a triangular arrangement. The final W is located in between the two layers in close proximity to the nucleotide recognition loop and forms an apex of the structure. In the molybdate-soaked crystals two layers containing four metal sites (Figure 5-6) were present with the apical Mo (corresponding in position to the apical W-site) being in plane with the bottom layer and coordinated tetrahedrally by surrounding oxygen atoms.

The metal sites were modeled as independent scatterers; however, it cannot be ruled out that a smaller number of discretely disordered molybdate/tungstate molecules exists. In fact, since some rather short metal-metal distanceswere observed (shortest Mo-Mo distance of 2.6 Å, shortest W-W distance of 2.7 Å), which would indicate the presence of metal-metal bonds with calculated distances of 2.74 Å for W-W and 2.76 Å for Mo-Mo single bonds (Pyykko and Atsumi, 2009) but are incompatible with the compounds used for soaking, it is safe to assume that disordered molybdate/tungstate molecules are in fact present. However,

my attempts to model discretely disordered molybdate/tungstate sites were unsuccessful. Common to both metal clusters is the apical site (#1) (Figure 5-6); not only is its location conserved but also the fact that at this site molybdate/tungstate could be clearly modeled resulting also in conserved positions for the oxygen atoms (Figure 5-5B and 5-6). The metal clusters were located between Ser630 from subdomain III and Arg670 from subdomain IV with Ser630 coordinating one of the oxygens of the molybdate/tungstate located at site #1 (Figure 5-5B and 5-6). For reasons outlined below I assume that this site represents, or is at least close, to the catalytically relevant molybdate/tungstate site. In addition, ITC experiments revealed that molybdate and tungstate binds to the GephE-ADP complex with a 1:1 stoichiometry and an affinity of ~1.1 and ~3.5 mM, respectively (Figure 5-6).

To derive insights into the mechanism of Mo-insertion the structure of the Cnx1 G-domain in complex with the AMP-MPT dinucleotide was superimposed with the ternary GephE-ADP-Mo structure (Figure 5-5C). This analysis revealed that the metal clusters were in close spatial proximity of the Mo/W-ligating dithiolene moiety. In particular the apical Mo was close tothe two S-atoms in the dithiolene group (Figure 5-5D) with metal-sulfur distances between 3.9 Å and 5.2 Å (the corresponding W-S distance were 3.8Å and 5.3 Å). This result suggested that the soaking experiments revealed the position the metal adopts before it is incorporated into the apo-form of Moco. Ser630 would not only directly coordinate the critical molybdate/tungstate by forming a hydrogen bond to one of the metal-coordinating oxygen atoms but could also play a role during catalysis.

5.3.5 Framework for Moco Biosynthesis is Evolutionarily Conserved

Multiple sequence alignments of gephyrin with homologs from different evolutionary domains were generated. As representative species *E.coli* MoeA, *A.thaliana* Cnx1 and *Rattus norvegicus* gephyrin are shown in Figure 5-7A; however, the clusters of conserved residues are also present if sequences from 8 different model organisms representing different phylogenetic kingdoms are aligned (Figure 5-4B).

Three clusters of conserved residues, D-S/T-N-R (red), T/S-S-G-G-V-S (blue) and L-P-G-N-P-V-S (orange), together with three conserved acidic residues (green) seem particularly noteworthy. These regions have been mapped onto the surface of GephE (Figure 5-7B) as they represent the adenine-binding region, nucleotide recognition loop, Mo/W-binding region and the residues contributing to Mg^{2+}-ligation, respectively.

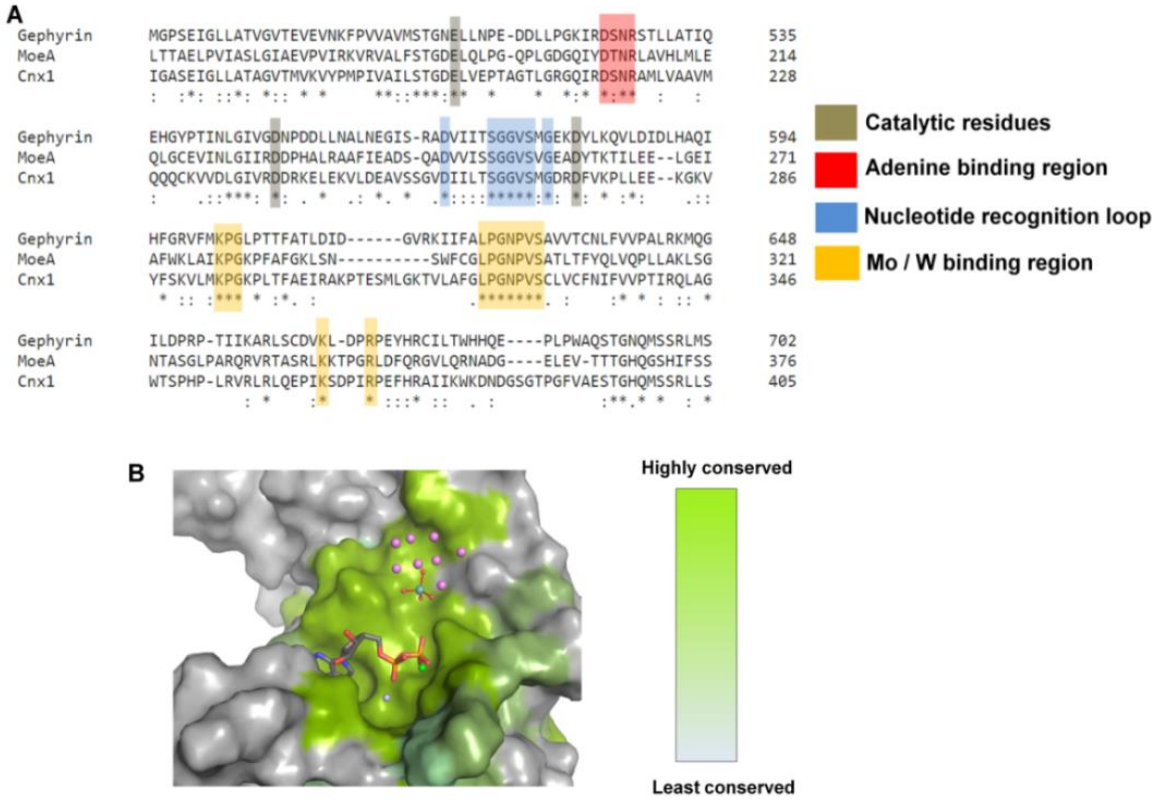

Figure 5-7. Sequence Conservation in the E Domain. (Fig.4 in the published manuscript). (A) Excerpt from the sequence alignment of *Rattus norvegicus* gephyrin, *E.coli* MoeA and*A. Thaliana* Cnx1. Conserved residues are indicated by asterisks, and type-conserved residues with either a colon or a period. Surface exposed stretches of conserved residues are highlighted in color. **(B)** Surface representation of the nucleotide-binding pocket with sequence conservation indicated in shades of green ranging from full (bright green) to no conservation (gray). This figure is based on a multiple sequence alignment of gephyrin and its homologs from 8 different organisms (*R. norvegicus, Homo sapiens, Xenopus laevis, E.coli, A. thaliana, Neurospora crassa, Drosophila melanogaster, Danio rerio*).

Mutational analysis and functional studies with *E. coli* MoeA (Nichols et al., 2007) have identified Glu188, Asp228 and Asp259 as being either important for substrate-binding or catalysis and these residues correspond to Glu509, Asp549, and Asp580 of GephE (Figure 5-8). As stated above, Asp580 directly ligates the second Mg^{2+}-ion, Glu509 interacts with the 2'-OH group of the ribose and also ligates one of the Mg^{2+}-ions through a water molecule while Asp549 also ligates the same Mg^{2+}-ion via a second water molecule. In addition to the residues mentioned above, a subdomain II deletion mutant of MoeA also displayed a diminished level of Moco biosynthesis.

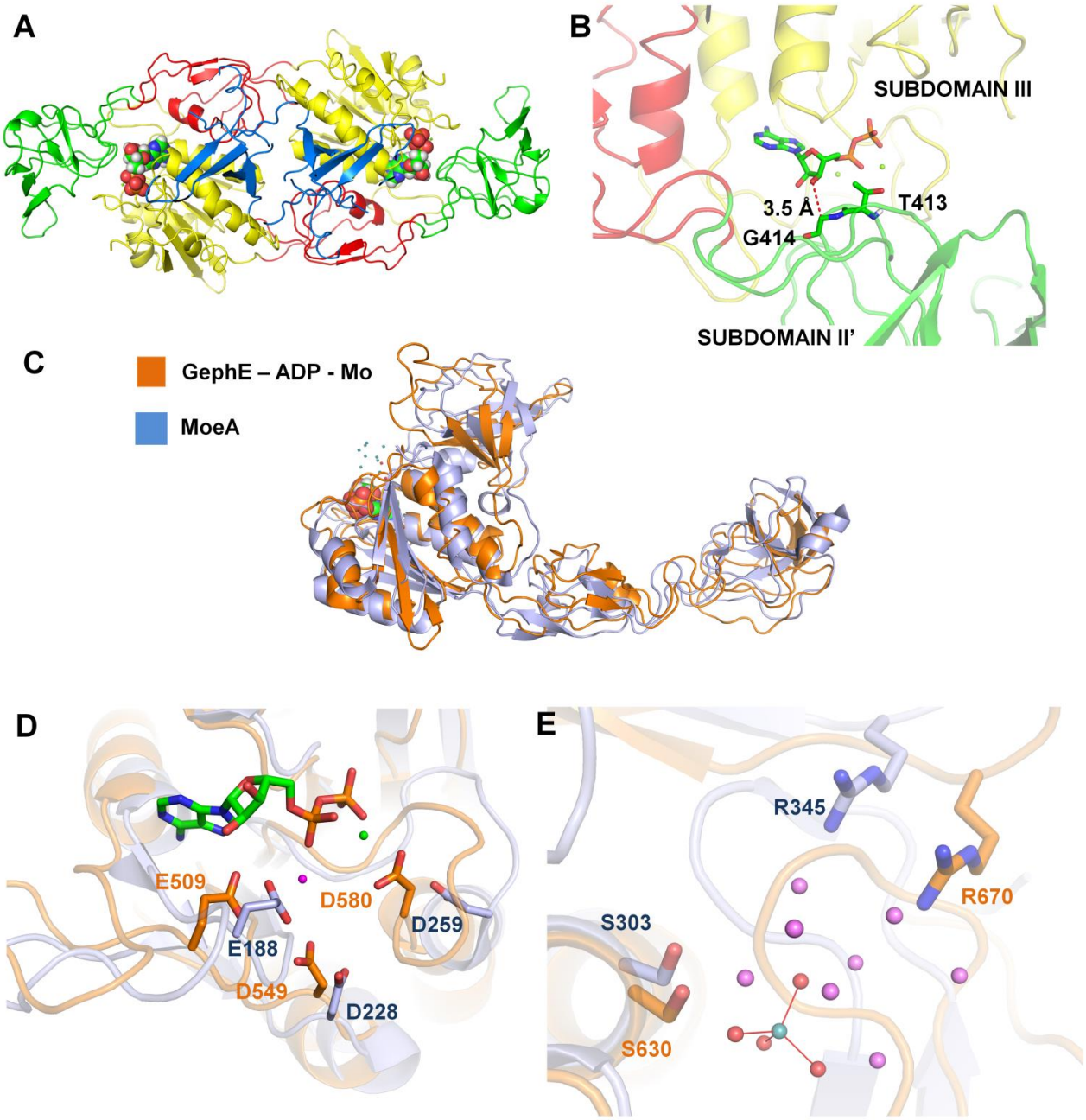

Figure 5-8. Comparison of GephE with MoeA: (Supplemental Fig.4 in the published manuscript). (A) Structure of the GephE-ADP structure viewed along the twofold axis of symmetry. **(B)** Enlarged view of the nucleotide-binding pocket illustrating the importance of Gly414 from subdomain II of the second monomer in nucleotide binding. **(C)** Superposition of GephE and MoeA based on subdomain III. **(D and E)** Enlarged views of the nucleotide and metal-binding regions in GephE and MoeA colored as in **(C)**. Critical residues are represented as sticks.

Our structures revealed that subdomain II from the second monomer is in close proximity of the nucleotide-binding pocket and, in particular, Gly414 is at a distance of 3.5Å from the 3'-OH group of the ribose and hence this strictly conserved residue also seems to play a critical

role during nucleotide-binding (Figure 5-8). Finally, Ser630 and Arg670, which are located on either side of the metal cluster, are strictly conserved. While a direct participation of Ser630 in the metal incorporation process seems straightforward given the close proximity of the molybdate/tungstate to site #1 of the cluster (see above), a direct binding of Arg670 to the single molybdate/tungstate could be easily accomplished by conformational changes in its side chain. The strict conservation of these residues (Figure 5-7B) demonstrates that Moco biosynthesis is conserved throughout evolution.

Table 5-3. Data Collection and Refinement Parameters.

Parameters	**Structure**		
	GephE-Mn^{2+}-ADP	GephE-ADP-$GABA_AR$	GephE-ADP-Glyβ R
Beamline	ESRF ID 30A-3	ESRF ID 30A-3	BESSY- ID 14.1
Wavelength (Å)	0.9640	0.9640	0.9696
Space group	I 222	I 222	I 222
Unit cell Parameters (a, b, c in Å)	87.93, 99.61, 112.32	86.96, 99.22, 111.61	88.09, 99.65, 113.00
Resolution limits (Å)	43.96 – 2.0	25– 1.6	25– 1.95
R_{sym}[a]	0.195 (1.589)	0.071 (0.609)	0.111 (0.527)
R_{pim}[b]	0.081 (0.67)	0.057 (0.50)	0.098 (0.46)
$CC_{1/2}$	0.991 (0.532)	0.997 (0.689)	0.989 (0.698)
Redundancy	12.9 (12.8)	4.5 (4.2)	3.7 (3.5)
Unique reflections	33,205	62,920	36,353
Completeness	1.0 (1.0)	0.98 (0.97)	0.99 (0.99)
$<I/\sigma I>$[c]	11.6 (1.8)	10.3 (1.9)	6.9 (2.0)
R[d] /R_{free}[e]	0.162/0.201	0.165/0.203	0.203/ 0.245
Deviation from ideal values in			
Bond distances (Å)	0.009	0.028	0.0181
Bond angles (°)	0.990	2.2190	1.875
Ramachandran statistics (%)[f] (Preferred/Allowed/Outliers)	97.6/2.4/0.0	97.9/1.7/0.5	96.9/1.7/0.4
Overall average B factor($Å^2$)	34.54	28.72	32.61
Coordinate error (Å)[g]	0.20	0.05	0.12

All the terms in the table are defined as according to the Table 2-1.

5.3.6 Implications for Human Health

Mutations in the enzymes catalyzing Moco biosynthesis result in Moco deficiency, a fatal disease accompanied by severe neurological impairments and early death. Most mutations

have been mapped to enzymes catalyzing earlier steps in this pathway. Of the twoclinically reported mutations in gephyrin, one is due to a frameshift in GephG after 21 amino acids resulting in a non-functional protein (Reiss et al., 2001). The second mutation, the homozygous D580A substitution (Reiss et al., 2011), completely abolished Moco biosynthesis and resulted in severe neurodevelopmental deficiencies in the affected patient Strikingly, our biochemical and structural data show that Asp580, which is conserved throughout evolution as described above, undergoes a large structural rearrangement upon nucleotide-binding and based on its proximity to the second Mg^{2+} I have postulated a catalytic role for this residue during the hydrolysis of the AMP-MPT dinucleotide.

5.3.7 Structure of a GephE-ADP-receptor derived peptide complexes provide clues towards the integration of gephyrin's dual functionality.

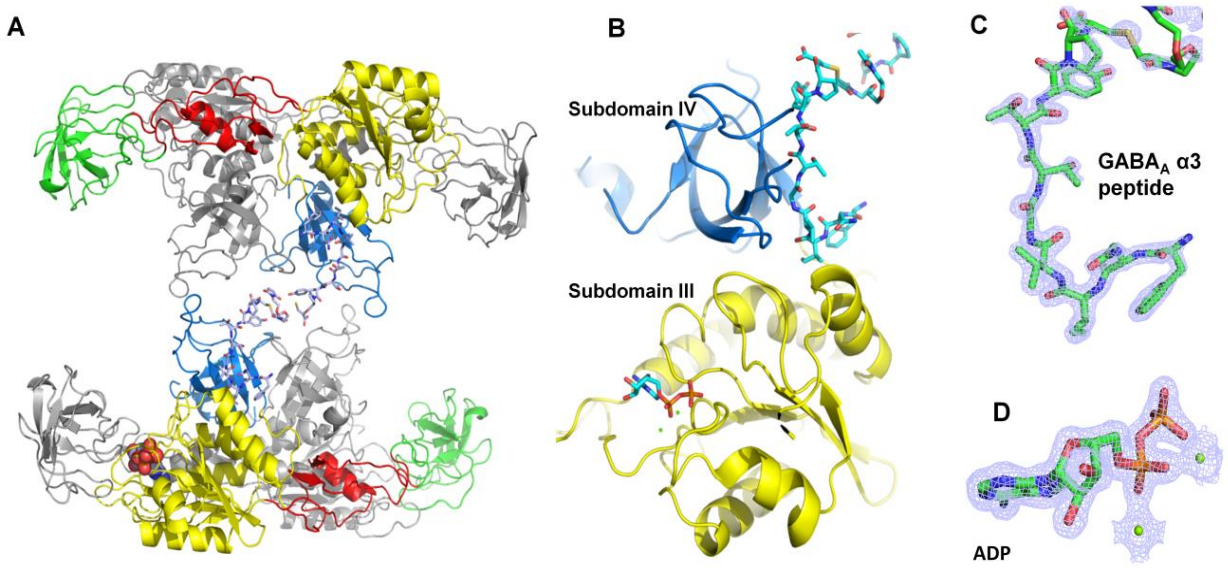

Figure 5-9: GephE-ADP-GABA$_A$R α3 complex: (Unpublished data). (A) Overall architecture of GephE-ADP-GABA$_A$R α3 subunit derived peptide complex. Subdomains are colored according to Fig. 1B. The peptide is represented as sticks and ADP in space filling representation. **(B)** Enlarged views of subdomains III and IV with the respective bound ligands. $2F_o$-F_c electron density contoured at 1.5 rmsd for the bound peptide **(C)** and ADP **(D).**

A comparison of the GephE-ADP structures with structures of GephE in complex with peptides derived from either the GlyR β-subunit or GABA$_A$R α3-subunit derived peptides revealed that the nucleotide binding and peptide binding pockets are ~20 Å apart (Kim et al., 2006; Maric et al., 2014b). In addition, structural comparison of the peptide binding pocket in the ADP bound structure with that of the GephE-Apo structure did not display major structural rearrangement in the peptide binding pocket. To determine whether there is any communication between the two sites, the ternary GephE-ADP-GABA$_A$R α3 (Figure 5-9)and

GephE-ADP-GlyR β complexes were crystallized. These complexes again crystallized in the orthorhombic I222 spacegroup with cell dimensions similar to the binary complexes (Table 5-3) and identical crystallization conditions (Table 5-1). In both ternary complexes, the overall architecture was similar to that of the binary complexes and a comparison of the bound nucleotide and peptide in the ternary complex with the respective binary complexes revealed only minimal structural rearrangements in either the peptide or nucleotide. Although the major site for the Moco biosynthesis in the human body is the liver, it has been already shown that local Moco biosynthesis takes places in the CNS. In addition, the clinical mutations which impair Moco biosynthesis did not display an altered clustering of the receptors at the postsynapses hinting towards the independency of these two functions from eachother (Reiss et al., 2011; Smolinsky et al., 2008). These ternary complexes thus structurally integrate the two independant cellular functions of gephyrin.

5.4 CONCLUSIONS

The data presented here provide valuable insights into the deadenylation and metal incorporation step during Moco biosynthesis. The crystal structures clearly demonstrate how the AMP moiety of the AMP-MPT substrate of the E domain is recognized by an adenine-binding region which selects against guanine and pyrimidine bases. Binding of the pyrophosphate linkage appears to be coupled to significant conformational changes, especially in the nucleotide recognition loop located in subdomain III and foremost in Asp580. Interestingly, substitution of this residue with alanine leads to Moco deficiency in humans. Finally, the ternary GephE-ADP-Mo/W complexes showed that the metal is bound at another conserved site, in close proximity to where the metal-accepting dithiolene group is predicted to reside. Thus, the data represented here help to decipher the terminal step of the evolutionarily conserved Moco biosynthetic pathway at an atomic level. In addition, the ternary complexes provide first critical insight into the simultaneous participation of gephyrin in two distinct cellular functions, i.e. Moco biosynthesis and neurotransmitter receptor anchoring.

5.5 EXPERIMENTAL PROCEDURES

5.5.1 Protein Expression and Purification

GephE (gephyrin P1 splice variant residues 318-736) was expressed in *E.coli* BL21DE3 and induced at an optical density of 0.8at 600 nm with 0.5 mM isopropyl β-D-1-

thiogalactopyranoside (IPTG) and grown overnight at 30°C. Purification involved initial affinity chromatography with chitin beads, cleavage of the intein tag, followed by anion exchange chromatography with a MonoQ 10/300 (GE Healthcare) column. Finally, the protein was purified by size exclusion chromatography on a Superdex 200 26/60 (GE Healthcare) column to homogeneity in 20 mM Hepes pH 8.0, 150 mM NaCl and 5 mM β-mercaptoethanol. Nucleotides were purchased from Sigma Aldrich.

5.5.2 Isothermal Titration Calorimetry (ITC)

GephE was dialyzed overnight into 20 mMHepes pH8.0, 100 mMNaCl, 2mM $MgCl_2$ and 5 mM β-mercaptoethanol (ITC buffer). All experiments were performed using an ITC200 (GE Healthcare) at 37 °C and 500 rpm stirring. Specifically, for the nucleotide titrations, 40 µl of a solution containing either 15 mM ADP or 30 mM AMP was titrated into the 300 µl sample cell containing 700µM of GephE. For the molybdate and tungstate titrations, 100 mM molybdate or tungstate was dissolved in ITC buffer and titrated into 250µM GephE-ADP complex in the cell. In each experiment, a volume of 2.4 µl of ligand was added at a time resulting in 16 injections. The reference titrations of ligand to buffer were subtracted from the ligand to protein titrations to obtain the final titration curves. Data were analyzed with a single site binding model with the OriginLab software.

5.5.3 Protein Complex Crystallization and X-Ray Data Collection

Complexes of GephE and AMP/ADP were prepared by mixing the protein with 2-5mM nucleotides and either 5mM $MgCl_2$ or 5 mM $MnCl_2$, followed by incubation at 4 °C for 30min. The complexes were crystallized by the sitting dropvapor diffusion method at 20˚C at a concentration of 3 mg/ml. The crystallization of the ternary complexes of GephE-ADP and receptor derived peptide complex was crystallized by incubating GephE with 2mM ADP and 1:2 molar ration of receptor derived peptide and crystallized at a concentration of 3mg/ml as described for the binary complex of GephE-ADP. For structural analyses of the GephE-ADP-tungstate and GephE-ADP-molybdate complexes, GephE-ADP co-crystals were soaked in 15 mM sodium tungstate or 15 mM sodium molybdate for 2 minutes. Diffraction data were collected at beamlines ID29 and ID30A-3 of the ESRF inGrenoble and beamlines P13 and P14 of PETRA III in Hamburg. Crystallization conditions are summarized inTable 5-1.

5.5.4 Structure Determination and Refinement

Data were indexed and integrated with XDS (Kabsch, 2010) further scaling and merging were done with the CCP4 suite (Bailey, 1994).The structures were solved by molecular replacement with PhaserMR (McCoy et al., 2007)using PDB entry 4PD0 as initial model (Maric et al., 2014c) except for the tungstate-soaked crystals, where the structure was solved by SAD phasing. For experimental phasing, the SHELXC/D/E (Sheldrick, 2008) pipeline followed by automated model building with ARPWarp (Langer et al., 2008) was utilized. Refinements were carried out with PHENIX (Adams et al., 2010). The data collection

and refinement statistics are summarized in Tables 5-2 and Table 5-3 . All figures representing crystal structures were prepared using PyMol (http://www.pymol.org).

5.6 ACCESSION NUMBERS

The coordinates have been deposited in the Protein Data Bank with the following PDB codes: 5ERQ, 5ERR, 5ERS, 5ERT, 5ERU and 5ERV.

5.7 AUTHOR CONTRIBUTIONS

Experiments were designed by VBK and HS. VBK performed all experiments. VBK and HS analyzed the data and wrote the manuscript.

5.8 ACKNOWLEDGEMENTS

We thank Dr. Petra Hänzelmann and Dr. Jochen Kuper for critical reading of the manuscript and Dr. Bodo Sander for the help with ITC. We also thank Dr. Gleb Bourenkov, beamline P14 of PETRAIII and all other beamline scientists at ESRF and PETRA III for excellent technical assistance during data collection. This work was supported by the Deutsche Forschungsgemeinschaft (Schi425/8-1 and FZ 82) to HS.

6. Characterization of the Gephyrin-Microtubule Interaction

6.1 INTRODUCTION

Gephyrin, the central organizer at inhibitory postsynapses was co-purified initially with the GlyR and microtubules (Kirsch et al., 1991). Gephyrin anchors receptors such as $GABA_AR$ (Maric et al., 2014b) and GlyR (Kim et al., 2006; Meyer et al., 1995) to the postsynaptic membrane by acting as a bridge between the receptors and cytoskeletal elements. Besides the interaction with the microtubules, it has been already shown that gephyrin also interacts, at least indirectly, with the other major cytoskeletal component, namely F-actin (Giesemann et al., 2003). Nevertheless, only limited knowledge exists about how gephyrin interacts with the cytoskeleton (microtubules and microfilaments), despite the fact that these interactions are important for the intracellular transport of at least the GlyRs and for clustering of both types of inhibitory neurotransmitter receptors. Disruption of microtubules in cultured spinal cord neurons caused a rapid reduction of gephyrin clusters and, quite interestingly, disruption of the tubulin or actin cytoskeleton in mature cultured hippocampal neurons, however, did not affect gephyrin clustering. GlyRs were shown to be retrogradely co-transported with gephyrin via the GlyR β-subunit mediated direct interaction, and this transport depends cytoskeletal elements; incontrast $GABA_AR$ transport remains poorly characterized (Maas et al., 2006). Although it is known that gephyrin interacts with microtubules, solid experimental evidence is still missing to pinpoint the interaction, apart from initial clues derived from *in situ* experiments and bioinformatics analyses. The studies presented in this thesis narrowed down the interaction site on gephyrin for tubulin to the residues encoded by exon 14, which is part of the linker region in gephyrin and shares high sequence homology to the Tau protein, a classical microtubule-associated protein (Ramming et al., 2000). The data presented here, which were obtained mainly though co-sedimentation assays, discover an additional binding site for tubulin rather than the one which was already shown, thus providing valuable insights into the critical gephyrin-tubulin interaction.

6.2 AIMS

The main aim is to map the binding site of the microtubule on gephyrin and structurally characterize the gephyrin-tubulin complex by X-ray crystallography and to derive insight into the significance of this interaction in maintianing the architecture of the synapse.

6.3 MATERIALS AND METHODS

6.3.1 Purification of gephyrin constructs, DARPin and RB3-SLD.

Different gephyrin constructs used in the interaction studies were Full-length (FL), Linker + GephE (LE), GephG + Linker (GL), GephG, GephE and the Δ14 construct, which carries a deletion of exon 14. The FL, LE, GL, GephG and Δ14 constructs were expressed in the *E coli* BL21DE3 strain and were induced with 0.5mM IPTG at an optical density of 0.8 at 600 nm and grown overnight at 15°C. The cells were harvested by centrifuging the culture at 8000 x *g*. In all cases, purification involved a 3-step protocol with initial nickel affinity, followed by anion ion exchange chromatography by using a MonoQ 10/100 column (GE Healthcare) and finally size exclusion chromatography by using a SD 26/60 column (GE healthcare). The cells were resuspended in 150 ml lysis buffter (100 mM Hepes pH 8, 500 mM NaCl, 10% glycerol, 1mM EDTA and 5 mM β-mercaptoethanol), supplemented with 3 cocktail protease inhibitor tablets (Roche Diagnostics) and cell lysis was performed with a cell disruptor (Microfluidizer M-110P, Microfluidics) by passing the resuspended cells twice through the machine at a pressure of 1500 bar. The supernatant was separated by two step centrifugation step: 1) centrifuging the lysate at 58000 X *g* by using a JA 25.50 rotor for 10 mins and, 2) the supernatant was transferred to new centrifugation tubes and again centrifuged for 20 mins more at the same speed (Beckmann). The separated supernatant was then loaded onto 14 ml Ni-beads which were pre-equilibrated with lysis buffer and the elution was carried out with 5 CV of elution buffer (50 mM Hepes pH 8, 250 mM NaCl, 250 mM imidazole and 5 mM β-mercaptoethanol). The fractions containing protein was pooled and subsequently MonoQ anion exchange chromatography and SEC was carried out. The SEC buffer contained 20 mM Hepes pH 8.0, 150 mM NaCl and 5 mM β-mercaptoethanol. In all linker-containing constructs, native PAGE was carried out after the MonoQ step to separate higher-order oligomers. In the native PAGE analysis, only those protein fractions which displayed a single band in the gel were pooled and subsequently carried forward for size exclusion chromatography. Those fractions which displayed multiple protein bands were considered to be mixtures of higher order oligomers and were discared after the anion exchange chromatography.

GephE (gephyrin P1 splice variant residues 318-736) was expressed in *E.coli* BL21DE3 and induced at an optical density of 0.8 at 600 nm with 0.5 mM IPTG and grown overnight at 30°C. Purification involved initial affinity chromatography with chitin beads, cleavage of the intein tag, followed by anion exchange chromatography with a MonoQ 10/300 (GE Healthcare) column. Finally, the protein was purified by size exclusion chromatography on a Superdex 200 26/60 (GE Healthcare) column to homogeneity in 20 mM Hepes pH 8.0, 150 mM NaCl and 5 mM β-mercaptoethanol.

The DARPin gene was chemically synthesized and was cloned into the pET28a plasmid by Genescript. DARPin was expressed following the Geph-FL expression protocol (see above) with minor modifications. The only change applied during the course of expression is that the culture was incubated at 18°C overnight post induction with 0.5mM IPTG. Cell harevesting was carried out as decribed for the FL-Geph construct. The cells were resuspended in lysis buffter (50mM Hepes pH8, 300mM NaCl, 5mM β-mercaptoethanol) and cell lysis was performed with a cell disruptor (Microfluidizer M-110P, Microfluidics) by passing the resuspended cells twice through the machine at a pressure of 1500 bar. The supernatant was separated by centrifuging the lysate at 58000 x *g* by using a JA 25.50 rotor (Beckmann). The lysate was loaded onto 5 ml Ni-beads which were pre-equilibrated with lysis buffer and the elution was carried out with 5 CV of elution buffer (50mM Hepes pH 8, 300 mM NaCl, 250 mM imidazole and 5 mM β-mercaptoethanol). The fractions containing the proteins were pooled and purified to homogeneity by size exclusion chromatography by using a Superdex SD 26/60 column (GE healthcare)

The RB3-SLD construct in the pET8c plasmid was kindly provided by Dr. Patrick Curmi. The protein was expressed in *E.coli* BL21 DE3 cells grown at 37°C until the OD_{600} reached 0.6-0.7. Then the culture was induced with 0.5 mM IPTG and grown further for 4 hours post induction. The RB3-SLD domain was purified according to (Charbaut et al., 2001) with slight modifications. The cell pellet was resuspended in 50 mM Hepes pH 8.0, 250 mM NaCl and 5 mM β-mercaptoethanol and cells were lysed with a cell disruptor. The lysate was centrifuged at 58000 x *g* by using a JA 25.50 rotor (Beckmann Coulter) for one hour at 4 °C and the supernatant was heated to 80°C for 5 min. Next, the precipitant was centrifuged at 400000 x g by using a TLA 100 rotor (Beckmann Coulter) for 30 min at 4°C . The supernatant from this step was then diluted to a final salt concentration of 80 mM, followed by anion exchange chromatography with a MonoQ 10/100 column. Finally, the fractions containing RB3-SLD were pooled and purified to homogeneity by size exclusion chromatography on a Superdex SD 26/60 column (GE Healthcare)

6.3.2 Microtubule purification from cow brain.

Microtubules were purified from cow brain by using a multistep polymerization-depolymerization method (Castoldi and Popov, 2003) . 500g of cow brain were washed with 1XPBS (8g of NaCl, 0.2g of KCl, 1.44g of Na_2HPO_4,0.24g of KH_2PO_4in 1 litre, pH 7.4) and cleared of blood clots. The chopped brain pieces were transferred into ice cold depolymerization buffer ((DB), 50mM MES pH-6.6, 1mM $CaCl_2$,1 l per kg brain)) and homogenized with a hand mixer from Clatronic, twice for 1min. Cell debris was cleared from the supernatant by using a Beckman JLA 16.250 rotor at 29,000 x *g* for 60 min at 4 °C.In the first polymerization step, the cleared supernatant was supplemented with an equal amount

of warm (37 °C) high molarity PIPES buffer ((HMPB) (1M PIPES pH 6.8, 10mM $MgCl_2$, 20mM EGTA)), anhydrous glycerol, ATP (1.5mM final concentration), and GTP (1.5mM final concentrations). This mixture was incubated at 37 °C in a water bath for 1 h. The mixture was centrifuged at 225000 x *g* by using a Ti45 Beckman rotor for 60 min at 37 °C in an ultracentrifuge to pellet down the polymerized microtubules. The resulting microtubule pellet was resuspended in 100 ml of cold DB and incubated at 4 °C with on a rotating shaker. The depolymerized tubulin was subsequently centrifuged in a Ti 45 Beckman rotor at 110000 x *g* for 30 min at 4 °C. A second polymerization step was carried out with the supernatant as described above. The polymerized tubulin was pelleted in a Ti45 Beckman rotor at 225000 x *g* for 30 min at 37 °C.The microtubule pellet was resuspended in 1XBRB80 buffer (80mM PIPES pH6.8, 1mM $MgCl_2$, 1mM EGTA) and incubated at 4 °C on a rotating shaker. The depolymerized tubulin was centrifuged in a TLA 100.4 Beckman tabletop ultracentrifuge rotor at 165000 x *g* for 30 min at 4 °C to remove any aggregated materials.The tubulin supernatant was collected and its concentration was determined by measuring its absorption at 280nm using a molar extinction coefficient of 115,000 M^{-1} cm^{-1}.

6.3.3 Microtubule co-sedimentation assay.

Prior to the co-sedimentation assay, an additional polymerization - depolymerization step was carried out to remove inactive tubulin. Subsequently, tubulin was polymerized at 37°C for one hour by the addition of 2mM GTP, 5mM $MgCl_2$, in the presence of taxol to stabilize the microtubules. Microtubules were pelleted down in a TLA 100 rotor at 130000 x *g* for 30 min at 37°C. Pellets were suspended in BRB80 buffer. For the initial optimization of the assay, FL were mixed (5 µM) with different concentrations of microtubule (1-3 µM)-containing solution (20 µl solution) and incubated at 10°C for one hour in 0.1 M Pipes pH 6.8, 10 mM $MgCl_2$, 1 mM EGTA. As a control experiment, all proteins were incubated in the same buffer without microtubules. For assays with the different gephyrin constructs, proteins (20µl solution at a molar concentration of 10µM) were incubated with 5 µM concentrations of microtubule. Subsequently, the samples were loaded onto a 50% glycerol cushion (50µl) prepared in BRB80 buffer and centrifuged at 350000 x *g* for 20 min at 25°C by using a Beckmann TLA 120 rotor. The supernatant and pellet fractions were analyzed by SDS-PAGE.

6.3.4 Nano-gold labelling, negative staining and electron microscopic (EM) analysis of the microtubule-gephyrin complex.

Microtubule samples were prepared for EM studies as described earlier. The gephyrin-microtubule samples were prepared by mixing gephyrin and microtubules in a 2:1 molar ratio and were incubated at 10°C for one hour. Nano-gold labelling of gephyrin was carried out by incubating an anti-His Nanogold (5nm) solution from Nanoprobes with gephyrin in a 1:2

molar ratio at room temperature for 30 min. Unlabeled nano-gold beads were separated from labeled protein by centrifuging at 25000 x *g* for one hour at 4°C.

Microtubules, gephyrin and the microtubule-gephyrin complex were deposited on glow-discharged carbon coated grids. R 2/2 Cu 300 mesh grids were bought from Quantifoil. The carbon coating was carried out by using a Denton Vaccum Desk V and then glow discharged for 45 seconds at $2.2x10^{-1}$ tor by using a Harric plasma cleaner. The samples were then stained with 2% (w/v) uranyl acetate and the grids were washed twice with water to remove un-bound samples and excess staining solution. The EM images were recorded with a 120 kV Tecnai G2 spirit twin microscope by using an Eagle 4K camera at 42000X magnification.

6.3.5 Analytical size exclusion chromatography coupled to multi angle light scattering (SEC-MALS).

SEC-MALS experiments were carried out in buffer containing 20 mM Hepes pH 7.2, 100 mM KCl, 1 mM $MgCl_2$ and 0.5 mM EGTA. Complex formation between tubulin and DARPin was carried out by mixing the protein at a 1:2 molar ratio either at room temperature or at 4°C. Size exclusion chromatography was carried out by using a Superose6 10/300 column coupled to a MALS instrument (Wyatt technologies). Parameters such as the UV-absorbance at 280 nm, the light scattering (LS) and the differential refractive index (dRI) were measured. The LS and dRI were recorded by using a Dawn 8^+ detector from Wyatt technologies and a T-rEX refractomer, respectively. All MALS measurements were carried out at room temperature.

6.4 RESULTS AND DISCUSSIONS

6.4.1 Microtubule co-sedimentation assays provide hints at multiple binding sites for tubulin on gephyrin. All proteins required for the assay were purified to homogeneity. To check for the binding of FL to microtubules and to fine map the gephyrin-microtubule interaction, classical co-sedimentation assays were carried out.

Initially, the assay conditions were optimized for buffer composition, temperature and incubation time and also with respect to time, temperature and centrifugation speed to sediment the samples. This initial screening helped to identify the buffer composition as 0.1 M Pipes pH 6.8, 10 mM $MgCl_2$, 1 mM EGTA (assay buffer) to be the best suitable buffer with a one hour incubation at 10°C. The centrifugation conditions were optimized to 350000 x *g* for 20 min at 25 °C. The sedimentation of full-length gephyrin showed that the majority of the protein molecules were retained in the presence of microtubules, the majority of full-length gephyrin was pelleted with the microtubules (Fig. 6-1B). Control assays with different

constructs of gephyrin in the absence of microtubules showed that the majority of each protein is retained in the supernatant (Fig. 6-1A), in line with the behavior of the full-length protein.

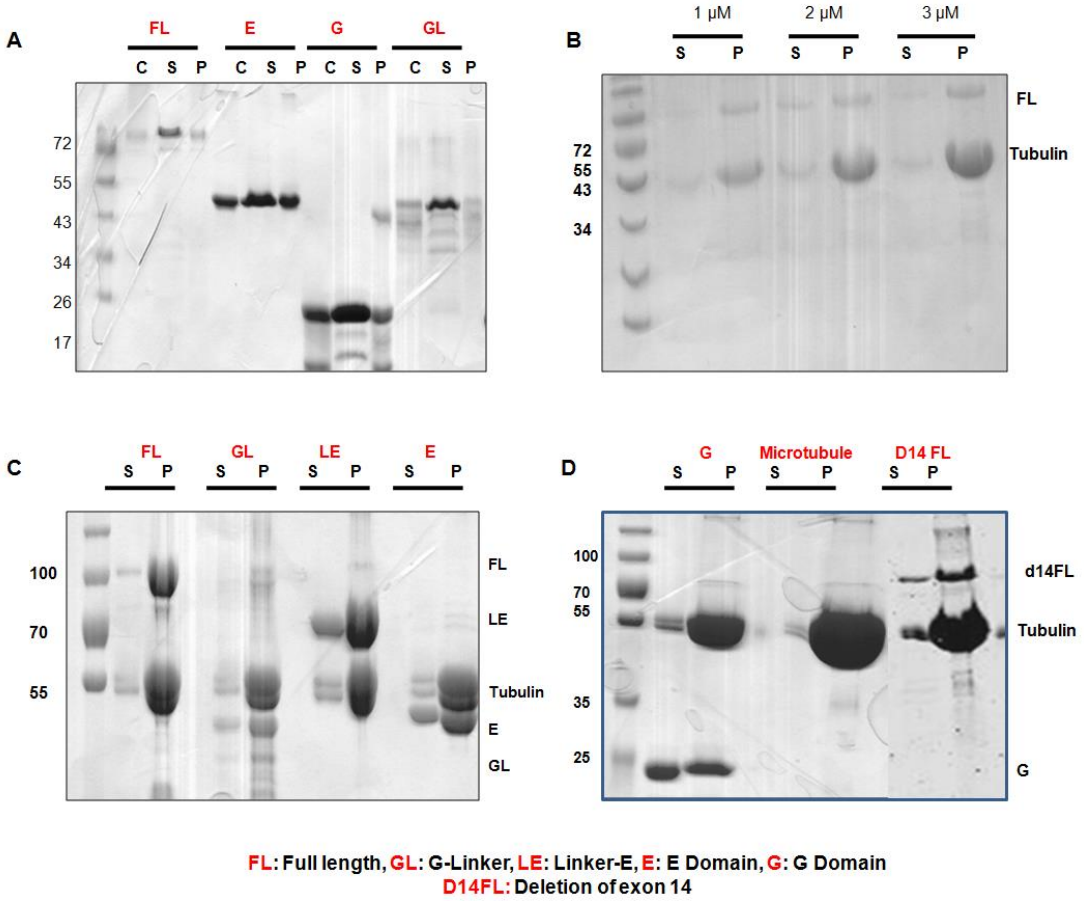

Figure 6-1: Microtubule co-sedimentation assay.(A) Control assays for the different gephyrin constructs. C, S and P refer to control, soluble and pellet fractions.In the control lane, 5 µM (5µl) of different proteins were loaded. **(B)** Optimization of the co-sedimentation assay with full-length gephyrin. The gel clearly demonstrates that with increasing amounts of microtubules (1-3 µM), the amount of FL-gephyrin proportionately increased. The concentration of FL-gephyrin remained constant at 5 µM. **(C, D)** Co-sedimentation assays with different constructs of gephyrin. The amount of protein being pelleted down compared to the supernatant fraction increased in all cases with the exception of the G domain. Please note that the SDS-PAGE presented in **(C)** was run for a longer time so that proteins with a molecular weight below 45 kDa ran through the gel, while proteins with similar molecular weights above 55 kDa were well separated. In all experiments, a constant concentration of microtubule (5µM) and different gephyrin contructs (always at a concentration of 10 µM) were used.

With this initial optimization, the assays were performed with the aforementioned gephyrin constructs. The assays clearly showed that GephFL, LE, GL, and E were pelleted down

more effectively in the presence of the microtubule in comparison to the control runs (Fig. 6-1A and 6-1C). Surprisingly, gephyrin witha deletion of exon 14 (D14FL) harboring the presumed binding site also co-sedimented with the microtubules, suggesting the presence of an additional microtubule binding site in gephyrin. A closer inspection of these results suggested that the additional and previously unknown binding site resides in the E domain of gephyrin as the GephE, GL and LE constructs also co-sedimented with microtubules (Fig. 6-1C). The negative binding of the G domain rules out any contribution of the G domain towards the gephyrin-tubulin interaction (Fig. 6-1A and 6-1D). Thus, the co-sedimentation assays helped to identify two different binding sites for microtubules in gephyrin, one residing in the linker region, specifically residues 320 to 334 (numbers according to P2 splice variant with the sequence VQSRCSSKENILRA) encoded by exon 14 and the other being located in the E domain.

6.4.2 Electron microscopy analysis of microtubules, gephyrin and the microtubule-gephyrin complex.

EM analysis of taxol-stabilized microtubules clearly showed the formation of microtubule filaments (Fig. 6-2A). In case of gephyrin, it was hard to analyze the morphology of the single particles due to a high deposition concentration in the absence of nano-gold labeling (Fig. 6-2B). Incontrast, the nano-gold labeled gephyrin sample typically showed single labeled beads with each bead presumably corresponding to a gephyrin trimer (Fig. 6-2E). This is due to the fact that full-length gephyrin trimerizes via its N-terminal G domain and the N-termini either not being far enough from each other to separate individual labeled nano-gold beads, as the distance between the N-termini of the each monomer is less than 50 nm, or only one nano-gold particle binding per trimer.

Analysis of the microtubule-gephyrin complex in the absence of nano-gold labeling indicated that the edges of the microtubule filaments were decorated with gephyrin as indicated by the arrows (Fig. 6-2C). Due to the high amount of gephyrin in the background it would be premature to stress this initial observation. To confirm this result complex formation was also carried out with nano-gold labeled gephyrin (Fig. 6-2D), however, the data failed to confirm the initial result obtained with unlabeled gephyrin. Further optimizations with the complex formation needs to be done to substantiate the initial result obtained with unlabeled gephyrin.

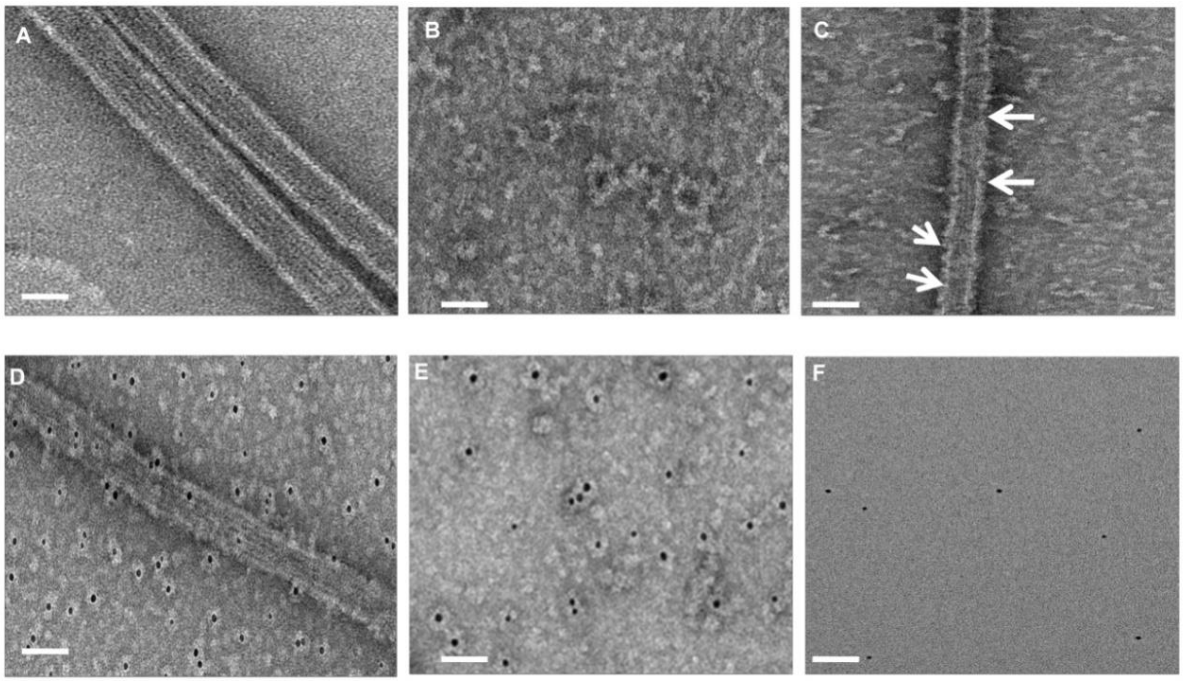

Figure 6-2: EM analysis of the gephyrin-microtubule interaction. (A) Negative stained particles of apo-microtubule and apo-gephyrin **(B). (C)** Particles of the gephyrin-microtubule complex. The microtubule filament clearly shows a decorated wall in comparison to apo-microtubules. **(D)** The gephyrin-microtubule complex, after gephyrin was labeled with 5 nm gold beads which specifically target its N-terminal His tag. Single dotted particle presumably represent the trimeric species of gephyrin**. (E)** Nanogold labeled and negatively stained apo-gephyrin particles. **(F)** EM micrograph of the naked nanogold beads serving as a negative control.

6.4.3. MALS provides insight into the temperature-dependent formation of the tubulin-DARPin complex.

To structurally characterize the tubulin-DARPin-gephyrin complex, it was essential to analyze the formation of the complex in solution before heading towards crystallization trials. Initially, to prove the existence of a stable complex between tubulin and DARPin, SEC-MALS experiments were carried out (Fig. 6-3). Interestingly, the analysis showed that it was not possible to obtain the complex by incubating the components at room temperature. Although the corresponding chromatogram showed symmetrical elution peaks, (Fig. 6-3B) the molecular weights corresponded to those of the individual components (Fig. 6-3A and Fig. 6-3D) rather than tubulin-DARPin complex. Changing the incubation temperature to 4 °C was required to achieve complex formation (Fig. 6-3D) and the corresponding analysis by MALS resulted in a molecular weight corresponding to a single DARPin bound to one αβ-tubulin heterodimer as documented by the agreement with the calculated molecular mass of the complex.

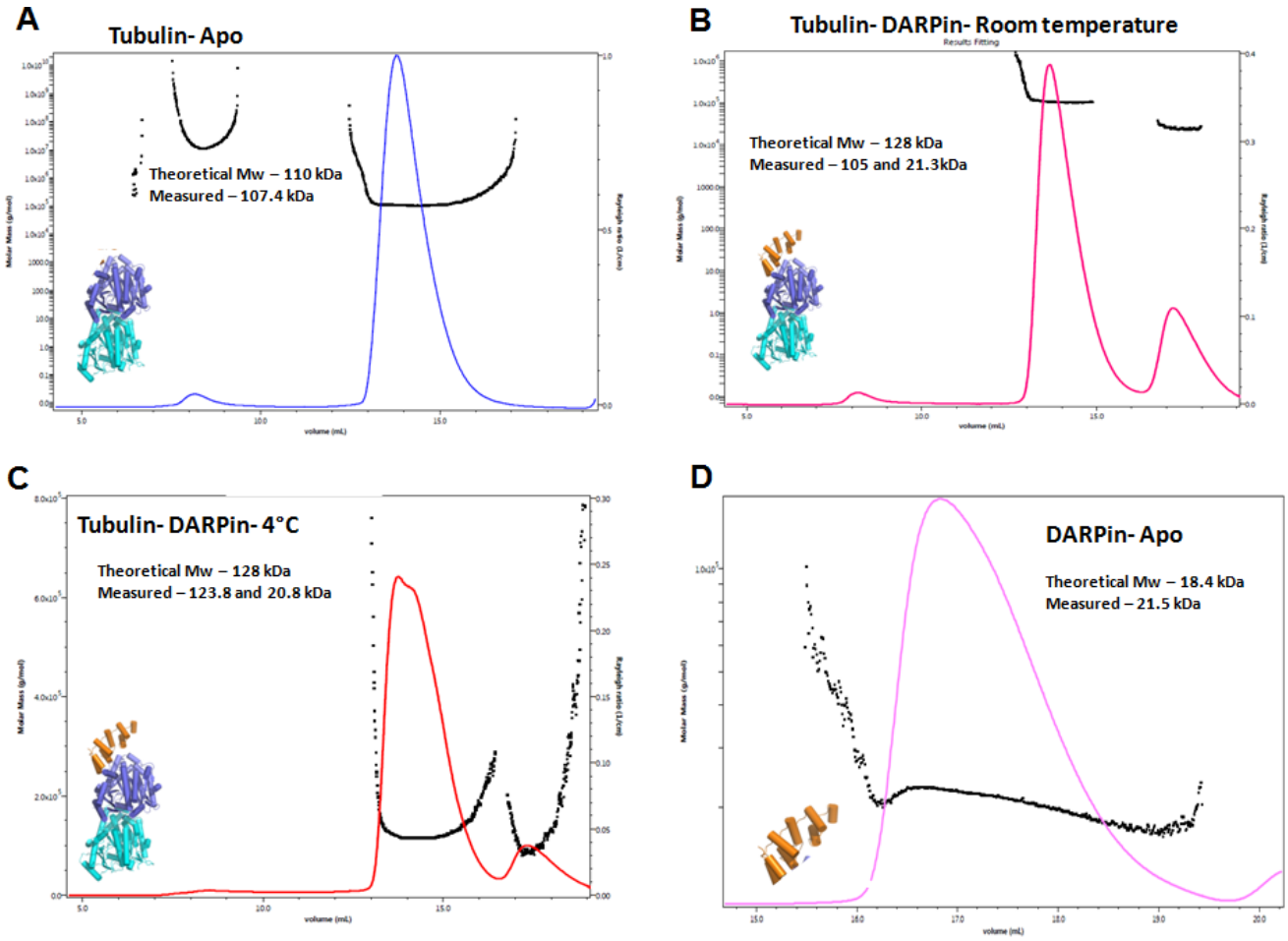

Figure 6-3: Analysis of the tubulin-DARPin complex by MALS. (A) Chromatogram of the tubulin heterodimer after one round of polymerization and depolymerization. **(B,C)** Analysis of the tubulin-DARPin complex after incubating the components at either room temperature or 4°C, respectively. **(D)** MALS analysis of apo-DARPin. The differential refractive indeces (dRI) are represented as differently colored curves and the respective measured molecular masses by black circles (scatter plot).

Due to time restrictions, a further analysis of the Tubulin-DARPin-gephyrin complex by SEC-MALS was not carried out. With respect to the structural characterization of this ternary complex, crystallization trials were carried out with a 1:1:1 molar ratio of Tubulin, DARPin and GephE, however, these were unsuccessful and did not result in the formation of crystals containing all three components.

7. Characterization of Cinnamon: A gephyrin ortholog from *Drosophila*

7.1 INTRODUCTION

Gephyrin was identified as the central organizer of inhibitory postsynapses almost three decades ago (Kirsch et al., 1991; Prior et al., 1992). Full-length gephyrin, a ~93 kDa protein, is composed of an N-terminal G domain and a C-terminal E domain. In isolation, the G domain forms a trimer and the E domain forms a dimer (Kim et al., 2006; Schwarz et al., 2001). The full-length protein predominantly trimerizes and utilizes the trimer interface of the G domain to accomplish that while the interface of the E domain is not utilized due to so far unknown reasons (Sander et al., 2013). Although crystal structures were determined for the individual domains, the full-length protein has been recalcitrant towards crystallization. The conformational heterogeneity of the unstructured linker region and its proteolytic sensitivity results inhighly heterogeneous protein preparations, thus preventing crystallization. Hence there is no crystal structure or atomic resultion cryo-EM structure available for full-length gephyrin or a gephyrin homolog containing both the G and the E domain. All gephyrin orthologs featuring the G and E domains also harbor an unstructured linker region, however, the length of this sequence stretch differs greatly. In Cinnamon, the *Drosophila* homolog of gephyrin (Kamdar et al., 1997; Kamdar et al., 1994; Wittle et al., 1999), the linker is rather short consisting of only 29 residues and hence this protein is an attractive candidate for crystallization and other structural studies such as cryo-EM.

7.2 AIMS

The main aim of the characterization of Cinnamon is to derive structural insights into a full-length gephyrin-like protein. If a medium to high resolution structure was obtained for the full-length protein, it would presumably allow to explain why E domain dimerization is inhibited in the context of the full-length protein and hence may provide important insight into gephyrin's role as a synaptic organizer.

7.3 MATERIALS AND METHODS

7.3.1 Cloning of Cinnamon constructs. cDNA of Cinnamon was ordered fromthe Drosophila genomic research center, Indiana University, Bloomington, USA. The cDNA was

subcloned into pETM14 and ColADuet vectors by sequence independent ligation cloning (SLIC) (Li and Elledge, 2007). Amplification and vector linearization were carried out as described in the Table 7-1, followed by DpnI digestion which was carried out by adding 1µl of the enzyme to 50 µL of PCR reaction mixture. The PCR product was purified by using the PCR and agarose gel purification kit from Macherey-Nagel, followed by T4 DNA polymerase digestion as carried out with the reaction mixture composition described in Table 7-2.

Table 7-1. PCR reaction scheme for gene amplification and plasmid linearization

Step	Temperature in °C	Time/ cycle
Initial denaturation	98	30 sec
30 cycles	98 60 72	10 sec 20 sec 3 min
Final extension	72	10 min
Hold	4	-

The ligation was carried out by mixing the T4 digested product with the plasmid DNA (2µl plasmid + 8 µl gene of interest + 10 µl ddH_2O), incubating the samples at 75 °C for 5 min and then slowly cooling them to 5 °C. The resulting expression plasmids were used to transform *E.coli* DH5α cells. The transformed cells were plated onto LB agar plates containing respective antibiotic and were incubated at 37 °C overnight. After overnight incubation, colony PCRs were carried out with selected clones following the protocol summarized in Table 7-2.

Table 7-2. Pipetting scheme for the T4-Digestion

	Cinnamon	pETM-14	ColA
PCR-Purified DNA	1 µg	1 µg	1 µg
NEB-Buffer (2)	1 µl	1 µl	1 µl
NEB-BSA	1 µl	1 µl	1 µl
T4-DNA-Polymerase	1 µl	1 µl	1 µl
ddH_2O	37.2 µl	33.4 µl	36.8 µl

Reaction scheme for colony PCR

Step	Temperature in °C	Time/cycle
Initial denaturation	95	3 sec
30 cycles	95 55 72	10 sec 20 sec 2 min
Final extension	72	10 min
Hold	4	-

Positive clones from the colony PCR results positive clones were confirmed by sequencing with the 5' primer specific to the T7 promoter sequence and the 3' primer specific to the T7 terminator DNA sequences.

7.3.2 Protein expression. Expression tests with full-length Cinnamon were carried out with different *E.coli* strains including BL21DE3, Rosetta II, ArcticExpress and OverExpress C43 as well as SoluBL21 (bought from amsbio). For all the test expression, the cells were induced with 0.5 mM IPTG at OD_{600} of 0.6-0.7. After an initial incubation temperature of 37°C, three different temperatures were tested for the post-induction incubation. 1) Cells were grown at 37°C for four hours. 2) Cells were grown overnight at 15°C and 3) at 20°C. All strains resulted in the expression of insoluble protein except for the SoluBL21 strain. The best soluble expression was observed with the 20°C overnight incubation tempreature when cells were induced with 0.5mM IPTG at an OD_{600} of 0.6-0.7. Subsequently the protein expression was optimized as follows. After the inoculation of the secondary culture with the priamary culture (20 ml of primary culture in 2l of secondary culture) and subsequent growth for 3-4 h at 37°C, the cells were induced with 0.5 mM IPGT at an OD_{600} of 0.7-0.8 and were grown overnight at 20°C. Cells were harvesting by centrifugation at 8000 X *g* at 4°C by using a JA 5.0 rotor (Beckmann).

7.3.3 Protein purification. The cell pellet was resuspend in 150 ml of lysis buffer (50 mM Tris pH 8, 250 mM NaCl, 5 mM β-mercaptoethanol and 5% glycerol) which was supplemented with two tablets of protease inhibitor cocktail (Roche diagnostics), 1 mM PMSF and 1 mM benzamidine hydrochloride. Cell lysis was performed with a cell disruptor (Microfluidizer M-110P, Microfluidics) by passing the resuspended cells twice through the machine at a pressure of 1500 bar. The supernatant fractions were separated from the pellet by centrifuging the lysate at 58000 x *g* for one hour at 4°C by using a JA 25.50 rotor (Beckmann).

The first step of the purification was carried out by affinity chromatography during which the supernatant fractions were passed through pre-equilibrated (with lysis buffer) Ni-IDA beads (5ml). The Ni-beads were washed with a buffer containing a high salt concentration (50 mM Tris pH8, 1M NaCl, 5mM β-mercaptoethanol and 5% glycerol) to minimize binding of impurities to Cinnamon. An additional washing step was performed with wash buffer (50 mM Tris pH8, 250 mM NaCl, 20 mM imidazole, 5mM β-mercaptoethanol and 5% glycerol) to prevent unspecific binding of proteins to the column. Bound proteins were eluted with five column volumes (CV) of elution buffer (50 mM Tris pH8, 250 mM NaCl, 250 mM imidazole, 5mM β-mercaptoethanol and 5% glycerol). Fractions were tested by SDS-PAGE before proceeding to the next step. Fractions containing the Cinnamon protein were pooled and diluted with dilution buffer (50 mM Tris pH8 and 5mM β-mercaptoethanol) so that the final concentration of NaCl was 80mM. The pooled fractions were loaded onto a MonoQ anion exchange chromatography column (10/100, GE Healthcare), which was pre-equilibrated with MonoQ buffer A (50 mM Tris pH8, 80 mM NaCl and 5mM β-mercaptoethanol) by using an AEKTA system (GE Healthcare). The elution was performed with MonoQ buffer B (50 mM Tris pH8, 1 M NaCl and 5 mM β-mercaptoethanol) with a two step gradient (Step 1–up to 30% buffer B and Step 2–up to 65% buffer B) and then finally with a step gradient to 100% of buffer B. With this protocol pure trimeric and hexameric fractions could be separated by anion exchange chromatography. These species were pooled separately and purified individually to homogeneity by size exclusion chromatography, which was performed by using a Superose 6 10/300 column (GE Healthcare) with SEC buffer (50 mM Tris pH8, 80mM NaCl and 5mM β-mercaptoethanol).

7.3.4 Electron microscopyand atomic force microscopy.

Soon after size exclusion chromatography, the trimer and hexamer fractions of Cinnamon were diluted to different concentrations (0.02 mg/ml, 0.04 mg/ml, 0.06 mg/ml, 0.08 mg/ml and 0.1 mg/ml) with grid buffer (50 mM Tris pH8, 250 mM NaCl and 5mM β-mercaptoethanol) and centrifuged at 25000 x*g* at 4°C to remove any aggregates followed by deposition on glow-discharged carbon coated grids. R 2/2 Cu 300 mesh grids were bought from Quantifoil. The carbon coating was carried out by using a Denton Vaccum Desk V and the grids were then glow discharged for 45 seconds at $2.2x10^{-1}$tor by using a Harric plasma cleaner. Samples were stained with 2% (w/v) uranyl acetate and the grids were washed twice with water to remove unbound samples and excess staining solution. The EM images were recorded with a 120 kV Tecnai G2 spirit twin microscope by using an Eagle 4K camera at 67000X magnification.

For AFM studies, hexamer and trimer samples were diluted to a final concentration of 20nM and deposited on freshly cleaved mica. The images were collected using a Molecular Force

Probe MFP-3D-BIO atomic force microscope (Asylum Research) in oscillating mode using Olympus OMCL-AC240 silicon probes with spring constants of ~2N/m and resonance frequencies of ~70 kHz. AFM images were flattened to third order using the IgorPro-based MFP software (Asylum Research). Peak volumes were measured using ImageSXM and translated into molecular mass via the previously established linear relationship: MM = (V + 5.9)/ 1.2, where MM is the protein molecular mass and V is the protein peak volume. The approximate molecular mass of the sample molecules was derived from the midpoint of a Gaussian fit to the mass distribution (Origin).

7.3.5 Analytical size exclusion chromatography coupled to multi angle light scattering (SEC-MALS).

SEC-MALS experiments for both oligomeric froms of Cinnamon were carried out in buffer containing 20mM Tris pH 8, 150 mM NaCl and 5 mM β-mercaptoethanol with a protein concentration of 2mg/ml. Size exclusion chromatography was carried out by using a Superose6 10/300 column coupled to a MALS instrument (Wyatt technologies). Factors such as the UV absorbance at 280 nm, the light scattering (LS) and the differential refractive index (dRI) were meansured. The LS and dRI were recorded by using the Dawn 8^+ detector and T-rEX refractometer from Wyatt technologies. All experiments concerning the MALS experiments were carried out at room temperature.

7.4 RESULTS AND DISCUSSIONS:

7.4.1 Protein purification and separation of different Cinnamon oligomers:

After the first step of the purification (Ni-affinity chromatography) the protein sample still contained a high amount of impurities. To further enhance protein purity, anion exchange chromatography was carried out as a second step. This resulted in the protein eluting in two distinct peaks. Since the fractions from both peaks contained the Cinnamon protein, the two peaks were pooled separately and purified to homogeneity by size exclusion chromatography using a Superose6 10/300 column. Strikingly, two different pools of Cinnamon eluted separately from the Superose column with a difference in the elution volume of 2 ml (Fig. 7-1A and 7-1B). The eluted samples were not only analyzed by SDS-PAGE but also by native PAGE. Although there was no difference in the running behavior of these samples on the SDS-PAGE, (Fig. 7-1C and 7-1D), the native PAGE analysis (Fig. 7-1E) clearly indicated two distinct oligomeric states of Cinnamon.

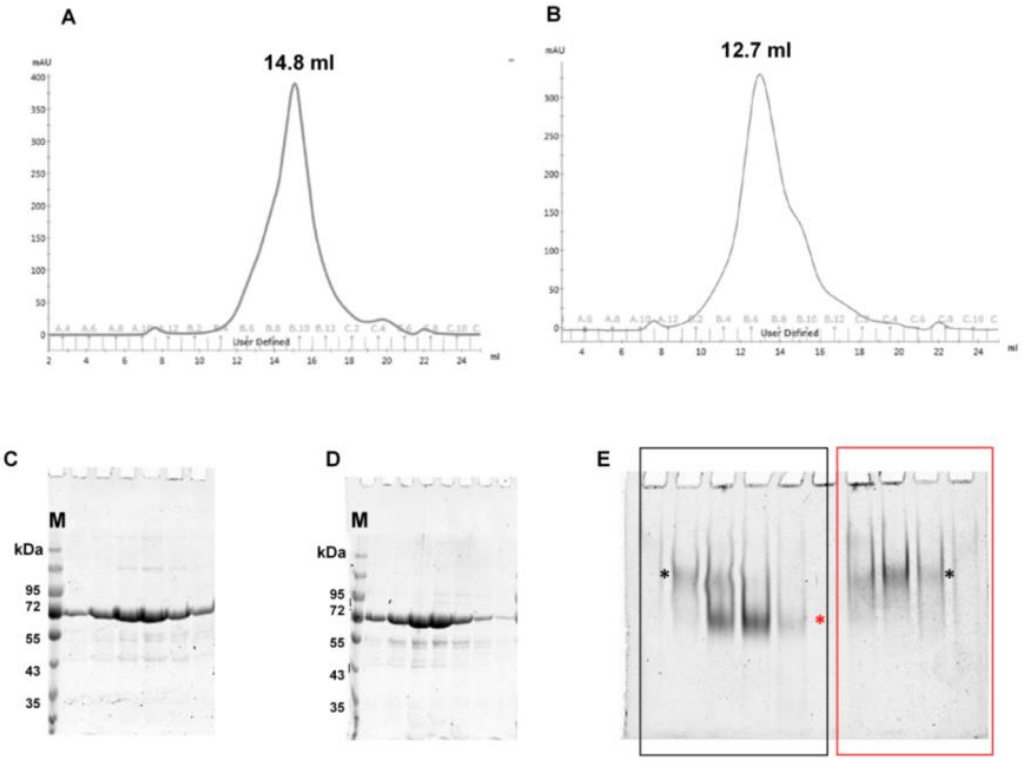

Figure 7-1: Purification of Cinnamon. Chromatograms of the Cinnamon trimer and hexamer fractions **(A and B). (C and D)** 12% SDS-PAGE of trimer and hexamer peak fractions from SEC. **(E)** 5% native PAGE of the trimer and hexamer fractions. Trimer fractions are highlighted witha black box and hexamer fractions with a red box. Black and red asterisks represent the two different oligomeric state of Cinnamon.

7.4.2 SEC-MALS of the different Cinnamon oligomers:

With initial size exclusion chromatography and PAGE analysis, it was clear that the full-length protein forms two distinct oligomeric states in solution. To further characterize these different states, SEC-MALS was carried out (Fig.7-2). Interestingly, the two distinct oligomeric forms turned out to be the trimeric (Fig.7-2A) and hexameric forms of Cinnamon (Fig.7-1B). Strikingly the measured molecular weight of these oligomeric state deviated considerably from the respective theoretical molecular weights (154 kDa for the trimeric fraction and 360 kDa for the hexameric fraction vs. calculated molecular weights of 200 kDa and 400 kDa). Although the native PAGE analysis of the samples showed single distinct bands for the proteins, the heterogeneous mass distribution of the protein under the curve in MALS measurements clearly indicate both oligomeric forms to display conformational heterogeneity in solution.

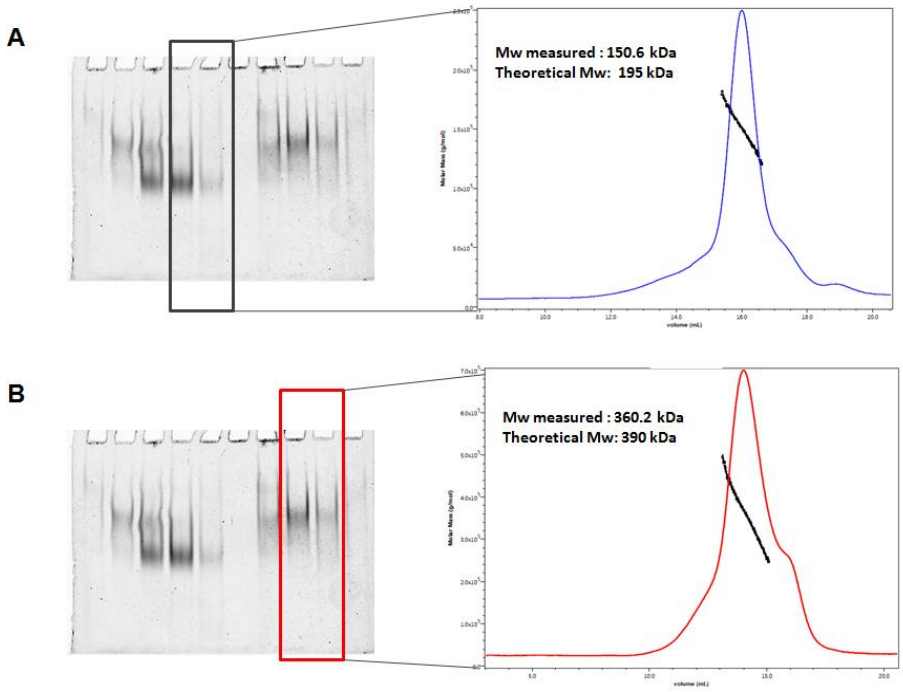

Figure 7-2: MALS analysis of the Cinnamon oligomers. (A) MALS analysis (right) of the trimeric species with pooled fractions from native PAGE (left panel). **(B)** MALS analysis (right) of the hexameric species with pooled fractions from native PAGE (left panel).

7.4.2 Electron microscopy and atomic force microscopy revealed a homogenous Cinnamon trimer and a heterogeneous hexamer

To get an initial idea about the shape of Cinnamon, preliminary studies were carried out by AFM and EM. AFM studies with the trimer fractions clearly revealed the trimer to adopt a compact state (Fig. 7-3A). In contrast, the hexamer displayed conformational heterogeneity (Fig. 7-3B) which consisted of multiple shapes including compact globular as well as elongated shapes (indicated with Arabic numerals 1-3). The volume analysis of the trimer fractions clearly displayed a Gaussian distribution corresponding to a mass of ~240 kDa, (Fig. 7-3C), which is in agreement with the theoretically calculated molecular mass (~200 kDa).

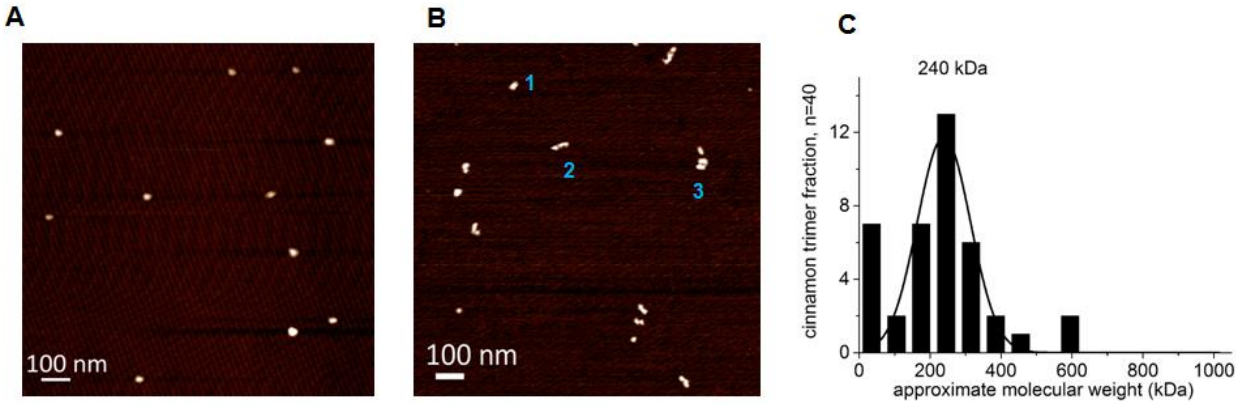

Figure7-3:Structural properties of Cinnamon revealed by AFM imaging. **(A, B)** AFM images of the trimeric (A) and hexameric (B) fractions of Cinnamon. Cinnamon molecules from the trimeric fraction display a compact architecture; incontrast, the hexamers exhibit structural heterogeneity (1: compact, 2:

elongated and 3: bi-lobed structures). **(C)** Volume analysis for the trimeric fractions, in which the midpoint of the Gaussian curve indicates a mass of 240 kDa.

Due to the conformational flexibility of the particles, automated volume analysis could not be carried out on the hexamer samples, where individual monomers were picked as separate particles and thus resulted in a molecular weight, which was far off from the expected molecular weight for the hexameric state of the Cinnamon. In addition, the linker region within the proteins could not be resolved in the AFM images due to its low height, contributing to the discrepancy between theoretical and experimentally derived molecular mass. In future analyses, volume measurements will have to be carried out manually, by summing up the separate volumes of individual peaks within the hexameric assemblies, as previously described for AFM experiments on gephyrin (Sander et al., 2013).

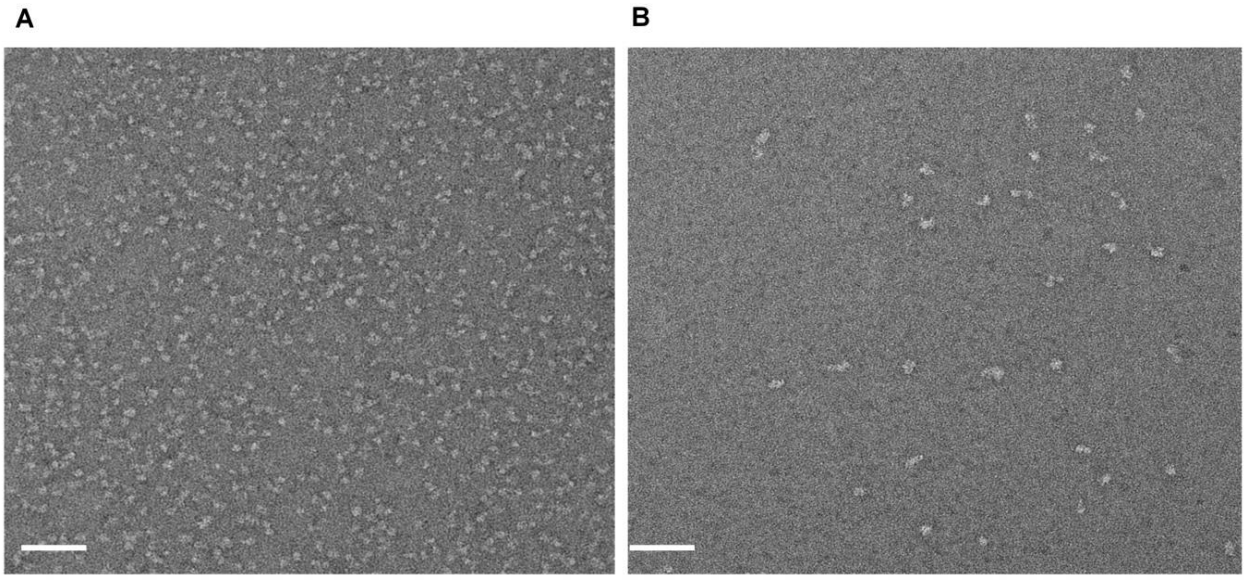

Figure7-4:Single particle analysis of Cinnamon by EM. (A, B) EM images of negatively stained particles of trimeric **(A)** and hexameric **(B)** fractions of Cinnamon. The trimeric fractions display a homogeneous appearance in contrast to the hexamer fractions, which display considerable structural heterogeneity.

Although the AFM studies provided initial clues about the morphology of the particles, to gain insight at the higher resolution, EM studies were carried out. Amongst the different concentrations tested for the deposition on EM grid for the negative staining, the best results for the trimeric fractions were obtained with a concentration of 0.02 mg/ml and with 0.03mg/ml for the hexameric fractions. The findings from EM were consistent with the AFM data analysis, where negatively stained trimer particles showed a “tri-lobed” shape (Fig. 7-4A) in contrast to the hexamer fractions which exhibited a mixture of different morphologies

(Fig. 7-4B). A 3-D reconstruction of the trimeric fractions was attempted by Dr. Petra Wendler, Gene Center, Munich. Unfortunately, this did not yield any structural information as this analysis revealed the trimers to still be a heterogeneous mixture, at least under the conditions of the current EM experiments.

8. DISCUSSION

8.1 Molecular basis of $GABA_A$ receptor clustering:

Previous biochemical and co-localization studies provided initial clues about the presence of a universal binding site for the GlyR and $GABA_AR$ on gephyrin (Kim et al., 2006; Mukherjee et al., 2011a; Schrader et al., 2004; Tretter et al., 2011; Tretter et al., 2012), however, the molecular basis for the receptor-specific interactions of gephyrin remained elusive. The first part of my work involved the structural characterization of the gephyrin-$GABA_AR$ interaction. For these structural studies, the α3 subunit of the $GABA_AR$ was chosen as it shows the highest affinity for gephyrin amongst all those $GABA_AR$ subunits, which were shown to bind to gephyrin directly (Maric et al., 2011). A biochemical characterization of this interaction was previously performed by Dr. Hans Maric, allowing to pinpoint the core binding motif of the $GABA_AR$-α3 subunit which mediates the interaction with gephyrin. Although the α3 subunit displays the highest affinity of all the $GABA_AR$ subunits with a K_D of ~180 μM, this relatively low affinity hindered initial crystallization trials (Fig. 3-2). For the structural studies, a chimeric peptide of the GlyR-β-$GABA_AR$-α3 subunits was designed by mutating two residues in the $GABA_AR$- α3 core binding motif into the corresponding GlyR β residues (Fig 3-10). This peptide bound significantly tighter as reflected in a K_D of ~8 μM, which was nearly to that of a GlyR β derived peptide of equal length. Crystallization trials with this and the WT peptide not only resulted in the structure of GephE bound to the chimeric peptide but, surprisingly, also to the WT-$GABA_AR$- α3 peptide. The relatively low resolution of these structures (3.5 Å for the chimeric and 4.1 Å for the wild-type) made it difficult to model the side chains of the residues in the interface (Fig.3-3C and D). Therefore, further optimizations of the crystallization conditions were carriedout which resulted in improved crystals diffraction to a resolution of 2.7 Å for the WT and the chimeric peptide complexes (Table 3-4). These structures elucidated the receptor-specific interactions of gephyrin in atomic detail.

The structures showed that the $GABA_AR$ α3 derived peptide indeed interacts with GephE through the same hydrophobic binding pocket where the GlyR β subunit binds (Fig.3-4A), consistent with previous biochemical findings (Maric et al., 2014c; Maric et al., 2011). The interaction is mainly mediated by subdomain IV and partially by subdomain III of GephE. The N-terminal region of the core binding motif (11 residue long peptide essential for the interaction of gephyrin-$GABA_AR$-α3, Phe368-Asn378) of $GABA_AR$-α3 interacts with GephE in a similar fashion as the GlyR β subunit, however, there are receptor-specific interactions at the C-terminus. The GlyR peptide resembles the letter ‘C’ (Fig. 3-5c) whereas the $GABA_AR$-α3 peptide follows a straight trajectory in the C-terminal half, thus resembling the letter ‘L’ (Fig 3-4a). The structures also provide a basis for understanding the differential affinity of GephE for the GlyR β and $GABA_AR$ α3 subunits. The structures revealed that Ser399 of

GlyR β forms a H-bond with Asp329 of GephE, in contrast to Asn369 in $GABA_AR$-α3, which due to the involvement of its side chain nitrogen in a separate H-bond does not have a suitable H-bond donor left to productively interact with Asp329. In addition to this difference, Leu404 of GlyR interacts more favorably with the hydrophobic pocket of subdomain IV of GephE. In the $GABA_AR$-α3 core binding motif, Leu404 is replaced by Thr374, which interacts less favorably with the surrounding hydrophobic environment of GephE.

As described above, most of the biochemical, biophysical and structural studies on the gephyrin-receptor interactions were mainly carried out either with the aid of the recombinantly purified intracellular loop of the GlyR β and $GABA_AR$ α1-3 subunits or with shorter chemically synthesized receptor-derived peptides. However, in the context of the intact pentameric receptors, it should be noted that more than one binding site for the E domain is available and that these binding sites are located in close spatial proximity. In other words, avidity affects will almost certainly play a crucial role in the gephyrin-receptor interactions. To check for possible avidity affects, GlyR β and $GABA_AR$ α3 receptor derived peptides of different lengths were dimerized with several crosslinkers (Fig 4-4). Initial studies were performed with a GlyR β–subunit derived peptide and the crosslinking reaction was carried out exploiting intrinsic cysteine residues (Fig 2-2).

Biochemical and biophysical characterizations showed that avidity effects play a crucial role in the binding affinities of the gephyrin-receptor interactions. To check if the dimeric peptides occupy both binding pockets of the E domain dimer, X-ray crystal structures of GephE with a $GABA_AR$ α3 dimeric peptide crosslinked with a PEG-based linker and a GlyR β derived dimeric peptide crosslinked with a p-phenyl-based linker were determined (Fig. 4-8 and 4-9). Interestingly, the dimeric E domain and peptide dimers crystallized in a domain-swapped arrangement and the path of the peptide to a symmetry related neighboring molecule was different in both structures (Fig. 8-1). This prompted the question as to whether these dimeric peptides crosslinked two E-domain dimers in solution. However, analysis of three E-domain-dimeric peptide complexes by SEC-MALS experiments revealed that the peptides indeed interact with both monomers simultaneously and independent of the concentration, a result which is consistent with the biochemical analysis of these interactions (Fig 4-7).

Finally, the structures of the GephE-dimeric peptide complexes were solved to a resolution of 2 Å. Due to this high resolution, these structures revealed additional details of the GephE-$GABA_AR$-α3 specific interaction that could not be resolved using the corresponding monovalent peptides (Maric et al., 2014b). The most important of these features was the unambiguous definition of Tyr375 in the $GABA_AR$-α3 peptide. This residue is conserved in the synaptically located $GABA_AR$ α1-3 subunits and was identified to be critical for the binding interaction of these $GABA_AR$ α1-3 subunits and gephyrin (Maric et al., 2014a; Maric

et al., 2011; Mukherjee et al., 2011a; Tretter et al., 2011). Tyr375 displays an inward facing conformation, which engages in critical hydrophobic interactions with Lys658, Val727,Pro685 and Leu686 of subudomain IV of GephE (Fig. 8-2).

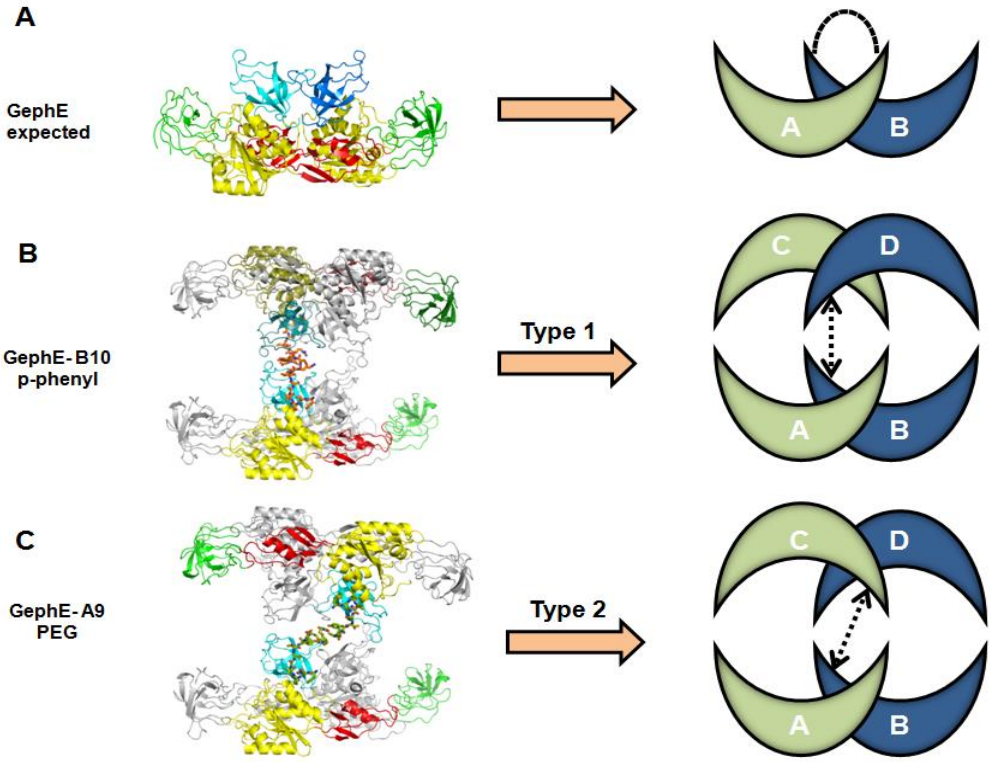

Figure 8-1. Domain swapping of the E domain in the presence of dimeric peptides. (A) Crystal structure of the GephE dimer (left) and the expected binding of the dimeric peptide shown with dashed lines in the right panel. **(B, C)** Crystal structures of GephE in the presence of a GlyR β-10 peptide crosslinked with a para-phenyl crosllinker and a $GABA_AR$ α3 derived peptide crosslinked with a PEG-based linker, respectively (left panels). The schematic diagrams of domain swapped peptides crosslinking two E-domain dimers where the four monomers are named with the letters **A-D**. The path of the peptides in the crystal packing is shown by the dashed double-headed arrows.

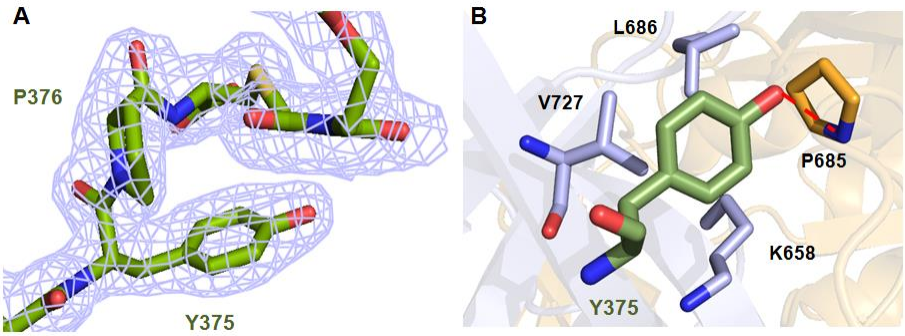

Figure 8-2. Structural features of the Tyr375 interaction. (A) Enlarged view of Tyr375 with the $2F_o$-F_c electron density map displayed at 1.5 rmsd. **(B)** Critical interaction of Try375 with residues in gephyrin. The dashed red line represents the hydrogen bond.

Another residue, which is critical for $GABA_AR$ α3 specific interaction with gephyrin, is Asn369. This residue could be modeled with two alternative side chain conformations (Figure 8-3). In the case of the GlyR β peptides, this side chain is a Ser which engages in productive hydrogen-bonded interactions with the main chain nitrogen of Val371 in the peptide and the side chain of Asp327 in gephyrin. The Asn in the $GABA_AR$ α3 subunit cannot simultaneously satisfy both interactions with a single conformation, due to its different distribution of H-bond donors and acceptors. Nevertheless, by adopting two conformations both interactions can be maintained, however,this is accompanied by negatively affecting the binding affinity.

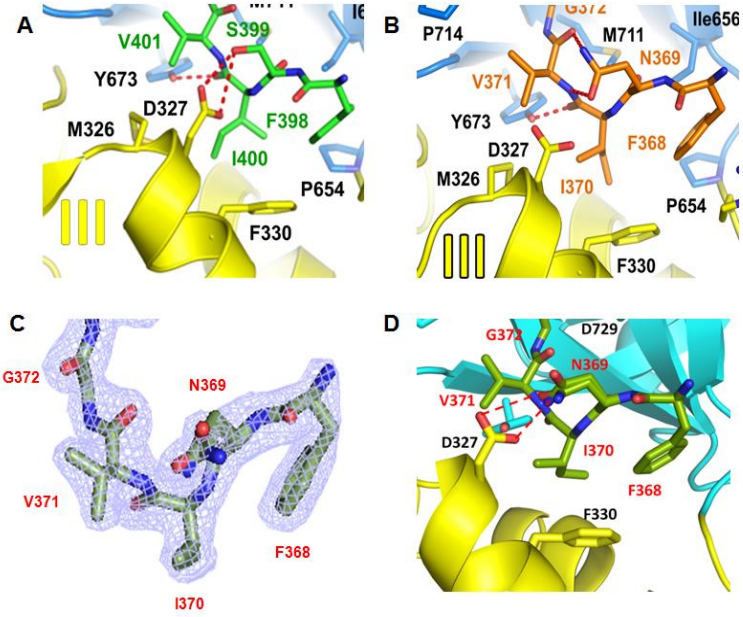

Figure 8-3: Comparison of the interaction of Asp327 of GephE and Ser399/Asn369 of the receptor-derived peptide. (A) Enlarged view of the interaction of Asp327 of GephE and Ser399 in the GephE-GlyR β-49 complex. **(B)** Enlarged view of the interaction of Asp327 of GephE and Asn369 in the GephE-$GABA_AR$ α3 derived monomeric peptide complex. **(C)** $2F_o$-F_c electron density map of the $GABA_AR$ α3 dimeric peptide (rmsd 2) where the side chain of Asn369 is modelled with two different conformations**. (D)** Enlarged view of the interaction of Asp327 of GephE and Asn369 in the GephE-$GABA_AR$ α3 PEG crosslinked dimeric peptide complex. In all structures subdomain III of the E domain is colored in yellow and subdomain IV in blue. H-bonds are represented as red dashed lines and peptides in stick representation.

The approach to use dimerized receptor fragments can also be used to analyze the binding of yet structurally uncharacterized GephE-binding receptor subunits such as the $GABA_AR$ α1, α2, β2 and β3 subunits.The monomeric peptides of the $GABA_AR$ α1 and α2 core binding motif display an affinity to GephE in the low micromolar range and this presumably prevented their co-crystallization with GephE. The sequence alignment of the core binding (minimal 11 residue long peptide) motifs clearly displays a high sequence identity with an conserved aromatic residue at the first position in the α1-3 subunits (Tyr340 in α1, Tyr339 in α2 and Phe368 in α3 subunits). In addition, the second and more critical aromatic residue is at postion 8 (conserved Tyr in α1, α2 and α3) of the core binding motif. This second aromatic residue has been shown to be one of the critical determinants of the gephyrin-receptor

interaction, *in vitro* studies demonstrated that any mutation of this critical residue completely abolished the interaction. In comparision to the α subunits, the binding sites on the β2 subunits have been mapped to a strech of 18 residues. These residues not only hardly share any sequence identity to that of the α subunits but also differ from eachother. Surface plasmon resonance (SPR) experiments showed an affinity of 50 μM for $GABA_AR$-β2 to gephyrin, which is similar to that of the previously determined affinity for the α subunits (Kowalczyk et al., 2013). Thus, the dimerization approach can potentially be extended towards all these subunit core binding regions so that the subunit specific interaction of gephyrin can be structurally depicted in atomic detail.

8.2 Structural basis for the terminal step of Moco biosynthesis:

In its moonlighting function, gephyrin also catalyzes the terminals steps of Moco biosynthesis. Mo-centers are catalytically inactive unless they are complexed with the special pterin-based cofactor called Moco. While previous studies focused mainly on Cnx1G, the plant homolog of the G domain, and hence shed light on the penultimate step of Moco biosynthesis, the terminal metal incorporation step still remained elusive. To better understand the molecular details of the terminal deadenylation and metal insertion reaction, which are both catalyzed by GephE, high resolution crystal structures of GephE in the presence of ADP, AMP and metals (W/Mo) were determined. The nucleotides were bound to subdomain III of GephE, which has a classical Rossmann fold architecture. The structures revealed that nucleotide binding imparts localized conformational rearrangements in subdomain III (which is structurally related to the N-terminal G domain), specifically in the nucleotide recognition loop. The striking structural rearrangement involves two residues, Lys579 and Asp580 (Fig 5-3) and seems to play a critical role in nucleotide-binding as Asp580 is linked to the nucleotide as it directly interacts with one of the metal ions which inturn interacts with both the α and β phosphates of ADP. In addition to these structural features, a single mutation leading to Moco deficiency has been reported for the homozygous substitution of Asp580 to Ala (Reiss et al., 2011). Recent studies with the recombinantly purified gephyrin, which harbors this mutation have demonstrated that the Asp to Ala substitution completely abolishes Moco biosynthesis (Dejanovic et al., 2015).Thus, these nucleotide-bound structures of GephE provide the molecular basis for the lethal disease Moco deficiency.

To gain insight into the metal insertion mechanism, GephE-ADP co-crystals were soaked with solutions containing either sodium tungstate or sodium molybdate. To unambiguously map the metal-binding site, data were collected at the X-ray absorption edges of the respective metal (Fig 5-6). In both cases, multiple anomalous scatterers were observed in close proximity of the nucleotide-binding pocket (Fig 5-6). The metal-binding pocket has a

characteristic positively charged surface, which is compatible with the binding of anionic ligands. Although there were discrete anomalous signals for the metals (9 for Mo and 10 for W) presumably originating from a smaller number of discretely disorderd sites (Fig 5-5), it was not possible to model the oxygens for all of them, except for one metal, located a tone end of metal cluster which is referred to as the apical site. Although some of the metal-metal distances were compatible with W-W and Mo-Mo bonds (Pyykko and Atsumi, 2009), a possible transformation of molybdate/tungstate to oligo-molybdates/tungstates was considered highly unlikely. The metal cluster is sandwiched between subdomains III and IV of the E domain. Ser630, in subdomain III directly interacts with the apical metal in the metal cluster. A second presumably important residue which comes into close proximity of the cluster is Arg670, which belongs to subdomain IV of the E domain. Since the metal site adjacent to Arg670 could not be modeled with its surrounding oxygens, it was not possible to evaluate this interaction in detail. Nevertheless, minor side chain rearrangements of Arg670 would allow this residue to directly interact with the metal cluster (Fig. 5-5).

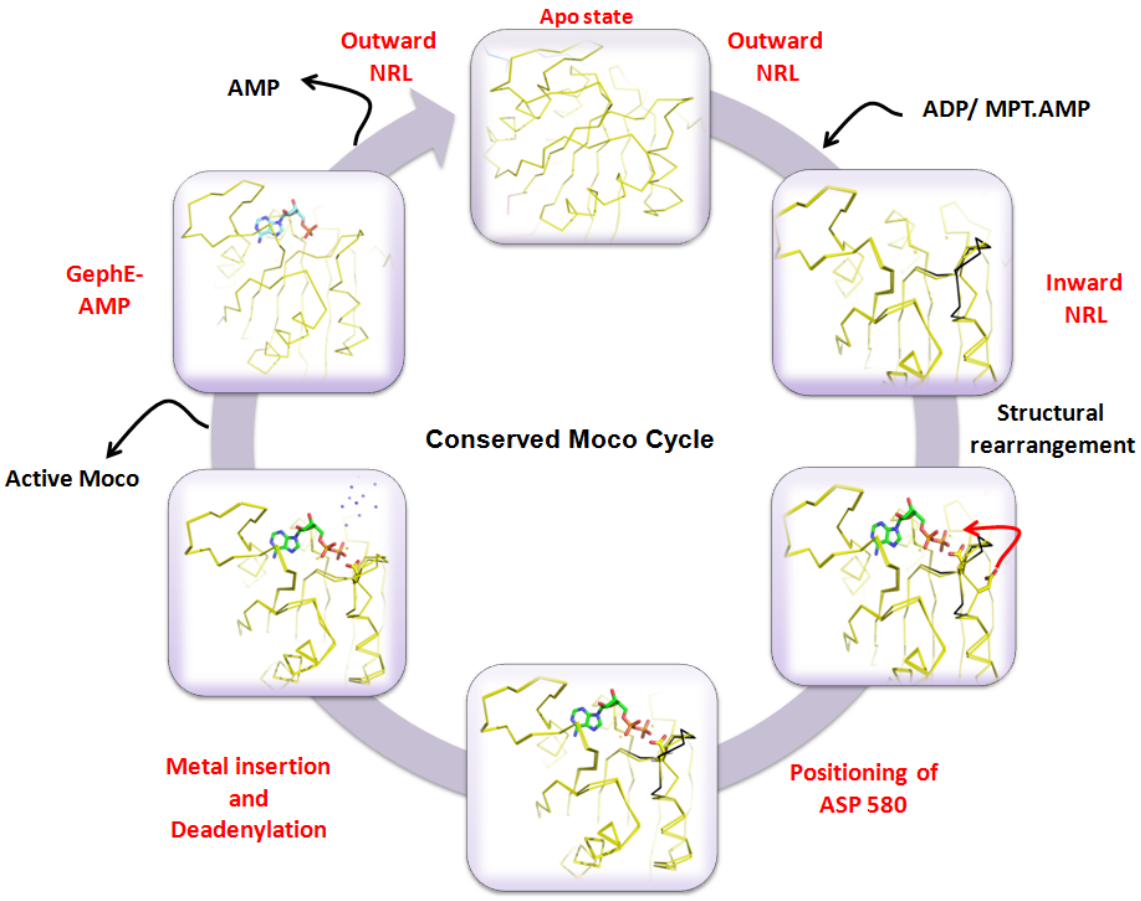

Figure 8-4.Schematic representation of the evolutionarily conserved terminal steps during Moco biosynthesis derived from the GephE-apo, GephE-nucleotide and GephE-ADP-metal complexes.

To understand the mechanism of metal incorporation, the GephE-ADP-W/Mo structures were superimposed with the structure of Cnx1G in complex with AMP-MPT (Kuper et al., 2004). The superimposed structures show that the apical metal, which directly interacts with Ser630 comes into close proximity of the dithiolene moiety and hence a catalytic role for this residue in the metal insertion mechanism seems likely. Interestingly, all those residues, which are important for nucleotide-binding and pyrophosphate hydrolysis as well as molybdate/tungstate binding region are conserved throughout evolution suggesting that the mechanism of metal insertion as deciphered in this study is conserved throughout evolution, from bacteria to humans (Fig. 5-7 and Fig 8-4).

8.3 Structural basis for the moonlighting function of gephyrin:

As mentioned before, in the brain and CNS one important function of gephyrin is to anchor $GABA_A$Rs and GlyRs and thus contribute to the formation of inhibitory synapses and hence signal processing in the brain. Co-crystal structures of GephE with peptides derived from the α3 subunit of the $GABA_A$R or with peptides derived from the GlyR β subunit deciphered the molecular basis for the receptor-specific interactions of gephyrin. Interestingly, comparison of the GephE-ADP structure with the GephE-receptor derived peptide complexes revealed that the receptor-binding pocket and nucleotide-binding pocket are ~20 Å apart from each other.

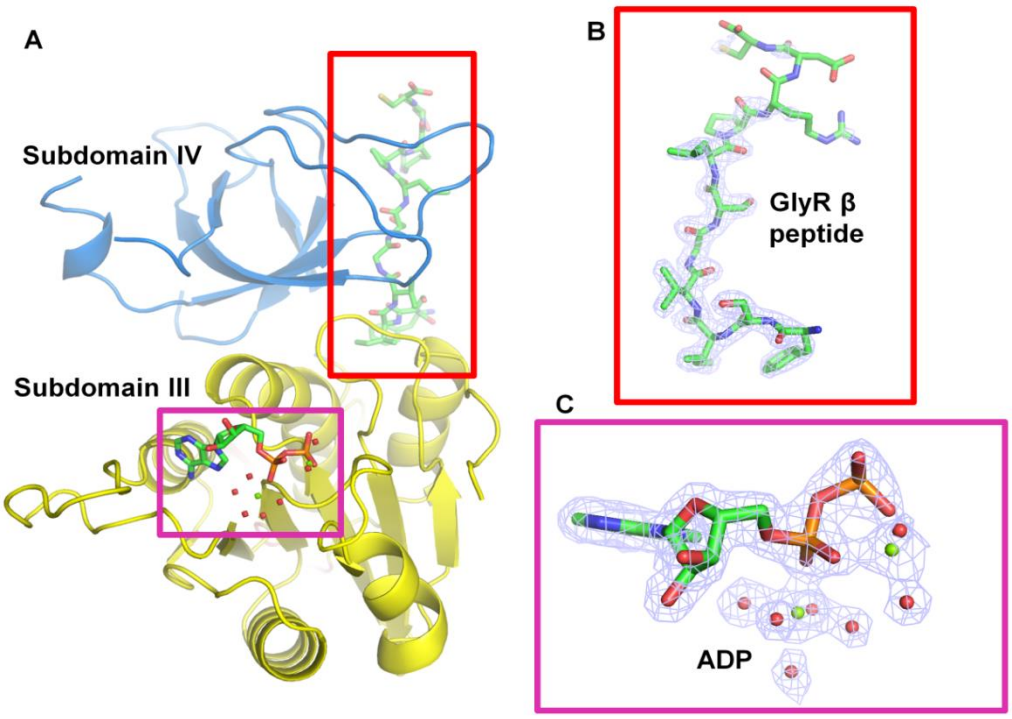

Figure 8-5. (A) Ternary complex of GephE-ADP-GlyRβ derived peptide. Side view of the the GephE-ADP-GlyR β complex with views focused on subdomains III and IV (shown in cartoon representation)

with the respective bound ligands (shown as sticks). $2F_o$-F_c electron density contoured at 1.5 rmsd for the bound peptide **(B)** and ADP **(C).**

To determine whether there is any communication between the two sites, ternary GephE-ADP-$GABA_AR$ α3 or GlyR β complexes were structurally characterized (Fig. 8-4 and 5-9). The overall architecture was similar to that of the respective binary complexes and a comparison of the bound nucleotide and peptide in the ternary complex with the binary complexes revealed only minimal structural rearrangements in either the peptide or nucleotide. These structures provide first insights into the integration of the two functions of gephyrin.

8.4 Gephyrin-microtubule interactions:

Gephyrin anchors receptors to the postsynaptic membrane by simultaneously interacting with cytoskeletal elements. Although gephyrin was co-purified initially with microtubules (Kirsch et al., 1991), the molecular basis of the interaction remained elusive. In the present study, the gephyrin-microtubule interaction was mainly probed by a microtubule-gephyrin co-sedimentation assay. A domain mapping of the interaction with different constructs revealed that the microtubules interact directly with gephyrin through two binding sites. One is provided by the linker region of gephyrin and the other is located in the E-domain (Fig 7-1). This finding was in contrast to previous studies, which were mainly based on *in situ* hybridization (Ramming et al., 2000). These studies revealed that the interaction is mediated by the linker region and predicted that the stretch of residues belonging to exon 14 mediates the interaction. Strikingly, the delta exon14 construct of the gephyrin full-length version retained binding to gephyrin in the co-sedimentation assay, thus confirming the presence of a second microtubule binding site in gephyrin.

8.5 Towards structural studies of gephyrin orthologs:

Although gephyrin was identified as the primary scaffolding protein at inhibitory postsynapses almost three decades ago, high resolution structural data of the full-length protein do not yet esist. The primary reason for this is the absence of multiple posttranslational modifications following expression of gephyrin in *E. coli* cells and foremost, the presence of the ~15 kDa unstructured linker region and its proteolytic sensitivity. Due to the presence of this unstructured region, a homogeneous protein sample is difficult to achieve. Nevertheless, it has been shown that full-length gephyrin is predominantly trimeric and uses the trimer interface of the G domain to oligomerize, while the dimer interface of the E domain is inactive (Sander et al., 2013). Low resolution AFM and SAXS studies were not successful in explaining why dimerization of the E domain is prevented and thus the

molecular architecture of the full-length gephyrin remains enigmatic. To gain insight into the architecture of the full-length protein, initial bioinformatics searches for homologous proteins were performed to identify gephyrin homologswith a significantly shorter linker region. This search identified the Cinnamon protein, the gephyrin ortholog in *Drosophila*. Cinnamon is a 65 kDa protein, which has a linker region of only ~3k Da, and is thus approximately five times shorter than the linker of gephyrin (Kamdar et al., 1997; Kamdar et al., 1994; Wittle et al., 1999). Although studies with the full-length Cinnamon protein are still in the initial stages, the preliminary characterization of the protein by MALS showed that two populations of the protein are formed upon expression in *E. coli* which correspond to trimers and hexamers with roughly a 3:2 ratio (Fig 7-1 and 7-2). This is in contrast to gephyrin where 90% of the protein is expressed in the trimeric from. In addition, AFM studies demonstrated that the Cinnamon trimer appears to be in a compact state (Fig 7-3), which is consistent with the construct of gephyrin in which the linker has been removed (Sander et al., 2013). Additional characterization of the Cinnamon trimer by negative-stain EM also showed a certain homogeneity, however, it is still insufficient to allow a structural characterization by cryo-EM (Fig 7-4). Nevertheless, these findings suggest that Cinnamon may be an attractive candidate for determining a high resolution structure of a gephyrin ortholog by using either X-ray crystallography or cryo-EM.

8.6 CONCLUSION:

During the course of the dissertation I was able to describe the two different functions of gephyrin, namely, receptor clustering and Moco biosynthesis, in atomic detail. These results will not only help us to understand the molecular basis for the receptor-specific interaction of gephyrin, but also provided important insights into the final step during Moco biosynthesis.

9. FUTURE PERSPECTIVES

9.1 Gephyrin- receptor interaction

The results presented in the current work decipher the molecular basis for the receptor (GlyR and $GABA_AR$) specific interaction of gephyrin. In addition to the $GABA_AR$ α3 subunit, it was shown that the α1 and α2 subunits also directly interact with gephyrin. Thus, in future, these studies can be extended, by applying the same methodology, i.e. dimerization of the peptide ligands to enhance their affinity towards GephE, to understand the $GABA_AR$ α1/2-subunit specific interactions of gephyrin.

9.2 Gephyrin-Microtubule interaction

The results from the co-sedimentation assays with different constructs of gephyrin and microtubules demonstrated that gephyrin relies on two binding sites to interact with microtubules. One of the binding sites resides in the linker region and and other in GephE. Instead of the clear binding results with polymerized tubulin, it has not been possible to show a conclusive complex formation between gephyrin and the tubulin α,β-heterodimer. Thus, an optimization of the gephryin-α,β-tubulin-heterodimer complex formation will have to be performed before proceeding with crystallization trials. In addition, to avoid a high amount of gephyrin background in the EM micrographs, a co-sedimentation assay can be performed before depositing the samples on the EM grid. Besides the optimization of sample preparations for structural studies, biochemical analysis of the interactions, maybe by ITC, will also help to better understand the stoichiometry and thermodynamic basis for this interaction and, inturn, will provide a better foundation for future structural studies.

9.3 The terminal step of Moco-biosynthesis

High resolution crystal structures of GephE in the apo-state and in the presence of nucleotides and metals have generated important insights into the terminal step during Moco biosynthesis. To gain additional insights into the molecular basis of the interaction, mutational analysis of the residues, which have shown to be important for the interaction should be carried out. For a better understanding the enzymatic framework of the terminal steps, adenylated molybdopterin will have to be co-crystallized with an active site mutant of GephE, for example the D580A variant which leads to MocD.

9.4 Structural studies on Cinnamon

Initial AFM and EM studies demonstrated that the trimeric form of Cinnamon adopts a compact conformation and will be a suitable candidate for crystallographic studies. If the crystallization trials fail, an alternative approach would be to carry out cryo EM studies. As the linker region in Cinnamon is comparatively shorter than in gephyrin, the crystal structures of the terminal domains will facilitate the cryo-EM studies of the full-length protein by providing the matching building blocks rather than having to rely on the known GephG and GephE structures.

10. SUMMARY OF PDB ENTRIES GENERATED IN THIS THESIS

PDB code	Structure
4PDO	1.7 Å resolution structure of the gephyrin E-domain
4PD1	Structure of the gephyrin E domain with a glycine receptor β subunit derived peptide
4TK1	Geph E in complex with a GABA receptor α3 subunit derived peptide in space group $P2_12_12$
4TK2	Geph E in complex with a GABA receptor α3 subunit derived peptide in space group $P6_1$
4TK3	Geph E in complex with a GABA receptor α3 derived double mutant peptide in spacegroup $P2_12_12$
4TK4	GephE in complex with a GABA receptor α3 subunit derived double mutant peptide in space group $P6_1$
4U90	GephE in complex with PEG crosslinked GABA receptor α3 subunit derived dimeric peptide
4U91	GephE in complex with para-phenyl crosslinked glycine receptorβsubunit derived dimeric peptide
5ERQ	Gephyrin E domain at 1.55 Åresolution
5ERR	GephE in complex with Mg^{2+}– ADP
5ERS	GephE in complex with Mg^{2+}- AMP
5ERT	GephE in complex with Mn^{2+}- ADP
5ERU	Ternary complex of GephE - ADP - molybdate cluster
5ERV	Ternary complex of GephE - ADP - tungstate cluster

11.LIST OF PUBLICATIONS

1. Maric, H.M., **Kasaragod, V.B.,** and Schindelin, H. (2014). Modulation of gephyrin-glycine receptor affinity by multivalency. *ACS Chem. Biol*. ***9***, 2554-2562.
2. Maric, H.M*., **Kasaragod, V.B*.,** Hausrat, T.J., Kneussel, M., Tretter, V., Strømgaard, K., and Schindelin, H. (2014). Molecular basis of the alternative recruitment of $GABA_A$ versus glycine receptors through gephyrin. *Nat. Commun*. ***5***, 5767.
3. Maric, H.M., **Kasaragod, V.B.,** Kedstrom, L.H., Hausrat, T.J., Kneussel, M., Schindelin, H., Strømgaard, K. (2015). Design and synthesis of high-affinity dimeric inhibitors targeting the interaction between gephyrin and inhibitory neurotransmitter receptors. *Angew. Chem. Int. Ed.****54***, 490-4.
4. **Kasaragod, V.B**. and Schindelin, H. (2016).Structural Framework for Metal Incorporation during Molybdenum Cofactor Biosynthesis.*Structure.****24*****,**782-8.

*** These authors contributed equally to this work.**

12. ACKNOWLEDGEMENTS

First and foremost, I would like to thank Prof. Dr. Hermann Schindelin for giving me the opportunity to do my PhD under his valuable guidance. Thank you Hermann, for funding me and helping me to acquire a solid foundation in macromolecular X-ray crystallography.

I would also like to thank Prof. Dr. Thomas Müller and Prof. Dr. Carmen Villmann for being members of my thesis committee and also for the valuable suggestions and evaluations during the annual committee meetings. I would also like to thank Prof. Dr. Caroline Kisker for all the support and suggestions, especially during the feedback meetings. Dr. Daniela Schneeberger played a critical role in my studies during the initial days of my PhD. I would like to thank her for all the support and guidance which she provided.

I am ever thankful towards Dr. Hans Maric, who had initiated the gephyrin-receptor interaction project and also for the subsequent fruitful collaboration. I would like to thank Dr. Bodo Sander for providing multiple gephyrin constructs and also for the fruitful discussions on the gephyrin topic.

I thank Dr. Florian Sauer for his support (academically and personally), guidance and being a wonderful bench mate throughout my PhD. I am also thankful towards Mohit Misra for his friendship and helping me during some of the critical times in the lab. I would like to thank Dr. Jochen Kuper, Dr. Petra Hänzelmann and Dr. Antje Schäfer for all the support. I would also like to thank Lena Ries and Dr. Christian Feiler for the wonderful memories. Besides, I would like to thank all members of lab 206 and office 00.017 for a nice working atmosphere.

I thank Christian Kraft for all the help with the EM experiments. I would also like to thank Dr. Ingrid Tessmer and Dr. Petra Wendler for their respective collaborations on the AFM and EM studies.

I thank Dr. Bernhard Froehlich for his excellent IT support. In the administrative point of view, I am thankful towards Andrea Heinzmann, Teresa Frank and Petra Baron.

I would like to thank those who travelled with me to different synchrotrons and stamping wonderful memories. I thank all past and present members of Schindelin, Kisker, Lorenz and Tessmer laboratories for helping me to learn many of the techniques in the lab and also for proving an excellent working atmosphere.

I would like to thank my family for all the sacrifices and being my backbone support, without which it would not have been possible for me to finish my studies.

Last but not least, I would like to thank God and my Dad for being my guardian angel.

13.ABBREVIATIONS

°	Degree
°C	Degree celcius
Å	Ångström
A280	Absorbance at 280 nm
ADP	Adenosine diphosphate
AFM	Atomic Force Microscopy
AMP	Adenosine monophosphate
Amp	Ampicillin
AMPA	α-amino-3-hydroxy-5-methyl-4-isoxazole propionic acid
aSEC	Analytical size-exclusion chromatography
ATP	Adenosine triphosphate
BLAST	Basic Local Alignment Search Tool
BRB80	Brinkley RB buffer 1980
BSA	Bovine serum albumin
cal	Calorie
Cam	Chloramphenicol
CB	Collybistin
CCP4	Collaborative computational project number 4
Cin	Cinnamon
CNS	Central nervous system
CV	Column volume
Da	Dalton
DARPin	Designed ankyrin repeat proteins
DB buffer	Depolymerization buffer
DLS	Dynamic light scattering
DNA	Deoxyribonucleic acid
DNase	Deoxyribonuclease
dRI	Differential Refractive Index
DSC	Differential scanning calorimetry
DTT	Dithiothreitol
E. coli	*Escherichia coli*
EDTA	Ethylenediaminetetraacetate
EGTA	Ethylene-bis(oxyethylenenitrilo)tetraacetic acid
ELS	Evaporative light scattering

EM	Electron microscopy
ESI-LCMS	Electospray liquid chromatography mass spectrometry
ESRF	European synchrotron radiation facility
Fig.	Figure
FPLC	Fast protein liquid chromatography
$GABA_AR$	Gamma-aminobutyric acid type A receptor
GDP	Guanosine diphosphate
Geph	Gephyrin
GephE	Gephyrin E domain
GephG	Gephyrin G domain
Gly β R	Glycine receptor beta subunit
GTP	Guanosine triphosphate
HEPES	4-(2-hydroxyethyl)-1- piperazineethanesulfonic acid
HMPB	High molarity polymerization buffer
HPLC	High performance liquid chromatography
HRMS	High resolution mass spectrometry
IPTG	Isopropyl-β-thiogalactoside
ITC	Isothermal titration calorimetry
J	Joule
K	Kelvin
Kan	Kanamycin
K_D	Dissociation constant
kDa	Kilo Dalton
kT	Kilo Tesla
LB	Lysogen broth
LCMS	Liquid chromatography-mass spectroscopy
M	Molar
MALS	Multi angle light scattering
MBP	Maltose binding protein
min	Minute
mIPSC	Miniature inhibitory postsynaptic current
mL	Milliliter
MLH	Missing linker half
mM	Millimolar
Mo	Molybdenum atom
MoCD	Molybdenum cofactor deficiency
Moco	Molybdenum cofactor

MoO_4^{2-}	Molybdate ion
MPD	2-Methyl-2,4-pentanediol
MPT	Molybdopterin
MPT.AMP	Adenylated molybdopterin
MR	Molecular Replacement
MS	Mass spectrometry
MWCO	Molecular weight cut off
n. a.	Not available
n.d.	Not determined
n.d.	Not determined
NL	Neuroligin
nm	Nanometer
nM	Nanomolar
NMDA	*N*-methyl-D-aspartate
PAGE	Polyacrylamide gel electophoresis
PDB	Protein Data Bank
PEG	Poly ethylene glycol
PH	Pleckstrin homology
pI	Isoelectric point
PIPES	1,4-Piperazinediethanesulfonic acid
PISA	Protein Interfaces, Surfaces andAssemblies
PMSF	Phenylmethylsulfonylfluoride
PSD	Postsynaptic density
rmsd	Root mean square deviation
RT	Room temperature
SAXS	Small-angle X-ray scattering
SDS	Sodium dodecyl sulfate
SH3	Src Homology 3 Domain
SLIC	Sequence and ligation independent cloning
SPR	Surface Plasmon resonance
T	Temparature
TCEP	Tris-(2-carboxyethyl)-phosphin
TLS	Translation, liberation, screw
TRIS	Trishydroxymethylaminomethane
UV	Ultraviolet
v/v	volume per volume
VV	Void volume

W	Tungsten atom
w/v	Weight per volume
WO_4^{2-}	Tungstate ion
WT	Wild-type
β-ME	β -mercaptoethanol
Δ14	Exon 14 deletion of Gephyrin
ΔH	Change in enthalpy
ΔS	Change in entropy
ε	Extinction coefficient
µL	Microliter
µM	Micromolar

14.EXPRESSION CONTRUCTS

Insert	Vector/ Tag-s / Protease cleavage site	Source
Gephyrin Full length P2 (1-750)	pET-28b/ N-term 6XHis/-	Sander, B.
Gephyrin E domain (318-736)	pTWIN/ Intein/ pH shift	Maric, H.M.
Gephyrin G domain	pET-28b/ N-term 6XHis/-	Sander, B.
Gephyrin G-Linker	pET-28b/ N-term 6XHis/-	Sander, B.
Gephyrin Linker-E	pET-28b/ N-term 6XHis/-	Sander, B.
Gephyrin delta exon 14	pET-28b/ N-term 6XHis/-	Sander, B.
Gephyrin- Missing linker half 1	pET-28b/ N-term 6XHis/-	Sander, B.
Gephyrin- Missing linker half 2	pET-28b/ N-term 6XHis/-	Sander, B.
MBP-Linker 1 (252-331)	pETM41/ N-term MBP 6XHis/TEV	Sander, B.
MBP-Linker 2 (303-331)	pETM41/ N-term MBP 6XHis/TEV	Sander, B.
Gephyrin E domain P713E	pTWIN1/ Intein/ pH shift	Maric, H.M.
Gephyrin E domain F330A	pTWIN1/ Intein/ pH shift	Maric, H.M.
Cinnamon- cDNA	---	DGRC, Indiana University
Cinnamon FL (1-601)	pETM-14/ N-term 6XHis/ 3C	Kasaragod, V.B.
Cinnamon FL (1-601)	ColA/ N-term Trx-6XHis/ 3C	Kasaragod, V.B.
Cinnamon FL (1-601)	pCDF/ N-term Trx-6XHis/ 3C	Kasaragod, V.B.
Cinnamon FL (1-601)	pCDF/ N-term Smt3-6XHis/ 3C	Kasaragod, V.B.
Cinnamon (12-601)	ColA/ N-term Trx-6XHis/ 3C	Kasaragod, V.B.
Cinnamon (1-592)	pETM-14/ N-term 6XHis/ 3C	Kasaragod, V.B.
Cinnamon (1-592)	pETM-14/ N-term 6XHis/ 3C	Kasaragod, V.B.
Cinnamon (12-592)	pETM-14/ N-term 6XHis/ 3C	Kasaragod, V.B.
Cinnamon (12-592)	ColA/ N-term Trx-6XHis/ 3C	Kasaragod, V.B.
Cinnamon (12-592)	pCDF/ N-term Trx-6XHis/ 3C	Kasaragod, V.B.
Cinnamon (24-601)	pETM-14/ N-term 6XHis/ 3C	Kasaragod, V.B.
Cinnamon (24-601)	ColA/ N-term Trx-6XHis/ 3C	Kasaragod, V.B.
Cinnamon (1-571)	pETM-14/ N-term 6XHis/ 3C	Kasaragod, V.B.
Cinnamon (1-571)	ColA/ N-term Trx-6XHis/ 3C	Kasaragod, V.B.
Cinnamon (24-571)	pETM-14/ N-term 6XHis/ 3C	Kasaragod, V.B.
Cinnamon (24-571)	ColA/ N-term Trx-6XHis/ 3C	Kasaragod, V.B.
Cinnamon (24-571)	pCDF/ N-term Trx-6XHis/ 3C	Kasaragod, V.B.
Cinnamon E domain (198-601)	pETM-14/ N-term 6XHis/ 3C	Kasaragod, V.B.
Cinnamon E domain (198-601)	ColA/ N-term Trx-6XHis/ 3C	Kasaragod, V.B.
Cinnamon G domain (1-157)	pETM-14/ N-term 6XHis/ 3C	Kasaragod, V.B.
Cinnamon G domain (1-157)	ColA/ N-term Trx-6XHis/ 3C	Kasaragod, V.B.

15. AFFIDAVIT

I hereby confirm that my thesis entitled "Biochemical and Structural Basis for the Moonlighting Function of Gephyrin" is the result of my own work. I did not receive any help or support from commercial consultants. All sources and / or materials applied are listed and specified in the thesis.

Furthermore, I confirm that this thesis has not yet been submitted as part of another examination process neither in identical nor in similar form.

Würzburg,

Place, Date *Signature*

Eidesstattliche Erklärung

Hiermit erkläre ich an Eides statt, die Dissertation „Biochemische und Strukturelle Basis für die duale Funktionalität von Gephyrin“ eigenständig, d.h. insbesondere selbständig und ohne Hilfe eines kommerziellen Promotionsberaters, angefertigt und keine anderen als die von mir angegebenen Quellen und Hilfsmittel verwendet zu haben.

Ich erkläre außerdem, dass die Dissertation weder in gleicher noch in ähnlicher Form bereits in einem anderen Prüfungsverfahren vorgelegen hat.

Würzburg, den

Ort, Datum *Unterschrift*

16. CURRICULUM VITAE

VIKRAM BABU KASARAGOD

vikrambabuk@gmail.com Cell: +4917672224332
Permanent address: SHREYAS", Near Lalitha Kala Sadan,
Beerantha Bail Road, Kasaragod.
Pin Code- 671121 Kerala State, India
Current address: Frankenstrasse, 203, 97078 Würzburg, Germany

---

EDUCATION

Doctor of Philosophy **Expected 2016**
Biomedicine / Structural Biology

Masters of Science in Genetics (78%) **July '11**
Mainly based on *Drosophila* as the model organism.
University of Mysore. India

Bachelor of Science (GPA **7.72/10**) **June '09**
Subjects: Biotechnology, Botany and Chemistry
St. Aloysius College, Mangalore, Karnataka, India

ACADEMIC PROJECTS

Biochemical and structural basis for the moonlighting function of gephyrin. **April 2013 - present**

.

Doctoral thesis project.
Rudolf Virchow Center, University of Würzburg.
Guide: Prof. Dr. Hermann Schindelin.

The structural studies on Bacterial translocon proteins **Sep'12 to March' 13**
Rudolf Virchow Center, University of Würzburg.
Guide: Dr. Shashi Bhushan, Group leader, Cryo-EM group.

- Purification of different translocon proteins such as SecA and SecB of E. coli .
- The purified proteins were studied for the complex formation and interaction studies by EM.
- Structural studies of the different proteins which are involved in the co-translational process by Cryo EM.

The structural studies on proteins from Humans and *Plasmodium*.Sep '11 to June 2012
International Centre for Genetic Engineering and Biotechnology, New Delhi.
Guide: Dr. Amit Sharma, Group Leader, Structural and computational Biology Group

- Structural studies of Different proteins from humans and the malaria parasite, *Plasmodium* by X-ray crystallographic studies.
- The work is mainly carried out in Human Liver Fatty Acid Binding proteins (LFABP) and Amino acyl tRNA protein transferase from *Plasmodium.*

The studies on the interaction of histones with their chaperones. July'10 and Aug '10
International Centre for Genetic Engineering and Biotechnology, New Delhi.
Guide: Dr. Amit Sharma, Group Leader, Structural and computational Biology Group

- The project was mainly based on the structural analysis by X ray diffraction
- The Nucleosome assembly proteins (*napl* and *naps ht of P.falciparum*) were cloned and purified.
- Purified proteins were co crystallized with histone peptides.
- Project helped in the optimization of the crystallization condition, which will help in deciphering the structure of complex.

The airborne pollen and fungal spore survey in urban and rural areas of Mangalore **June '08 to May '09**
Guide: Dr. K.V. Nagalakshamma, Co-ordinator, UG Department of Biotechnology,
St.Aloysius College, Mangalore, India.

- Project based on the pollen survey and fungal survey using the concept of Aerobiology.
- Also includes the clinical survey of the allergic microorganisms where the informationwere given by the reputed medical practitioners.
- This survey has helped the researchers in knowing the onset of fungal spore and pollination period.
- Helping the Doctors in finding the causative agents for the asthma and other dust allergies.

SKILLS

- **Molecular biology techniques:** Cloning, Human Karyotyping, Blotting techniques, etc.
- PCR, FPLC, Ion exchange chromatography, Gel permeation chromatography and crystallization works.
- Usage of Flourimeter, Thermoflour, Handling Gradient Machine for Ribosome preparation.
- Handling Robotics for crystallization, Operation of X-ray Diffractometer, CCP4i, PHENIX.

SIGNIFICANT ACHIEVEMENTS AND EXTRA CURRICULAR ACTIVITIES

- Secured **3rd rank** in MSc Genetics exams conducted by University of Mysore (2009-11).
- **Only student** in the MSc batch(2009-11-Total strength is 120 students) who got selected as the summer research fellow by **Indian Academy of Sciences, Bangalore**.
- Participations in many intercollegiate fests in Science quiz competition and bagged following prizes
    - **Ist Place**-Sciencio 2008- Milagres College, Kallianpur,Karnataka
    - **Ist Place**- Eureka 07- PoornaPrajnaCollege,Udupi,Karnataka
    - **Ist Place** - Amalgamation 09-Mahatma Gandhi Memorial College, Udupi

- **Joint Secretary** of the Biotechnology Association at St.Aloysius College for the academic year 2008-09.
- **Student Coordinator for arrangements** for IMPRINTS-08 i.e. the National Level Science fest at St. Aloysius College in 2008
- **Organizing Student Coordinator** for Hands on Workshop in Principles and techniques in Biological Science at St. Aloysius College in 2009

Würzburg,

Place, Date Signature

17. REFERENCES

Adams, P.D., Afonine, P.V., Bunkoczi, G., Chen, V.B., Davis, I.W., Echols, N., Headd, J.J., Hung, L.W., Kapral, G.J., Grosse-Kunstleve, R.W.*, et al.* (2010). PHENIX: a comprehensive Python-based system for macromolecular structure solution. Acta Crystallogr D Biol Crystallogr ***66***, 213-221.

Albuquerque, E.X., Pereira, E.F., Alkondon, M., and Rogers, S.W. (2009). Mammalian nicotinic acetylcholine receptors: from structure to function. Physiological reviews ***89***, 73-120.

Alushin, G.M., Lander, G.C., Kellogg, E.H., Zhang, R., Baker, D., and Nogales, E. (2014). High-resolution microtubule structures reveal the structural transitions in alphabeta-tubulin upon GTP hydrolysis. Cell ***157***, 1117-1129.

Bach, A., Chi, C.N., Olsen, T.B., Pedersen, S.W., Roder, M.U., Pang, G.F., Clausen, R.P., Jemth, P., and Stromgaard, K. (2008). Modified peptides as potent inhibitors of the postsynaptic density-95/N-methyl-D-aspartate receptor interaction. J Med Chem ***51***, 6450-6459.

Bach, A., Chi, C.N., Pang, G.F., Olsen, L., Kristensen, A.S., Jemth, P., and Stromgaard, K. (2009). Design and synthesis of highly potent and plasma-stable dimeric inhibitors of the PSD-95-NMDA receptor interaction. Angew Chem Int Ed Engl ***48***, 9685-9689.

Bach, A., Clausen, B.H., Moller, M., Vestergaard, B., Chi, C.N., Round, A., Sorensen, P.L., Nissen, K.B., Kastrup, J.S., Gajhede, M.*, et al.* (2012). A high-affinity, dimeric inhibitor of PSD-95 bivalently interacts with PDZ1-2 and protects against ischemic brain damage. Proc Natl Acad Sci U S A ***109***, 3317-3322.

Bach, A., Eildal, J.N., Stuhr-Hansen, N., Deeskamp, R., Gottschalk, M., Pedersen, S.W., Kristensen, A.S., and Stromgaard, K. (2011). Cell-permeable and plasma-stable peptidomimetic inhibitors of the postsynaptic density-95/N-methyl-D-aspartate receptor interaction. J Med Chem ***54***, 1333-1346.

Bailey, S. (1994). The CCP4 suite: programs for protein crystallography. Acta Crystallogr D Biol Crystallogr ***50***, 760-763.

Ballif, B.A., Carey, G.R., Sunyaev, S.R., and Gygi, S.P. (2008). Large-scale identification and evolution indexing of tyrosine phosphorylation sites from murine brain. J Proteome Res ***7***, 311-318.

Bard, L., Sainlos, M., Bouchet, D., Cousins, S., Mikasova, L., Breillat, C., Stephenson, F.A., Imperiali, B., Choquet, D., and Groc, L. (2010). Dynamic and specific interaction between synaptic NR2-NMDA receptor and PDZ proteins. Proc Natl Acad Sci U S A ***107***, 19561-19566.

Battye, T.G., Kontogiannis, L., Johnson, O., Powell, H.R., and Leslie, A.G. (2011). iMOSFLM: a new graphical interface for diffraction-image processing with MOSFLM. Acta Crystallogr D Biol Crystallogr ***67***, 271-281.

Bayram, E., Topcu, Y., Karakaya, P., Yis, U., Cakmakci, H., Ichida, K., and Kurul, S.H. (2013). Molybdenum cofactor deficiency: review of 12 cases (MoCD and review). European journal of paediatric neurology : EJPN : official journal of the European Paediatric Neurology Society ***17***, 1-6.

Bedet, C., Bruusgaard, J.C., Vergo, S., Groth-Pedersen, L., Eimer, S., Triller, A., and Vannier, C. (2006). Regulation of gephyrin assembly and glycine receptor synaptic stability. J Biol Chem ***281***, 30046-30056.

Belaidi, A.A., and Schwarz, G. (2013). Metal insertion into the molybdenum cofactor: product-substrate channelling demonstrates the functional origin of domain fusion in gephyrin. The Biochemical journal ***450***, 149-157.

Bell-Horner, C.L., Dohi, A., Nguyen, Q., Dillon, G.H., and Singh, M. (2006). ERK/MAPK pathway regulates GABAA receptors. J Neurobiol ***66***, 1467-1474.

Bittner, F. (2014). Molybdenum metabolism in plants and crosstalk to iron. Frontiers in plant science ***5***, 28.

Castoldi,M., and Povov, A.V., (2003). Purification of brain tubulin through two cyclesof polymerization–depolymerization in a high-molarity buffer. Protein Expes Purif. ***32.*** 83-88.

Charbaut,E., Curmi, P.A., Ozon, S.,Lachkar, S., Virginie Redeker, V., Sobel, A. (2001). Stathmin family proteins display specific molecular and tubulin binding properties. J Biol Chem. ***276****,* 16146-16154.

Chi, C.N., Bach, A., Gottschalk, M., Kristensen, A.S., Stromgaard, K., and Jemth, P. (2010). Deciphering the kinetic binding mechanism of dimeric ligands using a potent plasma-stable dimeric inhibitor of postsynaptic density protein-95 as an example. J Biol Chem ***285***, 28252-28260.

Chi, C.N., Bach, A., Stromgaard, K., Gianni, S., and Jemth, P. (2012). Ligand binding by PDZ domains. Biofactors.

Choudhary, C., Kumar, C., Gnad, F., Nielsen, M.L., Rehman, M., Walther, T.C., Olsen, J.V., and Mann, M. (2009). Lysine acetylation targets protein complexes and co-regulates major cellular functions. Science ***325***, 834-840.

Copley, S.D. (2003). Enzymes with extra talents: moonlighting functions and catalytic promiscuity. Current opinion in chemical biology ***7***, 265-272.

Dejanovic, B., Djemie, T., Grunewald, N., Suls, A., Kress, V., Hetsch, F., Craiu, D., Zemel, M., Gormley, P., Lal, D.*, et al.* (2015). Simultaneous impairment of neuronal and metabolic function of mutated gephyrin in a patient with epileptic encephalopathy. EMBO molecular medicine ***7*****,** 1580-1594.

Dejanovic, B., Lal, D., Catarino, C.B., Arjune, S., Belaidi, A.A., Trucks, H., Vollmar, C., Surges, R., Kunz, W.S., Motameny, S.*, et al.* (2014a). Exonic microdeletions of the gephyrin gene impair GABAergic synaptic inhibition in patients with idiopathic generalized epilepsy. Neurobiology of disease ***67***, 88-96.

Dejanovic, B., Semtner, M., Ebert, S., Lamkemeyer, T., Neuser, F., Luscher, B., Meier, J.C., and Schwarz, G. (2014). Palmitoylation of gephyrin controls receptor clustering and plasticity of GABAergic synapses. PLoS biology ***12***, e1001908.

Demirkan, G., Yu, K., Boylan, J.M., Salomon, A.R., and Gruppuso, P.A. (2011). Phosphoproteomic profiling of in vivo signaling in liver by the mammalian target of rapamycin complex 1 (mTORC1). PLoS One ***6***, e21729.

Dolgin, E. (2012). To serve and neuroprotect. Nat Med ***18***, 1003-1006.

Dorleans, A., Knossow, M., and Gigant, B. (2007). Studying drug-tubulin interactions by X-ray crystallography. Methods in molecular medicine ***137***, 235-243.

Du, J., Lu, W., Wu, S., Cheng, Y., and Gouaux, E. (2015). Glycine receptor mechanism elucidated by electron cryo-microscopy. Nature ***526***, 224-229.

Durr, K.L., Chen, L., Stein, R.A., De Zorzi, R., Folea, I.M., Walz, T., McHaourab, H.S., and Gouaux, E. (2014). Structure and dynamics of AMPA receptor GluA2 in resting, pre-open, and desensitized states. Cell ***158***, 778-792.

Essrich, C., Lorez, M., Benson, J.A., Fritschy, J.M., and Luscher, B. (1998). Postsynaptic clustering of major GABAA receptor subtypes requires the gamma 2 subunit and gephyrin. Nat Neurosci***1*****,** 563-571.

Feng, G., Tintrup, H., Kirsch, J., Nichol, M.C., Kuhse, J., Betz, H., and Sanes, J.R. (1998). Dual requirement for gephyrin in glycine receptor clustering and molybdoenzyme activity. Science ***282***, 1321-1324.

Flemming, A. (2012). Stroke: Can PSD95 inhibitors widen the therapeutic window? Nat Rev Drug Discov ***11***, 272.

Fritschy, J.M., Harvey, R.J., and Schwarz, G. (2008). Gephyrin: where do we stand, where do we go? Trends Neurosci ***31***, 257-264.

Fritschy, J.M., and Panzanelli, P. (2014). GABA receptors and plasticity of inhibitory neurotransmission in the central nervous system. Eur J Neurosci. ***39***, 1845-1865

Giesemann, T., Schwarz, G., Nawrotzki, R., Berhorster, K., Rothkegel, M., Schluter, K., Schrader, N., Schindelin, H., Mendel, R.R., Kirsch, J.*, et al.* (2003). Complex formation

between the postsynaptic scaffolding protein gephyrin, profilin, and Mena: a possible link to the microfilament system. J Neurosci ***23***, 8330-8339.

Gronenborn, A.M. (2009). Protein acrobatics in pairs--dimerization via domain swapping. Curr Opin Struct Biol ***19***, 39-49.

Gross, A., Sims, R.E., Swinny, J.D., Sieghart, W., Bolam, J.P., and Stanford, I.M. (2011). Differential localization of GABA(A) receptor subunits in relation to rat striatopallidal and pallidopallidal synapses. Eur J Neurosci ***33***, 868-878.

Harvey, K., Duguid, I.C., Alldred, M.J., Beatty, S.E., Ward, H., Keep, N.H., Lingenfelter, S.E., Pearce, B.R., Lundgren, J., Owen, M.J.*, et al.* (2004). The GDP-GTP exchange factor collybistin: an essential determinant of neuronal gephyrin clustering. J Neurosci ***24***, 5816-5826.

Heine, M., Groc, L., Frischknecht, R., Beique, J.C., Lounis, B., Rumbaugh, G., Huganir, R.L., Cognet, L., and Choquet, D. (2008). Surface mobility of postsynaptic AMPARs tunes synaptic transmission. Science ***320***, 201-205.

Herweg, J., and Schwarz, G. (2012). Splice-specific glycine receptor binding, folding, and phosphorylation of the scaffolding protein gephyrin. J Biol Chem. ***287***, 12645-56

Hines, R.M., Davies, P.A., Moss, S.J., and Maguire, J. (2012a). Functional regulation of GABAA receptors in nervous system pathologies. Current opinion in neurobiology ***22***, 552-558.

Hines, R.M., Davies, P.A., Moss, S.J., and Maguire, J. (2012b). Functional regulation of GABAA receptors in nervous system pathologies. Curr Opin Neurobiol ***22***, 552-558.

Iskenderian-Epps, W.S., and Imperiali, B. (2010). Modulation of Shank3 PDZ domain ligand-binding affinity by dimerization. Chembiochem ***11***, 1979-1984.

Jencks, W.P. (1981). On the attribution and additivity of binding energies. Proc Natl Acad Sci U S A ***78***, 4046-4050.

Johnson, J.L., Chaudhury, M., and Rajagopalan, K.V. (1991). Identification of a molybdopterin-containing molybdenum cofactor in xanthine dehydrogenase from Pseudomonas aeruginosa. Biofactors ***3***, 103-107.

Johnston, G.A. (1996). GABAA receptor pharmacology. Pharmacol Ther ***69***, 173-198.

Kabsch, W. (2010). Xds. Acta Crystallogr D Biol Crystallogr ***66***, 125-132.

Kamdar, K.P., Primus, J.P., Shelton, M.E., Archangeli, L.L., Wittle, A.E., and Finnerty, V. (1997). Structure of the molybdenum cofactor genes in Drosophila. Biochemical Society transactions ***25***, 778-783.

Kamdar, K.P., Shelton, M.E., and Finnerty, V. (1994). The Drosophila molybdenum cofactor gene cinnamon is homologous to three Escherichia coli cofactor proteins and to the rat protein gephyrin. Genetics ***137***, 791-801.

Kang, R., Wan, J., Arstikaitis, P., Takahashi, H., Huang, K., Bailey, A.O., Thompson, J.X., Roth, A.F., Drisdel, R.C., Mastro, R.*, et al.* (2008). Neural palmitoyl-proteomics reveals dynamic synaptic palmitoylation. Nature ***456***, 904-909.

Kasaragod, V.B., and Schindelin, H. (2016). Structural Framework for Metal Incorporation during Molybdenum Cofactor Biosynthesis. Structure ***24***, 782-788.

Keinanen, K., Wisden, W., Sommer, B., Werner, P., Herb, A., Verdoorn, T.A., Sakmann, B., and Seeburg, P.H. (1990). A family of AMPA-selective glutamate receptors. Science ***249***, 556-560.

Kim, E.Y., Schrader, N., Smolinsky, B., Bedet, C., Vannier, C., Schwarz, G., and Schindelin, H. (2006). Deciphering the structural framework of glycine receptor anchoring by gephyrin. Embo J ***25***, 1385-1395.

Kirsch, J., Langosch, D., Prior, P., Littauer, U.Z., Schmitt, B., and Betz, H. (1991). The 93-kDa glycine receptor-associated protein binds to tubulin. J Biol Chem ***266***, 22242-22245.

Kittler, J.T., McAinsh, K., and Moss, S.J. (2002). Mechanisms of GABAA receptor assembly and trafficking: implications for the modulation of inhibitory neurotransmission. Mol Neurobiol ***26***, 251-268.

Klosi, E., Saro, D., and Spaller, M.R. (2007). Bivalent peptides as PDZ domain ligands. Bioorg Med Chem Lett ***17***, 6147-6150.

Kneussel, M., and Betz, H. (2000). Clustering of inhibitory neurotransmitter receptors at developing postsynaptic sites: the membrane activation model. Trends Neurosci ***23***, 429-435.

Kneussel, M., Brandstatter, J.H., Laube, B., Stahl, S., Muller, U., and Betz, H. (1999a). Loss of postsynaptic GABA(A) receptor clustering in gephyrin-deficient mice. J Neurosci ***19*,** 9289-9297.

Kneussel, M., Hermann, A., Kirsch, J., and Betz, H. (1999b). Hydrophobic interactions mediate binding of the glycine receptor beta-subunit to gephyrin. J Neurochem***72***, 1323-1326.

Kowalczyk, S., Winkelmann, A., Smolinsky, B., Forstera, B., Neundorf, I., Schwarz, G., and Meier, J.C. (2013). Direct binding of GABAA receptor beta2 and beta3 subunits to gephyrin. Eur J Neurosci. ***37***, 544-554.

Kuhse, J., Kalbouneh, H., Schlicksupp, A., Mukusch, S., Nawrotzki, R., and Kirsch, J. (2012). Phosphorylation of gephyrin in hippocampal neurons by cyclin-dependent kinase CDK5 at Ser-270 is dependent on collybistin. J Biol Chem ***287***, 30952-30966.

Kuper, J., Llamas, A., Hecht, H.J., Mendel, R.R., and Schwarz, G. (2004). Structure of the molybdopterin-bound Cnx1G domain links molybdenum and copper metabolism. Nature ***430***, 803-806.

Kuper, J., Winking, J., Hecht, H.J., Mendel, R.R., and Schwarz, G. (2003). The active site of the molybdenum cofactor biosynthetic protein domain Cnx1G. Archives of biochemistry and biophysics ***411***, 36-46.

Langer, G., Cohen, S.X., Lamzin, V.S., and Perrakis, A. (2008). Automated macromolecular model building for X-ray crystallography using ARP/wARP version 7. Nature protocols ***3***, 1171-1179.

Leimkuhler, S., Charcosset, M., Latour, P., Dorche, C., Kleppe, S., Scaglia, F., Szymczak, I., Schupp, P., Hahnewald, R., and Reiss, J. (2005). Ten novel mutations in the molybdenum cofactor genes MOCS1 and MOCS2 and in vitro characterization of a MOCS2 mutation that abolishes the binding ability of molybdopterin synthase. Human genetics ***117***, 565-570.

Leimkuhler, S., and Iobbi-Nivol, C. (2015). Bacterial molybdoenzymes: old enzymes for new purposes. FEMS microbiology reviews.***40***, 1-18.

Li, M.Z., and Elledge, S.J. (2007). Harnessing homologous recombination in vitro to generate recombinant DNA via SLIC. Nature methods ***4***, 251-256.

Linsalata, A.E., Chen, X., Winters, C.A., and Reese, T.S. (2014). Electron tomography on gamma-aminobutyric acid-ergic synapses reveals a discontinuous postsynaptic network of filaments. J Comp Neurol ***522***, 921-936.

Liu, M.T., Wuebbens, M.M., Rajagopalan, K.V., and Schindelin, H. (2000). Crystal structure of the gephyrin-related molybdenum cofactor biosynthesis protein MogA from Escherichia coli. J Biol Chem.***275***, 1814-1822.

Llamas, A., Mendel, R.R., and Schwarz, G. (2004). Synthesis of adenylated molybdopterin: an essential step for molybdenum insertion. J Biol Chem. ***279***, 55241-55246.

Llamas, A., Otte, T., Multhaup, G., Mendel, R.R., and Schwarz, G. (2006). The Mechanism of nucleotide-assisted molybdenum insertion into molybdopterin. A novel route toward metal cofactor assembly. J Biol Chem. ***281***, 18343-18350.

Lummis, S.C. (2012). 5-HT(3) receptors. J Biol Chem***. 287***, 40239-40245.

Maas, C., Tagnaouti, N., Loebrich, S., Behrend, B., Lappe-Siefke, C., and Kneussel, M. (2006). Neuronal cotransport of glycine receptor and the scaffold protein gephyrin. J Cell Biol ***172***, 441-451.

Maric, H.M., Kasaragod, V.B., Haugaard-Kedstrom, L., Hausrat, T.J., Kneussel, M., Schindelin, H., and Stromgaard, K. (2015). Design and synthesis of high-affinity dimeric inhibitors targeting the interactions between gephyrin and inhibitory neurotransmitter receptors. Angew Chem Int Ed Engl ***54***, 490-494..

Maric, H.M., Kasaragod, V.B., Hausrat, T.J., Kneussel, M., Tretter, V., Stromgaard, K., and Schindelin, H. (2014b). Molecular basis of the alternative recruitment of GABA(A) versus glycine receptors through gephyrin. Nature communications ***5***, 5767.

Maric, H.M., Kasaragod, V.B., and Schindelin, H. (2014c). Modulation of gephyrin-glycine receptor affinity by multivalency. ACS chemical biology ***9***, 2554-2562.

Maric, H.M., Mukherjee, J., Tretter, V., Moss, S.J., and Schindelin, H. (2011). Gephyrin-mediated gamma-aminobutyric acid type A and glycine receptor clustering relies on a common binding site. J Biol Chem ***286***, 42105-42114.

McCoy, A.J., Grosse-Kunstleve, R.W., Adams, P.D., Winn, M.D., Storoni, L.C., and Read, R.J. (2007). Phaser crystallographic software. Journal of applied crystallography ***40***, 658-674.

Mendel, R.R. (2013). The molybdenum cofactor. J Biol Chem. ***288***, 13165-13172.

Mendel, R.R., and Leimkuhler, S. (2015). The biosynthesis of the molybdenum cofactors. Journal of biological inorganic chemistry : JBIC : a publication of the Society of Biological Inorganic Chemistry ***20***, 337-347.

Meyer, G., Kirsch, J., Betz, H., and Langosch, D. (1995). Identification of a gephyrin binding motif on the glycine receptor beta subunit. Neuron ***15***, 563-572.

Miller, P.S., and Aricescu, A.R. (2014). Crystal structure of a human GABAA receptor. Nature ***512***, 270-275.

Mukherjee, J., Kretschmannova, K., Gouzer, G., Maric, H.M., Ramsden, S., Tretter, V., Harvey, K., Davies, P.A., Triller, A., Schindelin, H.*, et al.* (2011a). The residence time of GABA(A)Rs at inhibitory synapses is determined by direct binding of the receptor alpha1 subunit to gephyrin. J Neurosci ***31***, 14677-14687.

Mukherjee, J., Kretschmannova, K., Gouzer, G., Maric, H.M., Ramsden, S., Tretter, V., Harvey, K., Davies, P.A., Triller, A., Schindelin, H.*, et al.* (2011b). The residence time of GABA(A)Rs at inhibitory synapses is determined by direct binding of the receptor alpha1 subunit to gephyrin. J Neurosci ***31***, 14677-14687.

Muller, E., Le Corronc, H., Triller, A., and Legendre, P. (2006). Developmental dissociation of presynaptic inhibitory neurotransmitter and postsynaptic receptor clustering in the hypoglossal nucleus. Mol Cell Neurosci ***32***, 254-273.

Munton, R.P., Tweedie-Cullen, R., Livingstone-Zatchej, M., Weinandy, F., Waidelich, M., Longo, D., Gehrig, P., Potthast, F., Rutishauser, D., Gerrits, B.*, et al.* (2007). Qualitative and quantitative analyses of protein phosphorylation in naive and stimulated mouse synaptosomal preparations. Mol Cell Proteomics ***6***, 283-293.

Nakane, P.K., and Kawaoi, A. (1974). Peroxidase-labeled antibody. A new method of conjugation. J Histochem Cytochem ***22***, 1084-1091.

Nichols, J.D., Xiang, S., Schindelin, H., and Rajagopalan, K.V. (2007). Mutational analysis of Escherichia coli MoeA: two functional activities map to the active site cleft. Biochemistry ***46***, 78-86.

Ogino, K., Ramsden, S.L., Keib, N., Schwarz, G., Harvey, R.J., and Hirata, H. (2011). Duplicated gephyrin genes showing distinct tissue distribution and alternative splicing patterns mediate molybdenum cofactor biosynthesis, glycine receptor clustering, and escape behavior in zebrafish. J Biol Chem***. 286***, 806-817.

Olsen, R.W., and Sieghart, W. (2008). International Union of Pharmacology. LXX. Subtypes of gamma-aminobutyric acid(A) receptors: classification on the basis of subunit composition, pharmacology, and function. Update. Pharmacol Rev ***60***, 243-260.

Paoletti, P., Bellone, C., and Zhou, Q. (2013). NMDA receptor subunit diversity: impact on receptor properties, synaptic plasticity and disease. Nature reviews. Neuroscience ***14***, 383-400.

Pecqueur, L., Duellberg, C., Dreier, B., Jiang, Q., Wang, C., Pluckthun, A., Surrey, T., Gigant, B., and Knossow, M. (2012). A designed ankyrin repeat protein selected to bind to tubulin caps the microtubule plus end. Proceedings of the National Academy of Sciences of the United States of America ***109***, 12011-12016.

Pereda, A.E. (2014). Electrical synapses and their functional interactions with chemical synapses. Nature reviews. Neuroscience ***15***, 250-263.

Petrini, E.M., Lu, J., Cognet, L., Lounis, B., Ehlers, M.D., and Choquet, D. (2009). Endocytic trafficking and recycling maintain a pool of mobile surface AMPA receptors required for synaptic potentiation. Neuron ***63***, 92-105.

Pfeiffer, F., Graham, D., and Betz, H. (1982). Purification by affinity chromatography of the glycine receptor of rat spinal cord. J Biol Chem ***257***, 9389-9393.

Prior, P., Schmitt, B., Grenningloh, G., Pribilla, I., Multhaup, G., Beyreuther, K., Maulet, Y., Werner, P., Langosch, D., Kirsch, J.*, et al.* (1992). Primary structure and alternative splice variants of gephyrin, a putative glycine receptor-tubulin linker protein. Neuron *8*, 1161-1170.

Pyykko, P., and Atsumi, M. (2009). Molecular single-bond covalent radii for elements 1-118. Chemistry ***15***, 186-197.

Rahman, J., Latal, A.T., Besser, S., Hirrlinger, J., and Hulsmann, S. (2013). Mixed miniature postsynaptic currents resulting from co-release of glycine and GABA recorded from glycinergic neurons in the neonatal respiratory network. Eur J Neurosci ***37***, 1229-1241.

Ramming, M., Kins, S., Werner, N., Hermann, A., Betz, H., and Kirsch, J. (2000). Diversity and phylogeny of gephyrin: tissue-specific splice variants, gene structure, and sequence similarities to molybdenum cofactor-synthesizing and cytoskeleton-associated proteins. Proceedings of the National Academy of Sciences of the United States of America ***97***, 10266-10271.

Ravelli, R.B., Gigant, B., Curmi, P.A., Jourdain, I., Lachkar, S., Sobel, A., and Knossow, M. (2004). Insight into tubulin regulation from a complex with colchicine and a stathmin-like domain. Nature ***428***, 198-202.

Reiss, J., Gross-Hardt, S., Christensen, E., Schmidt, P., Mendel, R.R., and Schwarz, G. (2001). A mutation in the gene for the neurotransmitter receptor-clustering protein gephyrin causes a novel form of molybdenum cofactor deficiency. American journal of human genetics ***68***, 208-213.

Reiss, J., and Hahnewald, R. (2011). Molybdenum cofactor deficiency: Mutations in GPHN, MOCS1, and MOCS2. Human mutation ***32***, 10-18.

Reiss, J., Lenz, U., Aquaviva-Bourdain, C., Joriot-Chekaf, S., Mention-Mulliez, K., and Holder-Espinasse, M. (2011). A GPHN point mutation leading to molybdenum cofactor deficiency. Clinical genetics ***80***, 598-599.

Reissner, C., Klose, M., Fairless, R., and Missler, M. (2008). Mutational analysis of the neurexin/neuroligin complex reveals essential and regulatory components. Proceedings of the National Academy of Sciences of the United States of America ***105***, 15124-15129.

Rizzi, M., and Schindelin, H. (2002). Structural biology of enzymes involved in NAD and molybdenum cofactor biosynthesis. Current opinion in structural biology ***12***, 709-720.

Rudolph, U., and Knoflach, F. (2011). Beyond classical benzodiazepines: novel therapeutic potential of GABAA receptor subtypes. Nat Rev Drug Discov ***10***, 685-697.

Sainlos, M., Iskenderian-Epps, W.S., Olivier, N.B., Choquet, D., and Imperiali, B. (2013). Caged mono- and divalent ligands for light-assisted disruption of PDZ domain-mediated interactions. J Am Chem Soc ***135***, 4580-4583.

Sainlos, M., Tigaret, C., Poujol, C., Olivier, N.B., Bard, L., Breillat, C., Thiolon, K., Choquet, D., and Imperiali, B. (2011). Biomimetic divalent ligands for the acute disruption of synaptic AMPAR stabilization. Nat Chem Biol ***7,*** 81-91.

Sander, B., Tria, G., Shkumatov, A.V., Kim, E.Y., Grossmann, J.G., Tessmer, I., Svergun, D.I., and Schindelin, H. (2013). Structural characterization of gephyrin by AFM and SAXS reveals a mixture of compact and extended states. Acta Crystallogr D Biol Crystallogr ***69***, 2050-2060.

Sassoe-Pognetto, M., Panzanelli, P., Sieghart, W., and Fritschy, J.M. (2000). Colocalization of multiple GABA(A) receptor subtypes with gephyrin at postsynaptic sites. J Comp Neurol ***420***, 481-498.

Schrader, N., Kim, E.Y., Winking, J., Paulukat, J., Schindelin, H., and Schwarz, G. (2004). Biochemical characterization of the high affinity binding between the glycine receptor and gephyrin. J Biol Chem ***279***, 18733-18741.

Schwarz, G., Mendel, R.R., and Ribbe, M.W. (2009). Molybdenum cofactors, enzymes and pathways. Nature ***460***, 839-847.

Schwarz, G., Schrader, N., Mendel, R.R., Hecht, H.J., and Schindelin, H. (2001). Crystal structures of human gephyrin and plant Cnx1 G domains: comparative analysis and functional implications. J Mol Biol ***312***, 405-418.

Schwer, B., Eckersdorff, M., Li, Y., Silva, J.C., Fermin, D., Kurtev, M.V., Giallourakis, C., Comb, M.J., Alt, F.W., and Lombard, D.B. (2009). Calorie restriction alters mitochondrial protein acetylation. Aging Cell ***8***, 604-606.

Sheldrick, G.M. (2008). A short history of SHELX. Acta crystallographica. Section A, Foundations of crystallography ***64***, 112-122.

Singh, R. (1994). A sensitive assay for maleimide groups. Bioconjug Chem *5*, 348-351.

Smolinsky, B., Eichler, S.A., Buchmeier, S., Meier, J.C., and Schwarz, G. (2008). Splice-specific functions of gephyrin in molybdenum cofactor biosynthesis. J Biol Chem. ***283***, 17370-17379.

Sobolevsky, A.I., Rosconi, M.P., and Gouaux, E. (2009). X-ray structure, symmetry and mechanism of an AMPA-subtype glutamate receptor. Nature ***462***, 745-756.

Sola, M., Bavro, V.N., Timmins, J., Franz, T., Ricard-Blum, S., Schoehn, G., Ruigrok, R.W., Paarmann, I., Saiyed, T., O'Sullivan, G.A.*, et al.* (2004). Structural basis of dynamic glycine receptor clustering by gephyrin. Embo J ***23***, 2510-2519.

Sola, M., Kneussel, M., Heck, I.S., Betz, H., and Weissenhorn, W. (2001). X-ray crystal structure of the trimeric N-terminal domain of gephyrin. J Biol Chem *276*, 25294-25301.

Sommer, B., Burnashev, N., Verdoorn, T.A., Keinanen, K., Sakmann, B., and Seeburg, P.H. (1992). A glutamate receptor channel with high affinity for domoate and kainate. EMBO J ***11***, 1651-1656.

Soykan, T., Schneeberger, D., Tria, G., Buechner, C., Bader, N., Svergun, D., Tessmer, I., Poulopoulos, A., Papadopoulos, T., Varoqueaux, F.*, et al.* (2014). A conformational switch in collybistin determines the differentiation of inhibitory postsynapses. EMBO J ***33***, 2113-2133.

Specht, C.G., Grunewald, N., Pascual, O., Rostgaard, N., Schwarz, G., and Triller, A. (2011). Regulation of glycine receptor diffusion properties and gephyrin interactions by protein kinase C. Embo J ***30***, 3842-3853.

Specht, C.G., Izeddin, I., Rodriguez, P.C., El Beheiry, M., Rostaing, P., Darzacq, X., Dahan, M., and Triller, A. (2013). Quantitative nanoscopy of inhibitory synapses: counting gephyrin molecules and receptor binding sites. Neuron ***79***, 308-321.

Studer, R., von Boehmer, L., Haenggi, T., Schweizer, C., Benke, D., Rudolph, U., and Fritschy, J.M. (2006). Alteration of GABAergic synapses and gephyrin clusters in the thalamic reticular nucleus of GABAA receptor alpha3 subunit-null mice. Eur J Neurosci ***24***, 1307-1315.

Tejada-Jimenez, M., Llamas, A., Sanz-Luque, E., Galvan, A., and Fernandez, E. (2007). A high-affinity molybdate transporter in eukaryotes. Proceedings of the National Academy of Sciences of the United States of America ***104***, 20126-20130.

Traynelis, S.F., Wollmuth, L.P., McBain, C.J., Menniti, F.S., Vance, K.M., Ogden, K.K., Hansen, K.B., Yuan, H., Myers, S.J., and Dingledine, R. (2010). Glutamate receptor ion channels: structure, regulation, and function. Pharmacol Rev ***62***, 405-496.

Tretter, V., Jacob, T.C., Mukherjee, J., Fritschy, J.M., Pangalos, M.N., and Moss, S.J. (2008). The clustering of GABA(A) receptor subtypes at inhibitory synapses is facilitated via the direct binding of receptor alpha 2 subunits to gephyrin. J Neurosci ***28***, 1356-1365.

Tretter, V., Kerschner, B., Milenkovic, I., Ramsden, S.L., Ramerstorfer, J., Saiepour, L., Maric, H.M., Moss, S.J., Schindelin, H., Harvey, R.J.*, et al.* (2011). Molecular basis of the gamma-aminobutyric acid A receptor alpha3 subunit interaction with the clustering protein gephyrin. J Biol Chem ***286***, 37702-37711.

Tretter, V., Mukherjee, J., Maric, H.M., Schindelin, H., Sieghart, W., and Moss, S.J. (2012). Gephyrin, the enigmatic organizer at GABAergic synapses. Front Cell Neurosci***6***, 23.

Triller, A., and Choquet, D. (2005). Surface trafficking of receptors between synaptic and extrasynaptic membranes: and yet they do move! Trends Neurosci ***28***, 133-139.

Tyagarajan, S.K., and Fritschy, J.M. (2014). Gephyrin: a master regulator of neuronal function? Nat Rev Neurosci ***15***, 141-156.

Tyagarajan, S.K., Ghosh, H., Yevenes, G.E., Imanishi, S.Y., Zeilhofer, H.U., Gerrits, B., and Fritschy, J.M. (2013). Extracellular signal-regulated kinase and glycogen synthase kinase 3beta regulate gephyrin postsynaptic aggregation and GABAergic synaptic function in a calpain-dependent mechanism. J Biol Chem ***288***, 9634-9647.

Varoqueaux, F., Aramuni, G., Rawson, R.L., Mohrmann, R., Missler, M., Gottmann, K., Zhang, W., Sudhof, T.C., and Brose, N. (2006). Neuroligins determine synapse maturation and function. Neuron ***51***, 741-754.

Vlachos, A., Reddy-Alla, S., Papadopoulos, T., Deller, T., and Betz, H. (2013). Homeostatic regulation of gephyrin scaffolds and synaptic strength at mature hippocampal GABAergic postsynapses. Cereb Cortex ***23***, 2700-2711.

Winsky-Sommerer, R., Knapman, A., Fedele, D.E., Schofield, C.M., Vyazovskiy, V.V., Rudolph, U., Huguenard, J.R., Fritschy, J.M., and Tobler, I. (2008). Normal sleep homeostasis and lack of epilepsy phenotype in GABA A receptor alpha3 subunit-knockout mice. Neuroscience ***154***, 595-605.

Wittle, A.E., Kamdar, K.P., and Finnerty, V. (1999). The Drosophila cinnamon gene is functionally homologous to Arabidopsis cnx1 and has a similar expression pattern to the mammalian gephyrin gene. Molecular & general genetics : MGG ***261***, 672-680.

Wu, X., Wu, Z., Ning, G., Guo, Y., Ali, R., Macdonald, R.L., De Blas, A.L., Luscher, B., and Chen, G. (2012). gamma-Aminobutyric acid type A (GABAA) receptor alpha subunits play a direct role in synaptic versus extrasynaptic targeting. J Biol Chem ***287***, 27417-27430.

Xiang, S., Nichols, J., Rajagopalan, K.V., and Schindelin, H. (2001). The crystal structure of Escherichia coli MoeA and its relationship to the multifunctional protein gephyrin. Structure ***9*****,** 299-310.

Xue, H. (1998). Identification of major phylogenetic branches of inhibitory ligand-gated channel receptors. J Mol Evol ***47***, 323-333.

Yang, Z., Taran, E., Webb, T.I., and Lynch, J.W. (2012). Stoichiometry and subunit arrangement of alpha1beta glycine receptors as determined by atomic force microscopy. Biochemistry ***51***, 5229-5231.

Zhang, R., Alushin, G.M., Brown, A., and Nogales, E. (2015). Mechanistic Origin of Microtubule Dynamic Instability and Its Modulation by EB Proteins. Cell***162***, 849-859.

Zhou, H.X. (2001). The affinity-enhancing roles of flexible linkers in two-domain DNA-binding proteins. Biochemistry ***40***, 15069-15073.

Zhou, H.X. (2003). Quantitative account of the enhanced affinity of two linked scFvs specific for different epitopes on the same antigen. J Mol Biol ***329***, 1-8.

Zita, M.M., Marchionni, I., Bottos, E., Righi, M., Del Sal, G., Cherubini, E., and Zacchi, P. (2007). Post-phosphorylation prolyl isomerisation of gephyrin represents a mechanism to modulate glycine receptors function. Embo J ***26***, 1761-1771.